Approche quasi-systématique du contrôle de la chaîne d'air des moteurs suralimentés, basée sur la commande prédictive non linéaire explicite

Jamil El Hadef

UNIVERSITÉ D'ORLÉANS

ÉCOLE DOCTORALE
ENERGIE, MATERIAUX, SCIENCES DE LA TERRE ET DE L'UNIVERS

LABORATOIRE PRISME

THÈSE présentée par

Jamil EL HADEF

soutenue le **22 janvier 2014**

pour obtenir le grade de **Docteur de l'Université d'Orléans**
Discipline : Energétique

Approche quasi-systématique du contrôle de la chaîne d'air des moteurs suralimentés, basée sur la commande prédictive non linéaire explicite

THÈSE dirigée par
Yann CHAMAILLARD Professeur, Université d'Orléans

RAPPORTEURS
Anna STEFANOPOULOU Professor, University of Michigan
Mazen ALAMIR Directeur de recherche CNRS, GIPSA-Lab, Université de Grenoble

PRESIDENT DU JURY
Nicolas PETIT Professeur, MINES Paris Tech

EXAMINATEURS
Sorin OLARU Professeur, SUPELEC
Vincent TALON Docteur, Renault SAS
Guillaume COLIN Habilité à Diriger des Recherches, Université d'Orléans

CONTENTS

NOMENCLATURE

A	Orifice area
AFR	Air/fuel ratio
c_p	Specific heat of the gas at constant pressure
c_v	Specific heat of the gas at constant volume
C	Gas velocity (Part 1) *or* set of scalar coefficients that weight each Laguerre function level (Part 2)
D	Compressor wheel exducer diameter
h	Specific enthalpy of the fluid
H	Enthalpy of the fluid
H_c	Control horizon
H_p	Prediction horizon
I	Mass moment of inertia of the turbocharger
$\mathcal{J}$	Cost function
k_{ech}	Amount of energy transferred to the exhaust gas
LHV	Lower heating value
m	Mass of the fluid (Part 1) *or* number of input variables (Part 2)
Ma	Mach number
n	Dimension of a vector space
N	Number of revolutions per cycles on a four-cylinder four-stroke engine (Part 1) *or* number of terms in the Laguerre functions expansion (Chapter 6) *or* number of points in a given set (Chapter 7)
N_e	Engine speed
N_c	Control horizon
N_p	Prediction horizon
p	Pressure
p_{crit}	Critical pressure at which the flow reaches sonic conditions
Q	Mass flow rate
Q_{eng}	Air mass flow entering the cylinders
Q_{fuel}	Fuel mass flow rate

r	Perfect gas constant
R	Fluid gas constant
S	Entropy
$\mathcal{S}$	Objective function
t	Time
u	Manipulated variable
u^*	Optimal vector of input variables
U	Internal energy of the fluid (Part 1)
Uc	Compressor wheel blade tip speed
V	Volume
V_{cyl}	Total engine displacement
V_{ns}	Reduced flow speed
x	States vector

Greek

γ	Ratio of specific heats
Γ	Torque
Δt_c	Control sampling time
ε	Error bound
η	Efficiency of a turbomachine
η_{vol}	Volumetric efficiency
θ	Temperature (Part 1) *or* hyper-rectangle vertex (Part 2)
Θ	Set of vertices of a hyper-rectangle
Π	Pressure ratio
ρ	Fluid density
σ	Vector of exogenous inputs
Φ	Validation point (Part 2)
Φ	Dimensionless flow rate (Part 1) *or* set of validation points (Part 2)
Ψ	Head parameter
ω_t	Turbocharger rotational speed

Subscripts

amb	Ambient
apc	Downstream compressor
ape	Upstream throttle
avc	Upstream compressor
avt	Upstream turbine
C	Compressor
ds	Downstream
eff	Effective
in	Inlet of the control volume
is	Isentropic
man	Intake manifold
out	Outlet of the control volume
red	Reduced
thr	Throttle
T	Turbine
us	Upstream
wg	Wastegate

INTRODUCTION

CONTEXT AND ISSUES OF THE STUDY

The hundreds of millions of passenger cars and other vehicles on our roads emphasize our society's reliance on internal combustion engines for the transportation of goods and people. However, despite striking reductions in pollutant emissions and fuel consumption since the 1960s, when the first legislation concerning the pollutant emissions of light-duty vehicles was passed in the United States, motor vehicles remain one of the most important sources of air pollution in modern urban areas. The effect on human health is tragic and has been pointed out by an increasing number of studies.

On the one hand, this public health issue leads the authorities to advocate increasingly drastic pollutant emission standards. On the other hand car manufacturers, in view of the need to reduce development time in order to remain competitive on a more and more globalized market, argue for moderate policy changes. Current legislation is a compromise between these two competing factors. An interesting fact is that standards limit vehicle emissions to a normalized driving cycle. Nothing else is taken into account. In particular crucial stages in product life cycle management, such as raw material extraction, manufacturing, transportation or recycling are not considered. For car manufacturers, the only focus of research and development is the vehicle itself.

Among all the technological solutions conducive to a reduction in pollutant emissions and fuel consumption, the engine is known to be the most cost-effective parameter. In particular, control of the air path has become a significant branch of research and development since the introduction of an increasing number of actuators, added to manage the phenomena related to control of the gas entering the cylinders. Since the gas composition is at the heart of the combustion process, managing it appropriately represents a cost-effective way to reduce pollutant emissions.

This study addresses the issue of the complexity of the air path caused by the fact that actuators are often added to meet additional engine performance requirements, such as pollutant emissions, fuel efficiency and drivability. The proposed solution involves the combination of a *physics-based engine model* and *nonlinear model predictive control*. Beyond the originality of such a combination, the distinctive feature of the method resides in the use of the so-called *explicit nonlinear model predictive control paradigm* in order to obtain a real-time implementable controller. Altogether, this thesis presents a combination of methods taken from physics and mathematics, which attempts to propose a quasi-systematic air path control design approach for turbocharged gasoline engines (figure below).

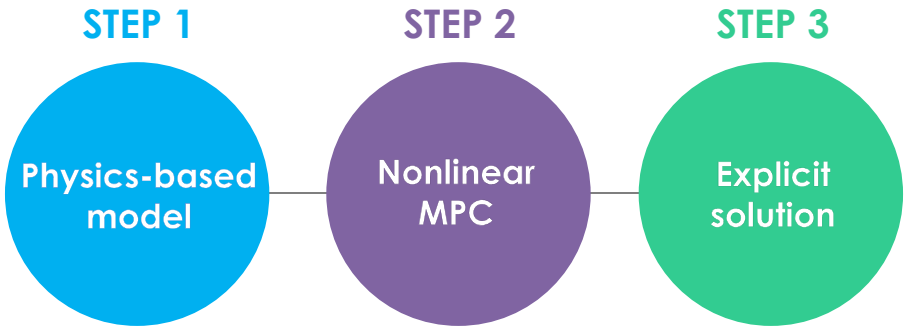

Figure – Overview of the control design approach proposed in this study

The present document has been organized in two main parts. The first three chapters lead to the construction of a control-oriented physics-based model of a turbocharged gasoline engine air path. The following chapters present the use of this model in an explicit nonlinear model predictive control framework, i.e. leading to a controller that is compatible with real-time requirements.

Part 1: Control-oriented physics-based model of turbocharged gasoline engine air path

It is clear that new technologies are urgently needed to reduce the pollutant emissions and fuel consumption of internal combustion engines. However, the compromise between emissions, fuel consumption and market competitiveness is not straightforward, and in order to find a suitable trade-off extensive simulations are increasingly used early on in the engine development process. In the present study we propose to investigate how engine control can make state-of-the art engine modelling even more attractive in the automotive industry.

Chapter 1 provides an overview of the behaviour of turbocharged gasoline engines that serves as an introduction to the modelling philosophy introduced in the rest of the chapter. Altogether it introduces the mean-value engine modelling philosophy as well as the zero-dimensional modelling approach that are used to describe the phenomena occurring through the air path. Lastly the quasi-static modelling approach used to model the compressor and the turbine is presented with an emphasis on the need for accurate turbocharger look-up tables.

Chapter 2 addresses the issues involved in the construction of the look-up tables that are at the heart of the quasi-static compressor and turbine sub-models. In practice, they are usually obtained by interpolating and extrapolating steady-state measurements directly provided by the manufacturer of the component. However, the absence of operating points at low turbocharger rotational speeds considerably complicates this task. The new interpolation and extrapolation methodologies presented here rely on an appropriate combination of physics, empirical observations and optimization. This is a clearly distinctive feature w.r.t. methods reported in the literature that are usually either physics-based and too complex in a control-oriented framework or purely mathematical and not sufficiently accurate.

Chapter 3 applies the philosophy and developments presented in the first two chapters to two practical cases of application, both validated with experimental test bench measurements. The first one concerns the design of a virtual turbocharger rotational speed sensor, for test bench applications. The second one concerns the design of a complete turbocharged gasoline engine air path model. It uses the modelling approach presented in chapter 1 and the turbocharger look-up tables obtained in chapter 2. Overall both examples tend to confirm the modelling hypotheses formulated in chapters 1 and 2. While the former is currently being implemented in an industrial framework at Renault SAS, the second one will be used in part 2, in a nonlinear model predictive control framework.

The overall modelling philosophy presented in these chapters is similar to the modelling approach usually chosen in the automotive industry when considering control applications[1]. As such, since it is beginning to be well-known by control engineers, it represents the perfect starting point of our approach toward a systematic air path control design.

[1] The novel interpolation and extrapolation strategies of the compressor and turbine data-maps, presented in chapter 2 and integrated into the zero-dimensional modeling philosophy used in chapter 3, are currently being implemented in an industrial tool as part of a partnership between Renault SAS and LMS®.

Part 2: Toward a real-time implementable nonlinear model predictive control of the air path of a turbocharged gasoline engine

Turbocharged gasoline engine air paths are intrinsically multi-input multi-output nonlinear systems, with active constraints on the inputs. In this framework, standard linear or even multi-linear control approaches have proved their limitations when considering engine control over an extensive part of the operating range. Additionally, the growing penetration of physics-based simulation in the automotive industry mostly remains limited to the validation of the control laws. In particular, control design processes that could use physics-based nonlinear models from the very beginning, to synthesize optimal, reliable and real-time implementable control laws, have long been awaited [9,46,47,62,100,103,104,114].

Chapter 4 reflects our intention to solve the problem in its industrial context, rather than provide a purely theoretical answer. It therefore proposes a summary of the main constraints that have to be taken into account when designing a control strategy in the automotive industrial framework. Far from claiming that this study provides an exhaustive answer to all these constraints, they mostly serve as a guideline for the study. Finally, before going into detail about our particular application, relevant contributions in the fields of engine model-based control and model predictive control are presented, with particular stress on the opportunities offered by the approach w.r.t. to air path control.

Chapter 5 presents the synthesis of an implicit nonlinear model predictive control (NMPC) that uses the physics-based model developed in chapter 3 and which is extensively used in the automotive industry, to compute the predictions. Altogether, this control scheme represents a novel combination in the field of gasoline engine air path model predictive control. We also take advantage of the physics-based model to introduce a novel thermodynamic-based objective function that maximises the engine efficiency explicitly. The significant performances obtained in simulation confirm the expectations of many authors about the use of physics-based engine models in nonlinear model predictive control [46,99] and contribute to opening up a new field of research. Finally, since the design of the controller proves to be compatible with the computation of a real-time implementable solution using the explicit NMPC paradigm, it represents the second step toward a quasi-systematic air path control design approach.

Chapter 6 proposes an alternative approach to the implicit NMPC law presented in chapter 5, based on a parameterization of the control increments trajectory. It can therefore be considered as a parameterized NMPC approach. The philosophy presented here is a direct extension to the nonlinear paradigm of the approach proposed in [133] in a linear framework and is motivated by the need to maintain the level of flexibility of the future control trajectory under tight computational requirements. The advantage of the approach lies in the encapsulation of the complexity/optimality compromise under a new set of easy-to-tune parameters. Altogether, the NMPC formulation remains easy to implement and compatible with the use of a physics-based model and an unconventional thermodynamic-based objective function.

Chapter 7 finally introduces the explicit NMPC framework and in particular a brief background about multi-parametric programming. The latter is at the heart of the approach and allows a piecewise affine approximation of an implicit NMPC law to be computed. The method itself draws on the most recent work in the field of explicit NMPC [53], and introduces the ability to handle computationally expensive prediction models as well as parallel computing. In particular, thanks to this distinctive feature the explicit approximation of the implicit NMPC law presented in chapter 5 can be computed. Once combined with an appropriate method of implementation on-board, namely using a binary search tree to store the piecewise affine explicit control law, it leads to a drastic reduction in computational

requirements w.r.t to implicit NMPC while maintaining very good tracking performances. Altogether, this makes it worth considering for a real-time implementation online and as such, represents the third and last step toward a quasi-systematic design approach for the control of the air path of turbocharged gasoline engines.

Overall, this second part leads to a real-time implementable controller, based on the piecewise approximation of a given implicit NMPC controller. By real-time implementable we mean a short and predictable computational time.

The main contributions of the study are:

- The derivation of a new set of algorithms for the interpolation and extrapolation of compressor and turbine quasi-steady-state data-maps. While these data-maps are at the heart of all control-oriented engine models that include a turbocharger, the accuracy of the methodology in the literature is not satisfying. The novel combination of physics, empirical observations and optimization proposed in this study proved to lead to more accurate data in the extrapolating zone, thus enhancing the robustness of the widespread quasi-static turbocharger models.
- The implementation of a horizon-1 nonlinear model predictive control (NMPC) scheme for the control of the inlet manifold pressure on a turbocharged gasoline engine. The distinctive feature of this scheme is the use of a physics-based engine model and a thermodynamic-based objective function.
- A proposal of a parameterized NMPC law based on the expansion of the future control increments trajectory on a set of orthonormal functions, namely Laguerre polynomials. Altogether, this unprecedented approach in the nonlinear framework facilitates the tuning of the closed-loop performance by encapsulating the complexity/optimality compromise in a set of two high level parameters.
- The computation of a piecewise affine solution of a 6-dimension multi-parametric nonlinear programming problem, that produces an explicit feedback control law which approximates the behaviour of the horizon-1 NMPC scheme suggested above, over the entire operating range of a turbocharged gasoline engine. Along with the use of a binary search-tree for the storage of the set of affine laws and the regions on which they are defined, the methodology considerably reduces the online computational time w.r.t. to implicit NMPC.

Altogether, this dissertation presents the first steps toward a systematic approach for the design of turbocharged gasoline engine air path optimal control.

INTRODUCTION *(in French)*

CONTEXTE ET ENJEUX DE L'ETUDE

Les centaines de millions de véhicules constituant le parc automobile mondial (tous véhicules) montrent la dépendance de notre société vis-à-vis du moteur à combustion interne pour le transport de biens et de personnes. Cependant, malgré des progrès considérables en termes d'émissions et de consommation depuis les années 60, date correspondant à la mise en place de la première règlementation concernant les émissions polluantes des véhicules légers aux Etats-Unis, les véhicules équipés de moteurs à combustion interne restent l'une des sources les plus importantes de pollution de l'air au sein des centres urbains modernes. Les effets sur la santé de l'Homme sont dramatiques et de plus en plus soulignés par les médias.

Du point de vue des autorités, cet enjeu sanitaire motive le renforcement des normes antipollution. Pour les constructeurs automobiles, au contraire, la nécessité de réduire les temps de développement afin de rester compétitifs sur un marché de plus en plus mondialisé, plaide en faveur d'un changement modéré de ces normes. La législation en vigueur est un compromis entre ces deux objectifs divergents. Il est intéressant de noter que ces règlementations limitent les émissions des véhicules sur un cycle de conduite normalisé. Aucun autre élément n'est pris en compte. En particulier, des étapes cruciales du cycle de vie du produit telles que l'extraction des matières premières, la fabrication, le transport ou le recyclage ne sont pas prises en considération. Au regard de la norme, le véhicule représente donc le seul axe de recherche et de développement des constructeurs automobiles.

Parmi toutes les solutions technologiques aboutissant à une réduction des émissions et de la consommation, le moteur est le paramètre le plus rentable. En particulier, le contrôle de la chaîne d'air rassemble une part importante de la recherche et du développement depuis l'augmentation du nombre d'actionneurs. Ces actionneurs sont précisément ajoutés pour contrôler les phénomènes liés à l'entrée des gaz dans le cylindre. En effet, la composition des gaz étant au cœur du processus de combustion, contrôler l'introduction des gaz dans le cylindre représente le moyen le plus avantageux pour réduire les émissions polluantes.

Cette étude répond au problème de complexité de la chaîne d'air, dû à l'ajout de nouveaux actionneurs afin d'atteindre de nouveaux besoins, incluant réduction des émissions polluantes et de la consommation, et confort de conduite. La proposition en elle-même repose sur la combinaison d'un *modèle moteur basé sur la physique* et d'une stratégie de *contrôle prédictif non linéaire*. Au-delà de la rareté de cette combinaison, l'originalité de la méthode repose sur l'utilisation de l'approche de *commande prédictive non linéaire explicite* pour l'implémentation en temps réel du contrôle. Dans son ensemble, cette thèse présente une combinaison de méthodes tirées de la physique et des mathématiques, qui propose une approche quasi-systématique pour la synthèse du contrôle de la chaîne d'air des moteurs essence suralimentés (voir figure ci-dessous).

Figure – Vue d'ensemble de l'approche de synthèse du contrôle proposée dans cette étude

Ce document est organisé en deux parties. Les trois premiers chapitres aboutissent à la construction d'un modèle, basé sur la physique et orienté pour le contrôle, de la chaîne d'air d'un moteur essence suralimenté. Les chapitres suivants présentent l'utilisation de ce modèle dans un cadre de commande prédictive non linéaire explicite, c'est-à-dire menant à un contrôle temps-réel.

Partie 1: Modèle physique pour le contrôle de la chaîne d'air des moteurs essence suralimentés

Il est clair que le besoin de technologies visant à réduire les émissions polluantes et la consommation des moteurs est important. Cependant, le compromis entre émissions polluantes, consommation et compétitivité n'est pas trivial. Sa détermination est de plus en plus obtenue au travers de la simulation, au plus tôt dans le processus de développement. Dans cette étude, nous proposons d'investiguer comment le contrôle pourrait encore valoriser d'avantages les efforts mener sur la modélisation dans l'industrie automobile.

Le Chapitre 1 fournit des généralités sur le comportement des moteurs essence suralimentés, servant d'introduction à la philosophie de modélisation présentée dans le reste du chapitre. Dans son ensemble, il présente l'approche de modélisation dite du moteur moyen et la modélisation zéro-dimensionnelle utilisées pour décrire les phénomènes mis en jeu dans la chaîne d'air. Finalement, un modèle quasi-statique du compresseur et de la turbine est présenté, et une attention particulière est portée sur le besoin de cartographies précises.

Le Chapitre 2 répond aux problèmes liés à la construction de ces cartographies. En pratique, elles sont souvent obtenues en interpolant et extrapolant des mesures en stabilisé directement fournies par le fabricant. Cependant, l'absence de points de fonctionnement aux bas régimes de rotation du turbocompresseur, complique considérablement la tâche. Les nouvelles méthodes d'interpolation et d'extrapolation présentées ici reposent sur un juste compromis de physique, d'observations empiriques et d'optimisation. Cela constitue un élément distinctif clair au regard des méthodes proposées dans la littérature, qui sont soit entièrement basées sur la physique et trop complexes pour le contrôle, soit purement mathématiques et imprécises en extrapolation.

Le Chapitre 3 représente la synthèse de la philosophie de modélisation présentée dans les deux premiers chapitres autour de deux cas d'application, tous deux validés expérimentalement. Le premier repose sur la construction d'un capteur virtuel du régime de rotation du turbocompresseur, avec un exemple d'intégration à un banc d'essai moteur. Le second concerne la synthèse complète du modèle de chaîne d'air d'un moteur essence suralimenté. Il utilise l'approche de modélisation présentée dans le chapitre 1 et les cartographies compresseur et turbine obtenues au chapitre 2. Ensemble, ces deux

exemples confirment les hypothèses de modélisation posées aux chapitres 1 et 2. Alors que le capteur virtuel est en train d'être implémenté industriellement chez Renault SAS, le modèle de la chaîne d'air, quant à lui, sera utilisé dans la partie 2 de l'étude dans un cadre de commande prédictive non linéaire.

La philosophie générale de modélisation présentée dans ces chapitres est similaire à celle utilisée dans l'industrie automobile[2] pour le développement du contrôle moteur. Ainsi, puisqu'elle commence à être bien connue des équipes responsables du contrôle moteur, elle représente le parfait point de départ de notre approche vers une synthèse systématique du contrôle de la chaîne d'air.

Partie 2: Vers un contrôle prédictif non linéaire temps-réel de la chaîne d'air des moteurs essences suralimentés

Intrinsèquement, la chaîne d'air des moteurs essence suralimentés est un système non linéaire multi-entrées multi-sorties, présentant également des actionneurs saturés. Dans ce contexte, les approches classiques de contrôle linéaire ou multi-linéaire ont atteint leurs limites, lorsque l'on prend en compte l'ensemble du champ de fonctionnement du moteur. De plus, la part croissante de la modélisation physique dans l'industrie automobile reste limitée si on considère uniquement la synthèse du contrôle en elle-même. En effet, les stratégies de contrôle pouvant utiliser ce type de modèles physiques non linéaires pour synthétiser des lois de contrôle optimales, robustes et implémentables en temps réel sont attendues avec un vif intérêt [9,46,47,62,100,103,104,114].

Le Chapitre 4 matérialise notre volonté de résoudre ce problème dans son contexte industriel, au lieu de fournir une solution purement théorique. Il propose ainsi un aperçu des contraintes principales qui doivent être prises en compte lorsque l'on conçoit une stratégie de contrôle pour l'industrie automobile. Loin de prétendre que cette étude répond de manière exhaustive à toutes ces exigences, elles servent surtout de fil conducteur à l'étude. Enfin, avant de rentrer dans les détails de notre cas d'application, les contributions les plus significatives dans le domaine du contrôle moteur dit « model-based » et du contrôle moteur prédictif, sont présentées et une attention particulière est portée sur les opportunités offertes pour le contrôle de la chaîne d'air.

Le Chapitre 5 présente la synthèse d'une stratégie de contrôle prédictif non linéaire qui utilise, pour le calcul des prédictions, le modèle moteur physique développé dans le chapitre 3 et largement utilisé dans l'industrie automobile. Dans son ensemble, cette stratégie de contrôle représente une association inédite dans le cadre du contrôle prédictif de la chaîne d'air des moteurs essence. On profite aussi de l'avantage d'utiliser un modèle physique pour introduire une fonction de coût inédite, basée sur la thermodynamique, maximisant explicitement le rendement moteur. Les performances significatives obtenues en simulation confirment les attentes de nombreux auteurs dans la littérature, vis-à-vis de l'utilisation de modèles moteur physiques dans un cadre de commande prédictive non linéaire [46,99], et participe à l'ouverture d'un nouveau champ de recherche. Finalement, puisque cette stratégie de contrôle a prouvé sa compatibilité avec une implémentation temps-réel utilisant une approche dite de commande prédictive non linéaire explicite, ce schéma de contrôle représente notre deuxième étape vers une approche quasi-systématique de la synthèse du contrôle de la chaîne d'air.

[2] Les nouvelles stratégies d'interpolation et d'extrapolation des cartographies compresseur et turbine, présentées dans le chapitre 2 et intégrées à la stratégie de modélisation zéro dimensionnelle utilisée dans le chapitre 3, sont actuellement en train d'être implémentées dans un outil industriel, dans le cadre d'un partenariat entre Renault SAS et LMS®.

Le Chapitre 6 propose une approche alternative au schéma de contrôle prédictif non linéaire présenté au chapitre 5, en se basant sur la paramétrisation de la trajectoire des futurs incréments de contrôle. Ainsi, elle entre dans la catégorie dite des commandes prédictives non linéaires paramétrées. La philosophie présentée ici est une extension directe au cas non linéaire de l'approche proposée par [133] dans un cadre linéaire, et est motivée par le besoin de maintenir le niveau de flexibilité de la future trajectoire de contrôle sous contrainte de temps de calcul. En pratique, l'avantage de l'approche repose sur l'encapsulation du compromis complexité/optimalité dans un nouveau jeu de paramètres faciles à régler. Dans son ensemble, cette formulation reste simple à implémenter et compatible avec l'utilisation d'un modèle basé sur la physique et d'une fonction de coût non conventionnelle basé sur la thermodynamique.

Le Chapitre 7 introduit, pour finir, le cadre de la commande prédictive non linéaire explicite, et en particulier un bref rappel théorique sur la résolution des problèmes multiparamétriques. Ces derniers sont au cœur de l'approche et permettent de calculer une approximation affine par morceaux d'une loi de contrôle prédictive non linéaire implicite. La méthode en elle-même s'inspire des travaux les plus récents dans le domaine de la commande prédictive non linéaire explicite [53], et introduit le support de modèles de prédiction complexes ainsi que le calcul parallèle. En particulier, ces derniers autorisent le calcul de la loi de contrôle explicite associée au schéma de contrôle prédictif non linéaire implicite présenté dans le chapitre 5. Une fois cette approche combinée à l'utilisation d'arbres binaires pour le stockage de la loi de contrôle affine par morceaux, elle permet une réduction significative du temps de calcul par rapport au schéma implicite, tout en maintenant d'excellentes performances en poursuite. Dans leur ensemble, ces résultats permettent d'envisager une implémentation en ligne en temps-réel et ainsi représentent notre troisième et dernière étape vers une approche quasi-systématique de la synthèse du contrôle de la chaîne d'air des moteurs essence suralimentés.

Cette deuxième partie mène à un contrôle temps-réel basé sur l'approximation d'un contrôle prédictif non linéaire donné. Par implémentation temps-réel, nous entendons présentant un temps de calcul court et prédictible.

Les contributions principales de l'étude sont:

- La synthèse de nouveaux algorithmes pour l'interpolation et l'extrapolation des cartographies quasi-statiques de compresseurs et de turbines. Alors que ces cartographies sont au cœur de tous les modèles moteurs incluant un turbocompresseur, la précision des méthodes disponibles dans la littérature n'est pas satisfaisante. La nouvelle association de physique, d'observations empiriques et de méthodes d'optimisation, proposée dans cette étude, a prouvé fournir de meilleurs résultats dans la zone extrapolée, améliorant ainsi la robustesse des modèles quasi-statiques de turbocompresseur, très utilisés.
- L'implémentation d'une commande prédictive non linéaire à horizon-1 pour le contrôle de la pression collecteur d'un moteur essence suralimenté. La particularité de ce schéma repose sur l'utilisation d'un modèle physique et d'une fonction de coût incluant un index de performance thermodynamique.
- Une commande prédictive non linéaire paramétrée basée sur la décomposition de la trajectoire des futurs incréments de commande, sur un ensemble de fonctions orthonormales, à savoir les polynômes de Laguerre. Dans son ensemble, cette approche inédite dans le cadre non linéaire facilite la calibration de la performance en boucle fermée en encapsulant le compromis complexité/optimalité dans un jeu de deux paramètres de haut niveau.
- Le calcul de la solution affine par morceaux d'un problème multiparamétrique non linéaire de dimension 6. Cette solution correspond à une loi de contrôle explicite approximant le comportement du schéma prédictif à horizon-1 cité ci-dessus, sur l'ensemble du domaine de fonctionnement d'un moteur essence suralimenté. Couplée à l'utilisation d'un arbre de recherche binaire pour le stockage des lois de contrôle affines et des régions sur lesquelles elles sont définies, la méthode réduit considérablement le temps de calcul en ligne par rapport à l'approche implicite.

Dans son ensemble, ce travail représente une première étape vers une approche quasi-systématique de la synthèse d'un contrôle optimal de la chaîne d'air des moteurs essence suralimentés.

PUBLICATIONS

Control-oriented engine modeling

Journal paper

- El Hadef J., Colin G., Chamaillard Y., and Talon V. *Physical-based Algorithms for Interpolation and Extrapolation of Turbocharger Data Maps*. SAE International Journal of Engines 5(2):2012

Conference proceedings

- El Hadef J., Colin G., Chamaillard Y., and Talon V. *Neural Model for Real-Time Engine Volumetric Efficiency Estimation*. 11th Conference on Engines and Vehicles (2013).

- El Hadef J., Janas, P., Colin G., Chamaillard Y., and Talon V. *Geometry-Based Compressor Data-Maps Prediction*. SAE World Congress 2013.

- El Hadef J., Colin G., Chamaillard Y., and Talon V. *Turbocharged SI Engine Models for Control*. 11th Symposium on Advanced Vehicle Control (IFAC - 2012).

- El Hadef J., Colin G., Chamaillard Y., and Talon V. *New Physics-Based Turbocharger Data-Maps Extrapolation Algorithms: Validation on a Spark-Ignited Engine.* IFAC Workshop on Engine and Powertrain Control, Simulation and Modeling (2012).

Engine nonlinear model predictive control

Conference proceedings

- El Hadef J., Olaru S., Rodriguez-Ayerbe P., Colin G., Chamaillard Y., and Talon V. *Nonlinear Model Predictive Control of the Air Path of a Turbocharged Gasoline Engine Using Laguerre Functions.* 17th International Conference on System Theory, Control and Computing (IEEE - 2013).

- El Hadef J., Olaru S., Rodriguez-Ayerbe P., Colin G., Chamaillard Y., and Talon V. *Explicit Nonlinear Model Predictive Control of the Air Path of a Turbocharged Spark-Ignited Engine*. Multi-Conference on Systems and Control (IEEE - 2013).

- El Hadef J., Colin G., Chamaillard Y., Olaru S., Rodriguez-Ayerbe P., and Talon V. *Explicit-ready Nonlinear Model Predictive Control of the Air Path of a Turbocharged Spark-Ignited Engine*. 7th IFAC Symposium on Advances in Automotive Control (2013).

Oral Presentation

- El Hadef J., *Quasi-Systematic Engine Air Path Control Strategy Based on Explicit Nonlinear Model Predictive Control. Graduate Student Workshop on Automotive Control*, Sophia University, Tokyo, Japan (2013).

PATENTS

Registered

- Fontvieille L., Talon V. and El Hadef J. *Procédé de régulation d'une suralimentation pour turbocompresseur couplé à une machine électrique, et dispositif turbocompresseur correspondant*. INPI No FR 1258518

- Talon V., El Hadef J., Fontvieille L., Chamaillard Y. and Colin G. *Procédé de régulation d'une suralimentation par turbocompresseur couplé à une machine électrique et avec une vanne de dérivation, et dispositif de suralimentation correspondant*. INPI No FR 1258519

- Talon V., Bordet N. and El Hadef J., *Estimations des émissions polluantes des moteurs essence, pour une application contrôle et sans capteur de pression cylindre*. INPI No FR 1355008

Submitted

- El Hadef J., Talon V., Olaru S. and Chamaillard Y. *Contrôle des systèmes VVT des moteurs dans un objectif de contrôle model-based des GMPs.*

- El Hadef J., Talon V., Chamaillard Y. and Colin G. *Observateur polytopique de la pression amont turbine pour les moteurs essence et diesel.*

- El Hadef J., Talon V., Chamaillard Y. and Colin G. *Observateur polytopique du régime de rotation du turbocompresseur pour moteur essence et diesel.*

PART 1

Control-oriented physics-based model of a turbocharged gasoline engine air path

CHAPTER 1

CONTROL-ORIENTED GASOLINE ENGINE MODELING

Amongst all advanced control strategies, a nonlinear model predictive control (NMPC) scheme that uses a physics-based prediction model is certainly one of the most promising approaches. However, it also carries the drawbacks of requiring a nonlinear model. In fact, while it benefits from the accuracy of a multivariable and nonlinear description of the system that is theoretically as close as possible to the real system, the development of such a complex model is often prohibitive, besides requiring the knowledge of many uncertain parameters. These critical issues have often motivated the development of alternative control approaches.

In the automotive industry, simulation has become a standard tool in powertrain and internal combustion engine development. In practice, the design and calibration of physics-based engine models are now sufficiently familiar to be included early on in the development processes of most car manufacturers. In fact, when considering the design and analysis of control systems, models have proved capable of achieving drastic development cost reductions. However, they have not made their way into the control strategies themselves and non-model-based approaches rather ironically still have the advantage of avoiding this time-consuming modeling phase. Finally, these simple approaches also benefit from a continuous optimization process that has lasted for more than twenty years. Nonetheless, regarding future pollutant emission standards and the increasing number of actuators in modern internal combustion engines, non-model-based control strategies may well have reached their limit.

In this context, this study attempts to combine the best of both worlds by using a physics-based model that is extensively used by car manufacturers to tackle the inherent modeling issue of NMPC approaches. This *physics-based NMPC* scheme can then be used to control the engine air path in a nonlinear and multivariable fashion. Among the abundant modeling variations proposed in the literature, the combination of a mean value engine model with zero-dimensional models of the pipes, in which the physical quantities are averaged on the volume, is probably one of the most mature modeling strategies for engine air path control [42,43,57,59]. For insiders it is straightforward since it allows complete engine models to be built from a given library of components. Moreover, the sub-models are interchangeable and usually configurable in terms of accuracy-complexity trade-off which makes it altogether an obvious candidate when considering an NMPC application.

This chapter gives an overview of the mean-value engine modeling approach when applied to the air path of a turbocharged gasoline engine. Key ideas about the functioning of gasoline engines are summed up in section 1.1. In section 1.2, the philosophy behind the mean value engine model is detailed. Finally, all the sub-models required to build the complete air path model of the engine involved in this thesis are detailed individually from sections 1.3 to 1.6. For each of them, the major nonlinearities are highlighted. The validation of the methodology on a practical case of application is postponed until chapter 3, besides other practical applications of this methodology.

1.1 Overview of turbocharged gasoline engines

In the automotive industry, internal combustion engines are used to transform the chemical energy contained in the fuel into a mechanical power that will propel the vehicle [65]. The engine speed N_e and torque are the result of the burning of an appropriate air-fuel mixture in the cylinders (figure 1.1). The work transfer that provides the desired power output directly occurs between the working fluids (fresh and burnt gases) and the engine mechanical components (piston).

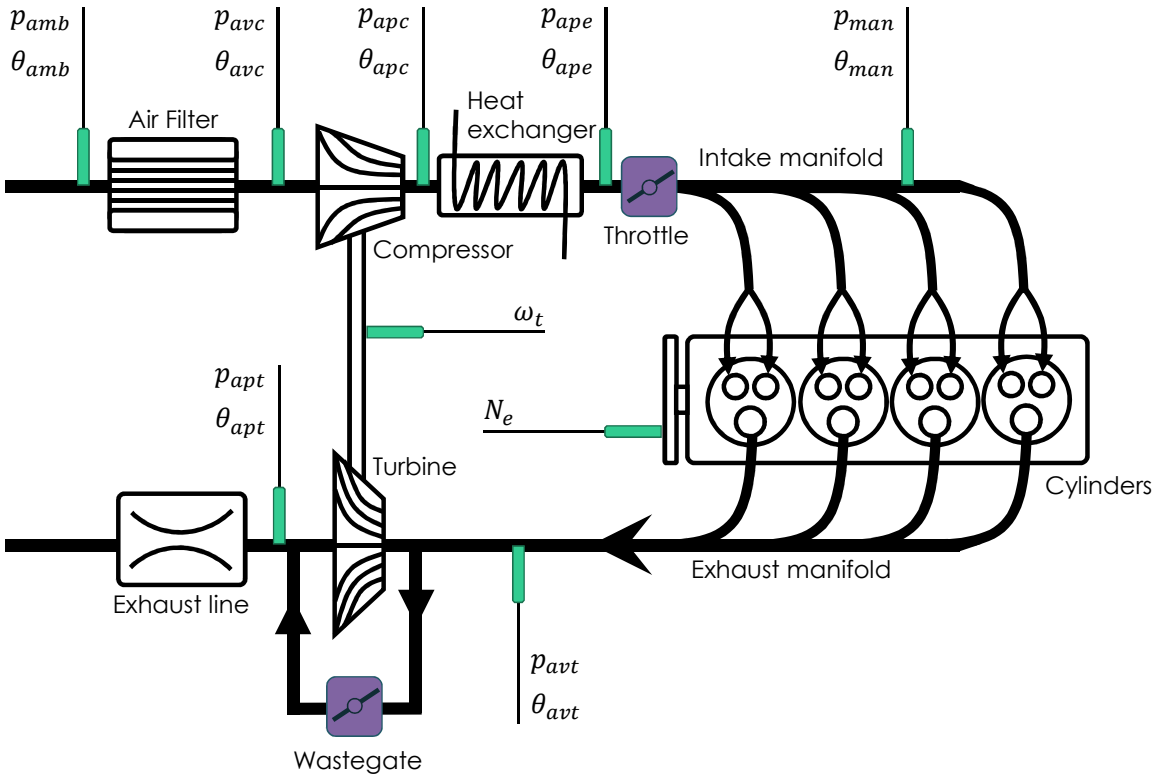

Figure 1.1 – Air path scheme of a 1.2L turbocharged spark-ignited engine. The throttle and the wastegate control the fresh air mass trapped in the cylinders for combustion.

Let us consider the turbocharged spark-ignited engine air path presented on figure 1.1. At the intake (p_{avc}, θ_{avc}), the compressor increases the pressure (p_{apc}, θ_{apc}) of the fresh air, possibly beyond atmospheric conditions $(p_{apc} > p_{amb})$, and a heat exchanger cools down (p_{ape}, θ_{ape}) the fresh air flow. Then, a variable flow restriction, namely the throttle, controls the flow entering the inlet manifold (p_{man}, θ_{man}). At the outlet of this volume, intake valves control the mass flow rate aspired by the engine Q_{eng}. At this stage, the air-fuel mixture is ignited at a time given by the spark advance. The combustion products, whose composition depends on the air-fuel ratio during combustion, leave the cylinders through a set of exhaust valves and enter the exhaust manifold (p_{avt}, θ_{avt}). At the outlet of this volume, the amount of burnt gases which exhaust to the atmosphere through the turbine is controlled by a by-pass valve, namely a wastegate. This energy, recovered at the exhaust, drives the compressor and its outlet boost pressure p_{apc} through a shaft (ω_t). This introduces a mechanical feedback path in the engine air path.

From a control-oriented point of view, the air path of a turbocharged gasoline engine model can be seen as a multi-variable nonlinear system that presents a set of saturated input and output signals, disturbances such as the engine speed and the air/fuel ratio, and exogenous inputs such as the atmospheric pressure and temperature conditions (figure 1.2). The input signals correspond to the manipulated variables of the actuators available to control one or more given physical quantities taken from the set of output signals (pressures, temperatures, flow rates). In the air path of a turbocharged gasoline engine such as the one presented on figure 1.1, two actuators, namely the throttle and the wastegate, are used to control the pressures and flows through the engine in order to obtain the appropriate quantity of fresh air trapped in the cylinders during combustion.

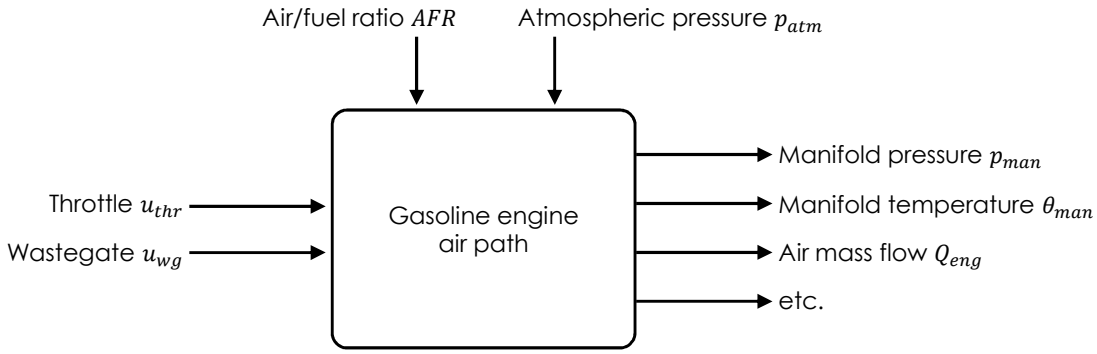

Figure 1.2 – Multi-input/multi-output description of a turbocharged gasoline engine

The air path of turbocharged spark-ignited engines essentially involves a combination of thermo- and fluid-dynamical processes that are highly complex. For a formal description, the reader is referred to [65]. However, when building a prediction model in an MPC framework, the challenge is no longer in matching experimental measurements at all costs, but in capturing only the essential dynamics and nonlinear behaviors while remaining small enough to be embedded in the control law. Precision is still necessary but no longer the main constraint. The crucial issue is to determine an appropriate trade-off between accuracy and computational requirements.

Mean value engine models (MVEM) are able to accurately describe the non-trivial multiple-input multiple-output phenomena that occur in the engine cylinders in order to provide a relevant input-output representation [57]. The zero-dimensional modeling approach that consists in suppressing all spatial dimensions by averaging the physical quantities over an entire volume leads to a minimum set of equations that can describe the pressure and temperature dynamics in the engine pipes [57]. The combination of these two approaches to model the complete engine air path (figure 1.1) can be used to build a low-order physics-based model that is in perfect agreement with model-based control strategies such as model predictive control and the use that is made of the prediction model. In this section, we present this general modeling approach, extensively used in the automotive industry, and that will later be used to build the engine air path prediction model that is at the heart of the NMPC control schemes presented in chapters 5 to 7.

1.2 Physics-based modeling philosophy

When analyzing the air path of car passenger engines, one remarkable thing is that both gasoline and diesel engines involve a similar set of components (pipes, air filters, heat exchangers, valve actuators, turbochargers). This observation argues for the development of a modular strategy based on individual sub-models that may be combined and are possibly also interchangeable. However, when put into practice, the assembled collection of accurate sub-models usually leads to unsatisfactory performances of the overall model. An additional calibration stage on the complete model is then required to obtain a relevant level of accuracy. It usually consists simply in optimizing the value of the most uncertain parameters of each sub-model in order to match experimental measurements [105].

Each component of the air path is either taken as:

- a control volume (also known as reservoir), in which mass and energy conservation equations are applied or,
- a flow component that determines the transport of mass and energy between the control volumes.

The notion of control volumes is quite intuitive and corresponds to the components where mass is collected such as pipes and manifolds. The flow components drive the flow between the control volumes. Examples of flow components are the valve actuators such as the throttle and the wastegate, the compressor and the turbine. The engine cylinders are assimilated to a volumetric pump that produces exhaust gases and therefore also falls into this category [57].

Before detailing the equations involved in each component, the interactions and exchange between these components must be clearly stated. As suggested above, the control volumes are governed by mass and energy equations while flow components determine the mass and energy transport. As a first step, it is natural to select the pressure and temperature, both measurable physical quantities, as states in the control volumes. The flow components will then transport the mass flows and temperature of the gas in the air path. Hence, the complete air path model consists in the simple succession of these two sub-elements: a flow component is followed by a control volume, itself followed by another flow component and so forth (figure 1.3).

Figure 1.3 – Example of a succession of control volumes and flow components in a 0D modeling framework.

In the following sections the components will be detailed separately and the equations presented along with the associated hypotheses.

1.3 Control volume

Control volumes are the basic building blocks to model the intake and exhaust part; they store mass and internal energy. Following the zero dimensional modeling philosophy, the thermodynamic states, i.e. pressure and temperature, are assumed to be uniform in the entire volume. Under the assumptions of static pressure and no heat or mass transfer through the walls, the simplified Euler mass and energy equations below apply in the volume:

$$\dot{m}(t) = \dot{m}_{in}(t) - \dot{m}_{out}(t) \tag{1.1}$$

$$\dot{U}(t) = \dot{H}_{in}(t) - \dot{H}_{out}(t) \tag{1.2}$$

where m, U and H respectively stand for the mass, the internal energy and the enthalpy of the fluid that depend on the instant t. The indices in and out respectively stand for the inlet and outlet of the control volume.

Assuming that the fluid behaves as a perfect gas, the ideal gas law also applies:

$$p(t)V = m(t) \cdot r \cdot \theta(t) \tag{1.3}$$

where p and θ are the pressure and temperature in the volume V and $r = c_p - c_v$ is the specific gas constant. c_p and c_v respectively stand for the specific heat of the gas in the volume at constant pressure and at constant volume.

Finally, the caloric relations below provide definitions of the internal energy and enthalpy flow:

$$U(t) = m(t) \cdot c_v \cdot \theta(t) \tag{1.4}$$

$$\dot{H}_{in}(t) = \dot{m}_{in}(t) \cdot c_p \cdot \theta_{in}(t) \tag{1.5}$$

$$\dot{H}_{out}(t) = \dot{m}_{out}(t) \cdot c_p \cdot \theta(t) \tag{1.6}$$

Some simple algebraic manipulations on the above equations lead to the well-known adiabatic formulation of pressure and temperature state equations in the control volume:

Adiabatic formulation

$$\dot{p}(t) = \frac{\gamma \cdot r}{V}\left(\dot{m}_{in}(t) \cdot \theta_{in}(t) - \dot{m}_{out}(t) \cdot \theta(t)\right) \tag{1.7}$$

$$\dot{\theta}(t) = \frac{r}{c_v \cdot V} \cdot \frac{\theta(t)}{p(t)}\left(\dot{m}_{in}(t) \cdot c_p \cdot \theta_{in}(t) - \dot{m}_{out}(t) \cdot c_p \cdot \theta(t) - \left(\dot{m}_{in}(t) - \dot{m}_{out}(t)\right) \cdot c_v \cdot \theta(t)\right) \tag{1.8}$$

where $\gamma = c_p/c_v$ is the ratio of specific heats.

It should be pointed out that the order of the model will be directly inherited from the number of control volumes of the engine model since, by definition, the states are exclusively contained in those volumes. However in each of these reservoirs, the question of which pressure and temperature states should be computed still remains.

There is no simple and systematic answer to this question, i.e. to determine whether or not the dynamic of a given physical quantity can be neglected or should be taken into account. An attempt to make such a

decision can be found in [57]. The authors propose to classify the behavior of the physical quantities into three categories according to their relative dynamic (figure 1.4). According to this classification, the physical quantities which present a settling time that is much smaller (signal ②) than the variable of main interest (signal ①) should be modeled as purely static variables. Their behavior can then be described by algebraic equations. On the other hand, the physical quantities that are much slower (signal ③) than the variable of main interest (signal ①) can be considered as constants. If necessary, they may depend on the operating point.

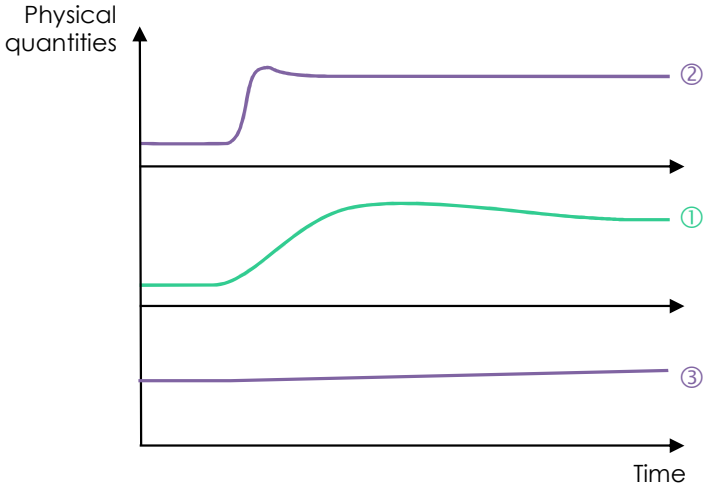

Figure 1.4 – Physical quantities classification used to determine whether or not the dynamic of a given physical value should be taken into account. The authors in [57] propose to classify the physical quantities into three categories according to their relative dynamic. Signal ① represents the variable of main interest. The settling time of signal ② is much smaller and can be modeled as a purely static variable obtained from algebraic equations. Signal ③ is very slow, compared to signal ① and can be taken as a constant. If necessary, they may depend on the operating point.

In the control volumes of an engine air path, the pressure is the variable of main interest since it is the one to be controlled. Then, depending on the configuration of the engine, the adiabatic formulation used in (1.7) and (1.8) may result in unnecessary computational complexity. In particular, in [60] it is shown that an isothermal hypothesis, characterized by $\dot{\theta}(t) = 0$, can be used without inducing any significant loss of accuracy. Neglecting the temperature dynamics leads to one-state control volumes [57], governed by the simplified set of equations:

Isothermal formulation

$$\dot{p}(t) = \frac{\gamma r}{V}\theta(t)\left(\dot{m}_{in}(t) - \dot{m}_{out}(t)\right) \tag{1.9}$$

$$\theta(t) = \theta_{in}(t) \tag{1.10}$$

1.4 Valve actuator

There is a wide variety of flow components involved in a turbocharged gasoline engine (figure 1.1). In particular, the engine cylinders, the compressor and the turbine deserve dedicated models that will be described in sections 1.5 and 1.6. The throttle and the wastegate, however, both fall in the category of isothermal orifices, i.e. where $\theta_{ds}(t) = \theta_{us}(t)$. This sub-section focuses on the description of this type of component.

In flow valves the upstream pressure p_{us} and downstream pressure p_{ds} drive the flow nonlinearly through the section. Assuming a barotropic fluid that behaves as a perfect gas and a unidimensional and isentropic steady flow, this nonlinear behavior of the flow can be described using the Barré de Saint-Venant equation [93]:

$$\begin{cases} Q(u) = \frac{p_{us}}{\sqrt{r\theta_{us}}} \cdot A_{eff}(u) \cdot \Pi^{\frac{1}{\gamma}} \cdot \sqrt{\frac{2\gamma}{\gamma-1} \cdot \left(1 - \Pi^{\frac{\gamma-1}{\gamma}}\right)} \\ \Pi = max\left(\frac{p_{ds}}{p_{us}}, p_{crit}\right) \end{cases} \tag{1.11}$$

where A_{eff} is the effective area of the orifice and depends nonlinearly on the actuator position u. $p_{crit} = \left(\frac{2}{\gamma+1}\right)^{\frac{\gamma}{\gamma-1}}$ is the critical pressure at which the flow reaches sonic conditions. Indices us and ds respectively stand for upstream and downstream.

Despite the fact that the hypotheses involved in this formulation are quite restrictive and rather difficult to verify in our particular application, the practical results are usually sufficiently accurate in a zero dimensional framework to be used to model valve actuators such as throttle, wastegate and, when needed, poppet valves [122]. However, one last issue needs to be taken into account. In fact, when $p_{us} = p_{ds}$, equation (1.11) shows an infinite gradient that would make (1.7) and (1.9) difficult to integrate due to the fact that they would cease to fulfill the Lipschitz conditions [57]. Since this is unacceptable for a control-oriented model, several simple pragmatic approaches to regularize (1.11) have been developed [33,57]. They are usually based on smooth polynomial approximations of (1.11) around a given threshold that describe the change in the nature of the flow, from turbulent to laminar. The resulting valve actuator model then shows a very good accuracy with respect to test bench measurements, making it possible to work on the complete range of actuator openings.

1.5 Engine cylinders

The mass flow in the cylinders pulsates with the opening and closing of the engine valves [33]. Following the MVEM philosophy, these pulsations can be averaged over one or more engine cycles, such that only the mean flow remains. This classical approximation meets the standard accuracy requirements of air path control. The following sub-sections successively describe the phenomena involved at the intake and at the exhaust of the cylinders.

1.5.1 Inlet mass flow rate

As suggested in section 1.2, the engine cylinders are approximated as a volumetric pump, in which the flow essentially depends on the upstream density and on the displaced volume [42,43,65]. The classical modeling philosophy for engine cylinders consists in correcting the theoretical mass flow rate that would be aspired at intake manifold conditions, by a correction factor.

This coefficient depends on the engine operating point and is known as the volumetric efficiency η_{vol}:

$$Q_{eng} = \left(\frac{p_{man}}{r \cdot \theta_{man}} \cdot \frac{V_{cyl} \cdot N_e}{60 \cdot N}\right) \times \eta_{vol} \tag{1.12}$$

where Q_{eng} is the engine mass flow rate, V_{cyl} the total engine displacement and $N = 2$ is the number of revolutions per cycle on a four-cylinder four-stroke engine. SI units apply except for the engine speed N_e that should be expressed in revolutions per minute.

The volumetric efficiency encapsulates the engine ability to aspire the air contained in the intake manifold [65] but its theoretical behavior is rather difficult to predict since various phenomena have to be taken into account. These include internal exhaust gas recirculation, ram and acoustic effects at the intake and cross-coupling between the cylinders [57]. Values can either be obtained from precise 3-dimension modeling of the fluid dynamic in the intake or reconstructed from steady-state test bench measurements of the physical quantities involved in (1.12). The volumetric efficiency is nonlinear and usually directly implemented as a look-up table or using a low order polynomial $f_{\eta_{vol}}$. Relevant inputs to be taken into account are the engine speed and the inlet manifold pressure and temperature:

$$\eta_{vol} = f_{\eta_{vol}}\left(N_e, \frac{p_{man}}{\theta_{man}}\right) \tag{1.13}$$

For more complex technical definitions, an alternative formulation of the nonlinear function $f_{\eta_{vol}}$ should be considered [30,68]. For example, we showed that neural-network based models can accurately describe the more complex phenomena involved when considering a turbocharged spark-ignited engine equipped with intake and exhaust variable valve timing [39].

1.5.2 Exhaust temperature and mass flow rate

In turbocharged engines, the exhaust enthalpy flow rate plays an important role by carrying a substantial part of the injected fuel energy [43]. It also represents the energy that can be recovered by the turbine for boosting and thus has a major influence on the intake conditions through the mechanical coupling with the compressor.

In practice, the exhaust temperature θ_{avt} can be computed by estimating the temperature increase over the engine. The formulation proposed here uses the inlet gas conditions, i.e. the inlet manifold temperature θ_{man} and the engine mass flow rate Q_{eng}:

$$\theta_{avt} = \theta_{man} + k_{ech} \frac{Q_{fuel} \cdot LHV}{c_p \cdot (Q_{fuel} + Q_{eng})} \tag{1.14}$$

where Q_{fuel} is the fuel mass flow rate, LHV stands for the lower heating value and k_{ech} estimates the amount of energy that is transferred to the exhaust gas. This quantity depends nonlinearly on many phenomena such as energy wall losses and blowdown at exhaust valve opening. It is therefore usually desirable to describe it using a look-up table or a low order polynomial $f_{k_{ech}}$ of steady-state test bench measurements assuming that the transient effects are neglected (signal ② on figure 1.4):

$$k_{ech} = f_{k_{ech}}\left(N_e, Q_{eng}, Q_{fuel}\right) \tag{1.15}$$

Finally, the mass flow rate at the exhaust is equal to the sum of Q_{eng}, the inlet mass flow rate presented in section 1.5.1 and Q_{fuel} the fuel mass flow rate. Both are linked by the so-called air-fuel ratio, denoted AFR, that characterizes the composition of the air-fuel mixture:

$$AFR = \frac{Q_{eng}}{Q_{fuel}} \tag{1.16}$$

If the engine does not operate at stoichiometric conditions, the air-fuel ratio is taken as an input disturbance of the model (figure 1.2). In that particular case, the influence of the mixture composition on the exhaust manifold temperature must be carefully taken into account in order to maintain the accuracy of the model. In practice a nominal engine-out temperature model is usually corrected afterwards by an algebraic correction function that depends on the air-fuel ratio. A similar approach is also used when modeling deviations from the nominal model due to the spark-advance [57].

1.6 Turbocharger

Compressors and turbines are the two remaining flow components in the engine technical definition involved in this study (figure 1.1). They play a key role in the coupling of the engine air path, while involving highly nonlinear phenomena [42,43,57] that will be described below.

From a control-oriented point of view, compressor and turbine modeling strategies are very similar. In particular, it is commonly assumed that the dynamic phenomena involved inside both components are much faster than the rate of change of their upstream and downstream boundary conditions. As suggested in section 1.3, the fluid dynamics can then be considered as a quasi-static phenomenon, which considerably simplifies the modeling approach.

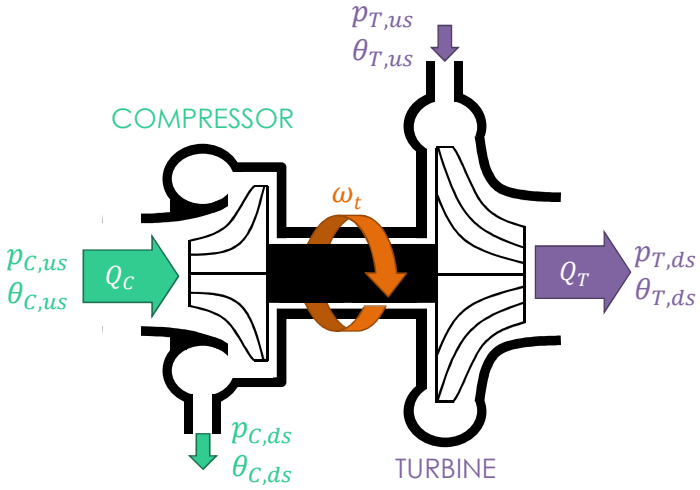

Figure 1.5 – Turbocharger side scheme.

The zero dimensional models of the compressor and turbine involve, in each case, two steps:

- First, assuming no losses, the transfer of energy between the component and the fluid is determined using a data-map that links the pressure ratio $\Pi_C = p_{C,ds}/p_{C,us}$ (respectively $\Pi_T = p_{T,us}/p_{T,ds}$), the mass flow rate Q_C (respectively Q_T) and the turbocharger rotational speed ω_t,
- Then, the losses occurring during the process are taken into account using a second data-map that links the isentropic efficiency of the compressor η_C (respectively η_T for the turbine), the rotational speed ω_t and either the pressure ratio Π_C (respectively Π_T) or the mass flow rate through the component Q_C (respectively Q_T) .

Thus, the modeling strategy consists in characterizing the behavior of the turbocharger through a set of four highly nonlinear look-up tables (figure 1.6).

1.6.1 Compressor

The compressor involved in this study is part of the family of fluid dynamic compressors, in opposition to mechanical superchargers that are directly driven by the engine crankshaft. Under a quasi-static hypothesis, the mass flow rate Q_C through the compressor is directly read in a quasi-static experimental data-map $f_{C,Q}$:

$$Q_C = f_{C,Q}(\Pi_C, \omega_t) \tag{1.17}$$

where the compression ratio $\Pi_C = p_{C,ds}/p_{C,us}$ and the turbocharger rotational speed ω_t are the two inputs of the look-up table.

In practice, the flow is distributed at a given temperature $\theta_{C,ds}$ which depends on the compressor isentropic efficiency η_c and is given by the adiabatic equation below:

$$\theta_{C,ds} = \theta_{C,us} \cdot \left(1 + \frac{1}{\eta_C} \cdot \left(\Pi_C^{\frac{\gamma-1}{\gamma}} - 1\right)\right) \tag{1.18}$$

where $\theta_{C,us}$ is the compressor upstream fluid temperature. In the engine presented on figure 1.1, it is assumed to be equal to the atmospheric temperature: $\theta_{C,us} = \theta_{amb}$.

Similarly to the mass flow rate, the isentropic efficiency of the compressor η_C is read in an experimental data-map $f_{C,\eta}$:

$$\eta_C = f_{C,\eta}(Q_C, \omega_t) \tag{1.19}$$

1.6.2 Turbine

The turbine is commonly assimilated to a flow restriction and as such, is logically considered as a flow component in the MVEM framework (section 1.2). Under the hypothesis of quasi-static dynamic, the mass flow rate across the turbine Q_T is directly read in an experimental data-map denoted $f_{T,Q}$:

$$Q_T = f_{T,Q}(\Pi_T, \omega_t) \tag{1.20}$$

where the expansion ratio $\Pi_T = p_{T,us}/p_{T,ds}$ and the turbocharger rotational speed ω_t are the input of the look-up table.

Similarly to the compressor case, the computation of the outlet flow temperature accounts for losses and depends on the isentropic efficiency of the turbine η_T:

$$\theta_{T,ds} = \theta_{T,us}\left(1 - \eta_T \cdot \left(1 - \left(\frac{1}{\Pi_T}\right)^{\frac{\gamma-1}{\gamma}}\right)\right) \tag{1.21}$$

where $\theta_{T,ds}$ is the turbine outlet temperature, $\theta_{T,us}$ is equal to the exhaust manifold temperature and η_T is directly read in a fourth experimental quasi-static data-map $f_{T,\eta}$:

$$\eta_T = f_{T,\eta}(\Pi_T, \omega_t) \tag{1.22}$$

1.6.3 Mechanical behavior

In turbocharged engines, the fact that the compressor and the turbine are mechanically linked induces an additional dynamic that can usually not be neglected when considering air path control. In particular, the turbocharger rotational speed ω_t has a significant influence on the intake pressures' transient response [33,42,43,57,65] and an additional state is required to compute it (1.23).

Neglecting friction, the rotational dynamic of the turbocharger is well described by the power balance between the two components and Newton's second law [92]:

$$\dot{\omega}_t = \frac{1}{I} \cdot \left(\Gamma_T(\omega_t) - \Gamma_C(\omega_t) \right) \tag{1.23}$$

where I is the mass moment of inertia of the turbocharger and Γ_T and Γ_C respectively represent the turbine and compressor torques:

$$\Gamma_C(\omega_t) = \frac{Q_C \cdot c_p \cdot (\theta_{C,ds} - \theta_{C,us})}{\omega_t} \tag{1.24}$$

$$\Gamma_T(\omega_t) = \frac{Q_T \cdot c_p \cdot (\theta_{T,us} - \theta_{T,ds})}{\omega_t} \tag{1.25}$$

where $\Gamma_C$and $\Gamma_T$both depend on the mass flow rate across the component $\{Q_C, Q_T\}$ and the upstream and downstream temperatures $\{\theta_{C,us}, \theta_{T,us}, \theta_{C,ds}, \theta_{T,ds}\}$, all computed from the four turbocharger data-maps $\{f_{C,Q}, f_{C,\eta}, f_{T,Q}, f_{T,\eta}\}$ (1.17-1.22). A lower turbocharger rotational speed saturation completes the model in order to avoid singularity when $\omega_t = 0$.

1.6.4 Compressor and turbine data-map issues

Modeling the behavior of the compressor and the turbine requires the introduction of an additional state, namely the turbocharger rotational speed ω_t. Its computation requires the knowledge of several physical quantities such as flow rate and isentropic efficiency that are all read in four quasi-static data-maps (figure 1.6). These are built from experimental test bench measurements and are often provided by the turbocharger manufacturer. It should be mentioned however that they are usually corrected for specified reference pressure and temperature conditions in ways that can depend on the manufacturer.

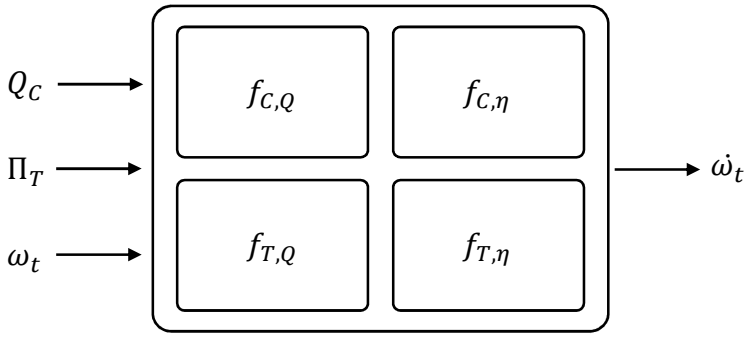

Figure 1.6 – Turbocharger rotational sub-model overview: $\dot{\omega}_t$ is obtained from the compressor mass flow rate Q_C, the pressure ratio across the turbine Π_T, the current turbocharger rotational speed ω_t and four quasi-static look-up tables $f_{C,Q}, f_{C,\eta}, f_{T,Q}, f_{T,\eta}$, usually partially provided by the turbocharger manufacturer.

The fundamental issue with the data-maps that are provided by the component manufacturer is that they never cover the entire operating range, but only the highest rotational speeds. Extrapolating these experimental data to low speed regions has then to be carried out by the user. Since these areas represent a significant part of the standard operating range of downsized engines (see chapter 2), several methods have been proposed in the literature to extrapolate the data-maps. However, when considering only those methods that do not require additional inputs than the four manufacturer data maps, none of the proposals available in the literature lead to sufficiently accurate results [33,57,92].

1.7 Conclusion

This first chapter has introduced the modeling philosophy that will be used to build a prediction model of the engine air path in chapter 3 and has underlined the numerous nonlinearities involved in such a model. The latter is control-oriented and will be used in various nonlinear model predictive control schemes from chapters 5 to 7.

In order to obtain an accuracy versus complexity trade-off compatible with nonlinear model predictive control requirements, we propose to combine a mean value engine model with a zero dimensional modeling of the air path. Both approaches are already widely used in the automotive industry and represent a significant part of current research into model-based control. At the heart of the proposal is the discretization of the air path into two types of elements: control volumes and flow components. While the former share a single set of equations based on mass and energy conservation laws, the latter usually require dedicated sub-models.

Amongst all these flow components, the turbocharger proved to be the element that requires the most attention since it introduces a fundamental coupling between the intake and the exhaust of the engine. As a result, it considerably impacts the overall accuracy of the model. However, the classical compressor and turbine modeling strategy is based on a set of four quasi-static data maps that are provided by the manufacturer, but need to be extrapolated in order to cover the entire operating range. And so far, no method in the literature has proved capable of conducting accurate extrapolation in a systematic manner.

This is the aim of the following chapter that, starting from the analysis of turbo-machinery equations, introduces a new set of physics-based extrapolation strategies of these four turbocharger data-maps.

CHAPTER 2

TURBOCHARGER DATA-MAPS EXTRAPOLATION

The approach most commonly found in the literature concerning turbocharger modeling consists in entering extensive mapping data in four quasi-static look-up tables (1.17), (1.19), (1.20) and (1.22) that are interpolated during the simulation (section 1.6). However, while engine mapping usually covers the entire operating range, the experimental data provided by the turbocharger manufacturer usually only cover the highest turbocharger rotational speeds (figure 2.1). In general, the relative speed range, i.e. the lowest over the highest rotational speeds, is roughly 40%. In other words, for a maximum turbocharger speed of 200,000 rpm, no measurements below 80,000 rpm are usually provided. This can be explained by the fact that large relative errors are encountered when measuring low pressure ratios and mass flow rates. Moreover at such low rotational speeds, the heat transfer between the turbine and the compressor becomes substantial with respect to the enthalpy flow of the fluid. Another important issue is that manufacturers' data-maps are usually provided in the form of iso-speeds that are generally poorly discretized (figure 2.1). This considerably complicates any interpolation and extrapolation initiative to obtain information in the empty zones and argues for physics-based methodologies. This is in contrast with the most popular model used in the literature [70] that is based on a mathematical representation of phenomenological observations rather than on turbo-machinery equations. However, while many alternative models exist in the literature [7,35,69,74,87,92,127,134], they usually require such a detailed knowledge of the components' geometry that they disqualify everyone but turbo-machinery specialists.

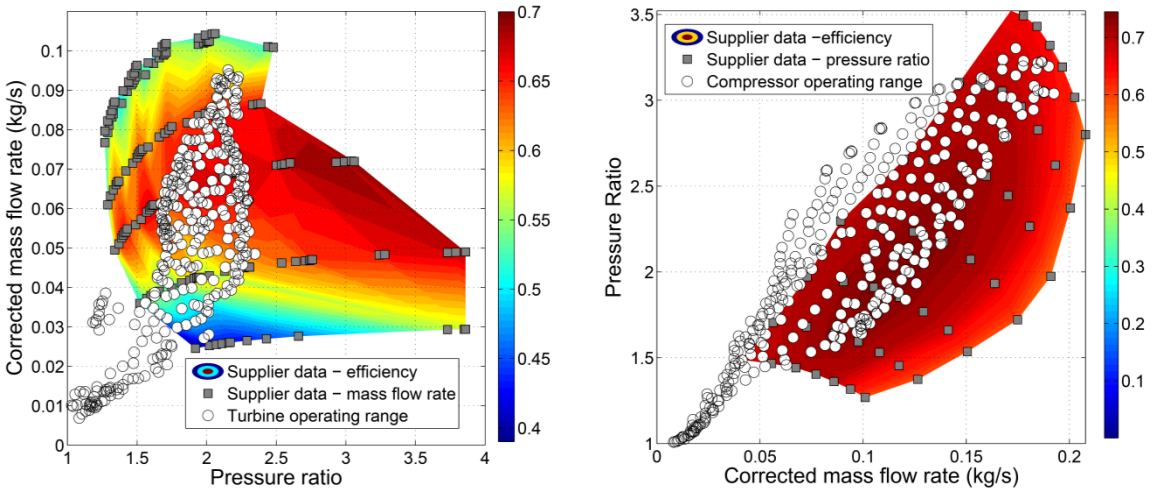

Figure 2.1 – Typical compressor and turbine quasi-static experimental data provided by the manufacturer from [88]. They respectively correspond to a finite set of operating points $(\Pi_C, Q_C, \omega_t, \eta_C)$ and $(\Pi_T, Q_T, \omega_t, \eta_T)$ for the compressor (left) and the turbine (right). It can be seen that while these data cover a wide variety of pressure ratios $\Pi_{C,T}$, mass flow rates $Q_{C,T}$ and isentropic efficiencies $\eta_{C,T}$, this information is available for only a few high turbocharger rotational iso-speeds.

The data in between these iso-speeds and at low turbocharger rotational speeds must then respectively be interpolated and extrapolated.

This chapter intends to propose a new set of extrapolation models that appropriately combine mathematics, empirical observations and turbo-machinery theory. In particular, a strong focus is placed on restraining the input requirements to the standard experimental operating points usually provided by turbocharger manufacturers. The scope of the new models is voluntarily limited to radial components since they are the only ones used in the automotive industry. These models also principally address single stage turbocharging configurations with fixed geometry turbines. However, variable geometry turbines can also be addressed by treating each position as a fixed geometry turbine. Finally, the robustness of the methodology is validated on a wide library of components representative of the variety of components set up on the Renault SAS vehicle line and includes about thirty compressors and thirty turbines (including variable geometry turbines), from different manufacturers including Garrett, BorgWarner, Mitsubishi and Bosch Mahle.

The major outcomes are: new empirical models for compression ratio and turbine flow rate extrapolations built in agreement with experimental observations; new robust and easy-to-implement algorithms, based on the combination of thermo-machinery equations, empirical knowledge and local optimization routines; and a significant improvement in the consistency of each thermo-machine sub-model obtained by creating a thermodynamic link between the pair of data-maps involved in each of them (section 1.6).

2.1 Compressor

This section presents a robust interpolation and extrapolation strategy for the compressor pressure ratio and isentropic efficiency data-maps (section 1.6). In the developments below, the focus is on the extrapolation stage as this represents the most challenging issue.

The first sub-section 2.1.1 details the operating principles of the compressor. The second sub-section 2.1.2 is dedicated to the extrapolation of the pressure ratio data-map $f_{C,Q}$ (1.17) and successively presents the theoretical extrapolation model (section 2.1.2.1), the practical extrapolation methodology (section 2.1.2.2), and the associated algorithm (section 2.1.2.3). Relevant results obtained for different compressors are presented in section 2.1.2.4. The third sub-section 2.1.3 concerns the isentropic efficiency data-map $f_{C,\eta}$ (1.19) and presents the extrapolation methodology following a similar layout.

2.1.1 Thermodynamic considerations

From inlet to outlet, a centrifugal compressor is usually composed of four elements: a static inlet such as a pipe (1), a bladed rotor or impeller, a diffuser, and a collector (2) (see left figure 2.2). The bladed rotor transfers the energy from the turbocharger shaft to the fluid, while the diffuser converts the kinetic energy of the gas into pressure by gradually reducing the gas velocity. Finally, the collector delivers the compressed air to downstream pipes: usually the engine air inlet system or another compressor.

The phenomena taking place in the rotor area are detailed on the h-S (specific enthalpy – entropy) diagram below (right figure 2.2). At the inlet, the air is at pressure p_1 and speed C_1. The rotor accelerates the gas up to speed C_{1b}. The enthalpy gain from 1 to $1b$ is due to the increase in kinetic energy (static pressure p_{1b} remains close to p_1). Then, the pressure is increased in the diffuser by transforming the kinetic energy into potential energy: the gas velocity decreases to C_2 while the static pressure reaches p_2 at the diffuser outlet. The total pressure p_{02} is then almost equal to the static pressure p_2.

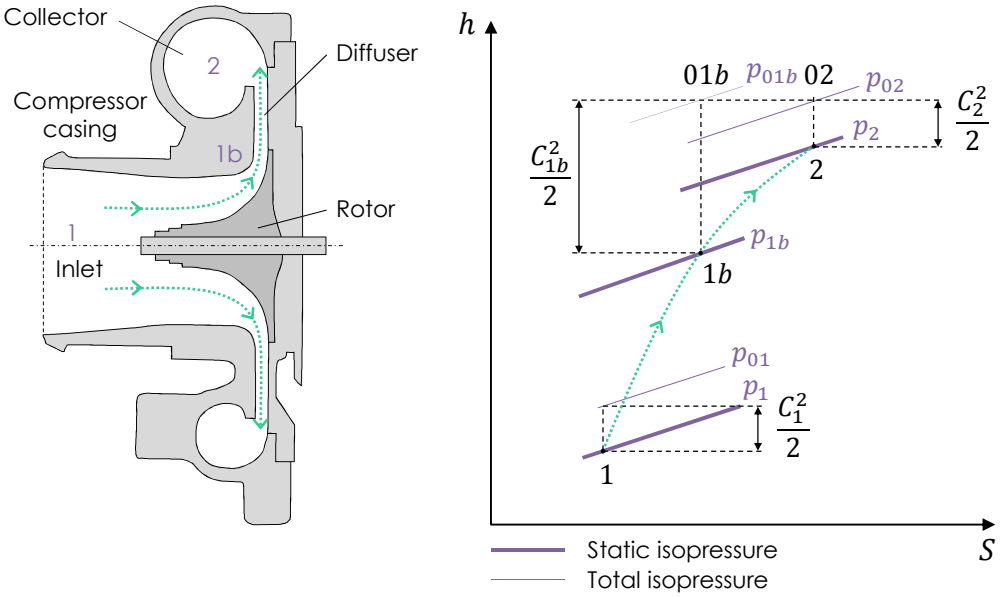

Figure 2.2 – Left: Side view of a centrifugal compressor,
Right: h-S diagram of a centrifugal compressor.
p_x and $p_{0x} = p_x + 0.5 \cdot {C_x}^2$ respectively stand for static and total pressure at x, C_x is the fluid speed.

It is this transfer of energy from the shaft to the fluid that is actually characterized by the data-map $f_{C,Q}$ that gives the pressure drop across the compressor. Moreover, as can be seen on figure 2.2, entropy is created, i.e. there are losses during the process. In fact, an ideal compression would be represented by a vertical straight line resulting in $\Delta S = 0$. These losses are characterized by a second data-map known as the compressor isentropic efficiency data-map $f_{C,\eta}$ (figure 2.3).

2.1.2 Extrapolation of the pressure ratio data-map $\Pi_c = f_{C,Q}(Q_C, \omega_t)$

The first look-up table involved in the compressor sub-model (1.17) describes the pressure ratio Π_C as a function of the mass flow rate through the compressor Q_C and the turbocharger rotational speed ω_t (figure 2.3).

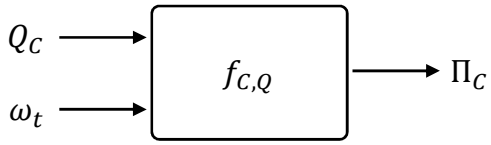

Figure 2.3 – Input/output description of the compressor pressure ratio Π_c data-map. Q_C stands for the compressor mass flow rate and ω_t for the turbocharger rotational speed.

The most popular formulation was introduced by Jensen and Kristensen in the 1990s [70] and is in fact a simplification of the model proposed by Winkler [135] in the 1970s. The compression ratio Π_C and compressor mass flow rate Q_C are respectively expressed in terms of two dimensionless quantities (2.1 and 2.2): the head parameter Ψ and the dimensionless flow rate Φ.

$$\Psi = c_p \cdot \theta_{C,us} \cdot \left[(\Pi_c)^{\frac{\gamma-1}{\gamma}} - 1 \right] \cdot \frac{2}{Uc^2} \tag{2.1}$$

$$\Phi = \frac{Q_C}{\rho \cdot \frac{\pi}{4} \cdot {D_C}^2 \cdot Uc} \tag{2.2}$$

where $\gamma = c_p/c_v$ is the ratio of specific heats, c_p and c_v respectively stand for the specific heat at constant pressure and at constant volume, $\theta_{C,us}$ is the inlet fluid temperature, ρ is the fluid density, $Uc = \frac{\pi}{60} \cdot D_c \cdot \omega_t$ is the blade tip speed and D_c is the compressor wheel exducer diameter.

The head parameter Ψ is then expressed as a function of the dimensionless flow rate Φ and the inlet Mach number M_a, using the empirical equation below:

$$\Psi = \frac{k_1 + k_2 \cdot M_a + k_3 \cdot \Phi + k_4 \cdot M_a \cdot \Phi}{k_5 + k_6 \cdot M_a - \Phi} \qquad with \qquad M_a = \frac{U_c}{\sqrt{\gamma \cdot R \cdot \theta_{C,us}}} \tag{2.3}$$

where $k_i, i = \{1, \dots, 6\}$ is a set of constants to be fitted on the experimental data provided by the manufacturer and R is the fluid gas constant.

When they have been identified, the head parameter Ψ and then the pressure ratio Π_C using (2.1) can be computed for any mass flow rate Q_C and turbocharger rotational speed ω_t. The construction of the first data-map $f_{C,Q}$ is then straightforward. The empirical model (2.3), while easy to implement, is known to lead to a data-map that is accurate only at medium rotational speeds. At high rotational speeds in particular, when new fluid characteristics should be taken into consideration [70], the inadequacy of the constant set of parameters k_i usually results in an inaccurate fit.

To overcome this issue, Martin et al. introduced in the 2000s a methodology in which all manufacturer iso-speeds are treated separately and a new set of k_i coefficients is fitted at each turbocharger rotational speed [87]. The extrapolation of the data-map at low rotational speeds is then obtained by using the set of coefficients corresponding to the lowest iso-speed provided by the manufacturer. The drawback of this method, while showing a better fit at high rotational speeds, is that the accuracy at lower speeds is not guaranteed since the set of k_i parameters is kept constant throughout the extrapolated area. In particular, if the lowest iso-speed provided by the manufacturer is too high, the set of parameters may be inadequate.

An alternative expression for the head parameter Ψ was also proposed in the 2000s [42,43] and directly based on Winkler's work [135]:

$$\Psi = \frac{k_1 + k_2 \cdot M_a + k_3 \cdot {M_a}^2 + k_4 \cdot \Phi + k_5 \cdot M_a \cdot \Phi + k_6 \cdot {M_a}^2 \cdot \Phi}{k_7 + k_8 \cdot M_a + k_9 \cdot {M_a}^2 - \Phi} \tag{2.4}$$

where $k_i, i = \{1, \dots, 9\}$ is a set of constants to be fitted on the experimental data provided by the manufacturer.

In this approach, the introduction of new parameters through the use of second order polynomials proved to improve the fit w.r.t. experimental measurements [42,43]. However in practice, the calibration of this model requires the identification of a set of nine coefficients which, without any prior knowledge on their optimal values, proved to be intractable. The model proposed below uses the philosophy proposed by Martin to overcome this issue.

2.1.2.1 Theoretical extrapolation model

The idea is that if iso-speeds are considered separately, the expression (2.4) that proved to be the most accurate can be considerably simplified. In fact, at constant turbocharger rotational speed, the flow Mach number M_a becomes constant and a new formulation for the head parameter can be obtained:

$$\Psi = \frac{A + B \cdot \Phi}{C - \Phi} \tag{2.5}$$

where A, B and C represent the new set of parameters that need to be identified for each of the manufacturer's iso-speeds, thus resulting in a set of parameter values that depend on the turbocharger rotational speed.

It should be noted that according to (2.4), A, B and C are second-order polynomials that are, at this stage, only known at a finite set of turbocharger rotational speeds (figure 2.4). To compute the pressure ratio in the extrapolated zone, i.e. for lower iso-speeds, these polynomials of ω_t must be explicitly defined. Thus, once A, B and C have been identified at each of the manufacturer's iso-speeds, a second step consists in identifying the parameters α_X, β_X and γ_X with $X = \{A, B, C\}$:

$$X(\omega_t) = \alpha_X \cdot {\omega_t}^2 + \beta_X \cdot \omega_t + \gamma_X \tag{2.6}$$

Once the parameters in (2.6) have been identified, the explicit formulation of the second order polynomials $A(\omega_t)$, $B(\omega_t)$ and $C(\omega_t)$ can be combined with (2.5) in order to compute the pressure ratio for any compressor mass flow rate and turbocharger rotational speed. The construction of the first data-map $f_{C,Q}$ is then straightforward.

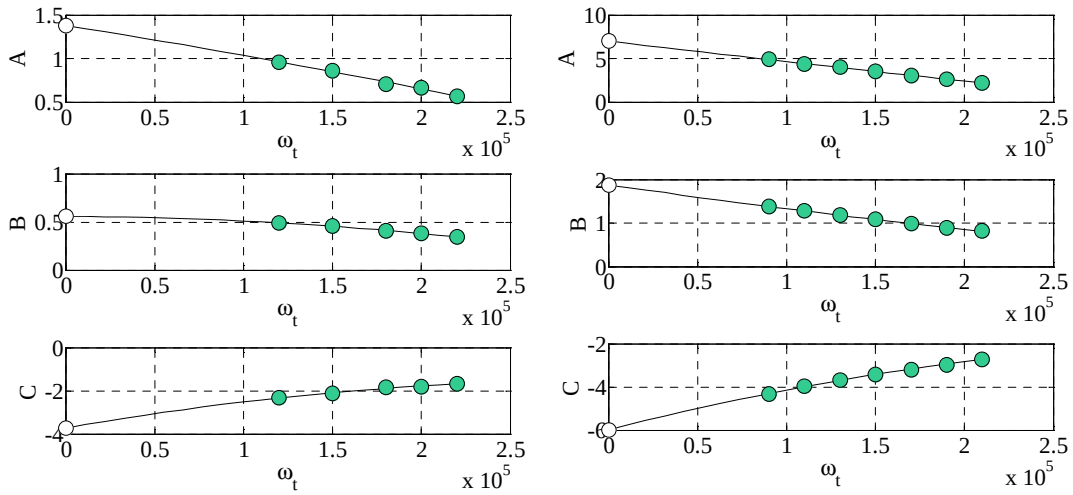

Figure 2.4 – Extrapolation model parameters A, B and C in (2.5), versus turbocharger rotational speed ω_t. A second order polynomial is fitted (solid lines) through the reference points (colored circles). In the final algorithm (section 2.1.2.3), the zero velocity point (white circle) must be noted down for later use.

This new model essentially presents two advantages regarding its accuracy and implementability:

- The second order formulation w.r.t. the turbocharger rotational speed takes into account the flow fluctuations across the operating range. Contrary to Jensen and Kristensen's model, homogeneous fit performances are obtained for every rotational speed. In particular, on the thirty compressors available for this study, this new model provides more accurate results than the affine model (2.3) that is currently widely used in practice. Practical results are presented in the following sections.
- The 3-parameter model (2.5) is particularly well adapted to the use of manufacturers' data-maps that sometimes contain no more than five to six experimental operating points for each iso-speed. Moreover, the calibration requires a simple gradient descent algorithm, while many other formulations require the use of a global optimization algorithm in order to overcome local minima.

2.1.2.2 Extrapolation practical methodology

On figure 2.4, it can be seen that the model (2.6) does not perfectly fit the experimental measurements provided by the manufacturer. This is due to the hypotheses that led to the formulation of the simplified model (2.6) but also more generally to measurement errors that cannot be overcome. As a consequence, and in order to improve the fit to the experimental data points, two practical recommendations are proposed below. They improve the fitting performances while preserving the smoothness and monotonicity properties of the results:

- The y-intercept of each second order polynomial function $A(\omega_t)$, $B(\omega_t)$, or $C(\omega_t)$, is determined using a second order model obtained with the classical Levenberg-Marquardt optimization algorithm [129],
- Then, the interpolation is obtained using a monotone piecewise cubic interpolation [50] based on cubic Hermite splines. They ensure that a smooth data-map is obtained while preserving its monotonicity. This interpolation method benefits from the flexibility offered by cubic splines as well as guaranteeing the monotonicity of the result [35].

These recommendations have been followed for the interpolation and extrapolation of about thirty pressure ratio data-maps $f_{C,Q}$ and showed an excellent robustness to the wide variety of compressors and operating points available for this study. A validation example of a fully interpolated and extrapolated pressure ratio data-map $f_{C,Q}$ is provided below. No additional measurements at lower iso-speeds than the one provided by the manufacturer could be carried out during this study. Thus, in order to prove the extrapolation accuracy of the methodology, the three lowest iso-speeds were excluded from the input data used for the model calibration. These experimental points, including the three excluded iso-speeds, are displayed below along with the model prediction and confirm the accuracy of the model (2.6) both in the interpolated and extrapolated zones (figure 2.5). Additional validation results are presented in section 2.1.2.4 below.

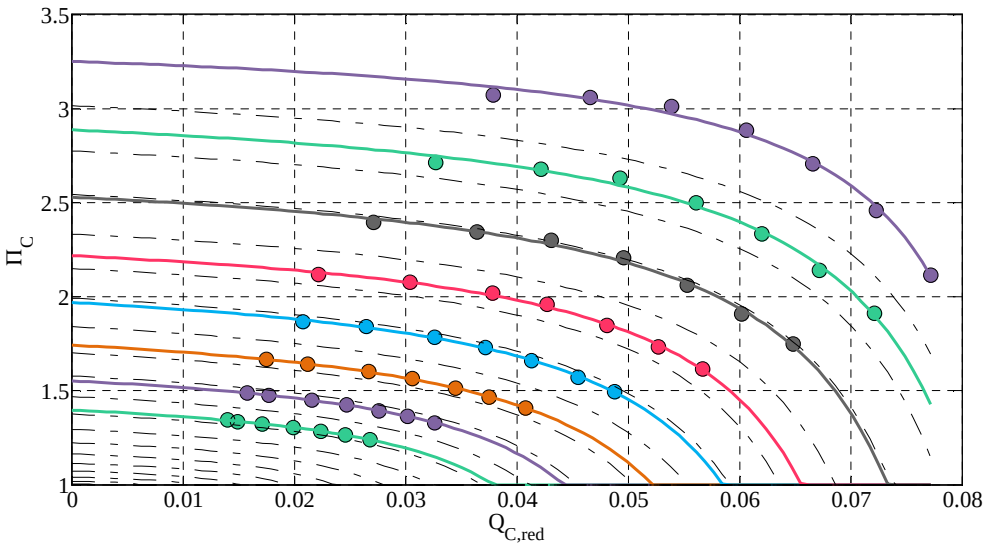

Figure 2.5 – Compression ratio Π_c versus normalized mass flow rate $Q_{C,red}$. For each supplier iso-speed, the pressure ratio is plotted (solid lines) and compared to the manufacturer's points (colored circles). New iso-speeds, interpolated and extrapolated, are also presented (dash-dot lines).

2.1.2.3 Final algorithm

The complete methodology to compute the pressure ratio data-map $f_{C,Q}$ can finally be summed up as below:

Inputs: Experimental operating points $\{\Pi_C, Q_C, \omega_t\}$ in the form of a finite number of turbocharger rotational iso-speeds.

Outputs: Complete extrapolated compressor pressure ratio data-map $\Pi_C = f_{C,Q}(Q_C, \omega_t)$

1- Compute Ψ and Φ for all the data points provided by the manufacturer using (2.1) and (2.2).

2- Treating each iso-speed separately, identify A, B and C according to the model defined in (2.5).

3- Determine the best second order polynomials which fit A, B and C w.r.t. ω_t (2.6). Then compute the y-intercepts of each second order polynomial, for A, B and C respectively, and add them to the values found at step 2 with the corresponding zero rotational speed.

4- Interpolate A, B and C through the entire operating range using monotone piecewise cubic interpolation.

5- Determine Ψ through the whole operating range using the interpolated values of A, B and C and (2.5).

6- Calculate Π_C through the entire operating range inverting (2.1).

2.1.2.4 Additional examples

One major issue, when developing such a model, is to make sure that it is robust enough to be applied to a wide variety of experimental data. This sub-section sums up a few results obtained on different compressor data-maps available for this study. In each case, the three lowest iso-speeds were excluded from the calibration data set but are displayed below to prove the accuracy of the model (2.6).

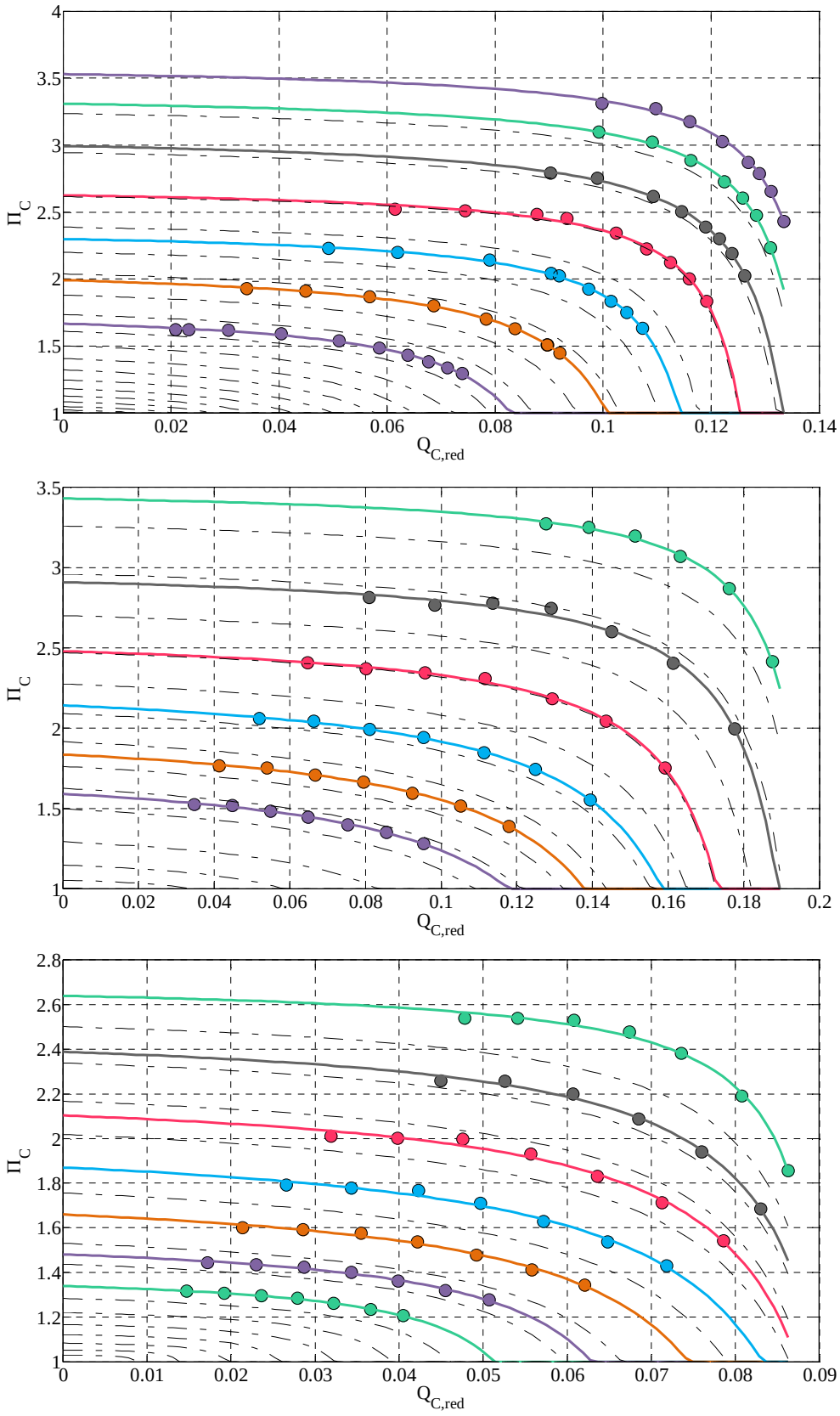

Figure 2.6 – Additional examples of extrapolated compression ratio data-maps $f_{C,Q}$ for three different compressors. The complete compression ratio data-map (lines) is fitted without using the three smallest iso-speeds which are here plotted for validation only.

2.1.3 Extrapolation of the isentropic efficiency data-map $\eta_C = f_{C,\eta}(Q_C, \omega_t)$

The second look-up table $f_{C,\eta}$ involved in the compressor sub-model (section 1.6) provides the compressor isentropic efficiency η_C as a function of the mass flow rate and the turbocharger rotational speed (figure 2.7). It takes into account the losses occurring during the compression process (figure 2.2).

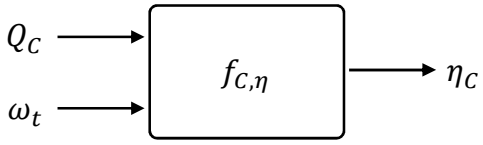

Figure 2.7 – Input/output description of the compressor isentropic efficiency η_C data-map. Q_C stands for the compressor mass flow rate and ω_t for the turbocharger rotational speed.

It is theoretically defined as the ratio of two physical quantities [134,135] that respectively correspond to the energy that is transferred to the fluid in the ideal or isentropic case and the energy transfer that is observed experimentally (figure 2.2):

$$\eta_C = \frac{\Delta h_{C,is}}{\Delta h_C} \tag{2.7}$$

where $\Delta h_{C,is}$ corresponds to the isentropic specific enthalpy exchange that would occur during an ideal compression process and Δh_C is the specific enthalpy exchange that actually occurs due to the losses. The two are linked by the following relation:

$$\Delta h_{C,is} = \Delta h_C - \Delta h_{C,losses} \tag{2.8}$$

where $\Delta h_{C,losses}$ corresponds to the compressor losses that mainly stem from blade incidence and viscous friction (figure 2.2).

Most of the extrapolation strategies in the literature use an alternative formulation for η_C rather than the physical one above (2.7). For instance, Jensen and Kristensen proposed to use a second order polynomial to describe the isentropic efficiency of the compressor at a given rotational speed [70]. Because of its phenomenological rather than physical foundation, it did not prove to lead to an accurate estimation of the isentropic efficiency for extrapolated operating points [87,92]. This motivated many investigations [35,74,92,127] into more physics-based models that usually go as far as using the detailed geometry of the compressor (blade and flow angles, inducer and exducer wheel diameters). In this study, we introduce an alternative approach based on the thermodynamic definition of the isentropic efficiency (2.7) but that does not require knowledge of the detailed geometrical characteristics of the compressor.

2.1.3.1 Theoretical extrapolation model

In order to compute the isentropic efficiency using (2.7), we introduce two separate sub-models for $\Delta h_{C,is} = f_{C,\Delta h_{is}}(Q_C, \omega_t)$ and $\Delta h_C = f_{C,\Delta h}(Q_C, \omega_t)$. Then, computing the isentropic efficiency at a given operating point $\{Q_C, \omega_t\}$ will comprise three steps:

- Computing the isentropic specific enthalpy exchange $\Delta h_{C,is}$ using $f_{C,\Delta h_{is}}$ (a),
- Computing the specific enthalpy exchange Δh_C using $f_{C,\Delta h}$ (b) and,
- Computing η_C using (2.7) (c).

a) Isentropic specific enthalpy exchange $\Delta h_{C,is} = f_{C,\Delta h_{is}}(Q_C, \omega_t)$

In a general framework, the isentropic specific enthalpy exchange $\Delta h_{C,is}$ is given by:

$$\Delta h_{C,is} = \left((\Pi_c)^{\frac{\gamma-1}{\gamma}} - 1 \right) \cdot c_p \cdot \theta_{C,us} \tag{2.9}$$

where the pressure ratio Π_c across the compressor is the only physical value that depends on the operating point $\{Q_C, \omega_t\}$. Its computation is straightforward since it can be obtained using the pressure ratio model $f_{C,Q}(Q_C, \omega_t)$ presented in section 2.1.2. Then, the explicit formulation of $f_{C,\Delta h_{is}}(Q_C, \omega_t)$ is straightforward and is obtained by replacing in (2.9) the term Π_c by the pressure ratio data-map $f_{C,Q}$. This makes it possible to compute the isentropic enthalpy exchange $\Delta h_{C,is}$ for any operating point $\{Q_C, \omega_t\}$.

A set of experimental values for $\Delta h_{C,is}$ was computed using (2.9) and the pressure ratio measurements provided by the manufacturer. These reference values are depicted on figure 2.8, along with the model estimations that were computed using the pressure ratio data-maps $f_{C,Q}$ obtained in section 2.1.2 (figure 2.5).

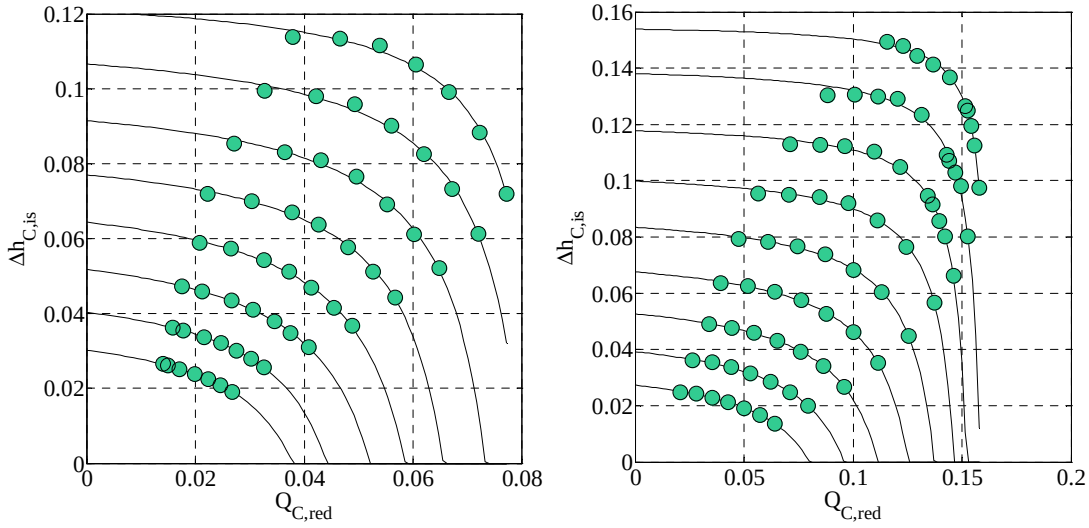

Figure 2.8 – Isentropic specific enthalpy exchange $\Delta h_{C,is}$ versus reduced mass flow rate $Q_{C,red}$ (2.9). The isentropic specific enthalpy exchange obtained with the model (solid lines) shows a good fit with the manufacturer's points used for model fitting (colored circles).

It can be noticed that the accuracy of the isentropic specific enthalpy exchange sub-model $f_{C,\Delta h_{is}}$ is directly linked to the accuracy of the pressure ratio model $f_{C,Q}$ obtained previously. This distinctive feature of the methodology represents a major advantage compared to other mean value formulations available in the literature, since it increases the overall consistency of the compressor model by creating a link between the pressure ratio and isentropic efficiency data-maps that it contains. In particular, if one wants to enhance the compressor model by taking into account additional effects on the pressure ratio data-maps, such as surge phenomena [87], this will implicitly modify the isentropic enthalpy exchange sub-model and thereby also adapt the efficiency data-map.

b) Specific enthalpy exchange $\Delta h_C = f_{C,\Delta h}(Q_C, \omega_t)$

Assuming no inlet guide vanes, i.e. no inlet pre-swirl effects, turbo-machinery equations provide a theoretical linear relationship that is valid at constant compressor rotational speed, between the specific enthalpy exchange Δh and the reduced mass flow rate $Q_{C,red}$ [87,95]:

$$\Delta h_C = b - a \cdot Q_{C,red} \tag{2.10}$$

where a and b are two constants that are fitted on each manufacturer iso-speed (this results in a set of parameter values that depend on the turbocharger rotational speed) and $Q_{C,red}$ is the reduced mass flow rate of the compressor:

$$Q_{C,red} = \sqrt{\frac{\theta_{C,us}}{\theta_{ref}}} \cdot \frac{p_{ref}}{p_{C,us}} \cdot Q_C \tag{2.11}$$

where, θ_{ref} and p_{ref} are the manufacturer's reference pressure and temperature during the measurements.

The same philosophy used for the calibration of the pressure ratio model in section 2.1.2 applies: each manufacturer iso-speed is treated separately and at a given rotational speed, values for the model parameters a and b are obtained by regression analysis [36] (figure 2.9). Reference values for this series of regression analyses are computed from the experimental operating points provided by the manufacturer and using the theoretical formulation below, that combines (2.7) and (2.9):

$$\Delta h_C = \frac{c_p \cdot \theta_{C,us} \cdot \left((\Pi_c)^{\frac{\gamma-1}{\gamma}} - 1 \right)}{\eta_c} \tag{2.12}$$

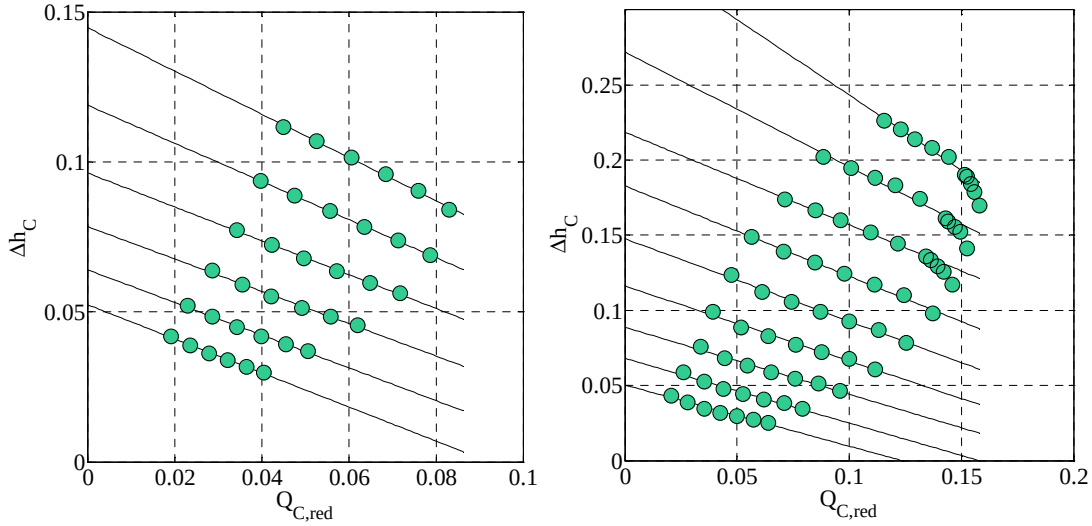

Figure 2.9 – Specific enthalpy exchange Δh_C versus reduced mass flow rate $Q_{C,red}$. The specific enthalpy exchange model fitting results (2.10) (solid lines) are presented against the manufacturer's reference points (2.12) (colored circles). The specific enthalpy exchange is linear w.r.t. the compressor reduced mass flow rate.

Since this affine relationship was obtained from physical-based turbo-machinery equations, in (2.10) the trend of the slope a and the y-intercept b w.r.t. the compressor rotational speed ω_t is known [87,95]. Assuming a constant inlet fluid density, relevant for single stage turbocharger configurations, a is expected to be proportional to ω_t. In particular, the curve is expected to go through origo: $a(0) = 0$ (figure 2.10). Similarly, b theoretically evolves as the square of the turbocharger rotational speed and hence also goes through origo: $b(0) = 0$ (figure 2.10).

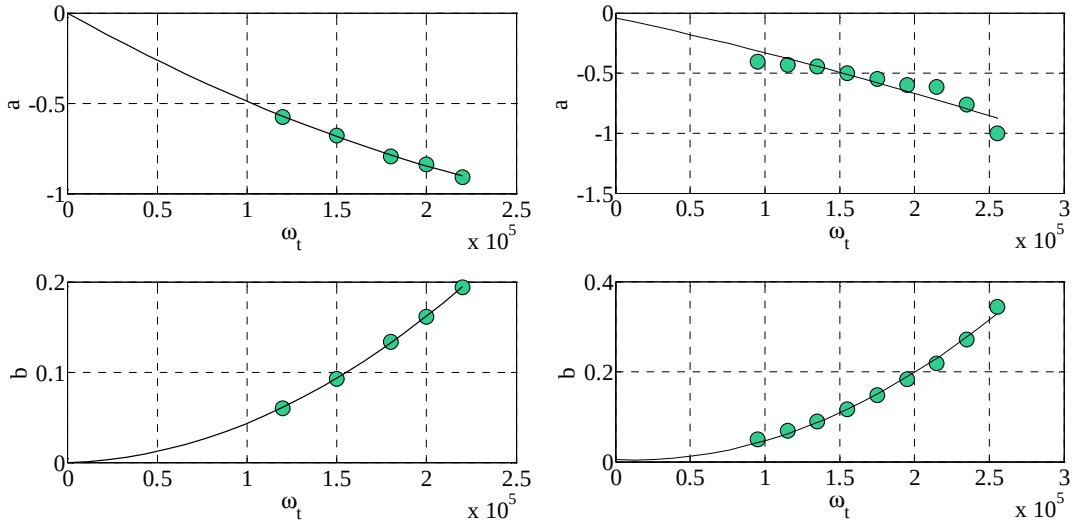

Figure 2.10 – Model parameters a and b versus rotational speed ω_t. The reference values are obtained by regression analysis on the manufacturer's data (2.12) (colored circles) and presented with a second order polynomial fit (solid line).

In practice the parameters a and b in (2.10) are usually not sufficiently descriptive [95]. This can be observed on the example depicted on figure 2.10 where it can be seen that the experimental reference operating points obtained with (2.12) do not perfectly fit the theoretical linear trend suggested above. For this reason, the parameters a and b can be used during the calibration to fine-tune the model prediction to the manufacturer's experimental operating points. This stage is fully described in section 2.1.3.2 below.

c) Isentropic efficiency $\eta_C = f_{C,\eta}(Q_C, \omega_t)$

At this stage, using respectively (2.9) and (2.10), the specific enthalpy exchanges $\Delta h_{C,is}$ and Δh_C involved in the calculation of the isentropic efficiency (2.7) can be computed for any operating point $\{Q_C, \omega_t\}$. The construction of the isentropic efficiency look-up table $f_{C,\eta}$ used in the compressor model (1.18) is then straightforward.

It can be noticed that the methodology directly inherits its accuracy from a set of hypotheses involved in the design of a simplified specific enthalpy exchange Δh_C model (2.10) and from the accuracy of the experimental measurements provided by the manufacturer. The latter are used during the calibration of the pressure ratio model $f_{C,Q}$ used to compute $\Delta h_{C,is}$ as well as for the identification of a and b. In order to increase the robustness of the model calibration, an iterative process will be put in place to fine-tune the shape of the isentropic efficiency curve to empirical observations. In particular, it is the position of the maximum efficiency point that is considered here and presented in the next sub-section.

2.1.3.2 Extrapolation practical methodology

In the theoretical extrapolation model detailed above, the linear regression used to determine the model parameters a and b in (2.10) is a very uncertain stage. In fact, even though an affine relationship is a very attractive formulation in a data fitting process, in practice, the experimental measurements provided by the manufacturer do not present a perfectly linear trend (figure 2.9). For instance, on the example presented in figure 2.10, the values for a and b can vary by about 15% from one set of points to another during the regression analysis stage. To obtain this figure, the regression analysis was performed at each iso-speed, on all the sets containing more than five points.

Since Δh_{is} in (2.7) is directly obtained from the pressure ratio model presented in section 2.1.2, the parameters a and b represent the only inputs of the extrapolation model to fine-tune the shape of the isentropic efficiency curve. In particular, for a given iso-speed, b controls the value of the maximum efficiency point $\overline{\eta}_C$ through (2.10). Additionally, in [87], it was observed that the curve connecting the isentropic maximum efficiency follows a parabola that goes through origo, w.r.t. the turbocharger rotational speed:

$$\overline{\eta}_C = max(\eta_C) = K_2 \cdot {\omega_t}^2 + K_1 \cdot \omega_t \tag{2.13}$$

where $K_i, i = \{1,2\}$ is a set of new parameters identified by regression analysis.

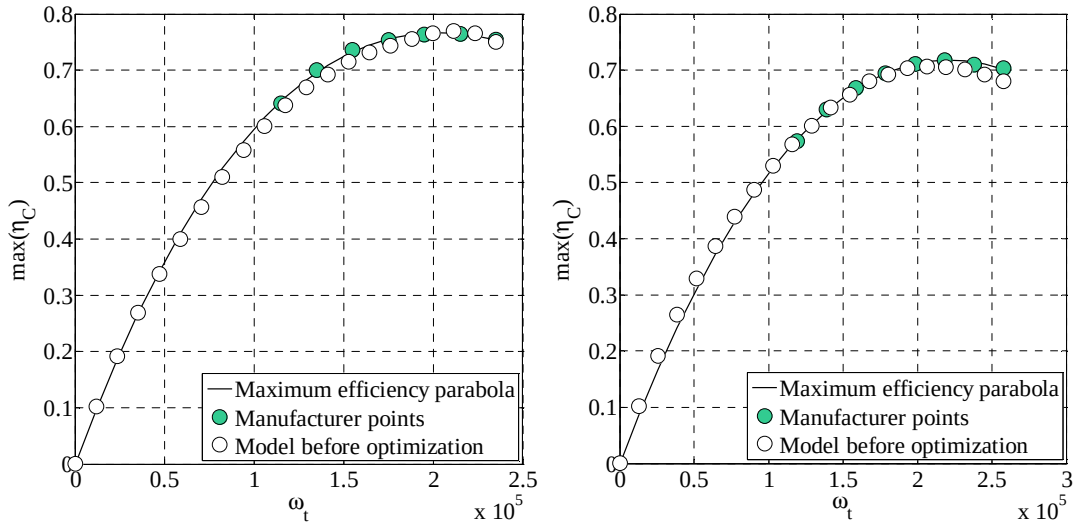

Figure 2.11 – Maximum compressor isentropic efficiency $\overline{\eta}_C$ versus rotational speed ω_t. The reference maximum efficiency for each iso-speed (green circles) can be extrapolated using a second order polynomial that goes through origo (2.13) (solid line). One can see that the maximum efficiency initially obtained with the theoretical model (2.7) (2.9) and (2.10) (white circles) does not follow this parabola.

This regression analysis requires a set of reference points. In practice, since the experimental maximum efficiency point of each iso-speed may not be provided by the manufacturer, it can be estimated by using the second order isentropic efficiency model proposed by Jensen and Kristensen [70]:

$$\eta_C = \delta_2 \cdot Q_C^2 + \delta_1 \cdot Q_C + \delta_0 \tag{2.14}$$

where the coefficients $\delta_i, i = \{0,1,2\}$ are identified using regression analysis on each manufacturer iso-speed.

Even though it is shown in [87,92] that this empirical model (2.14) leads to inaccurate extrapolations, it can still be used as an intermediate interpolation tool to estimate the maximum efficiency point $\overline{\eta}_C$ of each iso-speed. An example of the reference maximum efficiency points is depicted on figure 2.11, along with the parabola fit (2.13).

Once the equation of the maximum efficiency parabola (2.13) has been identified, the value of b can be fine-tuned until the corresponding iso-speed curve has its maximum efficiency point on the parabola (figure 2.12). In practice, in order to start with the best initial value of b at each iso-speed, the regression analysis (2.10) is performed for all the set of manufacturer operating points containing more than five points. The best set is the one that leads to the minimum sum of squared residuals w.r.t. the maximum efficiency parabola (2.13). The overall process is repeated for all the iso-speeds of the isentropic efficiency look-up table $f_{C,\eta}$. Examples of final results are depicted on figure 2.12.

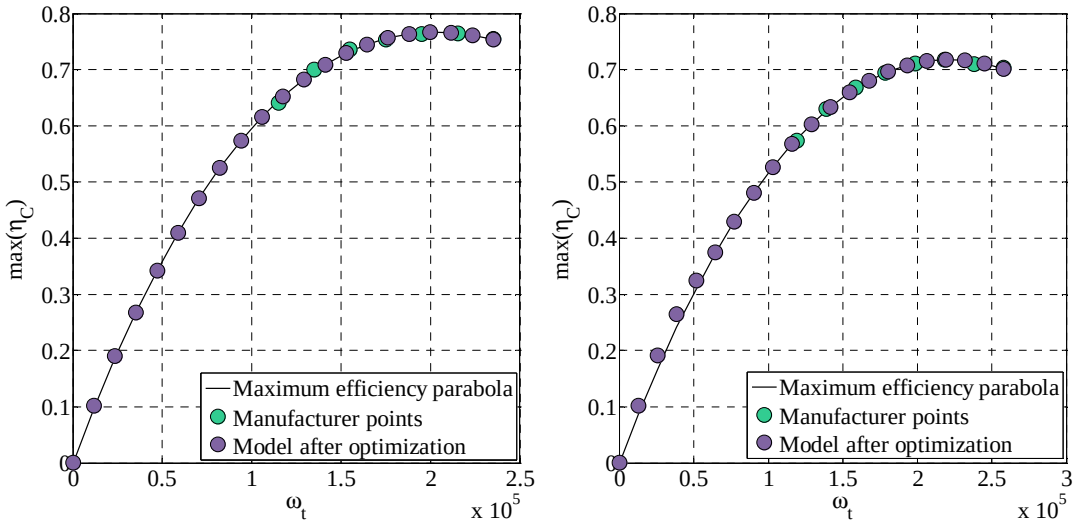

Figure 2.12 – Maximum compressor isentropic efficiency $\overline{\eta}_C$ versus rotational speed ω_t after optimization. The reference parabola (2.13) (solid line) is presented as well as the manufacturer's points (green circles). After optimization, the maximum efficiency points (purple circles) are now on the parabola both for the interpolated and extrapolated rotational speeds.

Altogether, it is a four-step process:

- obtain the maximum efficiency points at each iso-speed by using the second order model (2.14),
- use these reference points to determine the equation of the maximum efficiency parabola (2.13),
- determine at each iso-speed the set of manufacturer's points that minimizes the error between the maximum efficiency point of the isentropic efficiency curve (2.7) and the maximum efficiency parabola (2.13) and,
- fine-tune the values of b in (2.10) until the maximum efficiency point of all iso-speeds lies on the maximum efficiency parabola (2.13).

This single loop iterative algorithm was used to compute the isentropic efficiency map of about thirty compressors and gave a series of results in perfect agreement with empirical observations [136,137]. Thanks to the wide variety of manufacturer data-maps and compressor geometries available for this study, it also showed a high level of robustness.

A validation example of a fully interpolated and extrapolated compressor isentropic efficiency data-map $f_{C,\eta}$ is depicted on figure 2.13 below. As in the pressure ratio case, no additional measurements at lower iso-speeds than the ones provided by the manufacturer could be carried out during this study. Moreover, due to the particularly complex shape of the isentropic efficiency data-maps, it was not possible to exclude any of the iso-speeds during the model calibration stage. Still, the good accuracy of the methodology can be observed by comparing the manufacturer experimental operating points to the iso-speeds computed from (2.7) and the extrapolation methodology presented above. Additional validation results are presented in section 2.1.3.4 below.

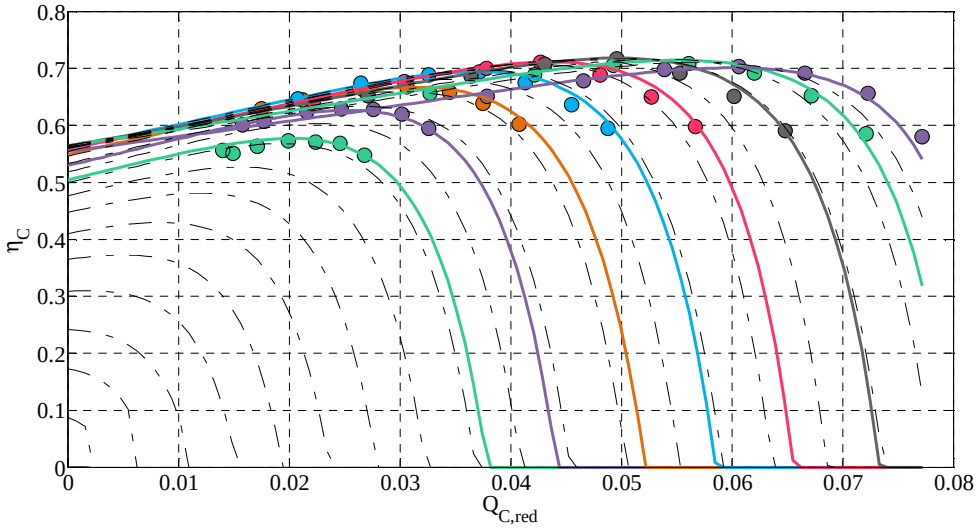

Figure 2.13 – Compressor isentropic efficiency η_C versus reduced mass flow rate $Q_{C,red}$. The extrapolated compressor efficiency (solid lines) shows a good fit with the manufacturer's data points (colored circles) through the entire flow rate range. Interpolated and extrapolated iso-speeds are also displayed (dash-dot lines).

2.1.3.3 Final algorithm

The complete methodology to compute the compressor isentropic efficiency data-map $f_{C,\eta}$ is summed up in the algorithm below and illustrated on figure 2.14 that provides an overview of the general stages of the algorithm:

Inputs: Experimental operating points $\{\eta_C, Q_C, \omega_t\}$ in the form of a finite number of turbocharger rotational iso-speeds. The compressor mass flow rate data-map $f_{C,Q}$.

Outputs: Complete extrapolated compressor isentropic efficiency data-map $\eta_C = f_{C,\eta}(Q_C, \omega_t)$

1- Evaluate $\overline{\eta}_C$ for each manufacturer data iso-speed using a local second order polynomial model using (2.14)

2- Determine the equation of the maximum efficiency parabola (2.13). One must set $\overline{\eta}_C = 0$ when $\omega_t = 0$.

3- Compute $\Delta h_{C,is}$ through the whole operating range using the pressure ratio data-map $f_{C,Q}$ obtained in section 2.1.2 and the isentropic specific enthalpy exchange sub-model (2.9).

4- Calculate the reference points for Δh_C using the experimental operating points $\{\eta_C, Q_C, \omega_t\}$ and (2.12).

5- Select a combination of experimental operating points $\{\eta_c, Q_C, \omega_t\}$ containing three or more points.

6- Identify the values of parameters a and b in (2.10) by regression analysis and using the set of reference points determined at step 5. Repeat step 6 for each iso-speed of the experimental operating points.

7- Extrapolate a and b as second order polynomials w.r.t. ω_t. Take into consideration the fact that $a(0) = 0$ and $b(0) = 0$.

8- Extrapolate Δh_C through the whole operating range using (2.10) and the extrapolated values of a and b.

9- Calculate η_C through the entire operating range using $\Delta h_{C,is}$ obtained at step 3 and Δh_C obtained at step 8 and (2.7).

10- Determine $\overline{\eta}_C$ for each extrapolated iso-speed.

11- Compute the residual for $\overline{\eta}_C$ obtained at step 10, w.r.t. the maximum efficiency parabola (2.13). It is equal to the sum of the squared difference between the parabola found at step 2 and the values evaluated at step 10. Save it.

12- If other experimental operating point combinations have not been evaluated, go to step 5. If not, find the combination of points with the smallest residual for $\overline{\eta}_C$ (saved at step 11) and use it from steps 6 to 10. Then go directly to 13.

13- For each iso-speed, optimize the value of b in order to reduce the residual for $\overline{\eta}_C$ w.r.t. the parabola identified at step 2. The initial value was computed at step 7.

14- Synthesize the full data-map $f_{C,\eta}$ using Δh_C calculated with the values of b obtained at step 13 and (2.10).

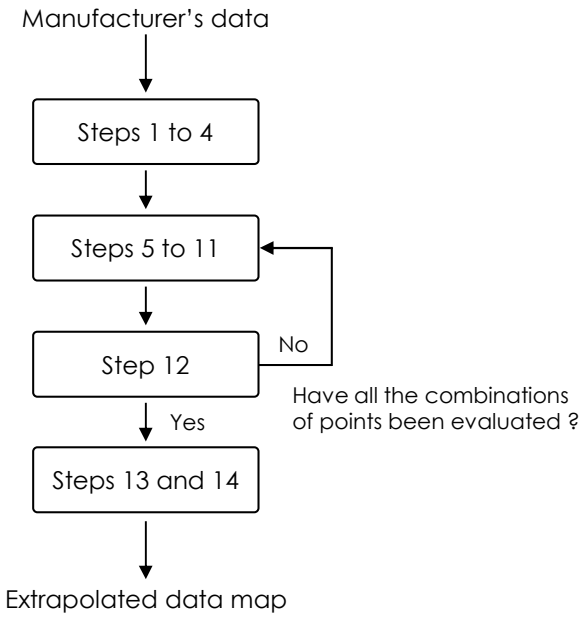

Figure 2.14 – Compressor isentropic efficiency data-map extrapolation algorithm overview.

2.1.3.4 Additional examples

A particular focus during the development of the methodology was to obtain sufficient robustness to build compressor data-maps from a wide range of experimental sets of operating points and for a wide variety of components. The method was therefore extensively tested on a set of about thirty compressors. Relevant examples of performance are depicted below (figure 2.15) and show a general good agreement with manufacturer experimental measurements.

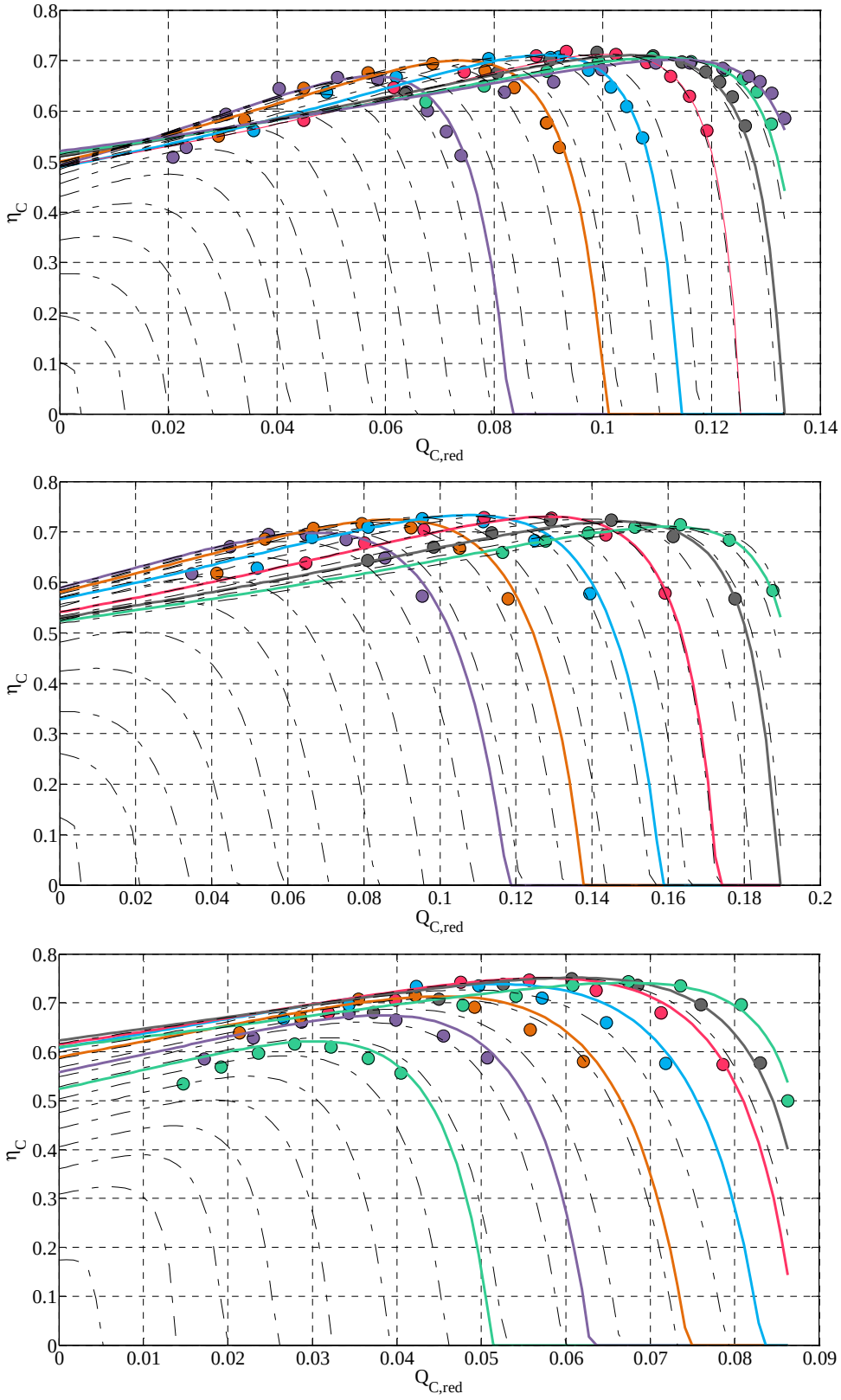

Figure 2.15 – Additional extrapolated compressor isentropic efficiency data-maps $f_{C,\eta}$. The fully extrapolated data-map for compressor isentropic efficiency (colored solid lines) is in good agreement with the manufacturer's points (colored circles) for any rotational speed and flow rate.

2.2 Turbine

Section 2.2 concerns the extrapolation of the two turbine look-up tables required in a standard turbocharger model (section 1.6). A similar layout to the compressor case is used here. Section 2.2.1 provides insight into the thermodynamic phenomenon that takes place during the expansion process. The second sub-section 2.2.2 concerns the extrapolation of the turbine look-up tables (figure 2.1) and successively presents the extrapolation model (section 2.2.2.1), the practical extrapolation methodology (section 2.2.2.2) along with the associated algorithm (section 2.2.2.3). Relevant results obtained for a set of fixed-geometry and variable geometry turbines are presented in section 2.2.2.4. The third sub-section 2.2.3 concerns the extrapolation of the turbine isentropic efficiency data-maps and follows the same layout.

2.2.1 Thermodynamic considerations

In this study, the turbine is assumed to be exclusively driven by the energy of the cylinder exhaust gases that are expanded toward the ambient pressure. From inlet to outlet, a radial turbine is usually composed of four elements: an inlet volute (3), a nozzle with static or moving blades (3b), a bladed rotor, and a static outlet, which is usually a simple pipe (4) (left figure 2.16).

The physical processes involved during the expansion of gases through the turbine are usually described on an h-S (specific enthalpy – entropy) diagram, as depicted below. In the inlet volute, the pressure is p_3 and the speed is equal to C_3. The nozzle accelerates the gas up to C_{3b}. At this stage, there is almost no change in specific enthalpy, i.e. h_{03b} is almost equal to h_{03}. There is mainly a change from potential to kinetic energy: the pressure loss from p_{03} to p_{03b} is compensated by the increase in speed from C_3 to C_{3b}. The transfer of work actually occurs though the rotor, designed to minimize the kinetic energy at the outlet. Then, in the static outlet, the total specific enthalpy h_{04} is significantly smaller than h_{03b} and the static pressure and gas speed decrease respectively to p_4 and C_4.

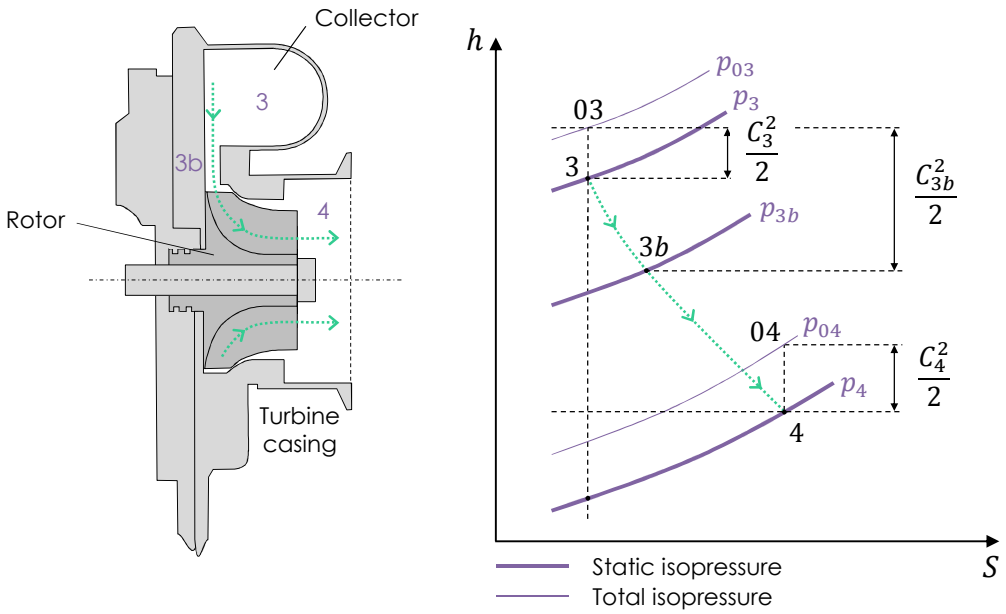

Figure 2.16 – Left: Side view of a radial turbine,
Right: h-S diagram of a radial turbine.
p_x and $p_{0x} = p_x + 0.5 \cdot {C_x}^2$ respectively stand for static and total pressure at x, C_x is the fluid speed.

This process is described by the first data-map of the turbine sub-model which gives the flow through the turbine. However, as for the compressor, the process is not ideal due to losses during expansion: the irreversibility can be seen on the h-S diagram since entropy is created (figure 2.16). An ideal expansion would indeed be represented by a vertical straight line resulting in $\Delta S = 0$. The losses are described by the second turbine data-map that gives its isentropic efficiency (figure 2.16).

2.2.2 Extrapolation of the turbine flow rate data-map $Q_T = f_{T,Q}(\Pi_T, \omega_t)$

The first look-up table $f_{T,Q}$ involved in the turbine sub-model (1.6.2) provides the mass flow rate through the turbine Q_T as a function of the pressure ratio across the turbine Π_T and the turbocharger rotational speed ω_t (figure 2.17).

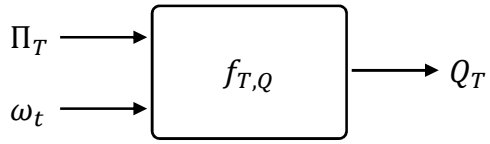

Figure 2.17 – Input/output description of the turbine mass flow rate Q_T data-map. Π_T stands for the pressure ratio across the turbine and ω_t for the turbocharger rotational speed.

The most popular approach to describe this behavior is based on the classical flow restriction model (1.11) and was initially presented by Jensen and Kristensen in 1991 [70]. Since then, many authors have attempted to enhance the formulation in order to improve the fit w.r.t. to experimental observations [87,92]. However, there is still no universal definition for the turbine equivalent section A_{eff}, required in general flow restriction formulations:

$$Q_T = A_{eff} \cdot C_{red} \tag{2.15}$$

where C_{red} is the reduced flow speed which depends on the subsonic or supersonic flow state (1.11).

Starting with the standard proposal by Jensen and Kristensen [70], it is widely admitted in the literature that A_{eff} is a function of Π_T, the pressure ratio across the turbine. However in practice, the theoretical formulation of this relationship is unknown and an affine relationship in Π_T is usually employed [70]. However, this formulation, while simple, does not fit the experimental trend of the turbine mass flow rate Q_T [136,137]. In particular, since C_{red} tends to a constant and $A_{eff}(\Pi_T) = a \cdot \Pi_T + b$ tends to $+\infty$ at high pressure ratios Π_T, the affine formulation leads to a turbine mass flow rate that would constantly increase with Π_T. This is in no way the theoretical behavior described by Bernouilli or Barré de Saint-Venant flow restriction models [122] which state that beyond a critical pressure ratio, the mass flow rate no longer increases: the flow is choked [102]. In the next sub-section, a new mathematical formulation $A_{eff}(\Pi_T)$ that matches this experimental flow behavior is proposed and used to build the turbine mass flow rate data-map $f_{T,Q}$.

Only a few measurements have been carried on an entire turbine operating range and the associated results are hardly ever published. However, it is still possible to make three hypotheses about the general turbine flow rate behavior involved in (2.15) [7,69,134]:

Empirical hypothesis on Q_T

$Hyp.1:$ $Q_T(\Pi_T)$ is strictly monotonic

$Hyp.2:$ $\lim_{\Pi_t \to 1} Q_T = 0$

$Hyp.3:$ $\lim_{\Pi_t \to +\infty} Q_T = \text{constant}$

Due to the shape of C_{red} in (2.15), the turbine flow rate Q_T inherits its variation ($Hyp.1$) and limits at the low and high pressure ratios ($Hyp.2-3$) from those of the equivalent section $A_{eff}(\Pi_T)$. In particular, the latter should comply with the same series of hypotheses.

2.2.2.1 Theoretical extrapolation model

In order to comply with the empirical observations ($Hyp.1-3$) detailed above, a new turbine flow restriction model that proved to fit the methodology and that is based on the reduced mass flow rate $Q_{T,red}$ and the flow Mach number M_a is introduced:

$$Q_{T,red} = A_{Mach}(\Pi_T) \cdot C_{Mach}(M_a) \tag{2.16}$$

where A_{Mach} is a new equivalent section formulation and V_{Mach} is the reduced flow speed given by:

$$C_{Mach} = \begin{cases} \sqrt{\frac{\gamma}{R}} \cdot \left(\frac{2}{\gamma+1}\right)^{\frac{\gamma+1}{2\gamma-2}} & if\ M_a > 1, \\ \sqrt{\frac{\gamma}{R}} \cdot \frac{M_a}{\left(1+\frac{(\gamma-1){M_a}^2}{2}\right)^{\frac{\gamma+1}{2\gamma-2}}} & otherwise. \end{cases} \tag{2.17}$$

The flow Mach number M_a is computed using:

$$M_a = \sqrt{\left(\frac{2}{\gamma-1}\right)\left({\Pi_T}^{\frac{\gamma-1}{\gamma}} - 1\right)} \tag{2.18}$$

and the reduced mass flow rate $Q_{T,red}$ normalizes the turbine flow rate w.r.t. reference pressure and temperature conditions (p_{ref}, θ_{ref}):

$$Q_{T,red} = Q_T \sqrt{\frac{\theta_{ref}}{\theta_{T,us}}} \cdot \frac{\Pi_T \cdot p_{T,ds}}{p_{ref}} \tag{2.19}$$

where $p_{T,ds}$ is the pressure at the turbine outlet.

Finally, using the alternative flow restriction formulation (2.16), the equivalent section definition below proved to describe accurately the behavior of the equivalent section at a constant turbocharger rotational speed:

$$A_{Mach}(\Pi_T) = k_1 \cdot \left(1 - e^{\left(1-\frac{1}{\Pi_T}\right)^{k_2}}\right) \tag{2.20}$$

where $k_i, i = \{1,2\}$ are model parameters identified using regression analysis on each manufacturer iso-speed (figure 2.18). This results in a set of parameter values that depend on the turbocharger rotational speed.

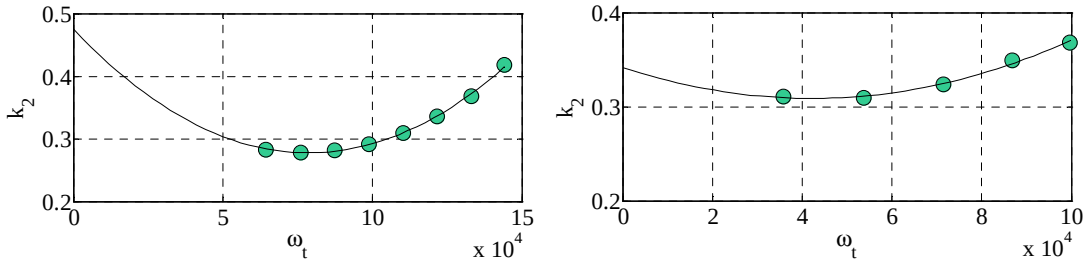

Figure 2.18 – k_2 extrapolation model parameter in (2.20) versus rotational speed ω_t. Reference values are displayed (colored circles) along with a second order polynomial fit (solid line). A_{mach} can then be calculated for any rotational speed using (2.20).

The turbine mass flow rate model (2.16-2.20) detailed above fulfills the three hypotheses above ($Hyp.1-3$) and leads to a turbine mass flow rate Q_T that is in perfect agreement with experimental observations [7,69,134]. It can therefore be used to obtain an accurate estimation of the turbine mass flow rate in the empty zone of the experimental data-map provided by the manufacturer.

2.2.2.2 Extrapolation practical methodology

The interpolation and extrapolation of the turbine mass flow rate using (2.16-2.20) requires the knowledge of the model parameters k_1 and k_2 over the entire turbocharger rotational speed range. In other words, it requires interpolating and extrapolating k_1 and k_2 from the finite set of values obtained by regression analysis on the manufacturer iso-speeds (see figure 2.1). The idea here is to combine empirical knowledge and extensive trials on our turbine data-base to determine an appropriate way to carry out this process.

As suggested before, the mass flow rate through the turbine Q_T is expected to become constant beyond a given critical pressure ratio. This is implicitly guaranteed by the extrapolation model (2.16-2.20) since it was explicitly built to fulfil $Hyp.3$. However, there is currently no single answer in the literature to the question whether it actually tends to a critical mass flow rate that depends or not on the turbocharger rotational speed [7,69,134]. It is not in the author's intent to provide a general answer to this complex question, but it can be noted that the formulation proposed here can fulfill both hypotheses, depending on the nature of k_1. In particular, if k_1 is kept constant in (2.20), then A_{Mach} tends to a unique constant value and so does Q_T. Then, k_2 usually corresponds to a second order polynomial in ω_t (figure 2.18). The turbine mass flow rate trend obtained is then in agreement with [7,69,134].

A validation example of a fully interpolated and extrapolated turbine mass flow rate data-map $f_{T,Q}$ is depicted on figure 2.19. Again, due to the great complexity of carrying out accurate turbine test bench trials, no additional measurements could be done during the study. Hence, the good accuracy of the methodology can only be justified by the relative position of the model with the experimental operating points provided by the manufacturer. Additional validation results are provided in section 2.2.2.4.

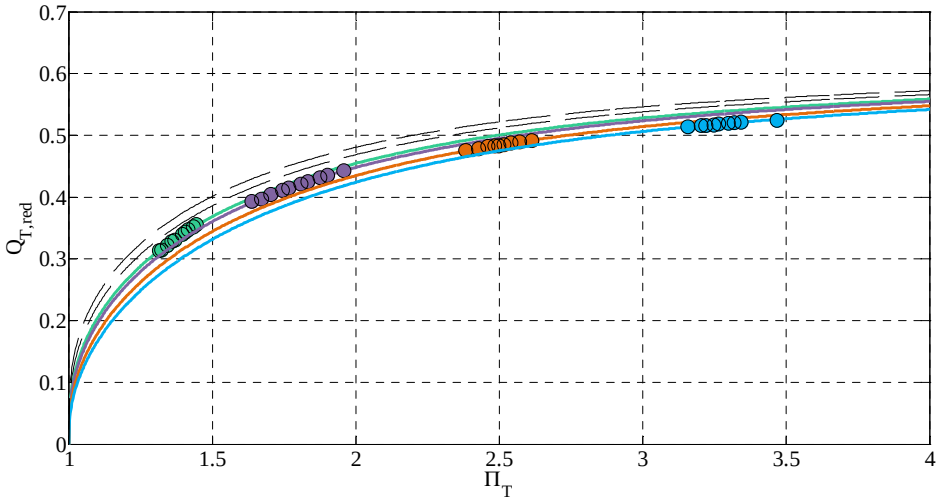

Figure 2.19 – Extrapolated reduced flow rate $Q_{T,red}$ versus pressure ratio Π_T. For each manufacturer iso-speed, the turbine flow rate extrapolated over the whole pressure ratio operating range is presented (solid line) as well as the reference points that have been used to fit the model (colored circles). Interpolated and extrapolated iso-speeds are also depicted (dash-dot lines).

2.2.2.3 Final algorithm

The complete methodology that uses the extrapolation model (2.16-2.20) to compute the turbine mass flow rate data-map $f_{T,Q}$ can be summed up as follows:

Inputs: Experimental operating points $\{\Pi_T, Q_T, \omega_t\}$ in the form of a finite number of turbocharger rotational iso-speeds.

Outputs: Complete extrapolated turbine mass flow rate data-map $Q_T = f_{T,Q}(\Pi_T, \omega_t)$.

1- Calculate A_{Mach} for every point of the data-map using (2.16-2.20).

2- Identify k_1 and k_2 as the best fit to A_{Mach} (each iso-speed must be taken individually) according to 2.20.

3- Replace all k_1 values by the mean value of the coefficients obtained at step 2.

4- Identify k_2 again using (2.20) and a constant value for k_1. Then, extrapolate k_2 using a second order polynomial w.r.t. the turbine rotational speed.

5- Calculate A_{Mach} for the whole operating range using the extrapolated k_1 and k_2 values and (2.21).

6- Compute the turbine reduced mass flow rate $Q_{T,red}$ with (2.16) and the mass flow rate Q_T by inverting (2.19).

2.2.2.4 Additional examples

Again, the biggest issue was to guarantee that the methodology is robust enough to be applied to a wide range of turbine and manufacturer experimental sets of operating points. This was validated by applying the methodology (section 2.2.2.3) to interpolate and extrapolate the mass flow rate data-map $f_{T,Q}$ of thirty different turbines. Relevant examples of data-maps are provided below:

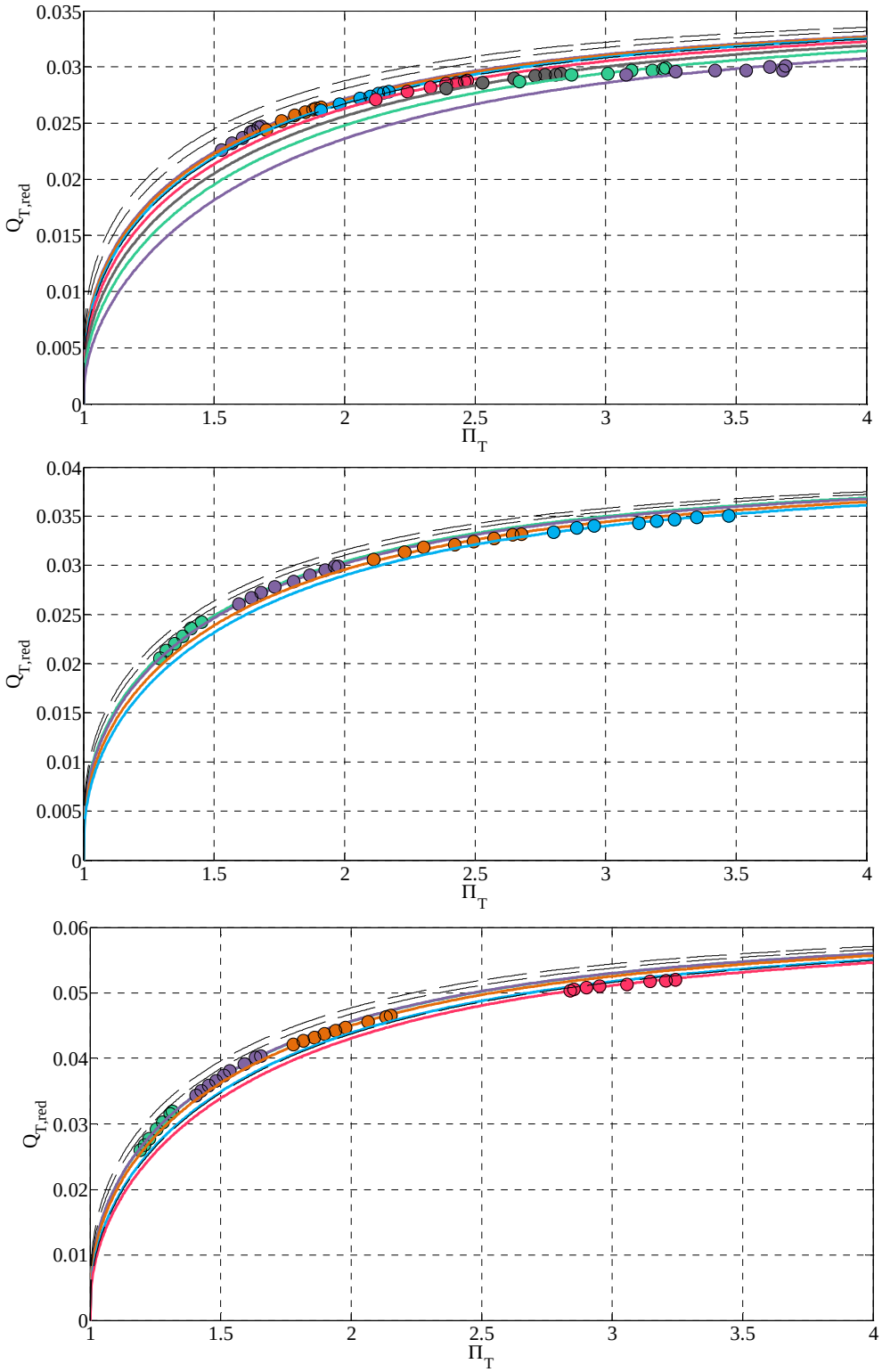

Figure 2.20 – Additional extrapolated reduced mass flow rate data-maps $f_{T,Q}$. The extrapolated turbine mass flow rate iso-speeds are plotted (solid lines). The manufacturer's data points (colored circles) demonstrate the good quality of the model.

2.2.3 Extrapolation of the isentropic efficiency data-map $\eta_T = f_{T,\eta}(\Pi_T, \omega_t)$

The fourth look-up table involved in the turbocharger sub-model presented in section 1.6 gives the isentropic efficiency of the turbine η_T as a function of the pressure ratio Π_T across the turbine and the turbocharger rotational speed ω_T (figure 2.21). It is used to characterize the losses occurring during the expansion process (figure 2.16).

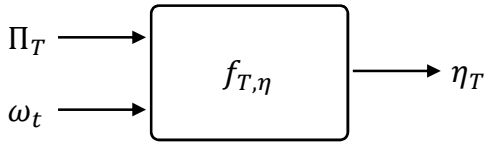

Figure 2.21 – Input/output description of the turbine isentropic efficiency η_T data-map. Π_T stands for the pressure ratio across the turbine and ω_t for the turbocharger rotational speed.

As in the compressor case (2.7), the turbine isentropic efficiency η_T is defined as the ratio of the ideal or isentropic specific enthalpy exchange $\Delta h_{T,is}$ and the specific enthalpy exchange Δh_T that actually occurs and accounts for losses:

$$\eta_T = \frac{\Delta h_T}{\Delta h_{T,is}} \tag{2.21}$$

On the h-S diagram presented on figure 2.16, it can be seen that $\Delta h_{T,is}$ and Δh_T are linked by the relation below:

$$\Delta h_{T,is} = \Delta h_T + \Delta h_{T,losses} \tag{2.22}$$

where $\Delta h_{T,losses}$ corresponds to the losses occurring during expansion which are mainly due to blade incidence and viscous friction (figure 2.16).

2.2.3.1 Theoretical extrapolation model

Similarly to the approach used for the compressor (section 2.1.3), it is proposed to use two sub-models $\Delta h_{T,is} = f_{T,\Delta h_{is}}(\Pi_T, \omega_t)$ and $\Delta h_T = f_{T,\Delta h}(\Pi_T, \omega_t)$ in order to compute the turbine isentropic efficiency η_T in (2.21). Computing the isentropic efficiency at a given operating point $\{\Pi_T, \omega_t\}$ is based on three steps:

- Computing the isentropic specific enthalpy exchange $\Delta h_{T,is}$ using $f_{T,\Delta h_{is}}$ (a),
- Computing the specific enthalpy exchange Δh_T using $f_{T,\Delta h}$ (b) and,
- Computing η_T using (2.21) (c).

a) Isentropic specific enthalpy exchange $\Delta h_{T,is} = f_{T,\Delta h_{is}}(\Pi_T, \omega_t)$

The theoretical isentropic specific enthalpy exchange definition is given by [87]:

$$\Delta h_{T,is} = \left(1 - \left(\frac{1}{\Pi_t}\right)^{\frac{\gamma-1}{\gamma}}\right) \cdot C_p \cdot \theta_{T,us} \tag{2.23}$$

It should be pointed out that it depends only on the pressure ratio across the turbine Π_T. In particular, it does not depend on the turbocharger rotational speed ω_t and therefore can be directly computed from its theoretical definition (2.23) for any operating point $\{\Pi_t, \omega_t\}$ (figure 2.22).

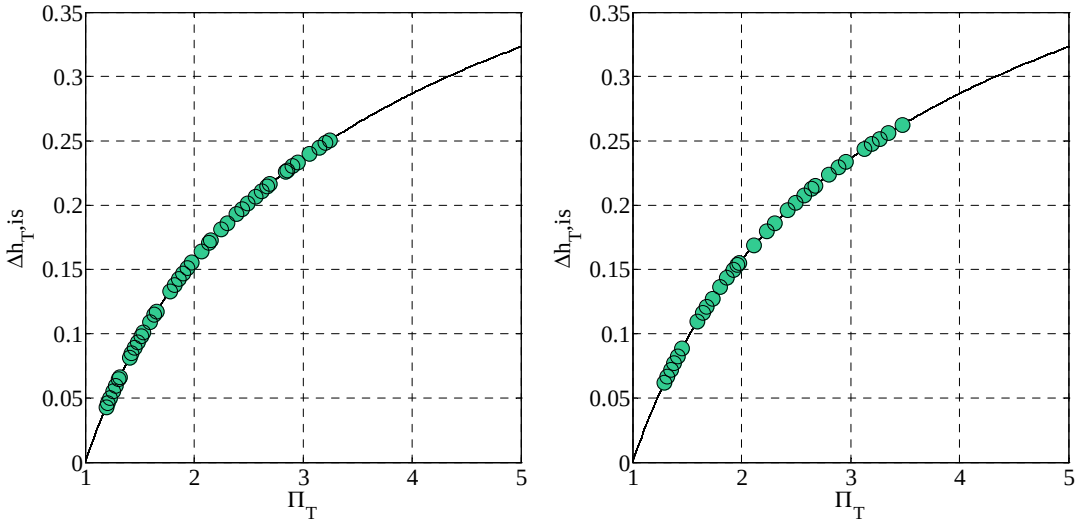

Figure 2.22 – Extrapolated isentropic specific enthalpy exchange $\Delta h_{T,is}$. It can be easily computed for all the manufacturer's points (colored circles) using the theoretical expression (2.23) and extrapolated to any rotational speeds ω_t and expansion ratios Π_T (solid line).

b) Specific enthalpy exchange $\Delta h_T = f_{T,\Delta h}(\Pi_T, \omega_t)$

Since for each experimental operating point, the manufacturer provides a measurement of the pressure ratio across the turbine Π_T as well as the corresponding isentropic efficiency η_T, the specific enthalpy exchange Δh_T at these operating points can be computed from the theoretical definition (2.24). This makes it possible to create a given reference set of operating points that can be used to calibrate the extrapolation model $f_{T,\Delta h}$ presented in this sub-section.

$$\Delta h_T = \left(1 - \left(\frac{1}{\Pi_T}\right)^{\frac{\gamma-1}{\gamma}}\right) \cdot C_p \cdot \theta_{T,us} \cdot \eta_T \tag{2.24}$$

As in the compressor case (2.10), simplified turbo-machinery equations provide at constant rotational speed a theoretical affine formulation for the specific enthalpy exchange Δh_T w.r.t. the reduced turbine mass flow rate $Q_{T,red}$:

$$\Delta h_T = a \cdot Q_{T,red} + b \tag{2.25}$$

where $Q_{T,red}$ is either obtained from the turbine mass flow rate data-map $f_{T,Q}$ obtained in section 2.2.2 or from the manufacturer's experimental operating points (see section 2.2.3.2 below for further details). a and b are two constants that can be identified using regression analysis on the reference set of operating points obtained with (2.24). Again, each iso-speed must be treated separately, which results in a set of parameter values that depend on the turbocharger rotational speed.

An example of this fitting process is illustrated on figure 2.23, where the reference points obtained from quasi-static measurements provided by the manufacturer are depicted along with the affine model estimation (2.22). This shows that the affine evolution expressed in (2.25) is verified experimentally. The associated set of model parameters $a(\omega_t)$ and $b(\omega_t)$ is provided on figure 2.24.

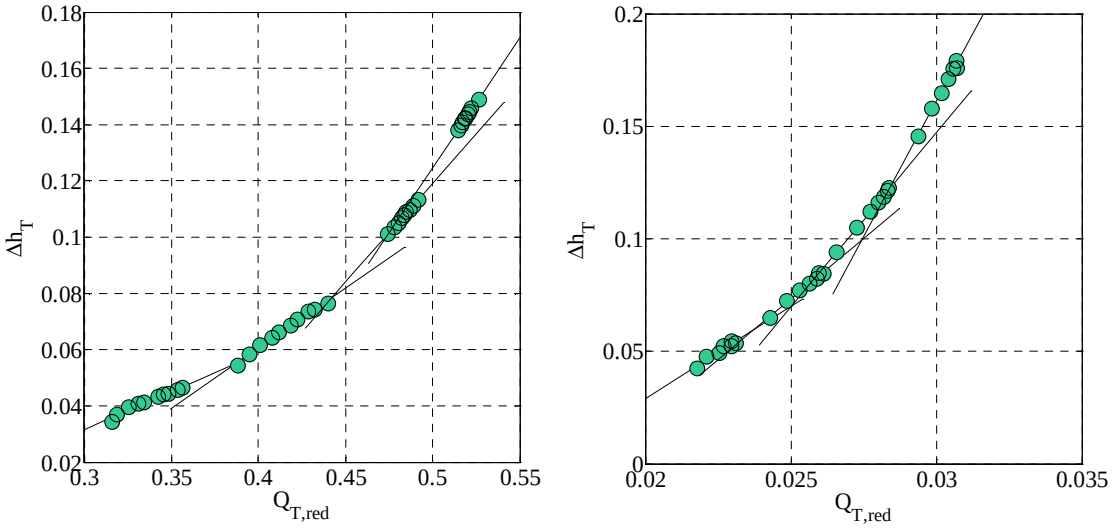

Figure 2.23 – Specific enthalpy exchange Δh_T versus reduced flow rate $Q_{T,red}$. From the supplier's data, one can obtain the reference values for specific enthalpy exchange (colored circles) and observe that it follows an affine trend (solid lines).

Since this theoretical formulation was obtained from physics-based turbo-machinery equations, the trend of the model parameters a and b w.r.t. the turbocharger rotational speed ω_t is known [87]: a and b are respectively affine and quadratic in ω_t. In particular, this means that at a standstill ($\omega_t = 0$), the specific enthalpy exchange Δh_T is a horizontal straight line, i.e. curves a and b both go through origo: $a(0) = 0$ and b(0) = 0.

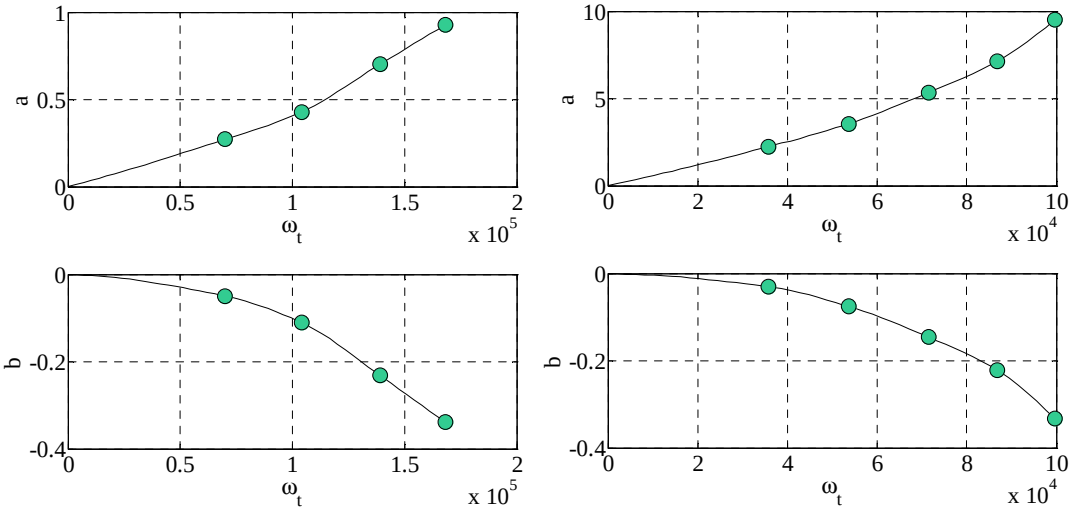

Figure 2.24 – Extrapolated model parameters a and b in (2.25) versus rotational speed ω_t. They are obtained by regression analysis on the reference specific enthalpy exchange (2.24) (colored circles).

As for the compressor, the practical example illustrated on figure 2.23 shows that these definitions may not be sufficiently descriptive. In particular, the regression analysis used to obtain $a(\omega_t)$ in (2.25) suffers from the same accuracy issue as with the compressor in (2.10) and the natural trend of a is closer to a parabola in ω_t than a straight line going through origo. This empirical observation, extensively tested on the thirty turbines available for this study, led to the use of a second order polynomial to describe the evolution of $a(\omega_t)$.

c) Isentropic efficiency $\eta_T = f_{T,\eta}(\Pi_T, \omega_t)$

Once the specific enthalpy exchange sub-model (2.25) has been calibrated on the manufacturer's experimental operating points, the isentropic efficiency η_T can be computed for any operating point $\{\Pi_T, \omega_t\}$ using (2.21). Then, the construction of the turbine isentropic efficiency data-map $f_{T,\eta}$ that is used in the turbine model (1.21) is straightforward.

As for the compressor, it can be noticed that the efficiency data-map $f_{T,\eta}$ directly inherits a significant part of its accuracy from the mass flow rate data-map since it is used in the specific enthalpy exchange sub-model in (2.25). This represents a particularly distinctive feature of the methodology that tends to increase the overall consistency of the extrapolated data-maps.

2.2.3.2 Extrapolation practical methodology

The similarities with the methodology used to obtain the compressor isentropic efficiency map (section 2.1.3) mean that the same issues are encountered. In particular, the weakest point of the methodology lies in the linear regression (2.25) used to identify a and b. Unlike the compressor case, no empirical knowledge about the curve shape proved to provide a sufficiently relevant accuracy criterion that could be used in an iterative scheme to fix the parameter values obtained by regression analysis, as was done in section 2.1.3.2. However, it was observed that if the values extracted from the mass flow rate data-map $f_{T,Q}$ (section 2.2.2) were used for $Q_{T,red}$ in (2.25), instead of the experimental values provided by the manufacturer, this naturally tends to line up $\Delta h_T(Q_{T,red})$. As such, it proved, through extensive tests on the turbines available for this study, to improve the determination of a robust set of values for slope a and the y-intercept b of the curve (figure 2.25).

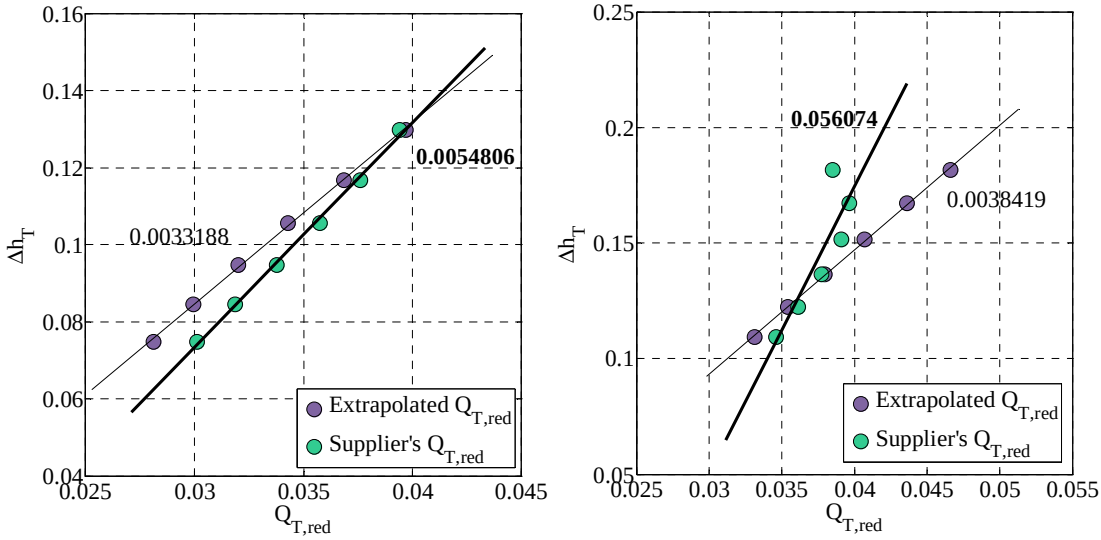

Figure 2.25 – Comparison of the use of supplier's data-map flow rate and extrapolated flow rate. The specific enthalpy exchange Δh_T is plotted versus the manufacturer's reduced mass flow rate $Q_{T,red}$ (green circles) as well as versus the extrapolated reduced mass flow rate (purple circles). The absolute value of the residual obtained for a standard linear fitting is also presented.

A validation example of a fully interpolated and extrapolated turbine isentropic efficiency data-map $f_{T,\eta}$ is depicted on figure 2.26. Again, no additional measurement campaign was carried out in the extrapolated area but the accuracy of the fit w.r.t the experimental measurements provided by the manufacturers confirms the physical foundation of the extrapolation model. Additional extrapolated data-maps are provided in section 2.2.3.4.

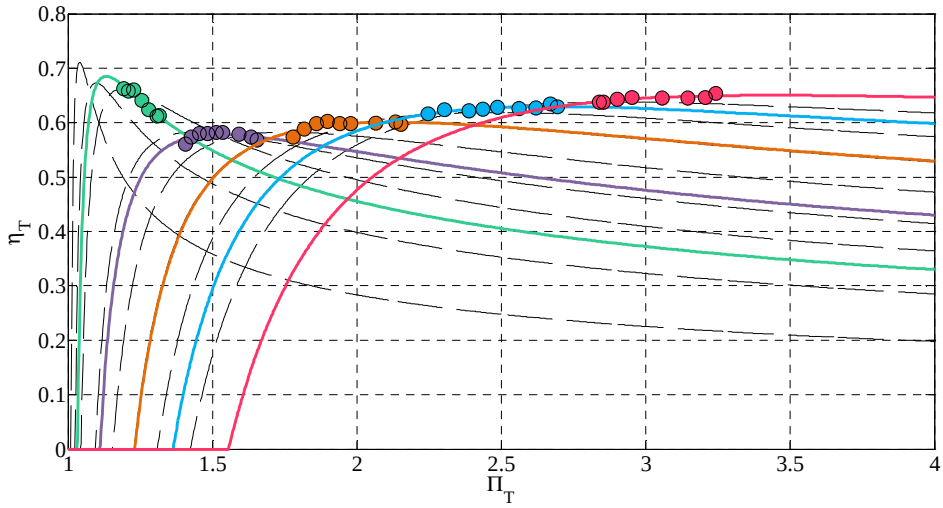

Figure 2.26 – Extrapolated isentropic efficiency η_T. The turbine isentropic efficiency is extrapolated over the entire expansion ratio range Π_T (solid lines) and compared to the reference values provided in the initial data-map (colored circles). Additional interpolated and extrapolated iso-speeds are also depicted (dash-dot lines).

2.2.3.3 Final algorithm

The complete methodology to compute the turbine isentropic efficiency data-map $f_{T,\eta}$ is summed up in the algorithm below:

Inputs: Experimental operating points $\{\eta_T, \Pi_T, \omega_t\}$ in the form of a finite number of turbocharger rotational iso-speeds. The turbine mass flow rate data-map $f_{T,Q}$.

Outputs: Complete extrapolated compressor isentropic efficiency data-map $\eta_T = f_{T,\eta}(\Pi_T, \omega_t)$

1- Compute $\Delta h_{T,is}$ for all the operating points $\{\Pi_T, \omega_t\}$ of the extrapolation range using (2.23).

2- Compute Δh_T for all the experimental operating points $\{\eta_T, \Pi_T, \omega_t\}$ provided by the manufacturer using the theoretical equation (2.24).

3- Identify a and b the parameters of the model presented in (2.25), treating all iso-speeds separately. $Q_{T,red}$ should be obtained from $f_{T,Q}$.

4- Interpolate and extrapolate the a and b values obtained at step 3 using a parabola that goes through origo in ω_t.

5- Compute Δh_T for all the operating points $\{\Pi_T, \omega_t\}$ of the extrapolation range using the extrapolated values of a and b and (2.25).

6- Compute the isentropic efficiency η_T as the ratio of $\Delta h_{T,is}$ obtained at step 1, Δh_T obtained at step 5 and the theoretical definition (2.21).

2.2.3.4 Additional examples

As previously suggested, a particular focus during the development of the methodology was to obtain sufficient robustness to interpolate and extrapolate the data-maps encountered in the automotive industry. The method was therefore extensively tested on a set of thirty turbines representative of a car manufacturer library. Relevant examples of performance are depicted below:

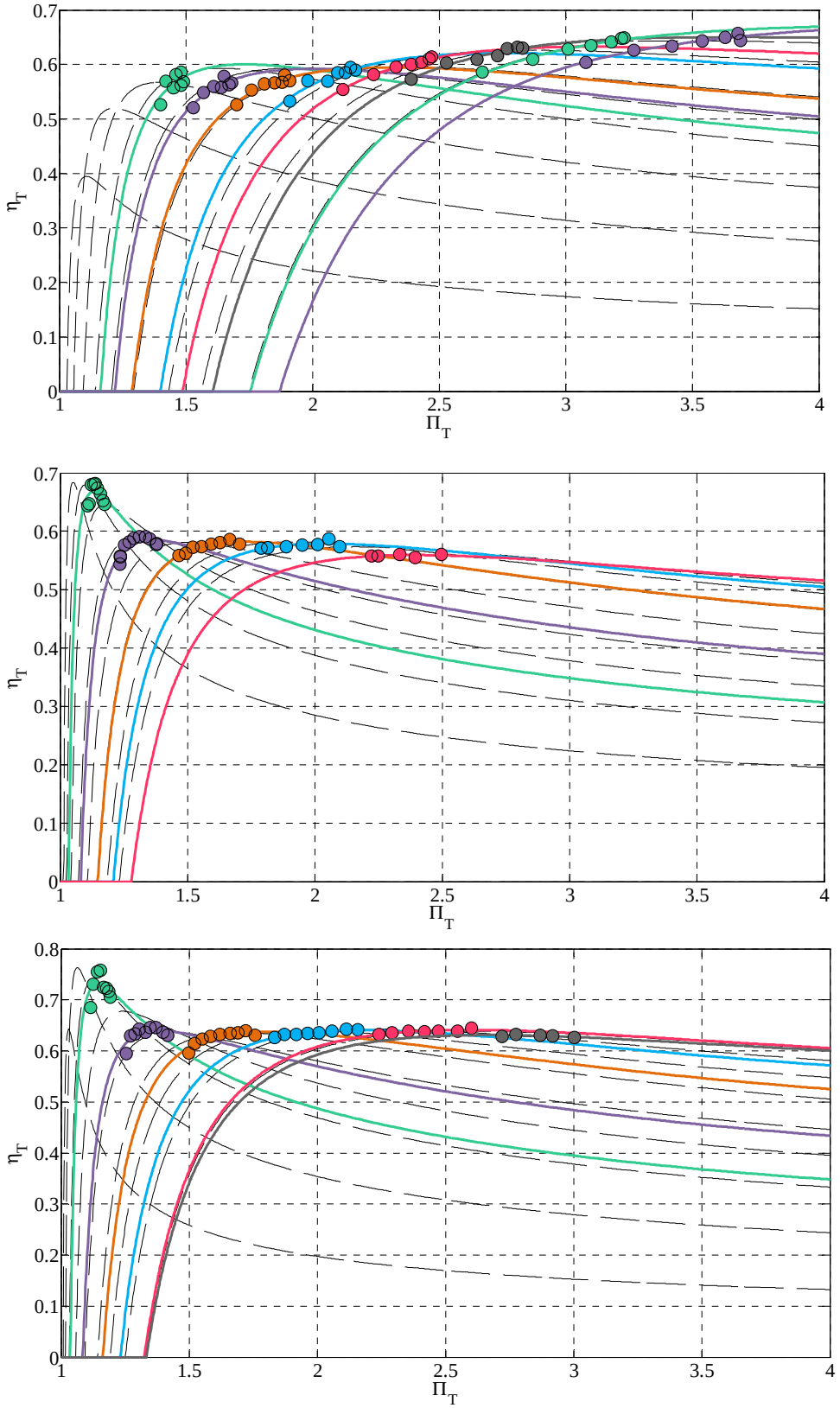

Figure 2.27 – Extrapolated isentropic efficiency data-map $f_{T,\eta}$. A complete extrapolated data-map is presented (lines). The results are in general good agreement with the supplier's data points (colored circles) which were used to fit the model.

2.3 Conclusion

Chapter 1 emphasized that the turbocharger sub-model is the cornerstone of mean value engine models, since it represents a mechanical coupling between the intake and the exhaust of turbocharged engines' air path.

The challenging objective of this study was to improve the extrapolation performances of current methods, while ensuring that any new proposals would still be based exclusively on a finite number of experimental operating points similar to those provided by turbo-machine manufacturers. This aim reflects the constant need to obtain an accurate mean value engine model early in the development process, before the first engine test bench trials even.

Starting from recent analyses of turbo-machinery equations [87,95], innovative physics-based methodologies for the extrapolation of the four compressor and turbine data-maps involved in a zero-dimensional turbocharger model have been derived (section 1.6). When the methods found in the literature were not satisfactory in terms of robustness or accuracy, they have either been improved or completely rewritten. *In fine*, a similar treatment is obtained for the compressor and the turbine, notably based on the linear trend of the enthalpy exchange and on the relation between the ideal and actual behavior of the turbomachines. These new proposals consistently rely on an original compromise between mathematics, empirical knowledge and physics that focuses on maximizing the robustness of the methodology. In particular, the four methods (2.1.1), (2.1.3), (2.2.2) and (2.2.3) presented in this chapter all associate an efficient theoretical extrapolation model[3] and a robust practical extrapolation algorithm that, together, provide much more robustness and accuracy than any equivalent method that can currently be found in the literature.

In the end, all the methodologies proposed in this chapter fulfill the initial objective so that, in practice, no dedicated test bench measurements are needed to extrapolate the four data-maps required in the turbocharger sub-model presented in section 1.6. A turbocharger rotational speed virtual sensor and a complete turbocharged spark-ignited engine model are presented in the following chapter. In both cases, steady-state and transient validation trials contribute to confirming the accuracy of the extrapolated data-maps obtained with these methods.

3 The actual operating range of turbo-machines is usually tighter than the extrapolation range presented here. In particular, phenomena such as surge usually limit this operating range and result in unpredictable turbocharger behavior, e.g. unstable flow [7,69,136,137]. Since these areas are usually well-known, additional constraints can be added directly in the control strategy, thus avoiding the need to take them into account during the extrapolation. It is this hypothesis that has been followed during this study. Still, if needed, an alternative approach would consist in afterwards correcting the extrapolated data-maps obtained at this stage by using a dedicated surge model [54,123].

CHAPTER 3

APPLICATION TO TURBOCHARGED GASOLINE ENGINES

In most standard gasoline engines, the sensor configuration usually only provides measurements for the ambient air temperature and the intake manifold pressure. On turbocharged engines, boost pressure and temperature measurements are usually added but no measurements are made in the exhaust manifold due to the harsh conditions that are encountered. Similarly, for reasons of safety and cost reduction, turbocharger rotational speed sensors that usually require drilling the casing are rarely put in place. However, in practice, this physical value is usually at the heart of the control and on-board diagnosis strategies. The knowledge of this physical quantity is of such crucial importance for car manufacturers that the development of virtual sensors has been the object of numerous patents filed in the past few years [1,58].

As underlined in chapter 1, another important challenge for the automotive industry is the use of simulation models in control applications. In fact, the automotive industry is still at present structured around non-model based control strategies and any additional efforts required to build a control-oriented model reduce the chances of a model-based strategy becoming a new standard. The cornerstone of the present study is to combine a mean value engine model with zero dimensional modeling in order to facilitate the construction of a physics-based nonlinear model that is compatible with the nonlinear model predictive framework.

This chapter addresses both issues with two practical examples of applications of the methodologies and developments presented in chapters 1 and 2. In particular, section 4.1 presents a turbocharger rotational speed open-loop estimator whose accuracy is directly inherited from the physics-based extrapolation methodology presented in chapter 2. Its steady-state and transient validation on a practical industrial case of application is also presented. Then, a complete control-oriented gasoline engine air path model is built and calibrated following the philosophy presented in chapters 1 and 2. Validation on both steady-state and transient experimental measurements are presented in section 4.2.

The major outcomes are: the design and experimental validation of an industrial turbocharger rotational speed virtual sensor that addresses both gasoline and diesel engines; a control-oriented turbocharger gasoline engine model that combines a mean value engine model and a zero dimensional air path model. This control-oriented physics-based model is especially designed to be used in nonlinear model predictive control laws (see chapters 5 and 6) that can be implemented in real time following the so-called explicit approach (see chapter 7).

3.1 Open-loop estimation of the turbocharger rotational speed ω_t

On most mass-produced turbocharged engines, most of the sensors are traditionally installed at the intake. Thus, in industrial engine management systems, the turbocharger rotational speed is commonly estimated by inverting the compressor sub-model, i.e. essentially the flow data-map $f_{C,Q}$ (figure 3.1). This data-map is usually provided by the manufacturer but it needs to be extrapolated and inverted to lower rotational speeds in order to cover the entire operating range of the engine.

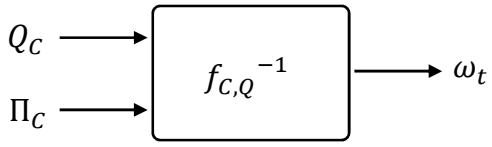

Figure 3.1 – Input/output description of the turbocharger rotational speed ω_t open-loop estimator. Q_C stands for the compressor mass flow rate and Π_C for the pressure ratio across the component.

Chapter 2 presented a new set of physics-based methodologies to extrapolate turbocharger data-maps from manufacturer quasi-static experimental measurements. In particular, assuming that the resulting compressor pressure ratio data-map $f_{C,Q}$ benefits from more accuracy, it is proposed to use it to estimate the turbocharger rotational speed ω_t. What follows therefore also contributes to validating the extrapolation strategy of the pressure ratio data-map $f_{C,Q}$ presented in chapter 2.

3.1.1 Estimation formulation

The open-loop estimator proposed in this study is directly based on the inverted compressor flow data-maps $f_{C,Q}$ obtained using the methodologies presented in chapter 2 (see section 2.1.2):

$$\omega_t = {f_{C,Q}}^{-1}\left(\Pi_C, Q_{C,red}\right) \tag{3.1}$$

where ω_t is the turbocharger rotational speed, Π_C is the compression ratio across the compressor and $Q_{C,red}$ is the compressor reduced mass flow rate (2.11).

Assuming that compression actually occurs, i.e. $\Pi_C > 1$, it can be seen that the compressor mass flow data-map obtained with the algorithm presented in section 1.2 is bijective (figure 2.12). Then, under this hypothesis on the pressure ratio Π_C, verified for relevant turbocharger rotational speeds ω_t, the inversion of $f_{C,Q}$ is straightforward (figure 3.2).

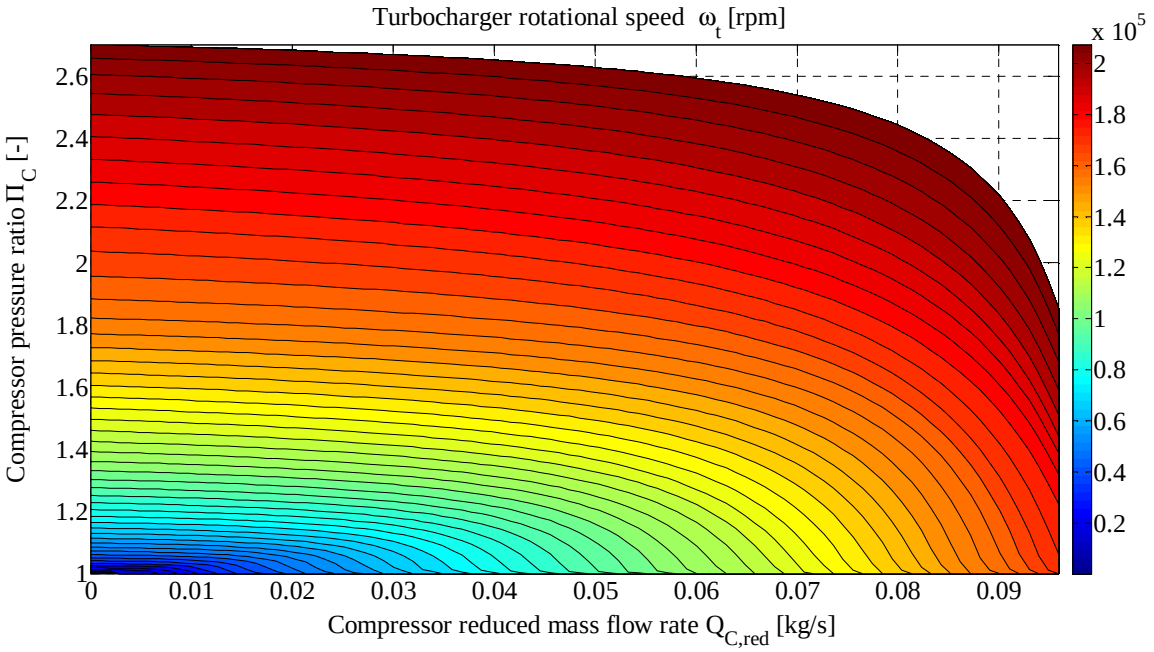

Figure 3.2 – Inverted compressor mass flow rate data map $\omega_t = {f_{C,Q}}^{-1}(Q_{C,red}, \Pi_C)$.

The physical inputs of the estimator are the upstream compressor pressure p_{avc}, the boosting pressure p_{apc} and the compressor mass flow rate Q_C (figure 1.1). In practice, they can either be measured or estimated by the engine management system. In the experimental validation stage that will follow, all the estimator inputs were measured using appropriate sensors, in order to avoid the risk of input estimation error. In particular, Q_C is provided by an air flow meter that is located upstream the compressor.

3.1.2 Steady-state performances

The first stage of the validation process involves the estimation of the turbocharger rotational speed ω_t at standstill conditions. Experimental test bench results are depicted on figure 3.3 and show an excellent agreement between the open-loop estimations and the measurements through the entire operating range. Figure 3.4 highlights that the absolute estimation error remains below 5,000 rpm for more than 98% of the 219 operating points presented here. At low turbocharger rotational speeds, the estimator tends to under-estimate the actual rotational speed, while at the highest speeds the estimation error is more homogeneously distributed.

In practice, the measurements (respectively estimations) of the pressures $\{p_{avc}, p_{apc}\}$ and of the compressor mass flow rate Q_C are uncertain. In particular, the turbocharger rotational speed ω_t estimations will be directly impacted by this uncertainty and it is of primary importance that the open-loop estimator should guarantee a certain level of robustness in those conditions. Thus, to conclude the validation of the steady-state performances of the open-loop estimator, a statistical analysis of the effect of these disturbances is presented on figure 3.5. The results of 1,000 trials, including the uncertainty of the sensors in the form of a gaussian distribution, are depicted along with the standard deviation obtained on each sample. The results show that the standard deviation on the turbocharger rotational speed ω_t remains below 5,000 rpm, while it is maximum at the lowest and highest rotational speeds.

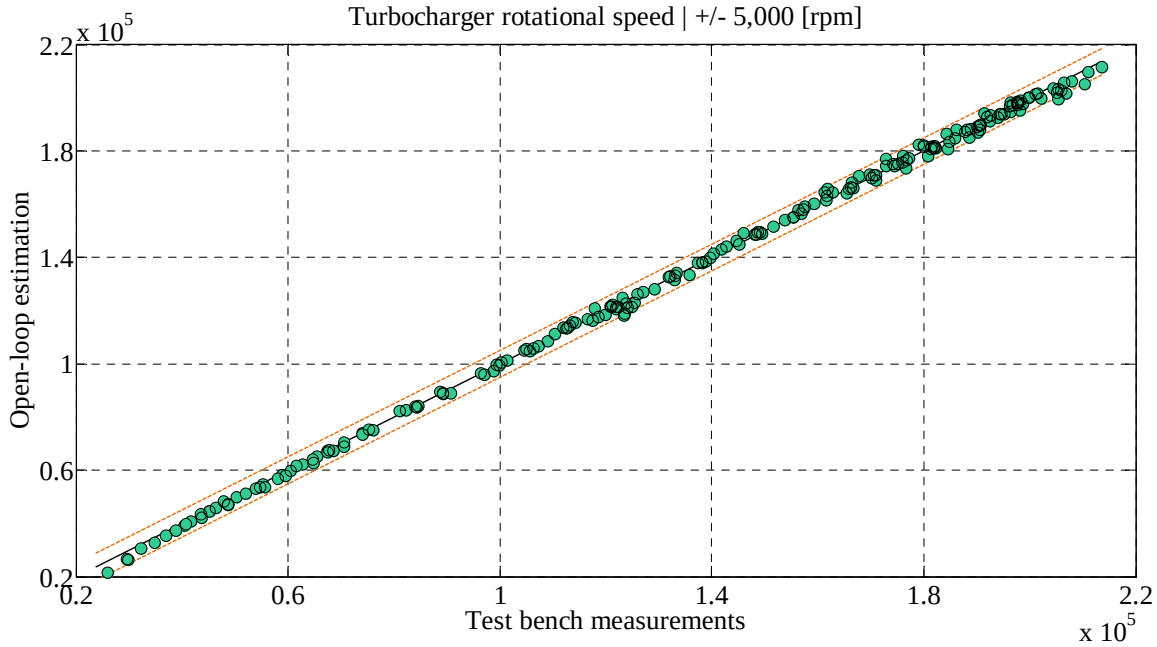

Figure 3.3 – Steady-state performances validation of the open-loop estimation using an inverted compressor pressure ratio data-map $f_{C,Q}{}^{-1}$, initially extrapolated using the methodology presented in chapter 2. Dashed lines represent a +/- 5,000 rpm estimation error: 98% of the operating points fall within this tolerance interval.

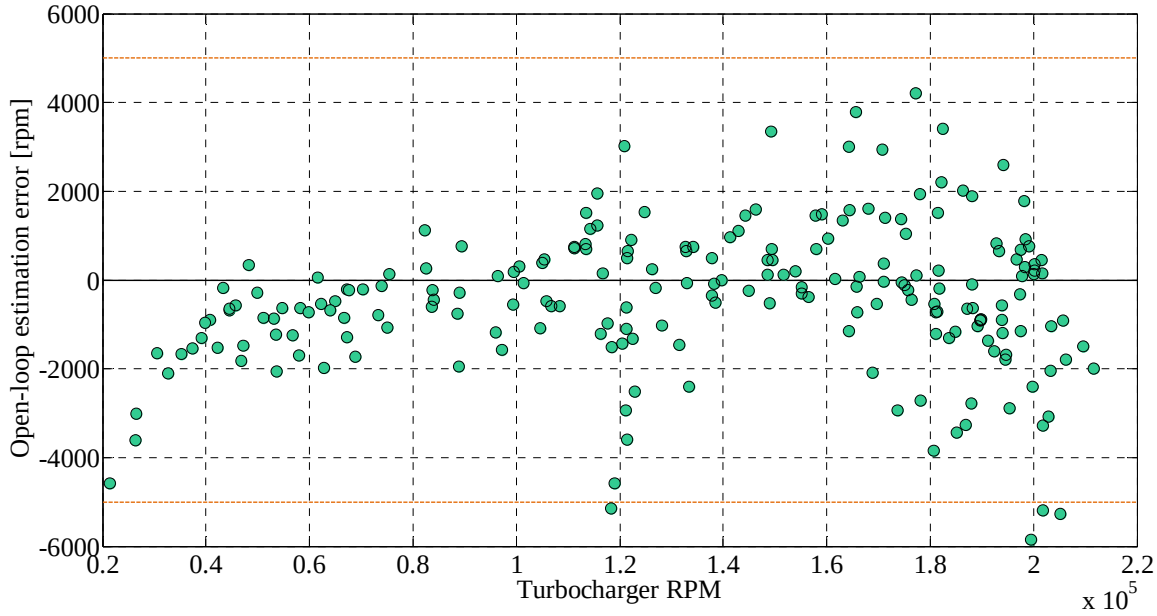

Figure 3.4 – Absolute estimation error versus turbocharger rotational speed measurements for steady-state operating points. The compressor pressure ratio data-map $f_{C,Q}$, extrapolated using the methodology presented in chapter 2, is inverted and used for the estimation in (3.1). The graph shows a homogenous distribution of the estimation error over the rotational speed range.

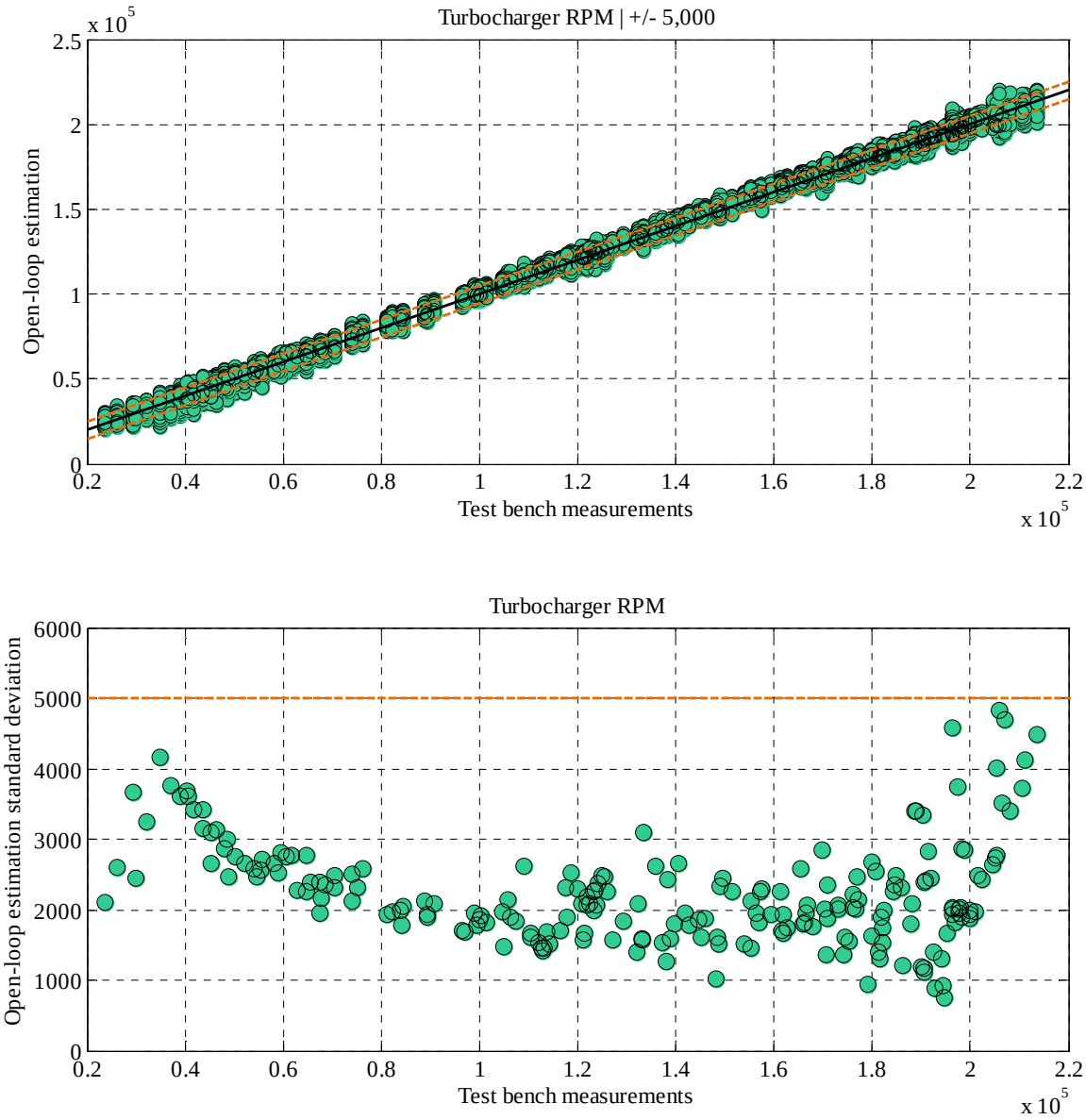

Figure 3.5 – Statistical analysis of the influence of sensor uncertainty on the open-loop estimation of the turbocharger rotational speed. Results are presented for 1,000 trials respectively including a 23 mbar and a 0.02 kg/s standard deviation for the pressure ratio Π_C and mass flow rate Q_C measurements.

3.1.3 Transient performances

The second validation stage consists in predicting the turbocharger rotational speed in real time and during slow transients on an experimental test bench. The cycle used at this stage consists in engine torque step changes that result in intake manifold pressure p_{man} and engine speed N_e transients (figure 3.6). It represents a sample of typical operating conditions of the test bench application considered for this study.

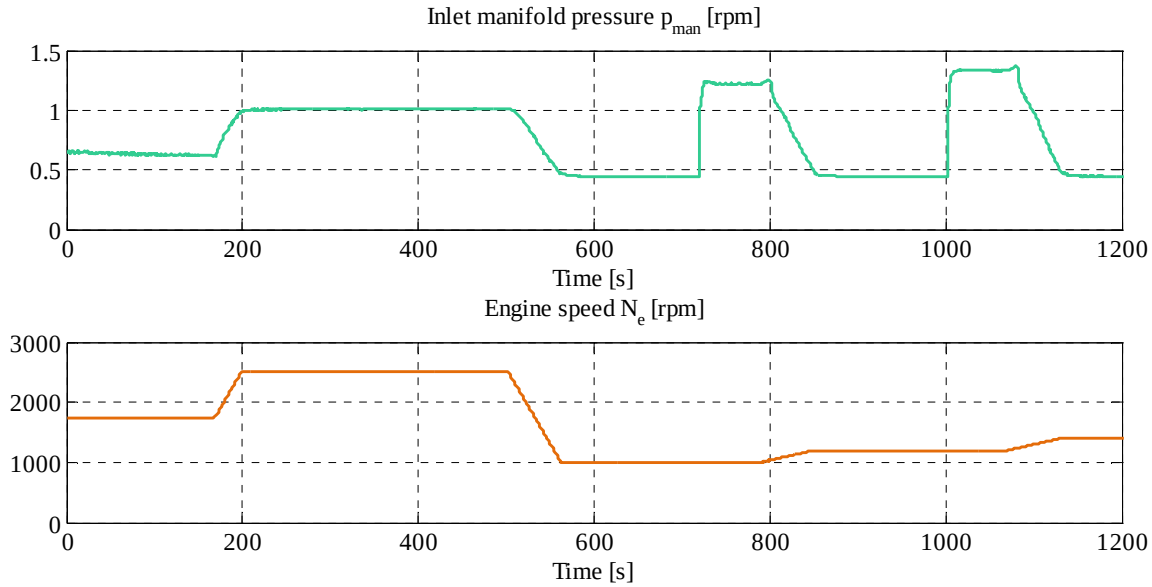

Figure 3.6 – Transient validation cycle: vehicle transient measurements of intake manifold pressure p_{man} and engine speed N_e.

The objective of this type of trial is to assess in an industrial framework whether a virtual sensor could be used to either diagnose the test bench turbocharger rotational speed sensor, or replace it in safety supervision processes. Experimental test bench results are depicted on figure 3.7. They show a general good agreement with the experimental measurements that were obtained from a turbocharger rotational speed sensor. In particular, the standstill phase of the cycle confirms the steady-state accuracy observed in the previous sub-section.

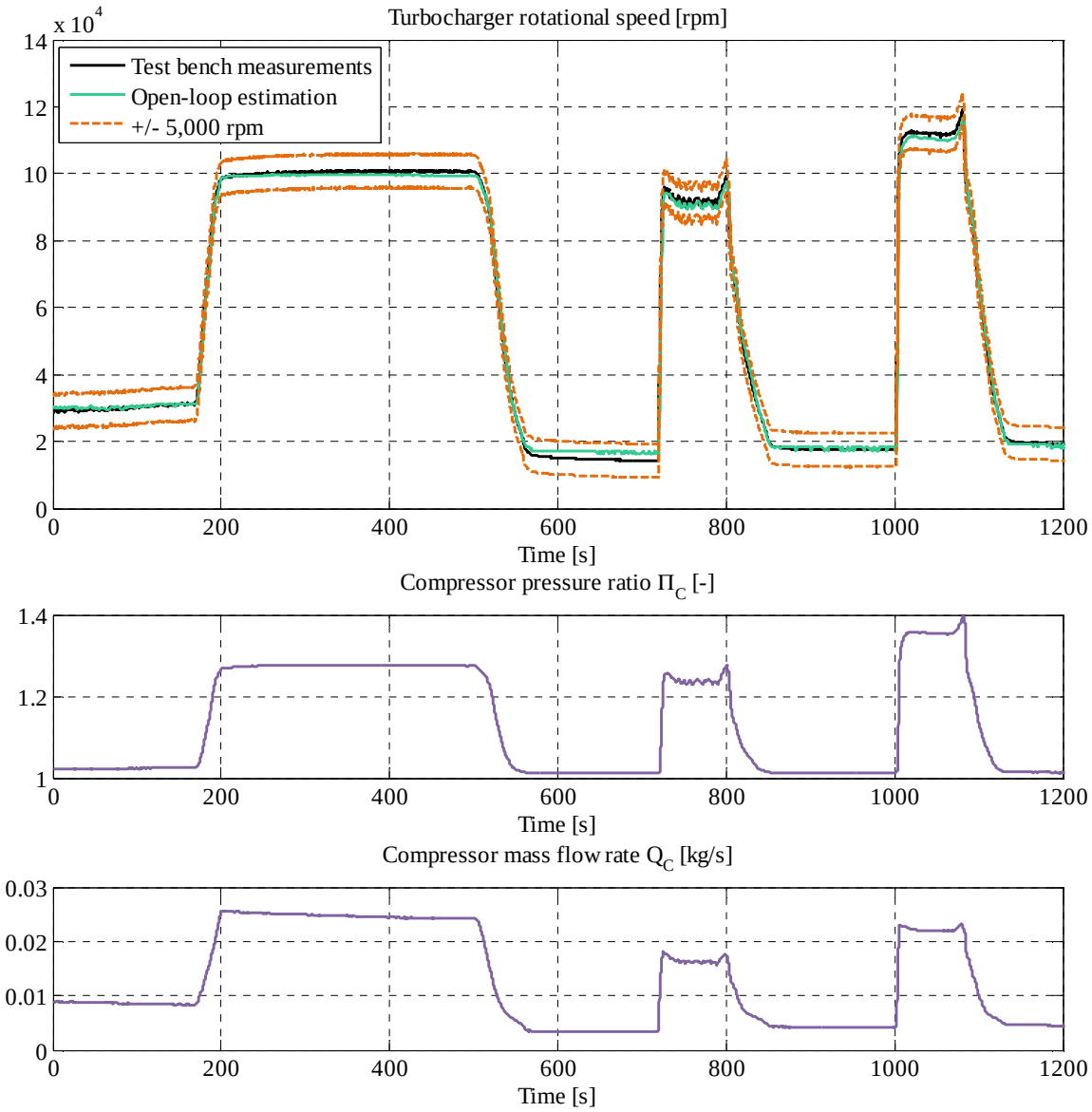

Figure 3.7 – Transient performances of the open-loop estimation of the turbocharger rotational speed ω_t on a test bench application. The inputs of the model are all measured (upstream and downstream compressor pressure and compressor mass flow rate). The rotational speed is predicted with less than 6% of relative error.

Figure 3.8 shows in greater detail how the rotational speed ω_t is estimated during the transient. In particular, while the estimation remains accurate during flow transients, the sudden increase in speed at time $t = 720s$ shows a significant estimation error, with a peak at roughly -18,000 rpm. Since a static map is used for the estimation, this underlines the existence of a neglected dynamic between the inputs and the turbocharger rotational speed.

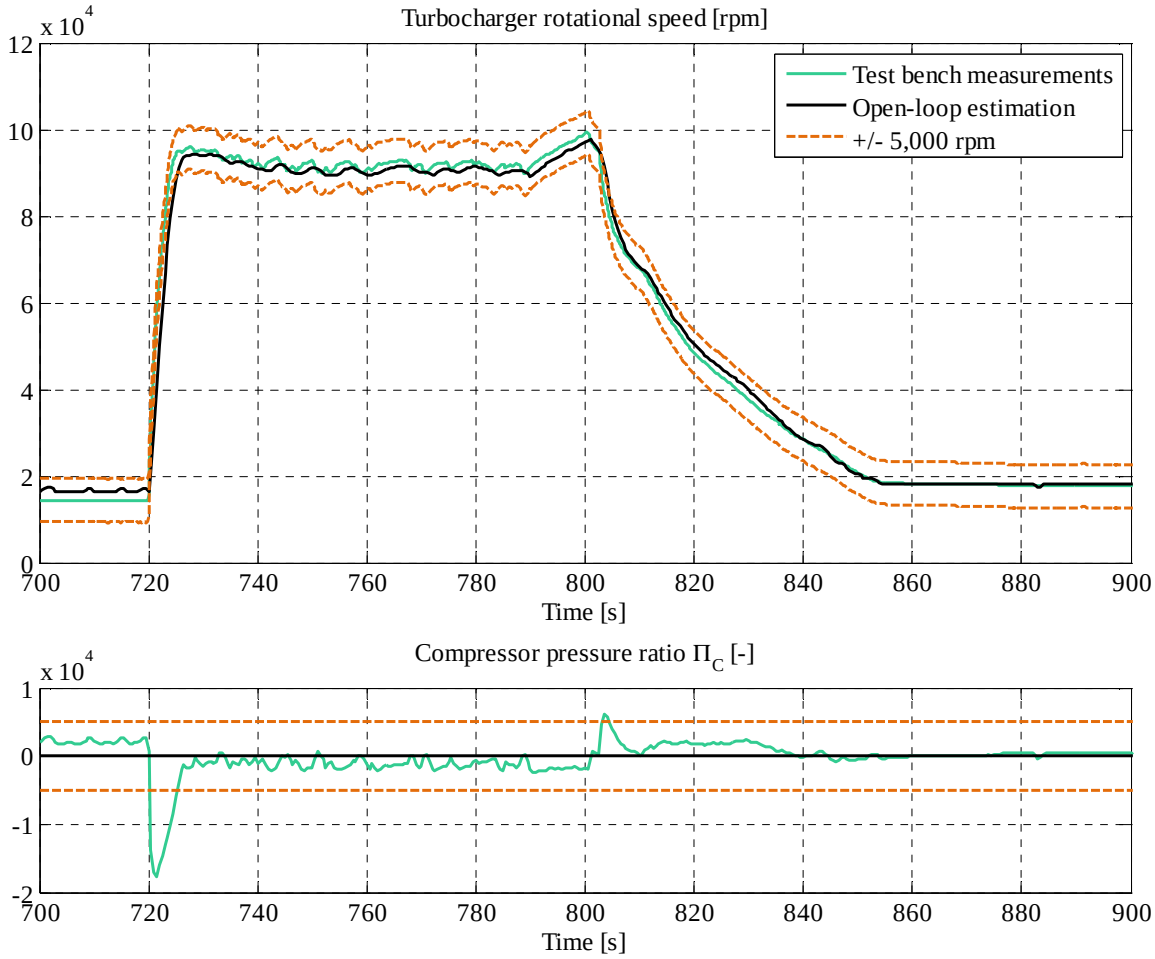

Figure 3.8 – Transient open-loop estimation error of the turbocharger rotational speed on a test bench application.

The overall accuracy obtained using a quasi-static data-map confirms that the actual time constants of the physical phenomena related to the compressor flow are small w.r.t. the turbocharger inertia [42,43,57,92]. In particular, it confirms that the compressor quasi-steady state modeling hypothesis made in chapter 1 is mostly relevant (section 1.6.1). Conversely, the lack of accuracy observed on fast transients highlights the limits of this widespread hypothesis.

3.1.4 Conclusion

This section has presented the performances of an open-loop estimator of the turbocharger rotational speed, based on the extrapolated compressor pressure ratio data-map $f_{C,Q}$ (section 1.6.1). The accuracy of the estimation is then directly inherited from the accuracy of this data-map. In this study, it was obtained from standard manufacturer experimental quasi-steady measurements using the new physics-based methodology presented in chapter 2. Compared to a potential closed-loop approach this open-loop estimation methodology (3.1) fundamentally benefits from its simplicity of implementation.

The estimator shows good performances both in steady-state and slow transient conditions from low to high rotational speeds. Combined with its very low computational requirements, this makes it a perfect candidate for the diagnosis or the replacement of turbocharger rotational speed sensors on automotive applications.

Since the estimation is based exclusively on compressor pressures and flow rate measurements, it addresses both fixed and variable geometry turbine configurations of gasoline and diesel engines.

Finally, the level of accuracy involved in this open-loop estimation also implicitly contributes to confirming the accuracy of the extrapolation methodology presented in section 2.1.2. It confirms the quasi-steady modeling hypothesis that will be used to implement a zero-dimensional compressor sub-model in the next section but also underlines its limits when considering fast transients.

3.2 Modeling a turbocharged gasoline engine

A preliminary requirement before applying a model-based control strategy is generally to implement a so-called control-oriented model of the system. This is particularly true when considering nonlinear model predictive control approaches since obtaining the nonlinear model is usually considered as a major issue [33,46,61,62,119]. We already suggested in chapter 1 that the automotive industry shows a very good maturity on this topic and that the combination of a mean value engine model and a zero-dimensional air path model could be particularly relevant to facilitate this stage.

In this section, starting from the turbocharged gasoline engine philosophy presented in chapter 1 and the turbocharger data-map construction methodology presented in chapter 2, a nonlinear physics-based model of the turbocharged gasoline engine involved in this study (figure 1.1) is implemented and validated. This model is intended to be used in the implicit and explicit nonlinear model predictive control laws presented from chapters 5 to 7.

3.2.1 Discretization of the air path

It is well-known that when building a control-oriented model, the objective is twofold: capturing the essential dynamics of the system, and keeping low computational requirements in order to allow its real-time implementation. In practice, these are two competing objectives. In fact, while the latter requires minimizing the number of states of the model, the former requires an exhaustive description of the dynamics of all the physical phenomena involved in the system. In order to overcome this issue, the engine modeling philosophy presented in chapter 1 provides a distinctive opportunity to control this trade-off thanks to the air path discretization stage (see section 1.2). In each control volume, only the relevant dynamics are retained, resulting in a minimum set of state equations that describes the air path dynamic (see section 1.3).

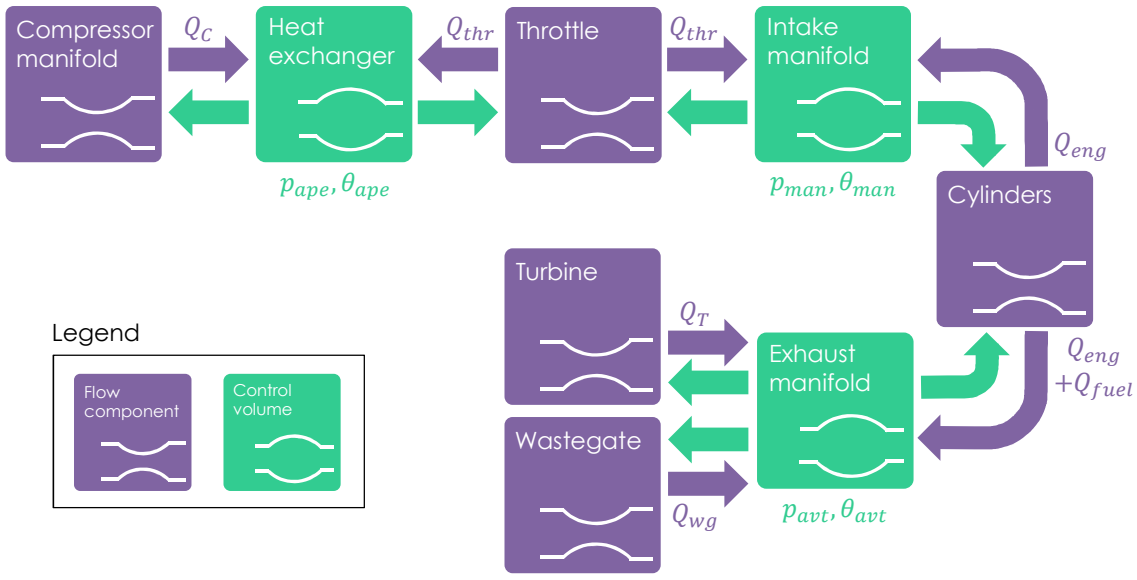

Figure 3.9 – Discretization of the air path of a turbocharged gasoline engine (figure 1.1). Three control volumes (in green) are considered. In each of them, only the pressure p is computed as a state of the model. The temperatures θ are assumed to be quasi-static and can therefore be described by algebraic equations. A fourth state, namely the turbocharger rotational speed ω_t, is required to describe the complete dynamic of the air path.

In the particular case of a turbocharged gasoline engine, four states are required to describe the pressure dynamic in three control volumes (the heat exchanger and both inlet and exhaust manifolds), as well as the rotational dynamic of the turbocharger (chapter 1). All are well-known as relevant dynamics when considering the air path control, while the temperatures in the control volume are commonly assumed to be quasi-static and modeled using algebraic equations or quasi-static maps [60]. Such an engine air path discretization leads to the model structure shown in figure 3.9.

It should be mentioned that the actuator dynamics, while having a significant influence on the air path [33], are neglected in the formulation proposed above. This is motivated by the fact that adding these dynamics to the model results in a significant number of additional states: usually one or two for each valve actuator. In a modeling framework, this shortage can easily be overcome by using the input measurements instead of the command signals. In the control framework that will follow from chapter 5 to 8, this assumption will be validated only if the controller can still hit the performance target.

3.2.2 Model formulation

Altogether, the model is governed by four nonlinear differential equations that govern the dynamic of the four states: boosting pressure, intake and exhaust manifold pressures and turbocharger rotational speed, respectively denoted p_{ape}, p_{man}, p_{avt} and ω_t (figure 1.1). The model inputs are: the throttle opening u_{thr}, the wastegate opening u_{wg}, the engine speed N_e , and the ambient pressure and temperature (p_{amb}, θ_{amb}).

In continuous time, the set of equations is given by:

$$\begin{cases} \dot{p_{ape}} = \frac{\gamma r}{V_{ape}} \cdot \left(Q_C \cdot \theta_{apc} - Q_{thr}(u_{thr}) \cdot \theta_{ape}\right) \\ \dot{p_{man}} = \frac{\gamma r}{V_{man}} \cdot \theta_{man} \cdot \left(Q_{thr}(u_{thr}) - Q_{eng}\right) \\ \dot{p_{avt}} = \frac{\gamma r}{V_{avt}} \cdot \theta_{avt} \cdot \left(Q_{eng} + Q_{fuel} - Q_T - Q_{wg}(u_{wg})\right) \\ \dot{\omega_t} = \frac{1}{I} \cdot (\Gamma_T - \Gamma_C) \end{cases} \tag{3.2}$$

where

- γ is the ratio of specific heats and r the specific gas constant,
- V_{ape}, V_{man} and V_{avt} are all known and respectively stand for: the volume between the compressor and the throttle including the heat exchanger, the volume of the intake manifold, and the exhaust manifold volume,
- Q_{thr} and Q_{wg} are respectively the throttle and wastegate flows, both obtained from the flow expansion equation (1.11) that involves the actuators' position,
- Q_C, Q_T, Γ_C and Γ_T respectively stand for the compressor and turbine flow rates and torques (section 1.6),
- I is the turbocharger mass moment of inertia and,
- θ_{apc}, $\theta_{ape} = \theta_{man}$ and θ_{avt} are computed using (1.18) and (1.14).

The model was discretized at a sampling time of 0.5 milliseconds using Euler's forward differentiation method and implemented on Matlab®.

3.2.3 Model calibration

Despite the intrinsically physical nature of the model proposed in this study, it is not possible to have access to all the parameters of the equations through physics or geometry. Hence it is necessary to identify the remaining ones from experimental input-output data. This stage is usually seen as calibrating the model (4.2).

3.2.3.1 Data set

In this study, an engine test bench and a vehicle were used to acquire respectively steady-state and transient data. In both cases, the complete set of pressures and temperatures, as well as the turbocharger rotational speed, were recorded following the sensor configuration presented on figure 1.1. The input signals of the model were also measured, except for the actual position of the wastegate, for which no sensor was available. Altogether, the steady-state data set contains 186 points which cover the entire operating range of the engine (figure 3.10). In the vehicle transients, engine speed varies from about 2,000 rpm to 6,000 rpm while throttle and wastegate openings are fully explored (figure 3.11 and 3.12).

Quasi-steady experimental compressor and turbine measurements provided by the turbocharger manufacturer were used as input for the interpolation and extrapolation strategies presented in chapter 2. The four data-maps $f_{C,Q}$, $f_{C,\eta}$, $f_{T,Q}$ and $f_{T,\eta}$ implemented in the turbocharger sub-model (section 1.6) are respectively presented on figures 2.5, 2.13, 2.19 and 2.26.

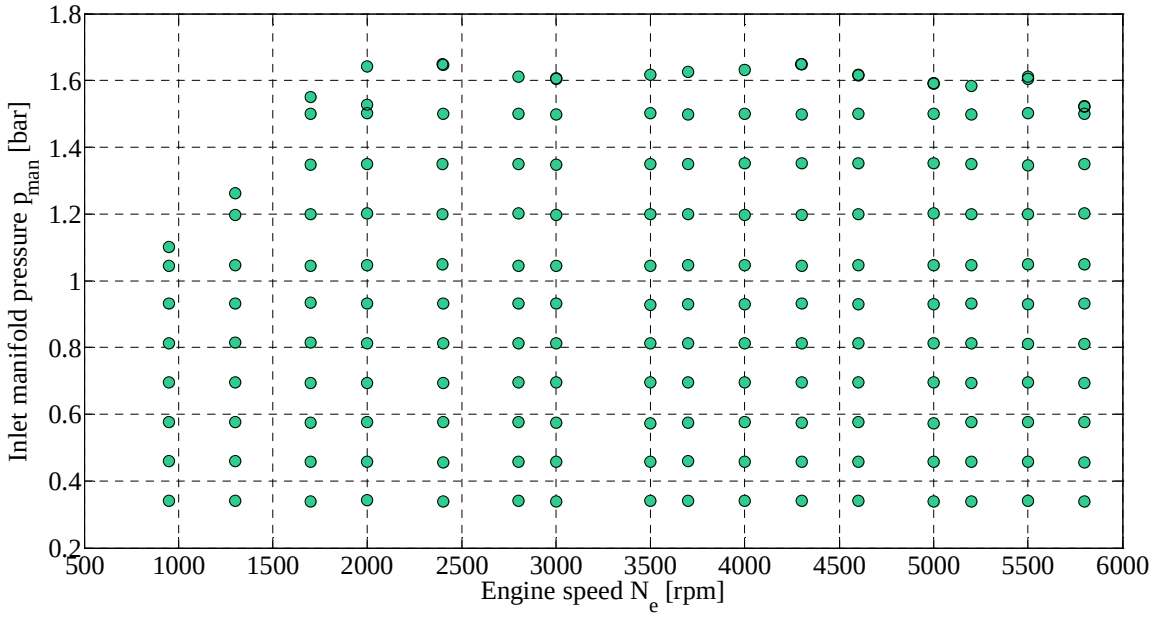

Figure 3.10 – Steady-state test bench operating points available for the study. Engine speed N_e and intake manifold pressure p_{man} are used to characterize the 186 steady-state operating points.

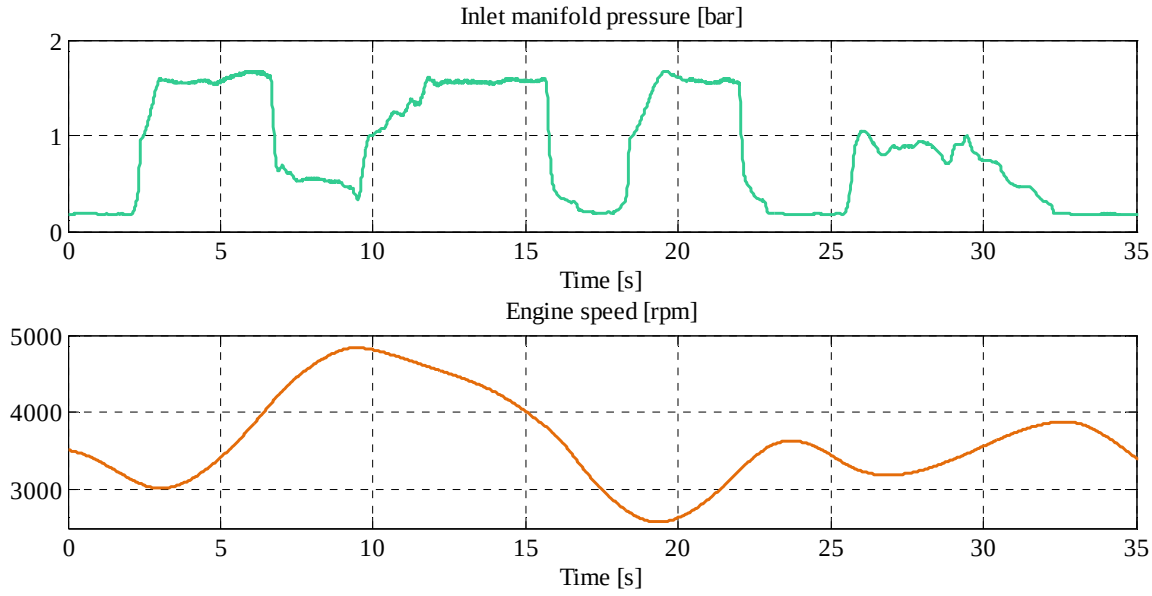

Figure 3.11 – Validation cycle #1 - Vehicle transient measurements of intake manifold pressure p_{man} and engine speed N_e.

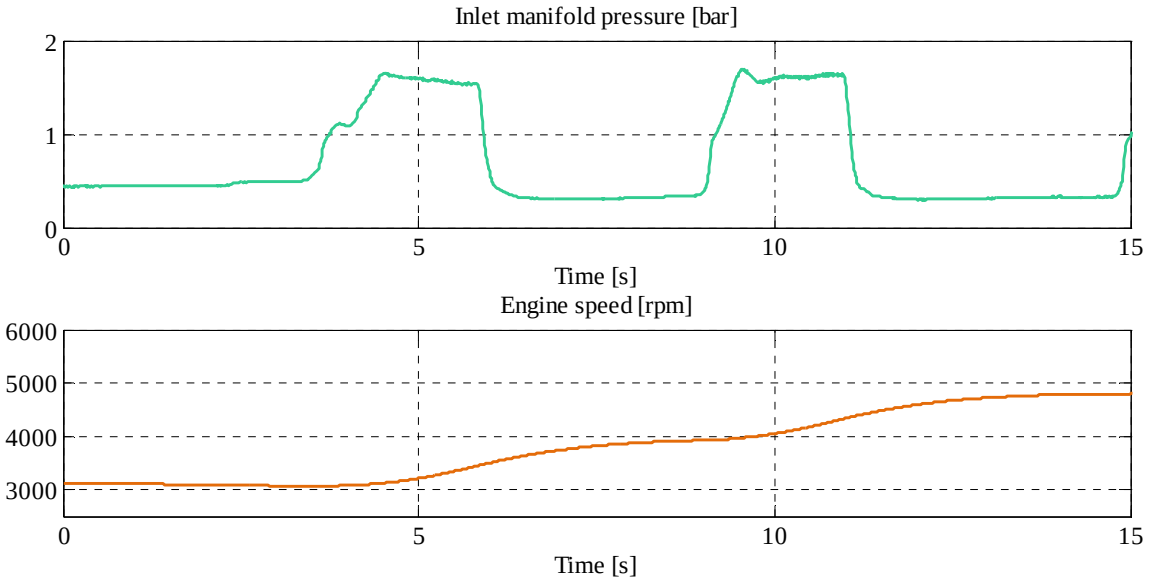

Figure 3.12 – Validation cycle #2 - Vehicle transient measurements of intake manifold pressure p_{man} and engine speed N_e.

3.2.3.2 Methodology

An automated identification process for the identification of turbocharged engine models based on first principles is not an easy task due to the severe nonlinearities in the equations involved in the model. In fact, when the model differential equations (3.2) are solved to evaluate the prediction error, it may become impossible to solve them numerically if for example, for some reasons, the model states become unreasonable [13] Moreover, internal combustion engine model identification usually also suffers from multiple local minima that require complex global optimization algorithm. These problems make the identification process reasonably difficult and currently argue in favor of a manual model calibration procedure even though attempts towards fully automated procedures remain a current research topic [14].

The modular description of the system presented above (figure 3.9) is well-adapted to manually calibrate one-by-one each component sub-model (e.g. compressor, valve actuators and cylinders) using steady-state experimental measurements (figure 3.10). However, initially, this usually leads to poor performances of the assembled model with respect to the experimental measurements even though each sub-model proves to be accurate. In fact, the accuracy can be significantly improved if the parameters are retuned using the complete engine model [14]. The parameter values obtained previously are then used as a warm initialization of the optimization routine. Finally, since the objective of a control-oriented model is to accurately capture the dynamic of the plant, a transient validation procedure usually completes the calibration stage.

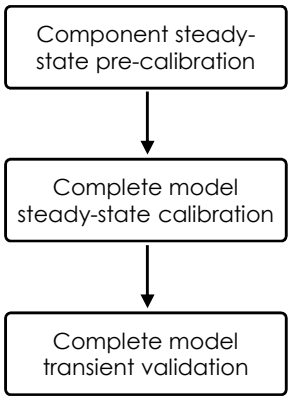

Figure 3.13 – Overview of the three-step physics-based model calibration methodology.

For this particular application, the optimal parameters were identified using a least-square algorithm initialized through prior knowledge based on the extensive experience of the different participants in the study. The optimal parameter value minimizes the sum of squared residuals over the 186 steady-state experimental samples (figure 3.10) while remaining in its nominal physical range, if such a range exists.

3.2.4 Steady-state performances

The steady-state performances of the model are obtained by simulating the 186 steady-state operating points available in the experimental data-set (figure 3.10) and the estimation error is analyzed on all the relevant physical values. For a turbocharged gasoline engine, they include the four states of the model $\{p_{apc}, p_{man}, p_{avt}, \omega_t\}$, the temperature in each control volume $\{\theta_{ape}, \theta_{man}, \theta_{avt}\}$ and the engine mass flow rate Q_{eng}. As the engine test bench available for this study did not include any turbocharger rotational speed sensors, no comparison with the model output could be carried out. Moreover, as stated before, the wastegate actual position could not be measured on the engine. Hence, since the model (3.2) does not

contain any actuator model, it is necessary to estimate this input during validation. This is achieved by minimizing the estimation error with the compressor outlet pressure experimental measurement (figure 1.1).

Pressure simulation results for the three control volumes of the model (3.2) are presented along with the experimental test bench measurements on figures 3.15.

- The boosting pressure shows no error at high loads due to the wastegate position estimation procedure described above. However, at low loads, when the wastegate sensitivity is too low, relative errors of about 5% appear.
- The other two pressures p_{man} and p_{avt} of the model are accurately estimated at high loads and the relative error remains below 5%. At low loads the least accurate estimation is the exhaust manifold pressure p_{avt} , for which the relative error locally reaches 17%.

To obtain an explanation for this phenomenon, it is interesting to have a look at how the exhaust manifold temperature θ_{avt} and the engine flow rate Q_{eng} are predicted. Figure 3.14 highlights the low relative error that is achieved on the engine mass flow rate Q_{eng}. The temperature simulation performances are presented in figure 3.16 and show that in most cases, the temperatures are predicted with less than 5% relative error. Altogether, it shows that the enthalpy flow in the exhaust manifold is accurately predicted and that the exhaust manifold pressure error spotted on figure 3.14 can probably be attributed to the turbocharger sub-model: the sum of the turbine and wastegate mass flow rates Q_T and Q_{wg} that exit from the exhaust manifold is too big.

Starting from this point, it becomes highly complex to understand in greater detail in which part of the sub-model the error is created. In fact, the difference between the experimental measurements and the simulation results is a global error which can usually be attributed to three different phenomena: pulse effects, thermal effects, and the extrapolation methodology that was used to build the data-maps (see chapter 2). The first two phenomena are only implicitly taken into account through the calibration process that actually tends to minimize this global modeling error, in opposition to determining the true value of the model physical parameters. As a result, the remaining part of the global error that can be attributed to each phenomenon cannot be quantified.

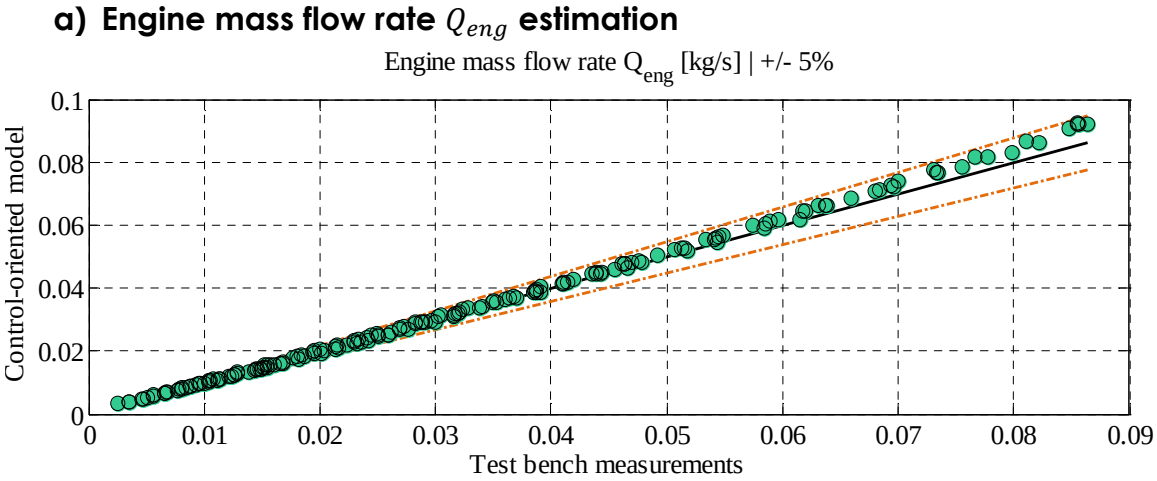

Figure 3.14 – Engine mass flow rate Q_{eng} estimation performances in steady-state operating conditions. A perfect model would give a 45-degree straight line. Dashed lines show the variation zones specified in the title.

b) Pressure estimation $\{p_{apc}, p_{man}, p_{avc}\}$

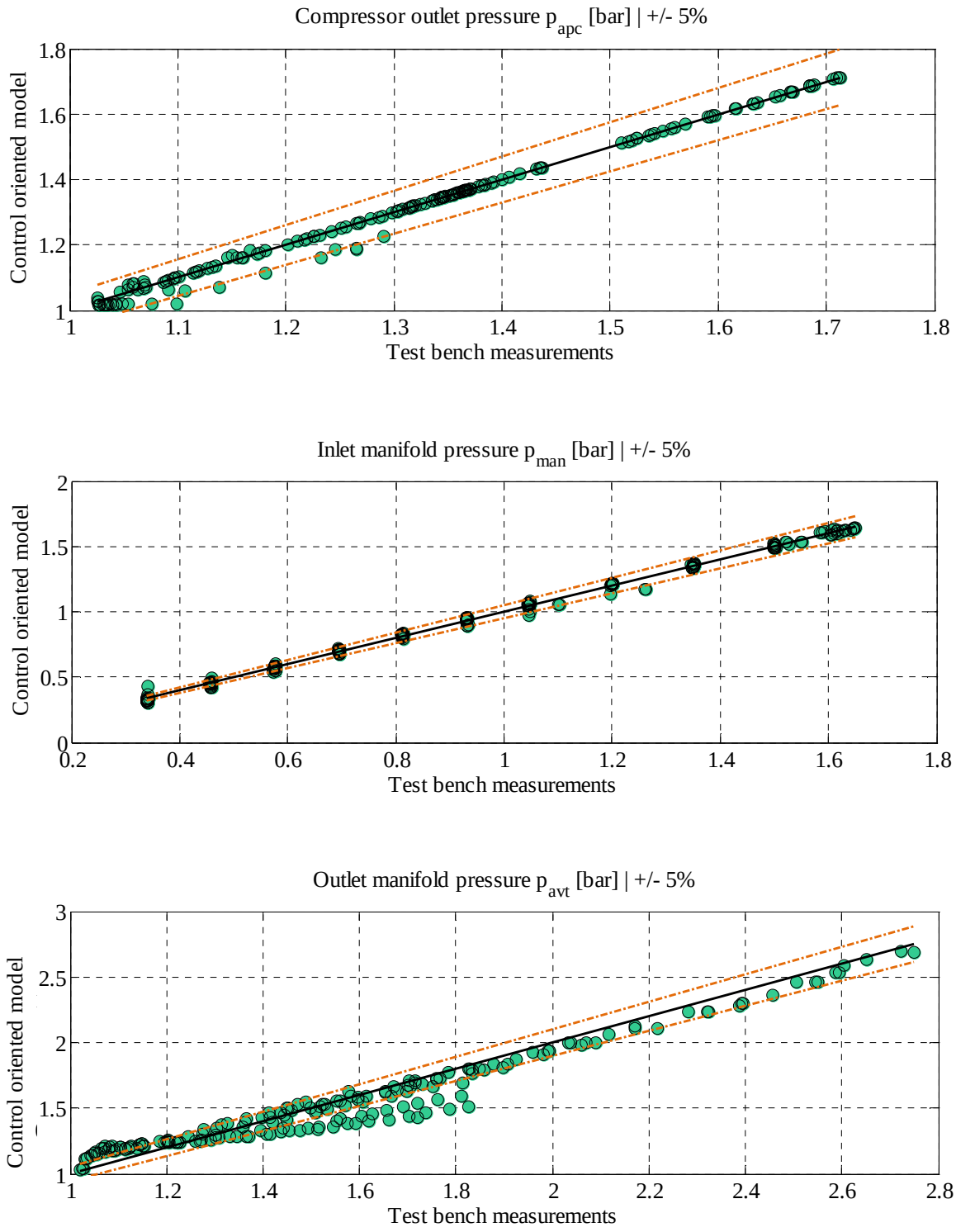

Figure 3.15 – Pressure estimation performances in steady-state operating conditions.

c) Temperature estimation $\{\theta_{apc}, \theta_{man}, \theta_{avc}\}$

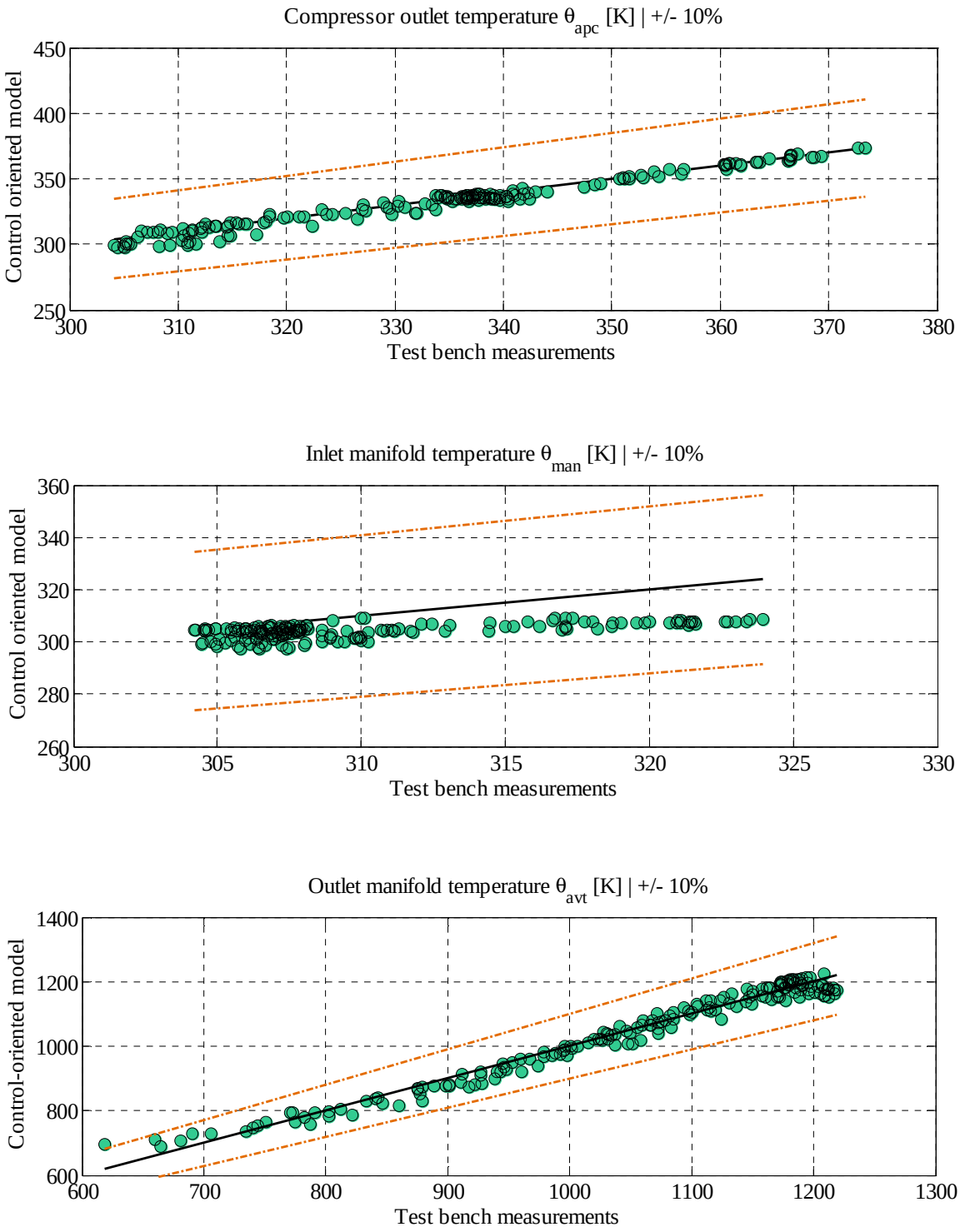

Figure 3.16 – Temperature estimation performances in steady-state operating conditions.

3.2.5 Transient performances

The dynamic properties of the model were investigated using a transient acquired on an actual vehicle. Again, no turbocharger rotational speed measurement was available during the trials. The objective here is to validate the overall accuracy of the model pressure estimation in opposition to the validation of a short horizon dynamic. This type of trial would indeed require a dedicated set of test bench trials such as actuator step transients. On figure 3.17 and 3.18, the three control volume pressure simulations are compared to the experimental measurements for the two different cycles (#1) and (#2) (figure 3.11 and 3.12). They show that the pressure dynamics are mostly well predicted on the overall cycle. This is a good indicator that the control volume sub-model parameters and the turbocharger inertia are appropriate since they govern the time constants of the model.

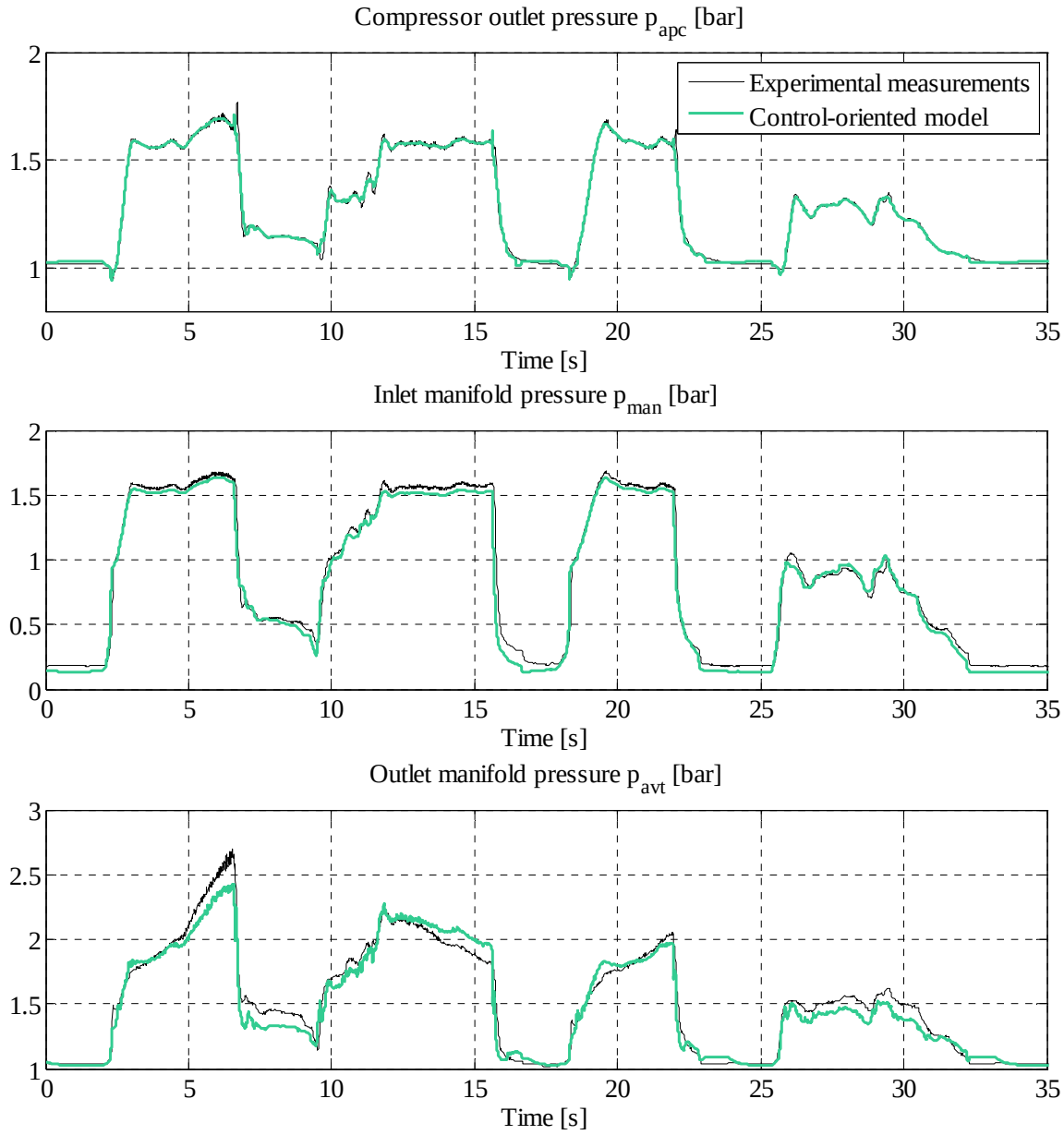

Figure 3.17 – Validation cycle #1: transient pressure estimation validation of the physics-based model (3.2).

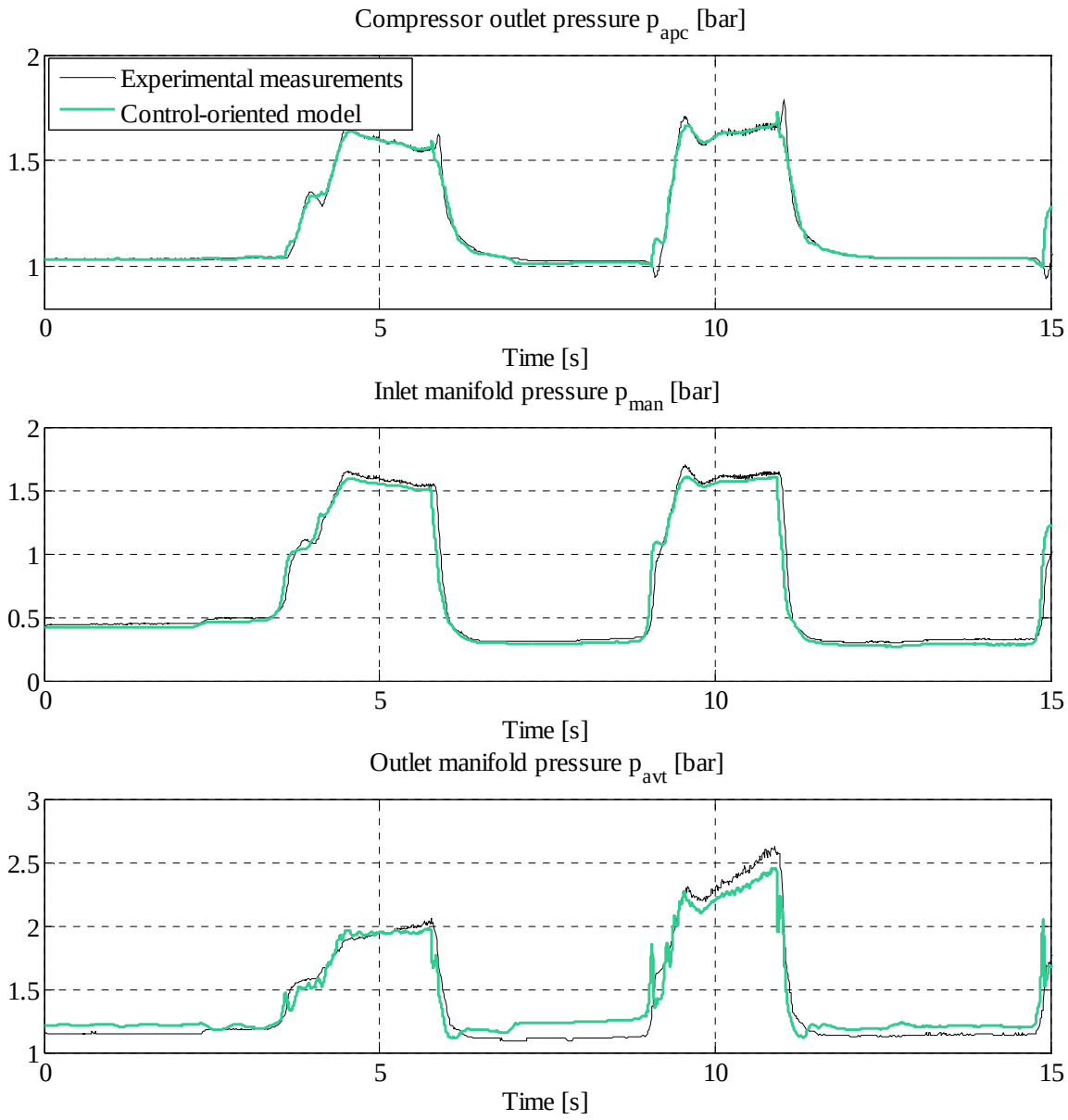

Figure 3.18 – Validation cycle #2: transient pressure estimation validation of the physics-based model (3.2).

3.2.6 Conclusion

The model presented in this section consist in the combination of the widespread mean value engine modeling and zero-dimensional air path modeling approaches. This philosophy makes it possible to build a simplified model of the engine in which the compromise between accuracy and complexity is explicitly chosen (chapter 1). In practice, this section shows that such a model can be calibrated from a standard set of steady-state test bench measurements that are commonplace in car manufacturer development processes. Moreover, once discretized and implemented, a minimum set of nonlinear differential equations already shows accurate steady-state and transient prediction performances. This makes it a perfect candidate when considering control-oriented applications such as nonlinear model predictive control [33,119].

3.3 Conclusion

Starting from the methodologies presented in chapters 1 and 2, two practical cases of application have been presented in this chapter.

The first one proposes to directly use the extrapolated compressor data-maps obtained in chapter 2 in order to estimate the turbocharger rotational speed of both turbocharged gasoline and diesel engines. This estimator is based on a simple open-loop structure that demonstrated a very high level of accuracy during experimental test bench trials. These performances have been confirmed in an industrial framework and for several engine technical definitions. As a result, the industrial implementation of this virtual sensor to replace physical sensors is under way at Renault S.A.S. Altogether, this example also provides evidence of the predictive capacity of the data-maps extrapolated using the new methodologies presented in chapter 2. It confirms the benefit of using a physics-based approach and underlines the growing importance of turbocharger data-maps in modern engine applications.

Other evidence of the accuracy of the compressor and turbine data-maps obtained using a physics-based approach (chapter 2) can also be found in section 3.2, where a complete air path model of a turbocharged gasoline engine is implemented, calibrated and validated on experimental steady-state and transient measurements. Altogether, the compromise that is obtained between computational requirements and accuracy makes it a perfect physics-based nonlinear control-oriented model.

***

Besides presenting a wide range of potential applications, these chapters also show a general modeling philosophy that can be followed when considering nonlinear control-oriented engine models. At the heart of this strategy are the mean value engine modeling and zero-dimensional air path modeling approaches presented in chapter 1. While the online computational requirements are currently still prohibitive in regards of current on board hardware, the modeling philosophy is already a perfect candidate for model-based control approaches that are mainly based on offline computation. As such, it represents our first step toward a systematic control design approach for turbocharged gasoline engines (figure 3.19).

Such a control strategy is presented in the second part of the manuscript, namely an explicit nonlinear model predictive control approach of the air path. [1]

Figure 3.19 – Overview of the control design approach proposed in this study.

PART 2

Toward a real-time implementable nonlinear model predictive control of the air path of a turbocharged gasoline engine

CHAPTER 4

OPPORTUNITIES AND CHALLENGES FOR ENGINE MODEL PREDICTIVE CONTROL

In the past few years, the increasing impact of economic considerations on engineering processes along with tighter environmental standards have led internal combustion engines to operate closer to their physical boundaries. In particular, the control of the air path has become more and more complex due to the introduction of innovative and more complex engine layouts (figure 4.1), that now result in multi-input multi-output constrained nonlinear systems with bounded inputs. In the presence of such challenging system, many traditional industrial control design strategies have difficulties in matching higher performance and cost objectives. This could motivate car manufacturers to introduce innovative control strategies that break with current approaches but in practice, the risk induced by a technological breakthrough usually favours minor changes. In particular, engine control development methodologies based on heuristic experimental test bench trials continue to play a major role despite their prohibitive cost. However, driven by the objective of remaining competitive in an increasingly globalised market, car manufacturers remain open to new proposals.

Motivated by the idea that any relevant new proposal in engine control should not only tackle the mathematical issues but solve the problem in its industrial context, this chapter starts by presenting the numerous industrial constraints that have to be taken into account when developing a new engine control strategy (section 4.1). They cover both hardware and software aspects but also provide general requirements that are important for the way control is practised by equipment manufacturers themselves. In the second part of this chapter (section 4.2), the most relevant contributions in advanced engine control will be summed up with an emphasis on linear and nonlinear engine model predictive control which, for practical cases of application, will be detailed in the following chapters.

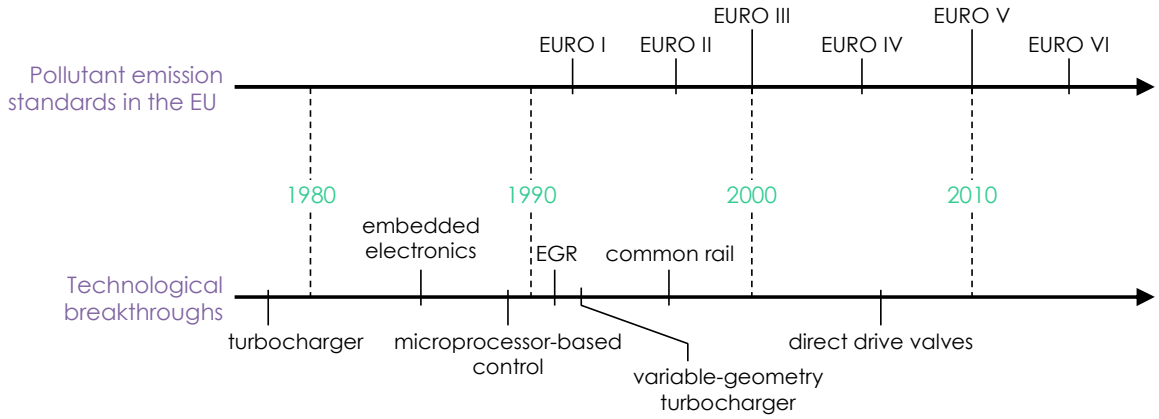

Figure 4.1 – Pollutant emission standards in Europe versus technological breakthroughs in internal combustion engine actuators since the 1980s.

4.1 Engine control research meets industrial constraints

The need for engine control did not wait for theoretical developments to find an answer. The first engine controllers in car passenger vehicles, for example, were purely mechanical. The compressor pop-off valve used in turbocharged engines is one example that remains in modern engines. Later, electronic control units (ECU) were introduced and enlarged the range of possibilities for controlling the engines. Rather than stopping to think about what new directions development could take, car manufacturers jumped at the opportunity to simplify what had become complex mechanisms. An electronic actuator along with a positioning data-map calibrated on a test bench was able to replace a complex mechanical system. Since then, the evolution of industrial engine control has mostly been incremental, with more and more look-up tables added to control an increasing number of actuators. The ever more stringent pollutant emission standards (figure 4.1) have therefore mainly resulted in an increasing number of operating conditions stored in these data-maps. Today, the complete control strategy of an engine represents thousands of pages describing the various tuning parameters and methodologies that have been implemented since the first ECU.

4.1.1 Engine control development process

Over the years, each car manufacturer and tier-one automotive supplier has developed and optimized a specific control development process that fits their needs and resources. However, from a high-level point of view, they all show a similar outline. It usually starts with steady-state test bench trials and terminates a few months later with the release of the software on the market. In between the different stages, described in the following sub-sections, numerous iteration loops slow down what appears to be a very expensive process (figure 4.2).

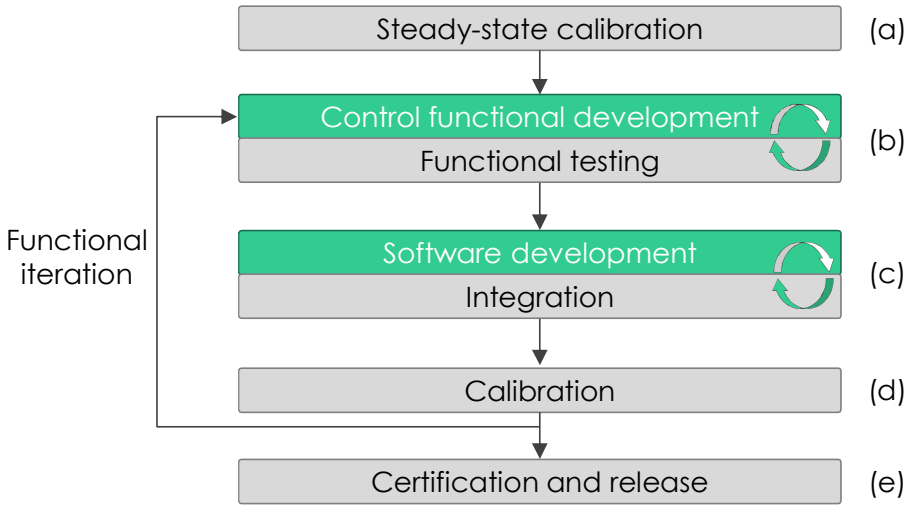

Figure 4.2 – General outline of the car manufacturers' engine control development process.

a) Steady-state engine calibration

When the engine is first started on the test bench, a pre-control phase that consists in mapping actuator positions at a coarse grid of engine speed and load points is initiated. The actuator positions are determined such that the first trade-offs on the steady-state behavior of the engine are established at this early development stage. In the worst case, this requires an exhaustive sweep of all the actuator positions but an appropriate experimental design usually allows a sparse exploration of the space. In all cases, it represents

a long and expensive experimental stage since a large part of the engine operating range must be explored. This phase is usually performed by insiders who have a thorough and quasi-intuitive knowledge of internal combustion engine behavior. In the end, it also provides a large experimental data-base that can for example be used to calibrate engine models such as the one presented in part 1 of the manuscript.

b) Control functional development and testing

In previous years and along with the growing complexity of engine technical definitions, the engine control architecture became modular. The core control strategy is now divided into functions (e.g. air and fuel paths) and sub-functions (e.g. after-treatment, exhaust gas recirculation, fuel injection) that usually correspond to actual sub-systems of the engine (figure 4.3). Theoretically, each of these functions or sub-functions can be individually replaced without impacting the rest of the control strategy. However, in practice, the interactions between the functions are so complex that a dedicated validation process is required after each update. This modular structure is completed by a high-level decision making strategy that delivers the set points (SP) to each sub-controller (figure 4.3).

Car manufacturers entrust this complex task to engine control teams composed of control engineers and internal combustion engine specialists. The primary objective of the engine control strategy is to match the steady-state trade-offs determined in the pre-control phase (a). The transient behavior of the engine is driven by the same functions but is tuned later in the development process. The control strategy must therefore provide enough flexibility to allow the engine to match the driving and pollutant emission standards when required. Usually this feature takes the form of a sufficient number of tuning parameters whose optimal values can be determined using an appropriate combination of test bench and vehicle experimental trials. Finally the last control development strategy constraint at this stage lies in the fact that the performances must be sustained throughout the lifetime of a large fleet of vehicles. In practice, the variability induced by the fact that the components will present differences in manufacturing and will age in different ways, requires the control strategy to show a certain level of robustness.

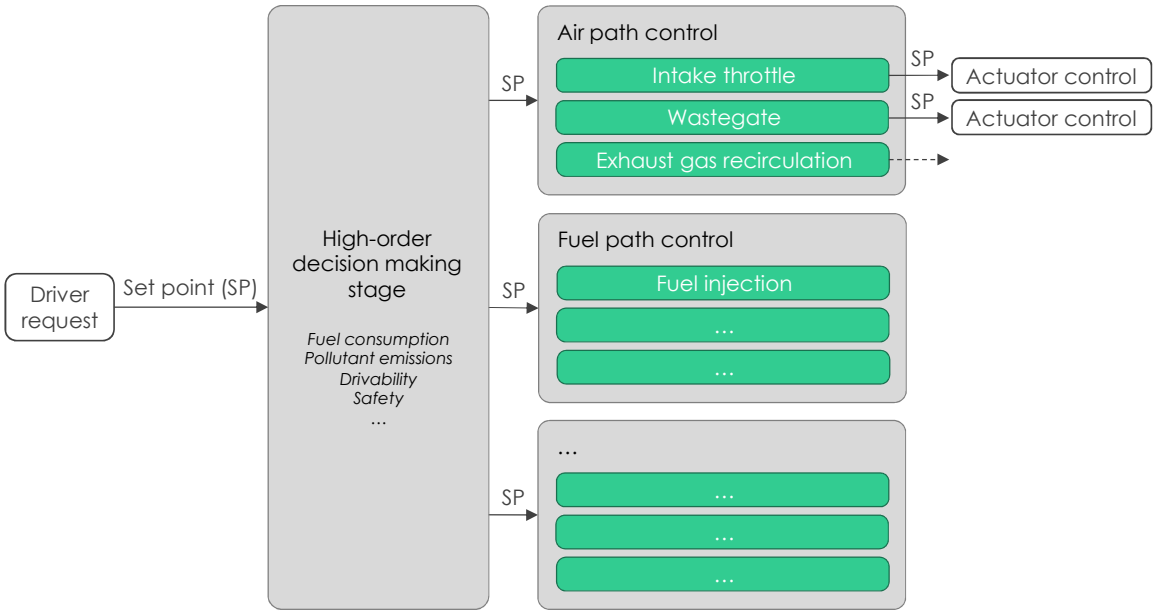

Figure 4.3 – General hierarchical architecture of the control engine software. The control is divided into a set of functions and sub-functions that can theoretically be replaced individually. A higher level controller provides the set points (SP) and constraints of each sub-controller based on the set point provided by the driver.

When the control strategy has been defined in the form of functional specifications, an individual functional testing stage is performed. Each functionality is progressively tested in simulation, on engine test benches and finally in a vehicle. The developers validate the behavior of each sub-controller, but also verify that the different control loops still deliver the expected performances once put together. The control strategy robustness to different ambient conditions and altitudes is usually also evaluated at this stage. In practice, this experimental validation is performed iteratively with the design of the control law (figure 4.2). High-level code such as Matlab® or Simulink® is typically compiled and integrated into rapid prototyping solutions that can bypass the standard ECU. This allows a fast evaluation of the control strategy, throughout its development process.

It should be pointed out that a substantial part of academic research currently focuses on providing new proposals for the design of one or more of these functional blocks.

c) Software development and integration

When the function specification has been written, software developers specify, code and test the desired sub-controller in the embedded software environment. These tasks are increasingly performed by a third party and/or achieved using auto-coding tools.

In practice, since subsequent re-entry into the software development process is extremely time-consuming and costly, the structure of the control is usually frozen at this stage of the development process. Only modifications of the tuning parameter values are allowed in the following steps. The key validation criteria for the software that is delivered at the end of this stage concern the memory and computational limitations of the ECU.

The final software is usually first integrated in an engine simulation environment in which a so-called Software in the Loop (SiL) validation is performed. The code is then tested and validated on engine test benches and on a vehicle.

d) Calibration

This phase consists in determining an appropriate value for all the steady-state and transient tuning parameters suggested above. The ultimate objective of this stage is to achieve a target trade-off between pollutant emissions, fuel consumption and drivability under emission legislation constraints. Efficient and intuitive tuning tools are required in order to facilitate this process, usually performed by test bench technicians. In particular, new tools must be well-integrated into the existing industrial calibration environment and methodologies.

If no calibration matches the target trade-off, the controller is classified as unacceptable and the entire software development cycle, starting from the control functional development stage is restarted (figure 4.2). This induces severe delays in the development process and must be avoided at all costs.

e) Certification and release

The certification of the software essentially concerns performing and documenting a given set of experimental tests that depend on the vehicle class and its geographical region of market release. Finally, once the control strategy and the software have been validated, it is released on the market, i.e. on a fleet of engines with a relative variability.

4.1.2 Industrial engine control requirements

This industrial control development process implies a certain number of requirements. Control strategies that do not respect these requirements are less likely to be industrialized. In the following sub-sections, only the main issues that are also related to air path control development are described. Further details and other specific requirements about the automotive industry can be found in [33,71,119].

a) Sensor set

The first question that arises when designing a controller often concerns the measurements and estimations that are available on the system for the control strategy, i.e. what physical quantities are known and with what accuracy. In the automotive industry, the sensor set can typically be chosen before the actual control development process starts.

In practice, this decision is the result of prior knowledge acquired on previous projects but is also highly motivated by the target cost of the engine. It is also chosen with diagnosis in mind, which generally also makes the addition of new sensors more complex. In fact, beyond the extra cost of the sensor itself, the risk of malfunction of the new sensor will also require rethinking part of the on-board diagnosis strategy.

b) Transferability

Motivated by substantial cost reductions, the standard practice in the automotive industry consists in maximizing the use of a given control strategy. This results in applying generic control architecture, functions and sub-functions to several engine technical definitions. While in practice, the complete control software cannot be recycled, the objective remains to maximize the number of functions or sub-functions that can be reused. As a result, a new control strategy is not likely to be carried through the entire development process described above (figure 4.2) if it cannot be applied to a sufficiently wide class of engines.

c) Tuning

Basically, the control system development process (section 4.1.1) can be split between design phases and calibration stages (figure 4.2). As suggested before, it is the responsibility of the group of engineers who design the control strategy to ensure that the control law will contain a set of tuning parameters that facilitate the task of the calibrators. In particular, parameters that are not physically meaningful or an absence of tuning parameters in the control law represent two important drawbacks when considering the adoption of a new control strategy.

This major constraint, when considering advanced control strategies, is motivated by the fact that there exists no exhaustive metrics that could be taken into account by the control law to describe such things as the drivability of a vehicle. A practical example of this situation is the fact that a given engine is typically used to propel a wide range of vehicles. Hence, adaptation to the different technical definitions (mass, performances) can only be achieved by taking into account the actual drivability of the different vehicles. Altogether, since manual calibration stages based on experimental trials cannot be avoided they should be made as intuitive as possible.

d) Computational resources

The amount of memory and the computational capabilities are usually very limited in passenger car ECUs in which the engine control software runs. Depending on the engine target and on the car manufacturer, figures such as 100 MHz and 6 MB of flash memory should be considered. In fact, the extreme conditions in which they are have to operate and the significant constraints on their reliability have slowed down the introduction of up to date hardware in the automotive industry. Moreover, since ECUs are used to control many features in the vehicle, they are usually heavily loaded. That is why in practice, the footprint of new control strategies should be as small as possible.

Finally, even if floating point arithmetic is becoming the new standard in many fields of application, including the automotive industry, some car manufacturers still use ECUs based on fixed point arithmetic. Similarly, the fact that the transition from 16-bit to 32-bit ECUs is not completed, should be taken into account when designing a control strategy for an industrial automotive application.

4.2 State of the art in engine air path model predictive control

Current production engine control strategies are obtained from a long iterative development process that is essentially based on heuristic experimental test bench and vehicle trials (section 4.1). The evolution of these strategies, mostly based on single-input single-output controller designs, is driven by an incremental engineering approach that started with the advent of electronic control units. More recently, several advanced engine control strategies have led to significant pollutant emission reductions [12,21,33,43,46,62,80,100] and have opened up a major field for both academic and industrial automotive research. In particular, a unanimously voted solution to the increasing complexity of internal combustion engines, namely the model-based control approach, has been the focus of most of the academic research and industrial developments in the past few years [19].

For all the stakeholders, the objective is twofold: handling the increasing complexity of modern combustion engines but also reducing the time and cost required to develop engine control strategies.

4.2.1 Engine model-based control approaches

The air path of combustion engines has been the subject of many examples of applications of model-based control strategies [19,21,71,114]. Because diesel engines are so popular (higher efficiency, better low speed torque, lower fuel consumption) and also represent a bigger challenge in terms of pollutant emission reductions, most of these studies are based on diesel engines. For example, [126] presents an overview of several controller approaches for the combined control of an exhaust gas recirculation (EGR) loop and a variable geometry turbine (VGT) on a diesel engine. A gain schedule multi-input multi-output controller, combined with a nonlinear feed-forward is presented in [12]. It is used for the control of the burnt mass fraction and air fuel ratio in diesel engines equipped with VGT. Many robust controllers of the air path of diesel engines have also been proposed, including one in [10,17]. It consists in a nonlinear controller with guaranteed robustness. The demonstration is classically based on the construction of a Lyapunov control function obtained from an input-output linearization. Other robust approaches were proposed in [16] and [8], both based on the definition of a linear parameter varying (LPV) model. Finally among many others, in [46], the authors propose a nonlinear controller based on flatness polynomials for the control of a turbocharged diesel engine.

In the meantime, model-based control of the air path of gasoline engines has been less popular. In fact, since at stoichiometric conditions the three-way catalyst achieves almost perfect conversion of the pollutants, the problem is usually considered as solved [14]. In practice, a few papers still present relevant model-based approaches that usually propose an alternative to the current industrial calibration methodologies. In [14] an overall model-based control strategy for the control of gasoline engines is described. It presents the high level control structure as well as the different loops classically involved in the control software. In [91], the author suggests a multi-variable control approach based on a mean-value engine model (MVEM) for a gasoline engine. The air path includes an EGR loop, variable valve timing (VVT) and tumble valves.

All these strategies show performance improvements in terms of pollutant emissions, fuel consumption and/or overall tuning efforts. They usually benefit from a multiple-input multiple-output philosophy but most of them suffer from the same drawbacks:

- They cannot directly incorporate performance specifications,
- They cannot handle input or state constraints,
- They have been designed to solve a specific problem while relying on knowledge that disqualifies everyone but a small group of specialists.

From a conceptual point of view, obtaining a control strategy that is devoid of complexity is the primary objective. Model-based control may not be the only solution to this end, but among all advanced control strategies, the past few years have shown an increasing interest in model predictive control (MPC), which can be considered the best example of this control philosophy. In particular, MPC has been applied on a new range of faster applications such that it now appears to be suitable for the control of modern combustion engines [33].

4.2.2 Engine model predictive control

The air path of internal combustion engines shows complex and coupled dynamics with bounded inputs. The inputs can either be physically bounded, like the opening of a valve which is limited to a given range of openings, or constrained by the purpose of avoiding damage to the engine (e.g. avoiding turbocharger over-speeding). In practice, in order to achieve the driving performances requested by the driver, the reference physical quantities' output y (e.g. engine torque Γ and speed N_e) must follow a given trajectory y^{SP} built under pollutant emission and fuel consumption constraints. This is a classical multi-objective problem for which optimal performances $\mathcal{S}^*$ along a given trajectory $\mathcal{T} = [k, k+N]$ can be obtained by solving the discrete finite horizon optimal control problem below:

$$\mathcal{S}^* = min_{u(.)}\, \mathcal{S}(x, y, u, \sigma, y^{SP}) \tag{4.1}$$

s.t

$$\mathcal{S} = \sum_{i=k}^{k+N} \mathcal{J}(x(i), y(i), u(i), \sigma, y^{SP}) \tag{4.2}$$

$$x(k+1) = f(x(k), u(k), \sigma) \tag{4.3}$$

$$y(k) = g(x(k), u(k), \sigma) \tag{4.4}$$

$$\underline{u} \leq u(k) \leq \overline{u} \tag{4.5}$$

where $\mathcal{S}$ is a given objective function to be minimized, $\mathcal{J}$ is called cost function, x is a vector of relevant states that describe the air path dynamics, f and g represent a discretized model of the engine, σ is a vector of exogenous inputs and $\underline{u}$ and $\overline{u}$ respectively stand for the lower and upper bounds on the manipulated variables.

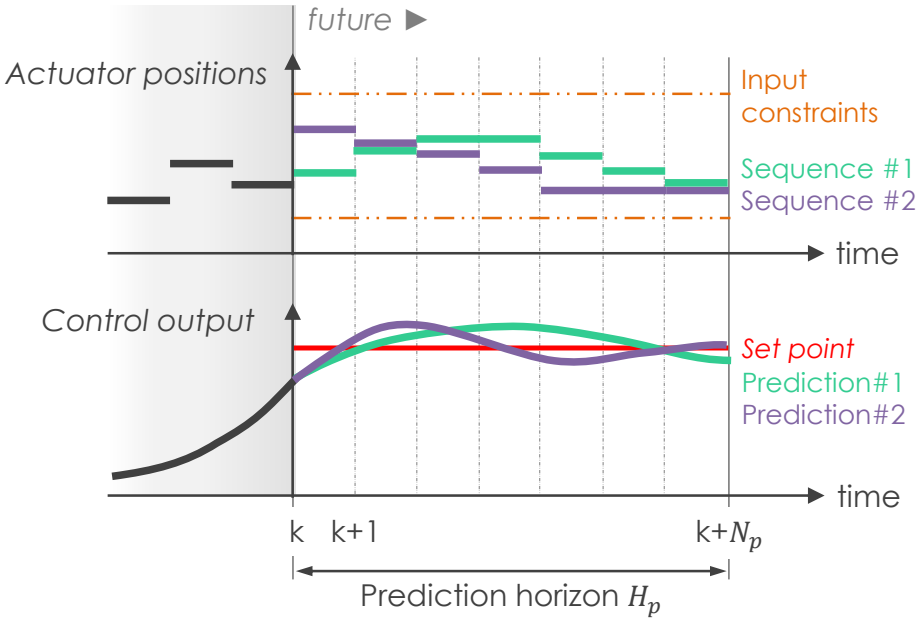

Figure 4.4 – Principle of the model predictive control approach.
An iterative finite-time open loop optimization is used to compute the optimal actuator positions w.r.t. the value of a given objective function $\mathcal{S}$ over the prediction horizon H_p .

In practice, solving such an optimization problem directly is not possible, even though attempts in this direction exist [114]. There are several explanations for this, among which the fact that this problem usually falls in the category of high-dimensional and non-convex optimization problems. This usually leads to prohibitive computational requirements with respect to actual engine control units. An alternative methodology to solve this problem is the so-called model predictive control approach [27,28,89]. Note that MPC does not solve the general optimal control problem (4.1) to (4.5) but leads to an approximate solution using the receding horizon principle (figure 4.4). This considerably reduces the computational requirements but still, in its simplest form, leads to a prohibitive computational load.

The approach was invented in the late 1950s and applied with success in the early 1980s to control multiple-input multiple-output complex linear plants with bounded inputs and constrained variables [9]. The first MPC industrial algorithms such as IDCOM (Identification and COMmand) and DMC (Dynamic Matrix Control, Shell® Oil) were developed for unconstrained MPC based on quadratic performance indices [32,110,111]. They were followed by algorithms dedicated to quadratic programs (QP), such as QDMC (Quadratic Dynamic Matrix Control), for solving constrained MPC problems [9] in the late 1980s. Later, an extensive theoretical effort was devoted to the analysis of such systems with the objective of providing conditions that would guarantee feasibility and closed-loop stability, as well as making explicit the intuitive relation that exists between MPC and linear quadratic regulation.

The first attempts to apply linear MPC to the control of internal combustion engines started in the early 2000s. In [115], a multivariable Generalized Predictive Control (GPC) was used for the air-management of a turbocharged diesel engine. This control scheme showed significant performance improvements with respect to a standard control scheme based on a double independent PI controller with anti-windup. A year later, in [113], a linear model predictive control was used for the simultaneous control of boost pressure and EGR rate of a turbocharged diesel engine. At that time, the benefits in terms of performances were clear but the real-time implementation of the controller was to remain an open question for the following two years. Finally in 2007, [47] presented a real-time implementable predictive controller for a real-world diesel engine. The approach was based on the online active set strategy presented in [45] and combined with a multi-linear engine model.

4.2.3 Engine explicit model predictive control

A relevant alternative to address the real-time implementation issue was presented the same year in [103] and proposed to combine a multi-linear diesel engine model with the so-called *explicit MPC* approach [10-12]. The latter consists in computing a piecewise affine control law that approximates the implicit MPC solution on a polytopic partitioning of the extended state space (further details are provided in section 4.3 below). In practice, the main drawback of this approach is straightforward and consists in the offline computational efforts required to approximate the implicit MPC solution in an n-dimensional state space. The idea itself, i.e. using linear programming for solving optimal control problems, was first proposed in the early sixties by Zadeh and Whalen [138] and by Propoi [107]. Since then, only a few authors have investigated the idea of combining MPC and linear programming [20,109], and even fewer have investigated the possibility of combining them in an engine control framework. The last relevant example is an engine explicit MPC scheme implemented on a standard modern ECU in 2008 [119].

Model predictive control can indeed be seen as a feed-forward approach and as such its performances are directly inherited from the model accuracy. In particular, the drawbacks of using poor models for feed-forward applications are well-known. In [34] it is summed up as follows: if the model information is too poor, it might be better not to use it at all. In fact, all these strategies show various enhancements in terms of performance but a common perspective is the need for more accurate engine models in order to improve

long-horizon predictions. Nonlinear model predictive control, by its ability to handle more complex models that can provide a more accurate description of the physics, is one way to address this issue.

4.2.4 Engine nonlinear model predictive control

Since its invention in the 1960s, linear MPC has become an increasingly popular control technique that is now used in more and more industries [52,108]. However, many systems such as internal combustion engines show an intrinsic nonlinearity that has to be taken into account in order to meet high performance requirements, product quality specifications and productivity demands. The linear paradigm cannot capture the process dynamics with sufficient accuracy and, in practice, a methodology to cope with nonlinearity must be put in place. Such an example is provided in [19], where the authors compare two different approaches to handle the nonlinearities of a turbocharged diesel engine air path, namely a multi-linear and a fully nonlinear MPC scheme. The conclusions of the study suggest that, while both philosophies lead to attractive tracking performances, the fully nonlinear control scheme shows a better potential, which would be revealed if the tuning effort were increased. In many industries, this inadequacy of linear control strategy to meet high performances has motivated the investigation of nonlinear model predictive control (NMPC) strategies.

In the NMPC framework, nonlinear models, multi-linear models or models that are linearized in real-time [29,31] are used to compute the optimal control trajectory, in opposition to MPC where a single linear model describes the system behaviour. While both approaches share a similar philosophy (figure 4.4), NMPC schemes are usually a lot more complex in practice. In fact, MPC problems usually fall into the category of linear or quadratic programming and are convex. Moreover, a wide variety of efficient numerical solvers and toolboxes are already available in the literature [63]. On the other hand, NMPC suffers from the challenge of guaranteeing a global solution to the optimization problem since convexity properties of the cost function to be optimized are usually lost. In practice, it is necessary to ensure that a close-to-global solution can be found within the real-time requirements. Further details about the problem formulation are provided in section 5.2.

The key properties of NMPC can be summed up as follows [4]:

- NMPC consists in minimizing a given objective function over a given temporal horizon,
- NMPC allows the direct use of a nonlinear model of the system,
- NMPC makes it possible to take explicitly into account state and input constraints,
- In NMPC, the predicted behaviour is usually different from the closed-loop behaviour,
- In standard NMPC, solving online an open-loop optimization problem is typically required and,
- In NMPC, the system states must be measured or estimated at each time step.

In 2006, the first applications of NMPC to an internal combustion engine were presented in [62], in which a third-order physics-based nonlinear model was combined with quasi-infinite horizon NMPC to control the air path of a turbocharged diesel engine. Two actuators, namely a variable geometry turbine and an exhaust gas recirculation valve, were simultaneously controlled to track an air-fuel ratio and EGR-rate trajectories. This first attempt showed an enhancement of the performances with respect to two other control strategies: a linear state feedback controller and an input-output linearization based control strategy. However, the real-time implementation of each controller was not addressed.

The online computational requirements issue of engine NMPC was first addressed in [46] and [29-31] with the control of the air path of a gasoline engine. In the former, the optimization problem was solved using a direct multiple shooting approach in which the intermediate states are treated as unknown variables, together with the control trajectory parameters. In [29,31], the nonlinear engine model was linearized in real time around the current operating point, enabling the use of a standard MPC scheme within a nonlinear

framework. While the nonlinearity issues are addressed in different ways, both studies show that NMPC can lead to significant improvement in gasoline engine control. A third approach was presented in 2009 in [104] for the control of a turbocharged diesel engine air path. The proposal combines a linear parameter varying model with the online active-set strategy presented in [45]. Again, the conclusion highlighted the fact that the NMPC scheme shows better tracking performances than a standard linear MPC in the two standard variables of fresh air mass flow and boost pressure.

General fast nonlinear model predictive control, that addresses the online computational requirements issue, has been an expanding field of research in the past few years. One of the approaches that emerged, besides explicit NMPC which was indeed never applied to internal combustion engines, involves recasting the primary optimization problem. This consists in retaining only the main degrees of freedom while minimizing the number of parameters. The approach is usually known as parameterized NMPC and has been successfully applied to the control of the air path of turbocharged diesel engines since 2009 [96-100]. In practice, the nonlinear model is used as a black-box for the computation of the optimal solution by a predictive controller that explicitly takes into account input constraints. The optimization routine is reduced to a low dimensional optimization problem that leads to a minimum computational time footprint. The tracking performances, when compared to those obtained with existing ECUs, show a great improvement and thus motivate further investigations. In particular, the use of a physics-based nonlinear model rather than an eighth-order data-based model is suggested by the authors.

4.3 Explicit model predictive control

Solving a nonlinear optimization problem online is known to be computationally overwhelming. This truism, either right or wrong, has traditionally limited the use of MPC in an industrial framework to slow processes such as chemical plants [4,52,108,110,111]. However, in practice, several approaches have also provided a real-time solution for the control of internal combustion engines (section 4.2). Among these approaches, computing the explicit solution of the optimization problem offline circumvented this issue [11,18,103].

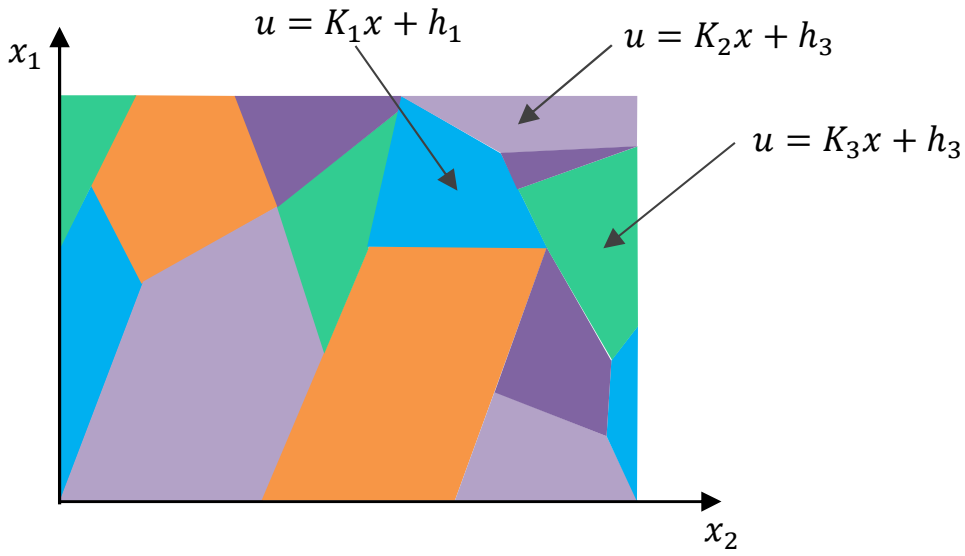

Figure 4.5 – Principle of the explicit model predictive control approach in a 2-dimension extended state space. The behavior of the implicit MPC law is approximated by a piecewise affine control law, defined on a set of a polytopic regions.

The explicit MPC approach consists in approximating the solution of the implicit MPC problem by a piecewise affine control law, defined on a polyhedral partition of the extended state space (figure 4.5). The latter usually includes the states of the model, the set points and a set of relevant exogenous inputs. In practice, this approximation can be as close as possible to the optimal solution of the problem and the explicit state feedback law that is obtained simply eliminates the need to execute a numerical optimization algorithm in real time [11,16,18]. On the other hand, it is also well-known that the curse of dimensionality represents its primary drawback, since the memory required to embed the numerous linear control laws can quickly become prohibitive for high dimension systems. However, generally speaking, the numerous benefits of an explicit solution make further investigations worthwhile. In fact, besides its low computational footprint, explicit MPC also allows verifiability of the implementation, a crucial property for the certification of safety-critical applications. It also leads to low complexity software since the core of the strategy consists of a simple look-up table. Finally, when considering NMPC the prospects are even higher since computational efficiency and verifiability issues are indeed more critical.

In a general framework, the main reasons that motivate the development of explicit NMPC can be summed up as follows [53]:

- Significant reduction in online computations by avoiding the computation of the solution of the optimization problem in real time,
- Significant reduction in software complexity since the embedded code only contains the determination of the appropriate polyhedral and the evaluation of the associated piecewise affine function,
- Formal analysis of performance, sub-optimality and stability of the approximated law can be performed since an explicit representation in the form of a state feedback law is available,
- The robust formulation of the explicit NMPC law usually does not lead to increased online computation with respect to standard formulation since the basic form of the controller is conserved and,
- All the appealing properties of NMPC (section 4.2.4), including the ability to combine a nonlinear model of the system with a physics-based performance specification index, are preserved.

4.4 Conclusion

Section 4.1 highlighted the most important constraints that have to be taken into account in order to give a new control strategy a chance of being adopted by the automotive industry. They concern hardware and software limitations but also the general practices of car manufacturers. Model-based control is one approach now unanimously voted in by academics and industrialists as a solution to handle growing engine complexity. Recent practical examples in fast engine NMPC confirm that predictive approaches represent a relevant alternative to handle the intrinsic nonlinearities of internal combustion engines. In particular, the possibilities of incorporating performance specifications, and handling input and state constraints, motivate further investigations into the nonlinear paradigm.

Concerning the real-time implementation itself, no approach seemed to make a sufficiently significant difference to become the new standard, and a certain number of other appealing theoretical approaches have not yet been applied to engine control. This is for example the case when considering the computation of the explicit solution of a NMPC scheme in an engine control framework, for which no practical example exists in the literature.

***

Chapters 1 to 3 introduced a control-oriented and physics-based engine model that directly benefits from the knowledge and data already available in the automotive industry. The following chapters will use this engine model in an NMPC framework and provide insights into the unprecedented combination of a physics-based engine model and an explicit NMPC approach.

CHAPTER 5

NONLINEAR MODEL PREDICTIVE CONTROL OF THE AIRPATH OF A TURBOCHARGED GASOLINE ENGINE

The importance of simulation in combustion engine development nowadays is undisputed and all original equipment manufacturers now include the development of an engine simulator in the earliest stages of their development process. In particular, this means that when reaching the stage of designing and calibrating a control strategy for a new engine, a physics-based nonlinear model is already available. These models, which are always calibrated using standard test bench measurements, are usually built using commercial software mainly based on first principles. Two of them currently dominate the automotive system modelling market: GT Power® developed by Gamma Technologies, and AMESim® developed by LMS. They both allow building and calibrating through a user-friendly interface and zero dimensional engine models that roughly follow the philosophy presented in chapter 1. They are also highly compatible with widespread control development tools such as Matlab® and Simulink®.

For the past few years, car manufacturers have started to integrate this new type of tool into their existing development processes. While initially they were only used to facilitate the decision process in the earliest stages of development, physics-based models have now proved sufficiently robust and accurate to completely replace selected experimental validation loops. However, even if developments in the next few years enlarge the range of possibilities by considerably reducing the computation time, there is still no evidence that these engine models will penetrate control development at earlier stages, and replace the current simple validation tools. In fact, most academic model-based control proposals currently rely on specific analytic models that require a dedicated experimental identification process [25].

In this chapter and the following, it is proposed to systematically build NMPC schemes that are based on a physics-based model such as those already widely used by car manufacturers and presented in chapter 3. This unconventional approach is the result of the combination of three considerations. First, the available computing power is exponentially increasing while accurate control-oriented physics-based models can already run faster than real-time on any standard desktop computers (chapters 1 to 3). Secondly, while NMPC has already proved able to improve the control performances of modern combustion engines, most expectations concern the used of physics-based prediction models (chapter 4). Finally, promising solutions for real-time implementations of MPC and NMPC laws already exist and have been successively applied in an engine control framework (chapter 4).

The main outcomes in this chapter are: a practical case of application of multi-input NMPC for the air path of a turbocharged gasoline engine, that benefits from the nonlinear physical engine model widely used in the automotive industry; a new thermodynamic objective function that implicitly maximises the engine cycle efficiency; and design and calibration recommendations for the computation of an explicit solution and its implementation in real time.

Section 5.1 presents the general objectives for the control of the air path of turbocharged gasoline engines. Section 5.2 serves as an introduction to the NMPC framework and the associated problem formulation. Finally sections 5.3 and 5.4 present the NMPC law and the performances obtained for a practical case of application, namely the control of the air path of a turbocharged gasoline engine (figure 1.1).

5.1 Control objectives in turbocharged gasoline engines

5.1.1 Engine torque production

Along with port injection gasoline engines, there are now more and more direct injection systems on the automotive market. Both types of engines usually combine stoichiometric combustion with an optimal spark advance. The latter provides the maximum torque that avoids damaging knocking [65]. The Otto cycle then describes the idealized behavior of the cylinder pressure and volume during the well-known four-stroke cycle. Such a pressure-volume (p-V) diagram is depicted on figure 5.1 below. The upper loop represents the work produced by the engine during the cycle, while the bottom loop represents the work consumed by the engine to suck up the air from the intake manifold, namely the pumping losses [65]. The losses and more generally the engine cycle efficiency defined as the ratio of the upper area on the total area, are then directly linked to the difference between the exhaust manifold and the intake manifold pressure, respectively p_{avt} and p_{man}.

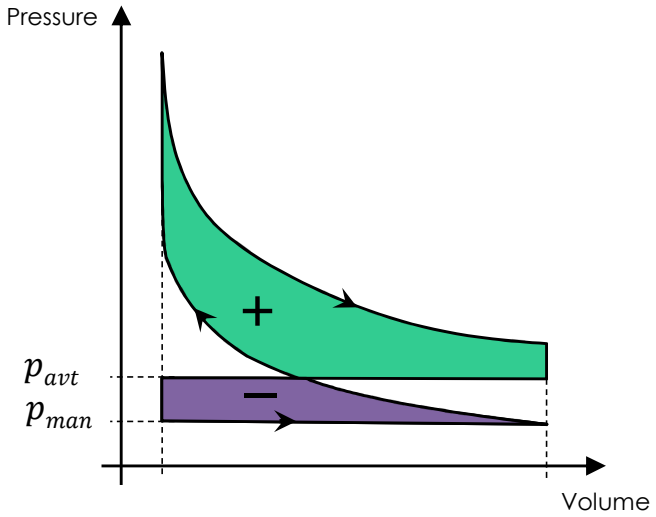

Figure 5.1 – Theoretical pressure-volume diagram inside the cylinder of a standard four-stroke internal combustion engine. The upper loop represents the work produced by the engine while the bottom loop represents the work consumed by the engine to suck up the air from the intake manifold.

In these conditions, i.e. at stoichiometry and optimal spark advance, the torque produced by a given gasoline engine is controlled by the air mass flow entering its cylinders Q_{eng}. At a given engine speed N_e, the latter directly depends on the intake manifold pressure p_{man}. Thus, from the air path control point of view, the torque of the engine is controlled by varying this pressure in the intake manifold p_{man}. With traditional fixed variable valve timing, a static look-up table calibrated on an engine test bench (section 4.1.1) is usually used to convert the torque set point, resulting from the driver request through the gas pedal, into an achievable corresponding intake manifold pressure set point p_{man}^{SP}. The objective of the air path controller is then to determine the positions of a given set of actuators that will achieve this pressure set point p_{man}^{SP}. The general construction of such engine set point trajectories under emission and fuel

consumption constraints is beyond the scope of this dissertation but further details can be found in [30,126].

5.1.2 Pollutant emission considerations

On European gasoline engines, an appropriate post-treatment system systematically ensures that the pollutant emissions remain below the regulatory level. In fact, while stoichiometric combustion mainly produces hydrocarbon (HC), carbon monoxide (CO) and nitrogen oxides (NOx), a very narrow air-fuel ratio window allows the so-called three-way catalyst to convert these three pollutants almost completely into carbon dioxide (CO_2) and water (see figure 5.2). If it exceeds pollutant emission standards, the particulate matter (PM) exhausted by the engine is captured by an additional element, namely the particulate filter. The complete post-treatment system is then known as a four-way catalyst. Thanks to these widespread technologies, pollutant emissions of spark-ignited engines are usually considered as a solved problem if the air/fuel ratio can be kept within the optimal conversion area (figure 5.2).

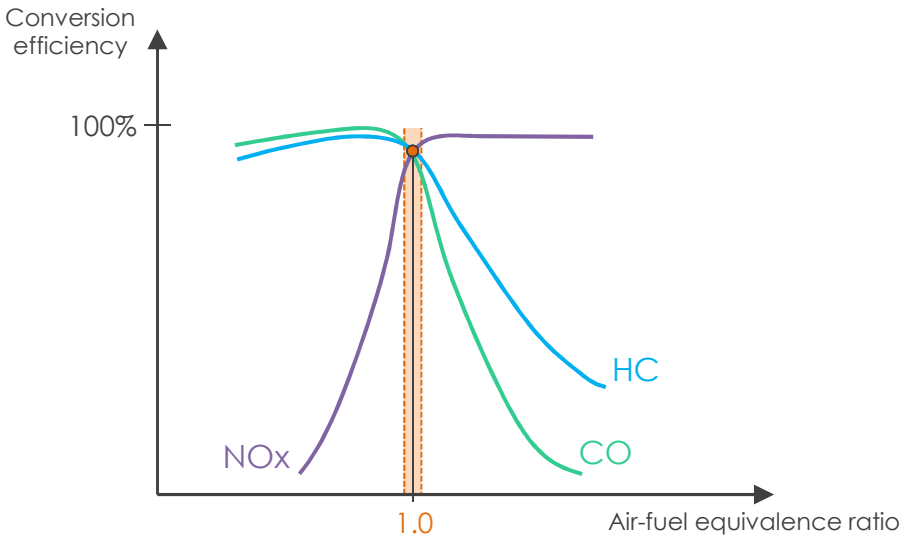

Figure 5.2 – Conversion efficiency diagram of a three-way catalyst (after light-off and at stationary behavior).

5.1.3 Application to turbocharged gasoline engines

In turbocharged spark-ignited engines, the throttle plate opening upstream the intake manifold u_{thr} and the wastegate position at the exhaust u_{wg}, make it possible to vary the pressures p_{apc} and p_{man} in a coordinated way. This combination of actuators is simple and reliable but can significantly reduce the engine efficiency due to two phenomena. Firstly, part loads are achieved by closing the throttle, i.e. producing pumping losses (figure 5.1). Secondly, the introduction of an additional flow restriction at the exhaust, namely the turbine, tends to increase the exhaust manifold pressure p_{avt}, i.e. the work consumed by the engine to suck up the air from the intake (figure 5.1). Since both tend to reduce the average brake-specific fuel consumption of turbocharged gasoline engines, the actual primary objective of the air path control loop is not to determine any actuator positions u_{thr} and u_{wg} that will achieve the pressure set point p_{man}^{SP}, but to determine among a wide range of solutions, the actuator positions u_{thr} and u_{wg} that will also minimize engine losses.

This multi-input $\{u_{thr}, u_{wg}\}$ and multi-objective control problem is usually divided into two single-input single objective problems [30,94]. The wastegate opening u_{wg} is used to achieve an additional compressor downstream pressure set point p_{apc}^{SP} while an appropriate throttle opening u_{thr} ensures that the intake manifold pressure set point p_{man}^{SP} corresponding to the driver's engine torque request is achieved. Then, a widely used method to reduce the pumping losses is to use the same set points for both problems [30]. In other words, the compressor downstream pressure, driven by the wastegate should also roughly follow the intake manifold pressure set point trajectory, i.e. $p_{apc}^{SP} \cong p_{man}^{SP}$. This can be explained by the fact that such an approach maximises the throttle opening u_{thr} by minimizing the pressure drop between the two control volumes (figure 3.9), and intuitively reduces the use of the turbocharger. The wastegate opening is then assumed to be maximised, thus reducing the flow restriction at the exhaust and the related engine losses. This is a typical manifestation of the way engine control theory has been used in the past few years: empirical observations translated into rules of thumb and other tricks, often based on strong hypotheses. However, faced with increasing engine complexity, this type of control strategy usually becomes intractable and explains the growing interest of car manufacturers for model based control approaches. For instance, the rule of thumb which consists in using two similar set point trajectories $\{p_{apc}^{SP}, p_{man}^{SP}\}$ falls apart when considering additional actuators such as variable valve timing. In fact, the engine torque then ceases to be given by the intake manifold pressure p_{man} which becomes an additional degree of freedom to maximise the engine cycle efficiency (figure 5.1).

In contrast, an NMPC scheme based on an accurate engine physics-based model would enable the physical behaviour of the engine to be explicitly taken into account. For instance, the maximum engine efficiency criteria deduced from the p-V diagram (figure 5.1), i.e. minimizing the pressure gap between the inlet and outlet manifold, can be taken directly into account in the objective function that is being minimized. The main advantage of this approach is that, as long as the related physics phenomena can be modelled, the philosophy can easily be extended to other technical definitions. For instance, if engine pollutant emissions are modelled, they can be minimized in a similar fashion. An example of an application of a thermodynamic-based performance index is fully detailed in section 5.3.

5.1.4 Car manufacturer specifications

In this study, the specifications for the intake manifold pressure p_{man} tracking are directly provided by a car manufacturer (figure 5.3).

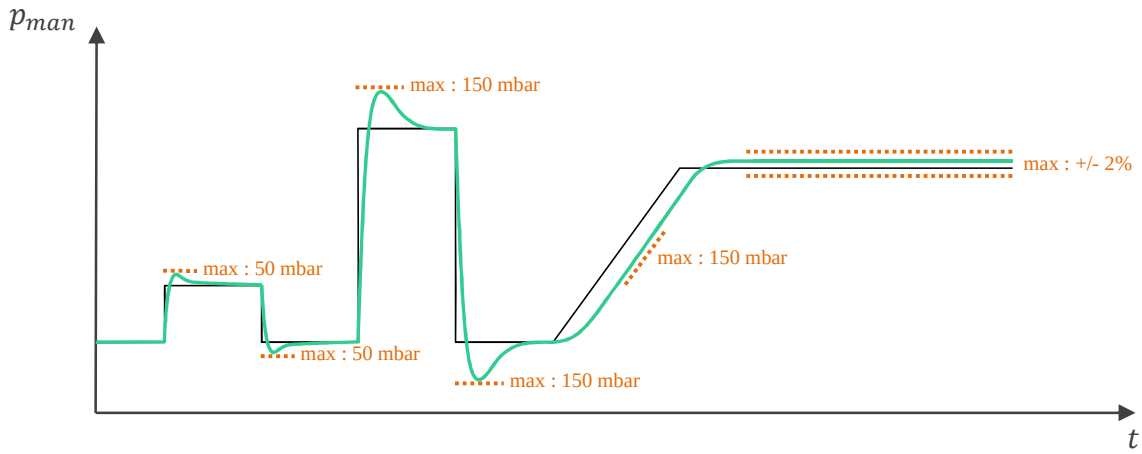

Figure 5.3 – Overview of standard car manufacturer intake manifold pressure set point tracking specifications for a turbocharged gasoline engine.

They are essentially motivated by the level of drivability to be attained on a given engine and address limits on the overshoots encountered for “small” and “big” set point changes (respectively a maximum value of 50 mbar and 150 mbar), tracking error during a ramp-type signal (150 mbar maximum) as well as a maximum steady-state error (2% of the set point value). They are summed up on figure 5.3.

Standard car manufacturer specifications also address issues such as upper limits on the turbocharger rotational speed ω_t and the engine exhaust temperature θ_{avt}, both motivated by major safety and reliability requirements. While NMPC schemes are particularly well-adapted to handle such state constraints, this also requires sufficiently accurate predictions of these physical values. Since for the model presented in chapter 3, the prediction accuracy cannot be guaranteed at such a safety level, the control schemes presented in this chapter and the following avoid such additional constraints.

5.2 Theoretical aspects of nonlinear model predictive control

The general MPC framework involves the solution of a finite horizon open-loop optimization control problem. The states are updated at each sampling time and a new optimization problem is solved repeatedly following the receding horizon approach. This optimization problem can be explicitly subject to system dynamics as well as input and state constraints. In this section, the main aspects related to NMPC are reviewed. The first sub-section starts with the formulation of the NMPC optimization problem in a general discrete time framework. Then the most relevant properties of NMPC are detailed along with theoretical considerations such as stability and robustness. Finally, before going into detail about the control of the air path of a turbocharged gasoline engine in section 5.3, considerations for the computation of the explicit solution of the NMPC law are provided.

5.2.1 Problem formulation

The system to be controlled is assumed to be described by a discrete-time model:

$$x(k+1) = f(x(k), u(k), \sigma) \tag{5.1}$$

where k is the discrete time index, $x(k) \in \mathbb{R}^n$ denotes the n system states and $u(k) \in \mathbb{R}^m$ represents the m input variables. f is a nonlinear function parameterized by a vector of exogenous inputs σ. The state and input control variables respectively remain in X and U, compact subsets of $\mathbb{R}^n$ and $\mathbb{R}^m$:

$$x \in X, u \in U \tag{5.2}$$

Given the current system state x_0 and the vector of exogenous inputs σ at time instant k, solving the NMPC problem consists in determining the optimal vector of input variables u^* with respect to a given objective function $\mathcal{S}$. Thus, the discretized NMPC problem that is addressed is given by:

$$\mathcal{S}^* = \mathcal{S}(u^*) = min_{u(.)}\, \mathcal{S}(x, y, u, \sigma) \tag{5.3}$$

s.t.

$$\mathcal{S} = \sum_{i=k}^{k+N_p} \mathcal{J}(x(i), y(i), u(i), \sigma(i)) \tag{5.4}$$

$$x(k+1) = f(x(k), u(k), \sigma(i)) \tag{5.5}$$

$$y(k) = g(x(k), u(k), \sigma(i)) \tag{5.6}$$

$$\underline{x} \le x(k) \le \overline{x}, \underline{u} \le u(k) \le \overline{u} \tag{5.7}$$

$$x(k) = x_0 \tag{5.8}$$

where $H_p = [k, k+N_p]$ is the so-called prediction horizon at time k and $\mathcal{J}$ denotes the so-called cost function. f and g are nonlinear functions describing the discrete-time system dynamics. It is assumed that they satisfy necessary regularity assumptions including smoothness and continuity. Finally $\underline{x}$, $\overline{x}$, $\underline{u}$ and $\overline{u}$ respectively stand for lower and upper bounds on the states and the control variables, and respectively define X and U.

The cornerstone in NMPC is the nonlinear model $\{f, g\}$, used to evaluate the set of admissible future control trajectories. It should be pointed out that the formulation of the NMPC problem proposed above does not take into account the model uncertainties induced by the modelling hypothesis, the unknown disturbances that can be encountered on a practical case of application, or the measurement errors that will normally occur. This is very unrealistic from a practical point of view and the question of predicting the real behaviour of the NMPC scheme once on board thus arises. This raises the more general issue of the stability and robustness of NMPC laws, which is the focus of much current research.

5.2.2 Issues of the stability and robustness of NMPC laws

5.2.2.1 Nominal stability

NMPC stability properties are notably inherited from the choice of the cost function and prediction horizon and are intrinsically linked to the system prediction model $\{f, g\}$. In practice, the fundamental issue is to decide whether or not the use of a finite horizon will lead to stability of the closed-loop system. In fact, while requiring significantly smaller computational resources, finite horizon optimal control problems are also known to provide an open-loop control trajectory that usually differs from the closed-loop trajectory of the nonlinear system since new information is obtained at each sampling time [4,27,28,89,110,111].

Different approaches to achieve closed-loop stability in the case of a finite horizon cost function are available, all motivated by drastic computational requirements. They usually lead to NMPC laws with guaranteed stability, i.e. the stability is achieved independently of the value of the calibration parameters. The most popular methods include: adding a terminal cost and/or terminal equality constraints to the standard set up, determining terminal set constraints, or any relevant combination of these. Note that along with guaranteeing stability, this type of strategy will usually lead to issues related to the feasibility of the optimization problem as well as to an increase in the computational requirements. Still, both issues are usually improved with respect to the infinite-horizon optimization case [4].

Finally, when dealing with stability considerations, one should also take into account that in NMPC, obtaining a suboptimal solution is usually sufficient to guarantee the stability of the closed-loop system [4,24,67,90,118]. This property is often used to decrease the on board computational requirements of the implicit solution, as well as to explain the inherent robustness of some industrial cases of application.

5.2.2.2 Robustness

Over the years, practical industrial cases of application have proven the inherent practical robustness of NMPC laws, which probably explains the growing popularity of the method [3,52,53,56,108]. The formal treatment of this inherent robustness of NMPC laws can be found in [22,84,89,117].

On the other hand, when combining short prediction horizons with state and terminal constraints, for example, robustness issues can appear [55]. To cope with this, a wide range of NMPC schemes that explicitly take into account modeling uncertainties and unknown disturbances has been designed. At least three main types of approach can be distinguished [4,56]: stochastic approaches based on a probabilistic description of the uncertainties, mechanisms to avoid steady-state errors based on the estimation of disturbances, and min-max reformulation of the nominal optimization problem. `

The latter is probably the most intuitive since it simply consists in taking into account, at each time step, the worst case uncertainty (or disturbance) out of given set. The minimization problem (5.3) is then transformed into a min-max optimization problem. In an open-loop fashion, it guarantees a certain level of performance whatever scenario is actually encountered, but usually leads to poor performances and obvious issues of feasibility. This min-max formulation usually avoids the use of any of the stability constraints described in section 5.2.2.1 [15,23,26]. Two key drawbacks explain the inherent conservativeness of the method: worst scenarios with a low probability of occurring have the same weight as more realistic nominal cases, and no advantage is taken of the feedback effect induced by the receding horizon strategy. A closed-loop formulation of the min-max approach that partially overcomes this drawback also exists [83,85,86]. It usually leads to less conservative performances but shares the same challenges w.r.t. the increasing computational complexity when compared to a standard NMPC

formulation (5.3) to (5.8) [53].

5.2.3 Computation and on-board exploitation of an explicit solution

When considering the on-board computational time in a general framework, a sensible approach has proved to be computing offline an approximate solution of the MPC (respectively NMPC) optimization problem under the form of an explicit control law (section 4.2). However, in practice, the methodology is not straightforward and several considerations have to be taken into account in the earliest stages of the development, in order to keep under control both offline and online computational requirements. Additionally, major characteristics of the trade-off between accuracy and complexity of the final explicit MPC (respectively NMPC) law are directly inherited by the implicit MPC (respectively NMPC) design. It is therefore of primary importance to take into account the potential offline and online numerical issues summed up below, in the very first stages of the implicit MPC (respectively NMPC) scheme design.

Offline, the computation of an explicit approximate solution to the NMPC problem (5.3) to (5.8) consists in the resolution of a multi-parametric nonlinear program (mp-NLP). Although the approach intrinsically suffers from the related curse of dimensionality linked to the order of the problem, the drawback can be overcome in three ways: better computing capabilities, efficient algorithms for solving mp-NLP, and the use of a low-order implicit NMPC scheme, i.e. with a minimum number of states. For the first, computing power naturally increases from year to year and what is currently intractable will soon become fast, easy and cheap - one has only to look back on how computational capabilities have increased since starting on one's studies or on a career. Secondly, concerning the construction of an efficient algorithm for the computation of the explicit solution, this study attempts to provide a relevant answer that is detailed in chapter 7. Finally, the constraint of computing the explicit solution from a low-order NMPC law typically corresponds to the considerations that have to be taken into account when designing the initial implicit NMPC scheme. A practical example for the construction of an explicit-ready NMPC scheme is provided in section 5.3.

Online, the exploitation of such an explicit NMPC law also induces its own set of constraints and involves two computational stages:

- determining the active region i, i.e. the polyhedral in which the system is currently performing (figure 4.5) and,
- computing the approximate optimal actuator positions, usually of the form $\hat{u}^* = K_i x + h_i$ from the controller parameters $\{K_i, h_i\}$ corresponding to the active polyhedral i.

In practice, the latter is usually not considered to be time-consuming since piecewise affine control laws are usually favoured. The computation of the optimal control then involves simple matrix algebra that will require only a few additions and multiplications. However, determining the active region among the total number of polyhedrals in the partition can become critical when a large number of regions are required to achieve good enough performances with the explicit control law. Additionally, in such cases, memory requirements can also become an issue since standard ECUs usually carry no more than 8 to 16 megabits of Read Only Memory (section 4.1.2).

Altogether, assuming that the computational capabilities available on-board are given, both the offline and online computational issues described above require minimizing the number of parameters of the mp-NLP to be solved. They include the number of states of the model, the number of set point trajectories to be followed, and the number of exogenous inputs to be taken into account. The implicit NMPC scheme

presented in section 5.3 explicitly takes this fact into account in order to enable the computation of an explicit solution of the NMPC problem in chapter 7.

5.3 NMPC of the air path of a turbocharged gasoline engine

5.3.1 Problem formulation

The air path NMPC scheme proposed in this chapter is based on the physics-based engine model presented in chapter 3. The problem fits into the formulation of an NMPC optimal control problem such as (5.3) to (5-8) if we respectively define the state vector x, the vector of inputs u and the vector of exogenous inputs σ as below:

$$x \coloneqq \left(p_{ape}, p_{man}, p_{avt}, \omega_t\right)^T \tag{5.9}$$

$$u \coloneqq \left(u_{thr}, u_{wg}\right) \tag{5.10}$$

$$\sigma = (N_e, p_{man}^{SP}, p_{amb}, \theta_{amb}) \tag{5.11}$$

As suggested before (section 5.1.4), no other constraint than saturation of the mechanical actuators is taken into account:

$$0 \leq u \leq 100\% \tag{5.12}$$

In this study, the prediction model is given by the widespread physics-based nonlinear model presented and validated in chapter 3. It combines a mean-value engine model and a zero-dimensional modelling of the air path, and considerably facilitates the calibration process while being sufficiently accurate for control-oriented purposes. The right-hand side in (5.5) is then given by the set of equations (3.2). For control design purposes, the equations are discretized at a sampling time of $\Delta t = 1\,ms$, using Euler's forward differentiation method:

$$\begin{cases} p_{ape}^{k+1} = p_{ape}^{k} + \frac{\gamma r}{V_{ape}} \cdot \left(Q_C \cdot \theta_{apc} - Q_{thr}(u_{thr}) \cdot \theta_{ape}\right) \cdot \Delta t \\ p_{man}^{k+1} = p_{man}^{k} + \frac{\gamma r}{V_{man}} \cdot \theta_{man} \cdot \left(Q_{thr}(u_{thr}) - Q_{eng}\right) \cdot \Delta t \\ p_{avt}^{k+1} = p_{avt}^{k} + \frac{\gamma r}{V_{avt}} \cdot \theta_{avt} \cdot \left(Q_{eng} + Q_{fuel} - Q_T - Q_{wg}\left(u_{wg}\right)\right) \cdot \Delta t \\ \omega_t^{k+1} = \omega_t^{k} + \frac{1}{I} \cdot \left(\Gamma_T - \Gamma_C\right) \cdot \Delta t \end{cases} \tag{5.13}$$

5.3.2 Algorithm

The optimization problem defined from (5.3) to (5.8) is addressed using the sequential approach known as direct single shooting [66,75,116]. The discretized set of equations (5.13) is solved using numerical simulations when evaluating the objective function $\mathcal{S}$ and the vector of control inputs u is treated as unknown. This is motivated by the fact that sequential approaches, in opposition to simultaneous approaches, use separate ordinary differential equation (ODE) and optimization solvers. Then during the optimization problem, the model is only used as a black-box to evaluate the objective function $\mathcal{S}$. This crucial feature enables any type of engine model to be used, in particular those designed on dedicated software (GT Power®, AMESim®) by specialists of the automotive industry. Additionally, the sequence of

simulate-optimize iterations is driven by a simple trust-region reflective algorithm implemented in Matlab®. The gradients are computed using the finite difference method.

The optimization solver, when initialized at the center of the control variable space (5.12), converged to a close-to-global solution within 20 iterations. This constitutes a cold start, in opposition to warm start approaches in which the iterative method is initialized using the solution obtained in the previous time step. This cold start increases the number of iterations required to reach the optimal solution but is a necessary feature regarding the computation of an explicit solution in chapter 7. Indeed, in the multi-parametric framework that will be put in place, there will be no such thing as a previous time step.

5.3.3 Calibration of the NMPC scheme

The calibration of the NMPC scheme (5.3)-(5.8) formulated above involves three stages that are detailed in the sub-sections below (figure 5.4). First, an appropriate cost function $\mathcal{J}$, with respect to the performance objectives, must be defined. Then, the prediction horizon H_p along with an appropriate parameterization of the control trajectory u can be determined by means of parametric analysis and/or experience.

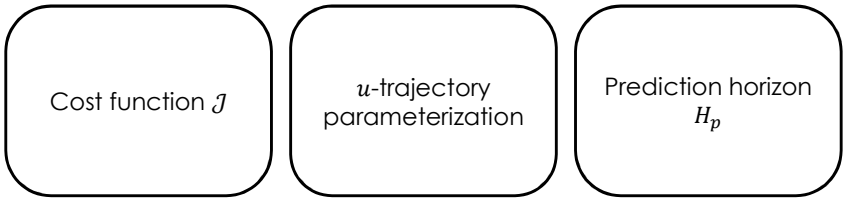

Figure 5.4 – Three calibration parameters of an implicit NMPC scheme.

5.3.3.1 Cost function $\mathcal{J}$

As detailed before, the physics-based NMPC approach involved in this study, takes thermodynamic criteria such as the engine cycle efficiency explicitly into account in the cost function $\mathcal{J}$ (section 5.1.3). In practice, besides the first classical quadratic term that ensures tracking of the intake manifold pressure set point p_{man}^{SP}, a second term p_{avt}/p_{man} is added in order to minimize the pressure ratio between the intake and exhaust manifolds. As indicated on figure 5.1, minimizing such a performance index naturally maximizes the engine cycle efficiency by reducing the area of the bottom loop of the Otto cycle. Altogether, the unprecedented thermodynamic cost function that is used in this study is given by:

$$\mathcal{J} = \alpha(p_{man}^{SP} - p_{man})^2 + \beta \frac{p_{avt}}{p_{man}} \tag{5.14}$$

where the weighting factors α and β are used to scale and penalize each term of this multi-objective cost function.

In practice, if the weighting factor α is small compared to β, the intake manifold pressure p_{man} will not reach its desired value p_{man}^{SP}. In fact it would become more favourable to minimize the second term p_{avt}/p_{man} than to achieve the required intake manifold pressure set point p_{man}^{SP}. With an appropriate choice of α and β, the engine cycle efficiency will be maximized only when the intake manifold pressure tracking error $p_{man}^{SP} - p_{man}$ is sufficiently small. Based on the author's experience, an initial guess for α and β can usually be obtained using a prediction horizon H_p (section 5.3.3.3) equal to the settling time of the system and a classical piecewise constant future control trajectory u. If the problem is intractable for computational considerations, one can first reduce the flexibility of the control trajectory so that it does not change at each time step. See section 5.3.3.2 below for further details.

This thermodynamic cost function formulation $\mathcal{J}$ avoids the use of any methods to formulate an NMPC with guaranteed stability (see section 5.2.2). This design choice is principally due to the parameterization of the optimization problem in σ which makes the definition of any terminal cost, terminal penalty term or terminal constraints intractable in this particular nonlinear paradigm. However, the closed-loop stability (in the sense of boundedness of state space trajectories) is ensured by the intrinsic dissipative properties of the engine as well as the physical bounds on the input control variables (5.12).

5.3.3.2 u-trajectory parameterization

Most of the time, in industrial engine control applications, the command of an actuator can only be changed at a given sampling time Δt_c and remains constant in between these sampling intervals. To cope with this, the unknown optimal control trajectory u must be described by a finite number of decision variables so that a finite-dimensional optimization problem can be solved using numerical optimization. A piecewise constant input signal u, with a regular sampling interval that matches the engine control set point changes, is usually used to fulfill these constraints.

In practice, the parameterization of the future control trajectory u will influence the controller closed-loop performances as well as the general computational requirements to compute the optimal actuator positions. On the one hand, it should be flexible enough to fully benefit from the control horizon H_p that is chosen, as well as approximate as well as possible the optimal trajectory of the original problem. On the other hand, even in the explicit NMPC paradigm, the optimization problem must remain implementable, i.e. capable of coping with the associated hardware and software computational issues (section 5.2.3). Altogether, the right compromise should provide a u-trajectory parameterization that contains a minimum number of parameters. It also has to minimize the computational requirements, the numerical sensitivity and later, facilitate the computation of the explicit solution [53].

Based on this practical point of view, it is usual to restrict the input variables from changing at each sampling instant on the prediction horizon. Usually, flexibility is given at the beginning of the prediction horizon by keeping the input variables constant after the so-called control horizon $H_c = [k, k + N_c]$ and until the end of the prediction horizon H_p (figure 5.5). There is no theoretical limit in this approach or in the distribution of the degrees of freedom over the prediction horizon. In fact, linear MPC laws with a constant input over the prediction horizon were already implemented successfully on industrial applications in the 1990s [108]. Horizon-1 model predictive control schemes are another popular example that uses this philosophy [64].

In this study, regarding the good computational capabilities available for tuning, a parametric analysis that consists in varying the number of control changes as well as their distribution over a sensible prediction horizon H_p has been used. Keeping in mind that the objective is to minimize the number of optimization parameters of the problem, a horizon-1 NMPC scheme proved able to provide enough flexibility to track the realistic vehicle driving cycles presented on figures 3.11 and 3.12, as well as handling sudden set point step changes. Since there are two manipulated variables, namely the throttle and the wastegate positions u_{thr} and u_{wg}, a horizon-1 NMPC scheme requires solving a 4-parameter optimization problem at each sampling time.

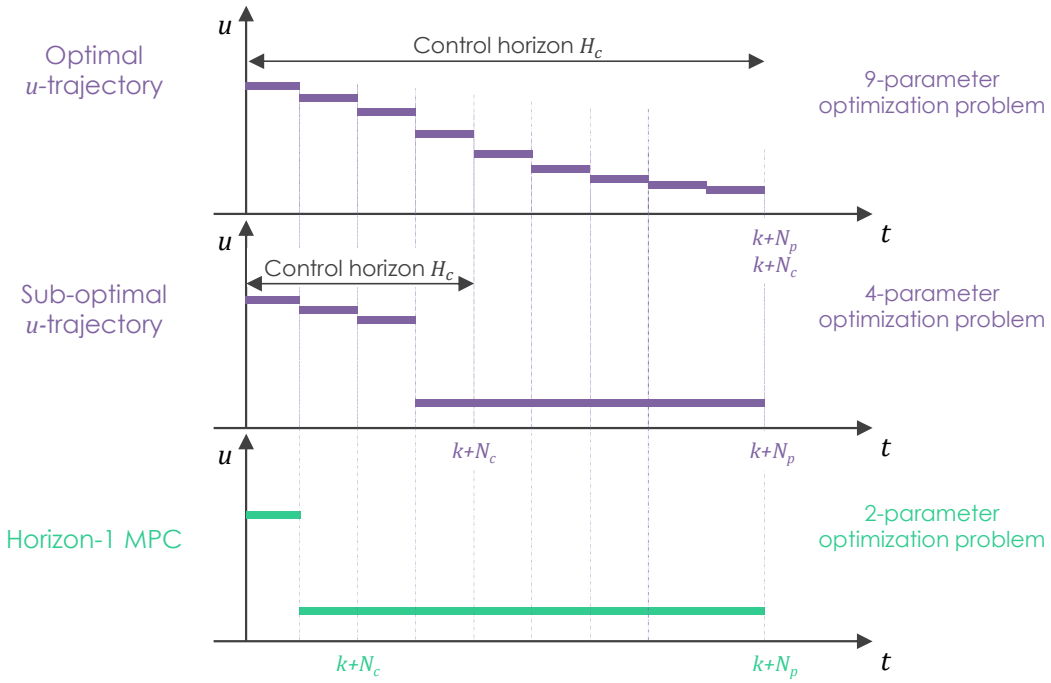

Figure 5.5 – Principle of the effect of a reduction in the control horizon H_c on the number of optimization parameters in (5.3) considering a single input system. The overall optimization problem complexity is usually reduced by reducing the number of degrees of freedom in the future control trajectory, i.e. H_c . However, the closed-loop performance of the control is usually also reduced.

In practice, the optimal parameterization also depends on the prediction horizon H_p that is used in (5.3): long prediction horizons usually require more flexibility, without which, NMPC performances considerably decrease. The evaluation of the different possibilities for the u-trajectory parameterization should indeed be made along with the determination of the prediction horizon H_p, following the recommendations presented in the following sub-section.

5.3.3.3 Prediction horizon H_p

From a theoretical point of view, it would be preferable to use an infinite prediction horizon in order to guarantee the intrinsic stability properties of the control law. Since such an optimal control problem is usually intractable in terms of computational time, finite horizons are usually favored. However, in practice, it is wrong to say that the repeated solution of a moving finite dimension problem is equivalent to the optimal solution of the infinite dimension problem. Intuitively, the difference increases when the length of the prediction horizon decreases, but practical experience shows that an appropriate choice of the prediction horizon usually approximates the behavior of the closed-loop infinite horizon NMPC sufficiently well, in a receding horizon framework [4,30,108,110,111,126].

In practice, when wishing to use a finite horizon H_p, one should still decide between using a constant and given prediction horizon or considering it as a free variable of the optimization problem, which is usually far more computationally challenging. Consequently, except in rare cases of application [44,49,101], the prediction horizon H_p is finite, constant and considered as a simple tuning parameter. In our particular discrete framework, it is also assumed to be an integer multiple of the control sampling time Δt_c.

A rough estimate of a relevant prediction horizon can usually be made in agreement with the dynamic behavior of the system [3,27,28,56,89]. In the case of a turbocharged gasoline engine, the settling time of the system is linked to the operating point. In particular, as suggested in chapter 1, the pressure transients are highly dependent on the engine speed N_e and on the turbocharger rotational speeds ω_t. For the 1.2L turbocharged gasoline engine depicted on figure 1.1, the physics-based model presented in chapter 3 showed that it varies roughly from 80 ms at low engine speed to 300 ms at high loads.

Again, a parametric analysis of the effect of the prediction horizon on the control performances is probably the easiest way to determine the most appropriate value w.r.t inlet manifold tracking specifications (section 5.1.4). Such an approach led to selecting a prediction horizon H_p of 200 ms that proved capable of tracking realistic vehicle transients (figure 3.11 and 3.12) as well as handling sudden set point step changes. This is in agreement with previous applications of the NMPC scheme to downsized turbocharged gasoline engines [31].

5.4 Simulation performances

Before computing the explicit solution of an implicit NMPC law, one should first ensure that the performances of the implicit scheme meet the specifications imposed by the car manufacturer (section 5.1.4). On this particular case of application, they include tracking performance criteria in order to achieve the torque requested by the driver as soon as possible, but also considerations about drivability that are difficult to take into account in simulation. In practice, we will first focus on verifying the general behavior of the controller on successive set point step changes (section 5.4.1) and compare it to the expected behavior based on extensive knowledge of the optimal behavior in such trivial cases. Next, the implicit NMPC scheme will be validated on realistic vehicle transients (section 5.4.2) and we will conclude on the performances of the implicit NMPC approach.

All the simulations were performed on an engine simulator running at a sampling period of 0.5 ms and based on the modeling philosophy presented in chapter 1. Compared to the prediction model described in chapter 3, additional throttle and wastegate first-order models were added to simulate the time response of both actuators. The sampling time of the air path control Δt_c is 10 ms, in accordance with the car manufacturer specifications.

5.4.1 Preliminary validation on set point step changes

Figure 5.6 illustrates representative closed-loop performances obtained under a sequence of successive positive and negative 300 to 400 mbar steps, followed by a positive and a negative 1,100 mbar step change on the intake manifold pressure set point p_{man}^{SP}. The engine speed is kept constant at 2,000 rpm, i.e. middle load. Figure 5.7 shows a similar set point trajectory at 5,000 rpm.

For both engine speeds the implicit NMPC scheme matches the car manufacturer specifications with no overshoot, a steady-state error below the 2% limit and a quasi-optimal settling time. In fact, at each set point step change, one can see that the throttle and the wastegate are immediately actuated, leading to an optimal settling time w.r.t the engine. In standard PI-control approaches, this type of behavior can only be obtained by the addition of a feed-forward action. During negative set point steps, the throttle is naturally used to quickly reach the set point, overcoming the turbocharger inertia. While the boost pressure and the turbocharger rotational speed slowly drop to minimize the pumping losses, the throttle is progressively opened again. This phenomenon can particularly be observed after the 1,100 mbar negative step change at time t = 2.5 s, and clearly demonstrates the benefits of a multi-variable control approach.

Altogether, the implicit NMPC scheme shows a very good general behavior w.r.t. the car manufacturer specifications (section 5.1.4) while requiring a reasonable calibration effort (section 5.3.3). In practice, the

opening of the two actuators is maximized, which reduces pumping losses due to the throttle and the blockage effect due to the turbine. This maximizes the engine efficiency and proves the validity of the thermodynamic objective function (5.14) proposed in this study.

In the next sub-section, the NMPC scheme is evaluated on a realistic vehicle transient, including a continuous change of the engine speed.

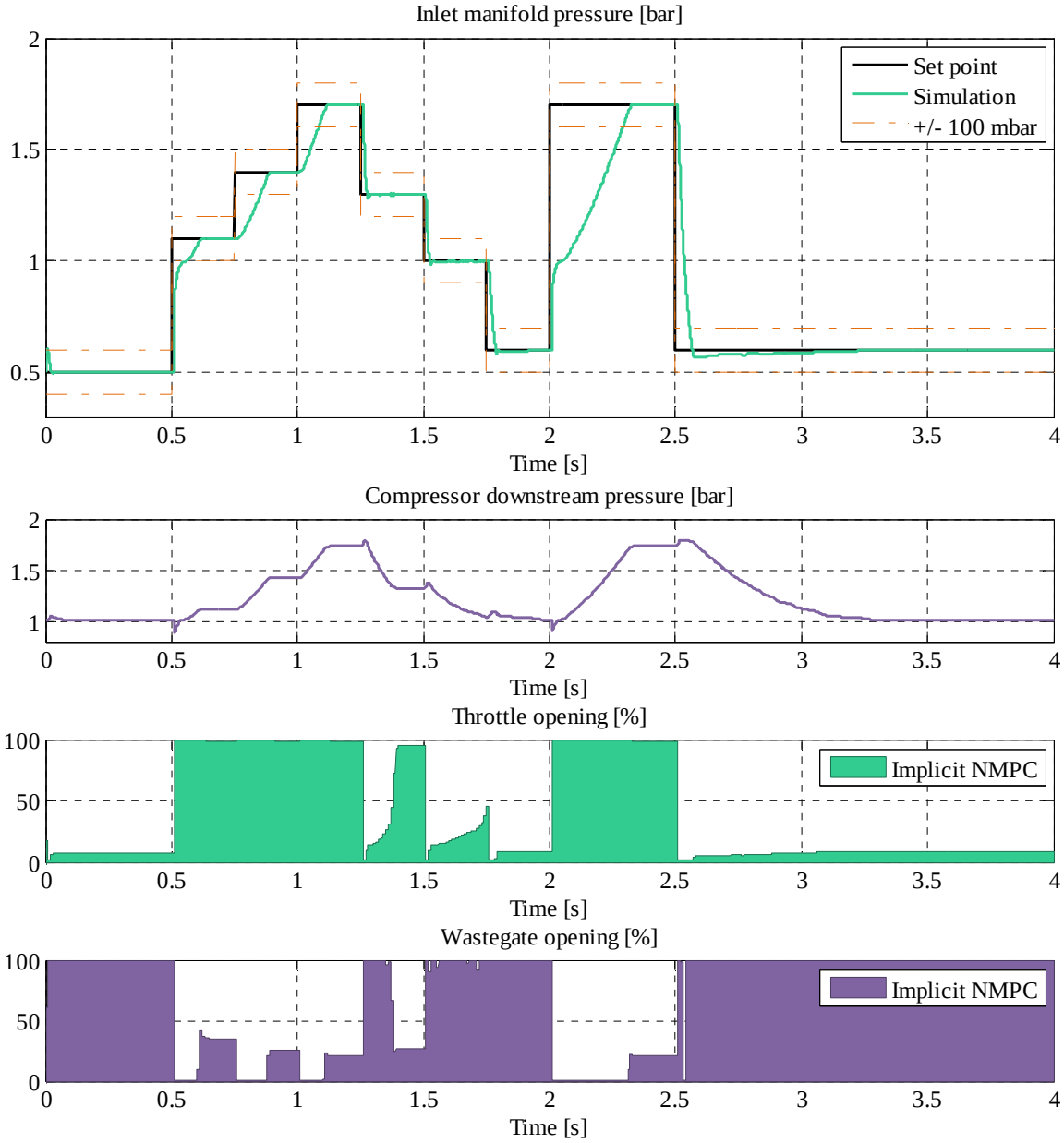

Figure 5.6 – Set point step validation graphs of the implicit NMPC scheme at constant engine speed (2,000 rpm).

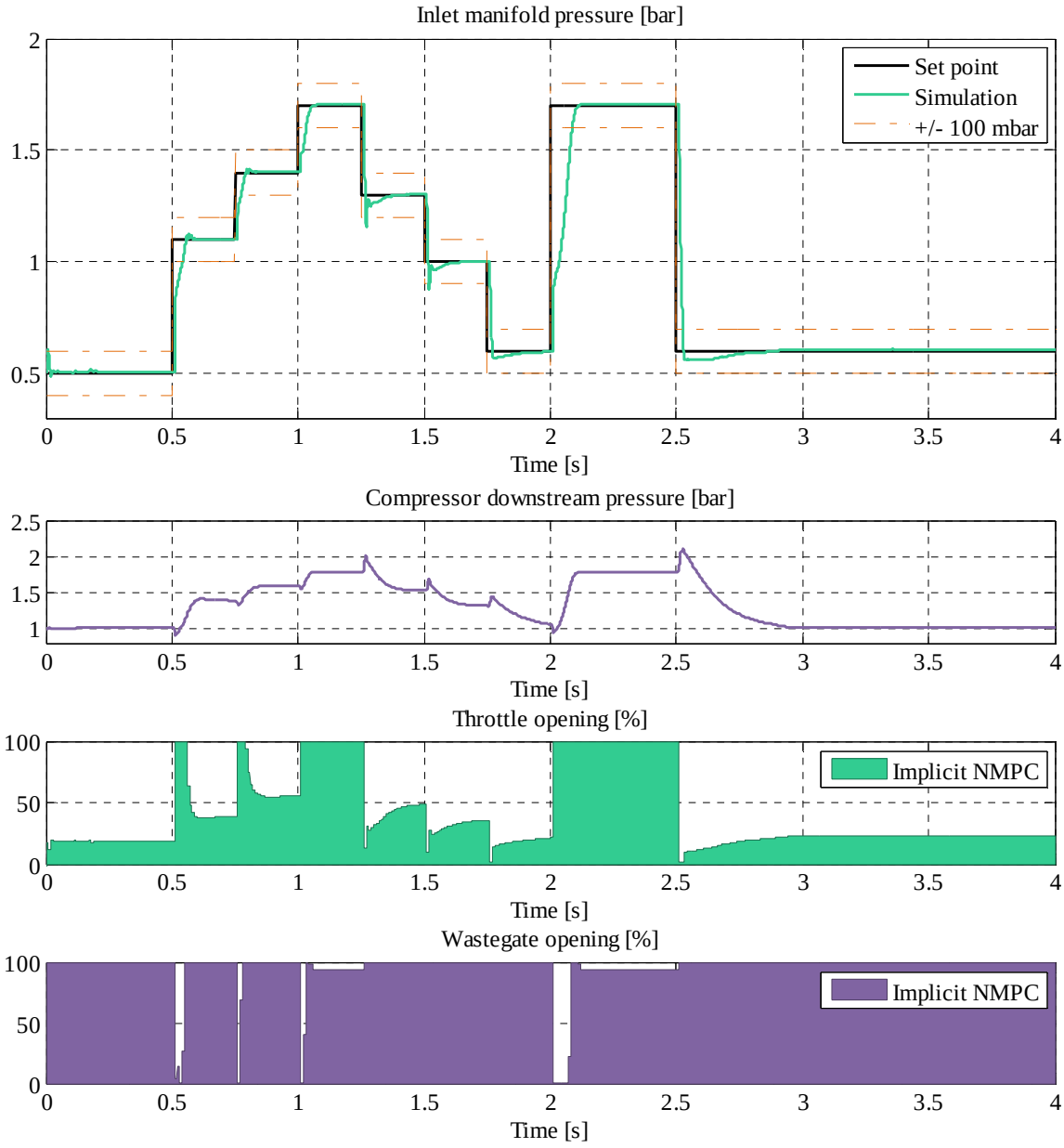

Figure 5.7 – Set point step validation graphs of the implicit NMPC scheme at constant engine speed (5,000 rpm).

5.4.2 Validation on realistic vehicle transients

In this sub-section, the performances of the implicit NMPC scheme are evaluated on two engine speeds and intake manifold pressure set point transients (figure 3.11 and 3.12). Both cycles represent samples of a driving sequence recorded on a vehicle equipped with the turbocharged gasoline engine presented on figure 1.1. The engine speed varies from 2,500 rpm to 5,000 rpm while the intake manifold pressure set point p_{man}^{SP} varies from 200 mbar (low load) to 1,700 mbar (high load). The cycle includes areas where the sensitivity of the wastegate is very low and set point change dynamics that require sudden opening and closing of the actuators.

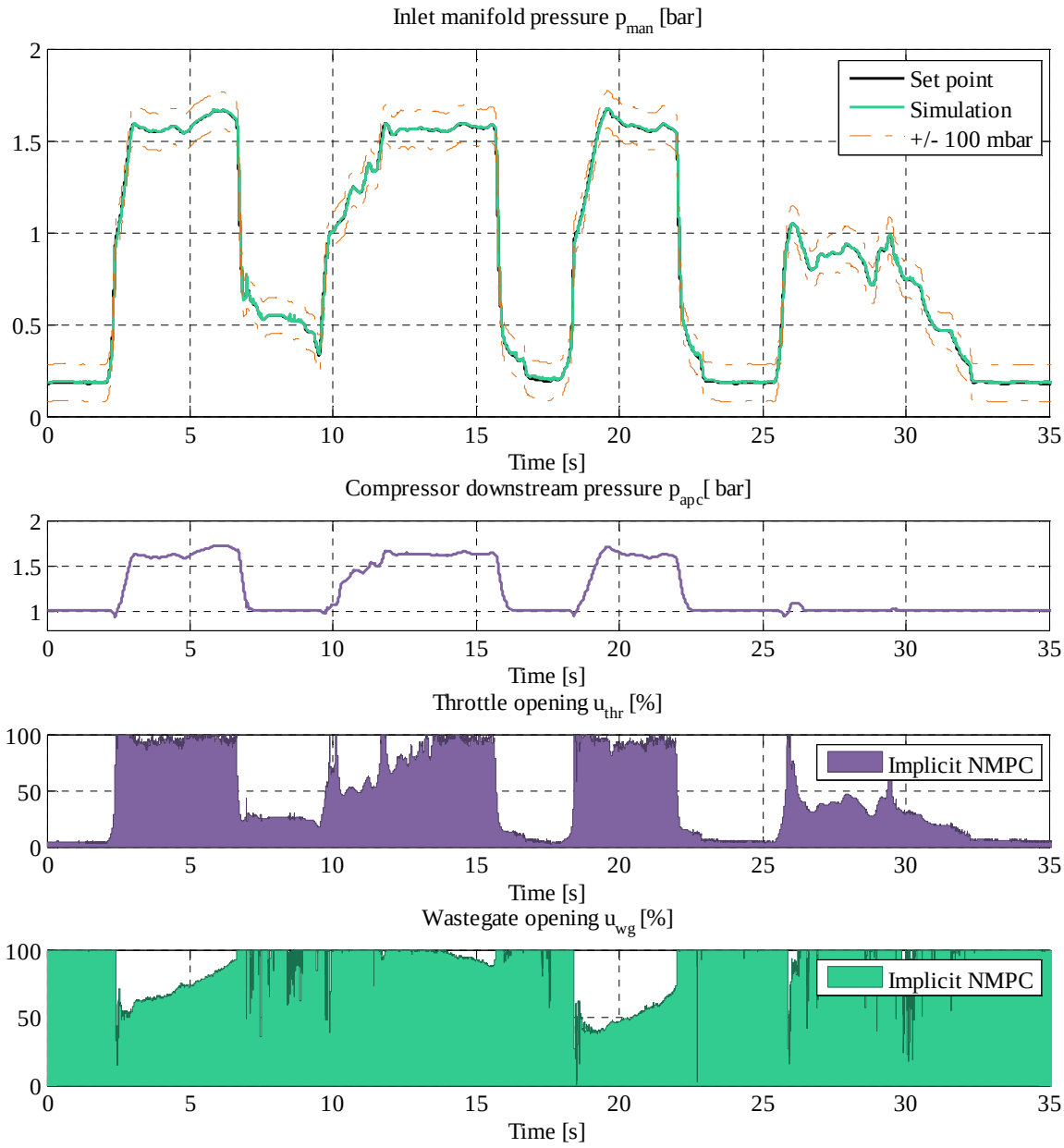

Figure 5.8 – Validation cycle #1: performance of the implicit NMPC scheme on a realistic intake manifold pressure set point transient p_{man}^{SP}. Note that the engine speed N_e varies continuously between 2,500 rpm and 5,000 rpm (figure 3.11).

Figures 5.8 and 5.9 respectively depict the performances that were obtained by simulating the behavior of the implicit NMPC scheme on the engine simulator that included the actuators' dynamics. Both show the ability of the controller to follow realistic intake manifold set point changes p_{man}^{SP} under continuous changes in engine speed N_e, i.e. conditions that are similar to real driving circumstances. In practice, the implicit NMPC scheme shows an average error that remains below 20 mbar. This is in perfect agreement w.r.t the car manufacturer specifications described in section 5.1.4, and similar to what is obtained by other advanced control strategies in the literature [5,6,31,62,99,100,119].

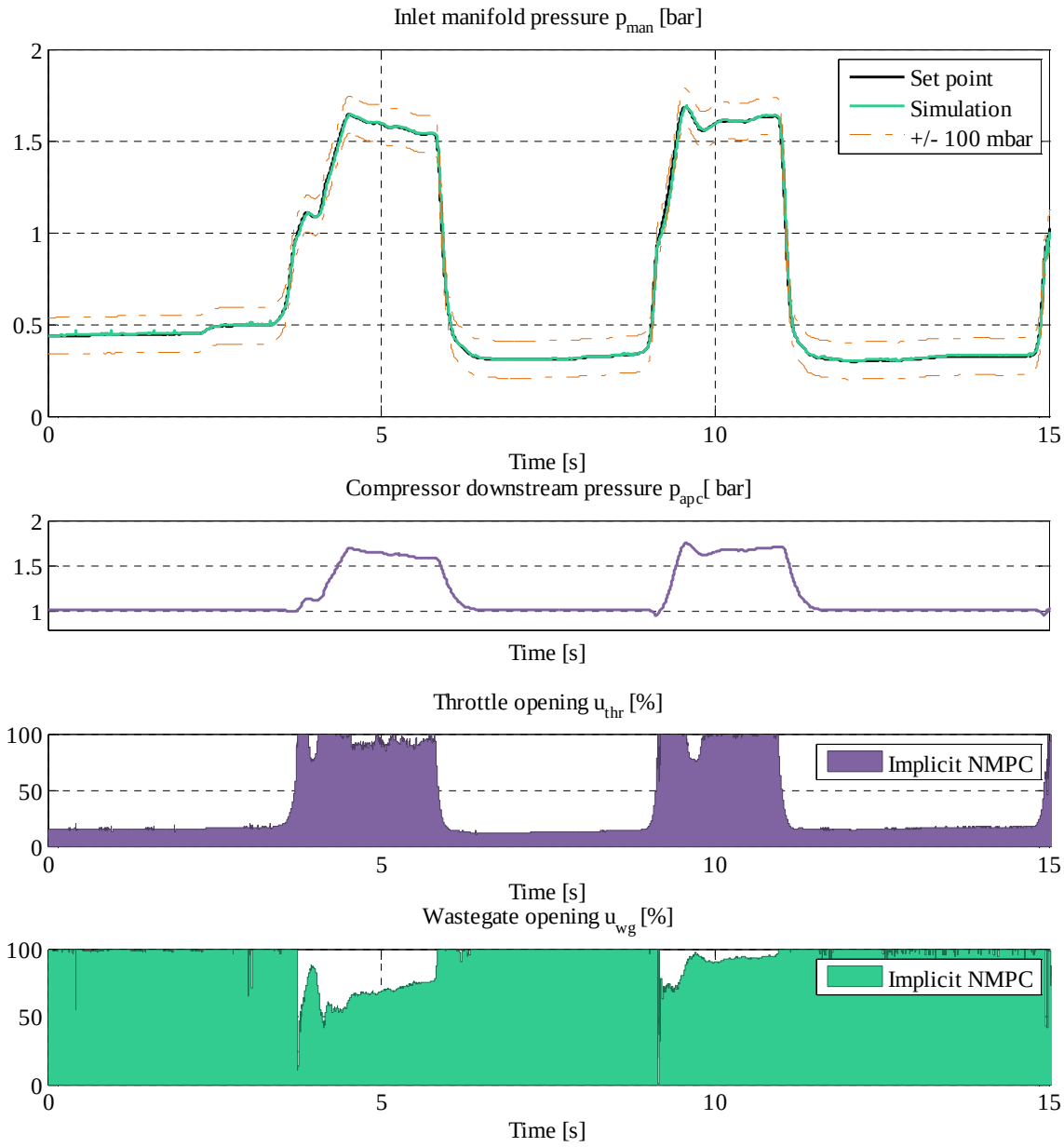

Figure 5.9 – Validation cycle #2: performance of the implicit NMPC scheme on a realistic intake manifold pressure set point transient p_{man}^{SP}. Note that the engine speed N_e varies continuously between 3,000 rpm and 5,000 rpm (figure 3.12).

5.5 Conclusion

This chapter has introduced a general implicit NMPC scheme and applied it to the control of the intake manifold pressure in a turbocharged gasoline engine. Two distinctive features of the control law must be particularly underlined. First, particular care has been taken to ensure that the implicit NMPC scheme can compute a real-time implementable solution, following the explicit NMPC paradigm. The actual computation and validation of the resulting piecewise affine controller is presented in chapter 7. Secondly, besides being based on a nonlinear physics-based model, the implicit NMPC scheme presented in this chapter directly includes a thermodynamic index factor, in the objective function of the optimization problem. It thus confirms the expectations of several previous authors concerning the benefits of combining physics-based engine models with NMPC [9,46,47,62,100,103,104,114]. Finally, the combination of these features turns this general implicit NMPC into a novel solution for the control of the air path of combustion engines.

The performances of the controller were validated in simulation on standard set point step changes, as well as on realistic vehicle transients that were acquired on an actual vehicle equipped with the engine considered in this study (figure 1.1). In all cases, the performances were in perfect agreement with standard car manufacturer specifications and were similar to standard results available in the literature. Indeed, the benefit of the approach does not concern fuel consumption or pollutant emission reductions but the time and effort that are required to obtain a controller that matches these specifications. Altogether, this chapter confirms the ability of NMPC approaches to handle the physics-based engine models already widely used in the automotive industry and thus represents our second step toward a systematic control design approach for the air path of turbocharged gasoline engines (figure 5.10).

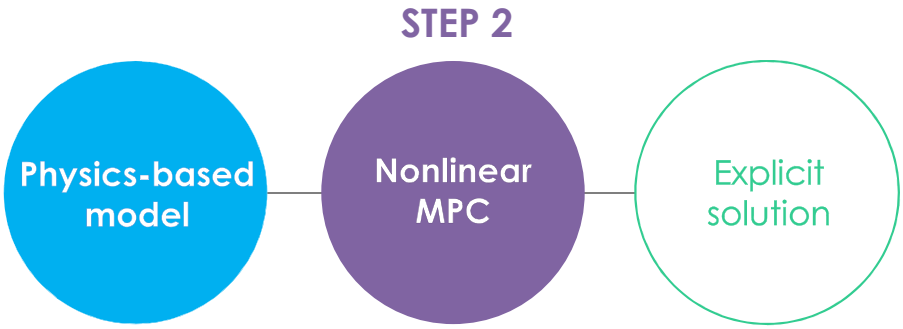

Figure 5.10 – Overview of the control design approach proposed in this study.

In section 5.3.3, it is emphasized that the parameterization of the control trajectory remains an open question when seeking to maximize the performances of the implicit scheme under tight computational constraints. Therefore, before moving on to the computation of the explicit solution of the NMPC scheme in chapter 7, the following chapter provides an alternative approach, based on a set of orthonormal functions, to parameterize the input control trajectory. Rather than simply reducing the control horizon in order to reduce computational requirements, it will provide more flexibility while maintaining the overall complexity of the optimization problem.

CHAPTER 6

ALTERNATIVE IMPLICIT NMPC SCHEME BASED ON FUTURE CONTROL PARAMETERIZATION

Most practical applications of MPC and NMPC are based on a discrete scheme [27,28,52,78,106,111,112,131]. This was indeed the case in the previous chapter where the use of the discrete framework was motivated by the fact that in standard combustion engines, the actuators' position can only be changed at a given sampling time Δt_c. In practice, it took a significant part of the overall calibration effort to determine how often the actuators' position should be allowed to change on the prediction horizon (section 5.3.3.2). The decision rests on a compromise between two competing objectives. On the one hand, the parameterization of the future control trajectory must be parsimonious in order to facilitate the optimization process, but on the other hand, it has to offer enough flexibility to approximate very closely the optimal control trajectory of the original problem.

In the linear framework, MPC schemes using a constant input over the prediction horizon were already successfully implemented in the 1990s [53,108]. In the nonlinear practical case of application presented in chapter 5, a horizon-1 NMPC was sufficient to control the air path of a turbocharged gasoline engine. At each time step, it requires solving a four-parameter optimization problem in order to obtain the optimal throttle and wastegate positions. The resulting computational requirements are particularly reasonable since a least squares solver and 20 iterations are sufficient to obtain the appropriate actuator positions. The performances of this discrete NMPC scheme were validated on set point step changes as well as on realistic vehicle transients. In each case, it matched standard car manufacturer tracking specifications (section 5.4); however in practice, it is well-known that reducing the control horizon may moderate the performances of the closed-loop system [4,27,28,132,133]. It is the search for an alternative constructive methodology to increase the control horizon while maintaining the computational requirements that motivates the developments presented in this chapter.

The philosophy consists in the parameterization of the future control trajectory by means of a set of orthonormal functions. This is an extension of the discrete MPC schemes introduced in [131-133] to the nonlinear framework. This approach, while being generic, provides a sufficiently parsimonious representation of the control trajectory for it to remain computationally efficient. To achieve this, the method uses a set of pre-chosen orthonormal basis functions, namely Laguerre polynomials [128], to decompose the future control increments trajectory. In this chapter, along with the formulation of the resulting NMPC scheme, foreseen in the original study [132,133], a practical case of application for the control of the air path of a turbocharged gasoline engine is presented. The performances are compared to the horizon-1 NMPC scheme presented in chapter 5 on set point step changes and realistic vehicle transients. Particular attention is paid to the calibration methodology required with the unfamiliar resulting NMPC formulation.

The main outcomes of this chapter are: the theoretical formulation of a discrete NMPC control scheme that uses the set of Laguerre functions to parameterize the future control trajectory; a calibration procedure proposal for the particular case of combustion engines; and a practical comparative study of the performances with respect to a horizon-1 NMPC scheme.

Section 6.1 starts by a brief background about orthonormal expansions, Laguerre polynomials and their application to the expansion of the future control trajectory. Finally in section 6.1.4, practical implementation considerations are provided in order to facilitate the use of the function. Then, section 6.2 provides a practical case of application, namely the control of the air path of the turbocharged gasoline engine presented and modeled in chapter 3. Finally in section 6.3, simulation results are provided and compared to the standard horizon-1 implicit NMPC scheme introduced in chapter 5.

6.1 Parameterization of the future control trajectory using Laguerre polynomials

6.1.1 Overview of orthonormal expansions

Assuming that $l_i, i \in \{1,2,...\}$ is an orthonormal and complete set of real functions over the interval $[0,+\infty[$, any arbitrary function $f(t)$ can be formally expanded on this set and expressed in terms of a series expansion [79]:

$$f(t) = \sum_{i=1}^{+\infty} C_i \cdot l_i\,(t) \tag{6.1}$$

s.t.

$$\int_0^{+\infty} l_i(t) \cdot l_i(t)\,dt = 1 \tag{6.2}$$

$$\int_0^{+\infty} l_i(t) \cdot l_j(t)\,dt = 1 \quad i \neq j \tag{6.3}$$

where C_i represents a set of scalar coefficients that weight each function.

This is a classical framework for function expansion, similar to the Fourier expansion. The latter is well-known in numerical analysis, for the approximation of functions in differential and integral equations [130].

Now, assuming that $f(t)$ is not arbitrary but falls in the category of piece-wise continuous functions satisfying:

$$\int_0^{+\infty} f(t) \cdot f(t)\,dt < +\infty \tag{6.4}$$

$f(t)$ can be approximated to any given tolerance $\varepsilon > 0$ using a truncated expansion of a finite number N of terms such that:

$$f(t) = \sum_{i=1}^{N} C_i \cdot l_i(t) \tag{6.5}$$

with

$$\int_0^{+\infty} (f(t) - \sum_{i=N+1}^{+\infty} C_i \cdot l_i(t))^2\,dt \leq \varepsilon \tag{6.6}$$

In summary, a truncated expansion of N terms (6.5) can be used to closely approximate any piecewise continuous function $f(t)$. In a general framework, this philosophy can for example be used to represent linear systems. In this chapter, we will use it to approximate the optimal future control increments trajectory. The next sub-section provides insight into the set of orthonormal functions l_i that was chosen for the expansion, namely the set of Laguerre polynomials [128,133].

6.1.2 Presentation of Laguerre polynomials

Among other orthonormal functions such as Legendre polynomials [37] that have already been successfully used in an MPC framework, the set of Laguerre functions (6.7) offers the advantage of programming simplicity. Indeed, it can be computed using a simple matrix difference equation [132,133].

$$L(k) = [l_1(k) \quad l_2(k) \quad \cdots \quad l_N(k) \ ]^T \tag{6.7}$$

where N corresponds to the number of Laguerre functions, i.e. the number of levels of the decomposition.

In the discrete-time framework that will follow, Laguerre functions are usually defined by their z-transfer. In particular, it is well-known that the z-transfer of the m-th Laguerre polynomial l_m takes the simple form below:

$$\mathcal{Z}(l_m) = \frac{\sqrt{(1-a^2)}}{z-a}\left[\frac{1-az}{z-a}\right]^{m-1} \tag{6.8}$$

where $a \in [0; 1[$ is a dimensionless parameter called scaling factor.

The effect of the scaling factor a on the temporal shape of the Laguerre function is illustrated on figure 6.1. It should be noted that Laguerre functions all converge to zero after a time that depends on the scaling factor a. As the value of the scaling factor increases, the convergence speed decreases and the trajectory becomes smoother. In the particular case where $a = 0$, the set of Laguerre polynomials becomes a set of pulses, respectively at $k = \{1,2, \dots N\}$.

Finally, as suggested above, the discrete values of Laguerre polynomials are computed very easily using the matrix difference equation below:

$$L(k+1) = \begin{bmatrix} a & 0 & 0 & \dots & 0 \\ b & a & 0 & \dots & 0 \\ -ab & b & a & \dots & 0 \\ a^2b & -ab & b & \dots & 0 \\ \vdots & \vdots & & & 0 \\ (-1)^{N-2}a^{N-2}b & (-1)^{N-3}a^{N-3}b & \dots & b & a \end{bmatrix} \cdot L(k) \tag{6.9}$$

where $b = 1 - a^2$ and the initial condition is given by:

$$L(0) = \sqrt{b} \cdot [1 \quad -a \quad a^2 \quad \dots \quad (-1)^{N-1}a^{N-1}]^T \tag{6.10}$$

6.1.3 Application to the expansion of the future control increments trajectory

In a receding control framework, Laguerre polynomials have proved to be suitable for parameterizing a future control trajectory when considering linear time invariant systems with closed-loop stability [37,131-133]. Assuming that, in this particular case, the control signal u converges to a constant after a set point change, its derivative converges to zero. Then, it is possible to expand the derivative of the control trajectory on the set of Laguerre functions, since the latter naturally converge to zero (figure 6.1).

Assuming that the control trajectory shows a similar behavior in a discrete time framework, an analogous approach consists in approximating the control increment trajectory Δu of a single actuator, by series with a finite number of terms:

$$\Delta u(k) = \sum_{m=1}^{N} C_m \cdot l_m(k) \tag{6.11}$$

s.t.

$$u(k) = u(k-1) + \Delta u(k) \tag{6.12}$$

where N is the number of terms l_m used to describe the control trajectory: as N increases, the degrees of freedom of the control trajectory increase. $C_m = [C_1 \quad C_2 \quad \dots \quad C_N]^T$ is the vector of weights to be identified.

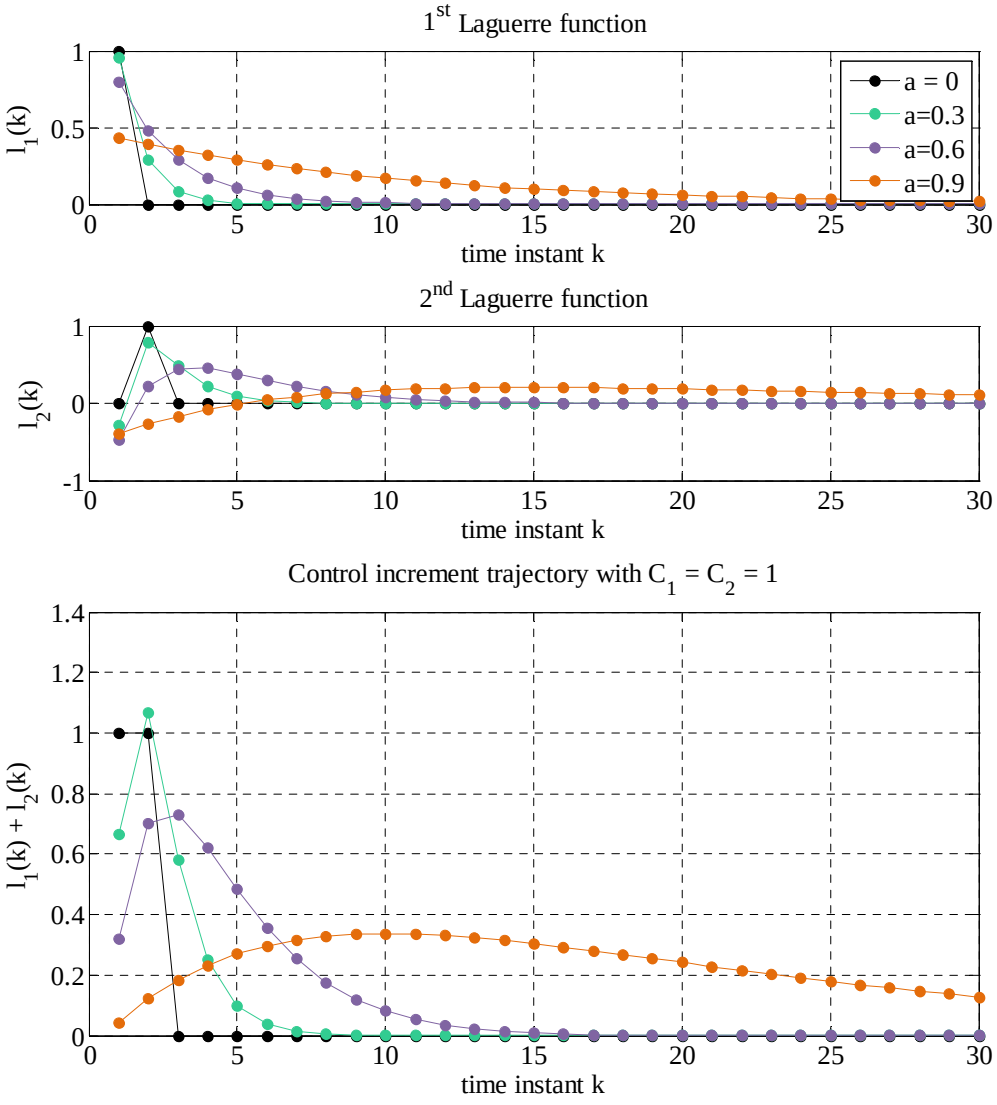

Figure 6.1 – The first two levels of expansion of the Laguerre polynomials are plotted for various values of the scaling factor ($a = 0$, $a = 0.3$, $a = 0.6$, $a = 0.9$). On the bottom graphs, the control increments trajectory (6.11) is plotted for $C_1 = C_2 = 1$. As the value of the scaling factor increases, the control horizon increases and the trajectory becomes smoother. When $a = 0$, the set of Laguerre polynomials becomes a set of pulses, respectively at $k = 1$ and $k = 2$.

In practice the problem of finding the optimal control signal u^* over a given prediction horizon N_p in the NMPC framework (5.3)-(5.8) is converted into determining an optimal vector of N weights C_m. This philosophy is illustrated on figure 6.1, where the control increments trajectory Δu, resulting from a 2-level Laguerre expansion with $C_1 = C_2 = 1$, is depicted on the bottom plot. The effect of the scaling factor a on the control trajectory, i.e. at each time instant k the sum of N terms $C_m \cdot l_m(k)$, is similar to what was observed on each Laguerre function in section 6.1.2.

6.1.4 Practical implementation considerations

In order to facilitate the use of Laguerre polynomials in the receding horizon framework, the complete future control trajectory u can be described in the form of a single vector that contains the control increments Δu over the prediction horizon N_p (figure 4.4).

Given the vector of parameters $C_m = [C_1 \quad C_2 \quad \dots \quad C_N]^T$ and using (6.11), the vector of control increments for a single actuator can easily be obtained from the matrix equation below:

$$\begin{pmatrix} \Delta u(k) \\ \Delta u(k+1) \\ \vdots \\ \Delta u(k+N_p) \end{pmatrix} = \mathbb{L} \cdot C_m \tag{6.13}$$

where each column of the matrix $\mathbb{L}$, contains the N_p successive values of the mth Laguerre polynomials $l_m(k)$. The N levels of expansion are then organized side by side so that the dimension of $\mathbb{L}$ is $N_p \times N$:

$$\mathbb{L} = \begin{pmatrix} l_1(k) & l_2(k) & \cdots & l_N(k) \\ l_1(k+1) & l_2(k+1) & \cdots & l_N(k+1) \\ \vdots & \vdots & & \vdots \\ l_1(k+N_p) & l_2(k+N_p) & \cdots & l_N(k+N_p) \end{pmatrix} \tag{6.14}$$

Similarly, the sequence of control signals over the prediction horizon is directly given by the matrix equation below:

$$\begin{pmatrix} u(k) \\ u(k+1) \\ \vdots \\ u(k+N_p) \end{pmatrix} = \mathbb{L}_\Sigma \cdot C_m + u(k-1) \tag{6.15}$$

where $\mathbb{L}_\Sigma$ corresponds on each column to the cumulated sum of the respective column in $\mathbb{L}$ (6.14):

$$\mathbb{L}_\Sigma = \begin{pmatrix} l_1(k) & l_2(k) & \cdots & l_N(k) \\ \sum_{i=1}^{2} l_1(k+i) & \sum_{i=1}^{2} l_2(k+i) & \cdots & \sum_{i=1}^{2} l_N(k+i) \\ \vdots & \vdots & & \vdots \\ \sum_{i=1}^{N_p} l_1(k+i) & \sum_{i=1}^{N_p} l_2(k+i) & \cdots & \sum_{i=1}^{N_p} l_N(k+i) \end{pmatrix} \tag{6.16}$$

Note that when $a = 0$, $L(k)$ becomes a set of pulses and the use of Laguerre polynomials for the parameterization of the control signal is then equivalent to the traditional NMPC approach (section 4.2.2) used in chapter 5. Conversely, for non-zero values, as a increases, the control horizon increases in the sense of temporal spectrum (figure 6.1).

6.1.5 Laguerre-based NMPC problem formulation

The general constrained nonlinear optimization problem associated to this parameterization differs only slightly from the formulation introduced in chapter 5, notably because control input increment Δu simply replaces the control input u in (5.3) to (5.8). The discrete formulation of a multi-input parameterized NMPC problem is given by:

$$\mathcal{S}^* = \mathcal{S}(\Delta u^*) = \min_{C_m} \mathcal{S}(x, y, u, \sigma) \tag{6.17}$$

s.t.

$$\mathcal{S} = \sum_{i=k}^{k+N_p} \mathcal{J}(x(i), y(i), \sigma) \tag{6.18}$$

$$x(k+1) = f(x(k), u(k), \sigma) \tag{6.19}$$
$$y(k) = g(x(k), u(k), \sigma) \tag{6.20}$$
$$u(k) = u(k-1) + \Delta u(k) \tag{6.21}$$
$$\underline{x} \leq x(k) \leq \overline{x}\ ,\ \underline{u} \leq u(k) \leq \overline{u}\ ,\ \underline{\Delta u} \leq \Delta u(k) \leq \overline{\Delta u} \tag{6.22}$$
$$x(k) = x_0 \tag{6.23}$$
$$u(k-1) = u_0 \tag{6.24}$$

where $H_p = [k, k+N_p]$ is the prediction horizon and $\Delta u(k)$ is given by (6.11). Together, f and g stand for the nonlinear model that describes the discrete-time dynamic of the system. $\underline{x}$, $\overline{x}$, $\underline{u}$, $\overline{u}$, $\underline{\Delta u}$ and $\overline{\Delta u}$ respectively stand for lower and upper bounds on the states, control variables and control increments.

Combining (6.15) and (6.22), the constraints on the amplitude of the inputs can be rewritten in a more practical way. In fact, for each input, the following system of inequalities applies:

$$\begin{cases} \mathbb{L}_\Sigma C_m < \overline{u} - u(k-1) \\ -\mathbb{L}_\Sigma C_m < u(k-1) - \underline{u} \end{cases} \tag{6.25}$$

When needed, a similar system of inequalities can take into account the constraints on the inputs' rate of change. It is obtained be combining (6.13) and (6.22):

$$\begin{cases} \mathbb{L} \cdot C_m < \overline{\Delta u} \\ -\mathbb{L} \cdot C_m < -\underline{\Delta u} \end{cases} \tag{6.26}$$

The distinctive feature of using Laguerre functions in a predictive framework is the fact that with an increase in the number of terms N, the orthonormal expansion will converge to the optimal control trajectory dictated by the objective function. This cannot be said of other arbitrary sets of exponential functions, assembled without taking orthogonality into account..

6.2 Application to the control of the air path

6.2.1 Problem formulation

The application to the control of the air path of a turbocharged gasoline engine is straightforward since the overall air path control problem formulation remains unchanged (section 5.1). Like the NMPC scheme presented in chapter 5, the objective is to track an inlet pressure manifold set point by means of two valve actuators: the throttle and the wastegate (section 5.1). Again, the physics-based engine model derived in chapter 3 is used to compute the state and output predictions. For the sake of completeness, the main characteristics of this NMPC problem are recapitulated below.

The vector of states x contains the four states of the model (6.27), the model outputs are the inlet manifold pressure p_{man} and the pressure upstream the turbine p_{avt} (6.28). Both actuators (6.29) are saturated

between closed and fully open. A vector of exogenous inputs σ takes into account the ambient conditions $\{p_{amb}, \theta_{amb}\}$, the engine speed N_e and inlet manifold pressure set point p_{man}^{SP} (6.30):

$$x \coloneqq \left(p_{ape}, p_{man}, p_{avt}, \omega_t\right)^T \tag{6.27}$$

$$y \coloneqq (p_{man}, p_{avt}) \tag{6.28}$$

$$u \coloneqq \left(u_{thr}, u_{wg}\right) \tag{6.29}$$

$$\sigma = (N_e, p_{man}^{SP}, p_{amb}, \theta_{amb}) \tag{6.30}$$

Finally, the outputs of the model p_{man} and p_{avt} are used to compute an objective function $\mathcal{S}$ that maximizes the engine cycle efficiency (section 5.3) besides ensuring an accurate inlet manifold pressure tracking, analogously to chapter 5:

$$\mathcal{S} = \sum_{k=1}^{Hp} \left(\alpha (p_{man}^{SP} - p_{man})^2 + \beta \left(\frac{p_{avt}}{p_{man}} \right) \right) \tag{6.31}$$

where α and β are used to scale and penalize each term of the cost function and should be chosen appropriately (section 5.3.3.1).

At this stage, all that remains is a reasonable choice for: the number of terms N in the expansion (6.11); the prediction horizon H_p ; and the scaling factor a in (6.9) and (6.10). The following sub-sections respectively describe the influence of each of these degrees of freedom and conclude with recommendations in order to determine an appropriate set of parameters. The final tuning is determined in agreement with the transient performances of the closed-loop and presented in section 6.3.

6.2.2 Calibration of the NMPC scheme

Based on the experience obtained on this particular example, the final number of terms in the expansion N (section 6.2.3), the prediction horizon H_p (section 6.2.4) and the scaling factor a (section 6.2.5) can be adjusted in that order, starting from the first interpretations obtained from a parametric analysis on a typical step response such as the one achieved above. However, even for insiders, the final tuning has to be performed by trial-and-error on transients, representative of the real operating conditions of the closed-loop system (section 6.3).

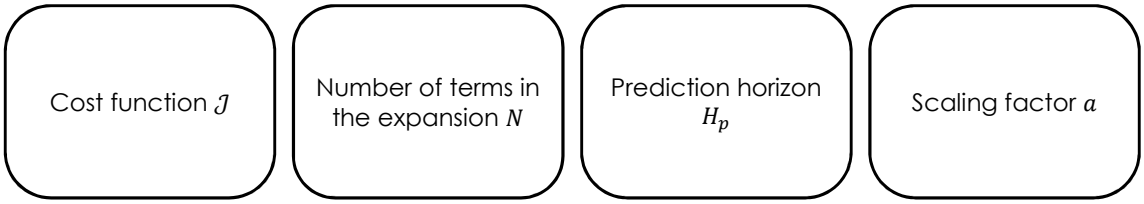

Figure 6.2 – Four calibration parameters of the NMPC scheme based on the expansion of the future control increments trajectory on a set of N Laguerre functions.

6.2.2.1 Number of terms N in the expansion

Similarly to what was observed in [131-133], increasing the number of terms N in the expansion (6.11) tends to increase the maximum flexibility of the future control trajectory. Along with this increase in flexibility, the trajectories are smoother (figure 6.1), resulting in a less aggressive controller. The main drawback is that the computational requirements to solve the optimization problem also increase with N.

The effect of a change in N can be observed on the closed-loop system response to inlet manifold set point step changes. Two constant engine speed cases are presented on figure 6.3 below. On the left, while the

engine speed is kept constant at 2,000 rpm, the inlet manifold pressure set point p_{man}^{SP} is moved from 0.6 bar (low load) to 1.6 bar (high load). On the right, p_{man}^{SP} is changed from 0.9 bar to 1.6 bar while the engine speed N_e remains constant at 5,000 rpm. In accordance with what was already observed on the effect of the engine speed on the engine dynamics (chapter 5), the time response at 5,000 rpm is substantially smaller.

During this first stage of the tuning methodology, the prediction horizon H_p and the scaling factor a are kept constant. A rough estimate of their optimal value is typically sufficient to be representative of the overall controller behavior. In this study, tests were performed using $a = 0.5$ and $H_p = 200$ ms. The latter was chosen in agreement with the settling time of the system (section 5.3.3.3).

Finally, figure 6.3 shows that using only one Laguerre polynomial to build the control trajectory tends to considerably slow down the system at both engine speeds. Then from $N = 2$ to $N = 5$, increasing the number of terms does not significantly influence the step response of the closed-loop. Since the primary objective remains to minimize the computational requirements (section 5.2.3), a 2-level expansion can be chosen in this study. This leads to determining, at each sampling time, two parameters for each actuator, i.e. solving a 4-dimension optimization problem. In this case, the computational requirements remain acceptable since the problem can be solved using a simple trust-region reflective algorithm method, as implemented in Matlab®. The algorithm converges within 20 iterations when initialized at $\Delta u(k) = 0, k \in [1, N_p]$.

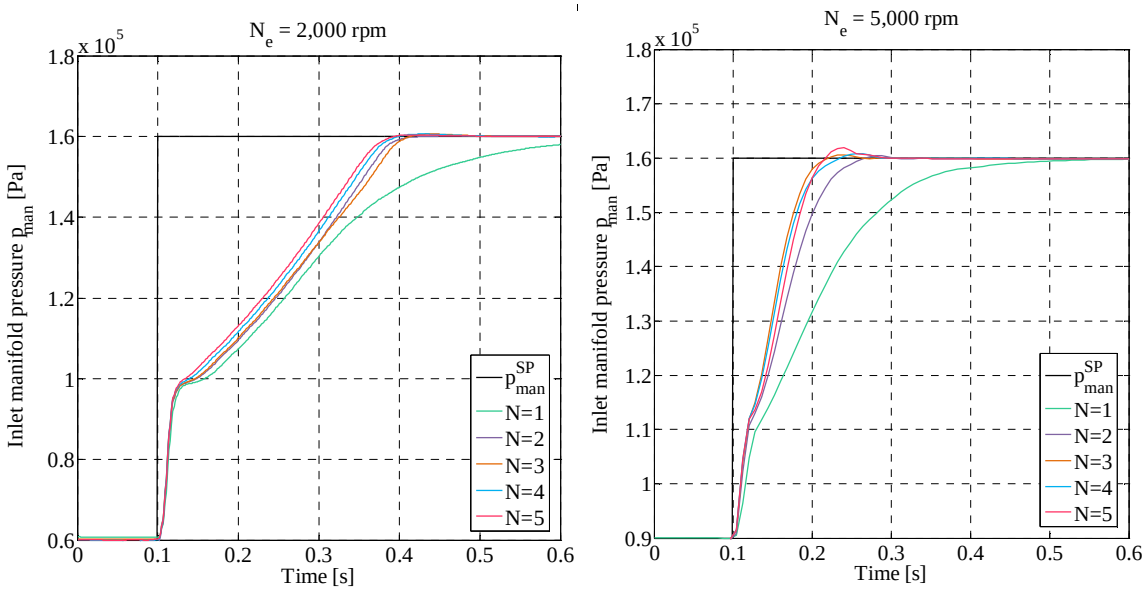

Figure 6.3 – Influence of the number of terms used in the expansion at 2,000 rpm (left) and 5,000 rpm (right). From $N = 2$ to $N = 5$ the control law presents similar performances. $H_p = 200$ ms and $a = 0.5$.

Altogether, the minimum number of terms N to be used in the expansion (6.11) should be given in agreement with the maximum acceptable time response of the system. Above this boundary, the decision is driven by the computational capabilities available to solve the optimization problem. In any case, an increase in the number of terms in the expansion will lead to the convergence of the control trajectory to the optimal trajectory dictated by the objective function.

6.2.2.2 Prediction horizon H_p

As in standard NMPC approaches [27,28], the prediction horizon H_p should be chosen in agreement with the settling time of the system. As suggested before, in the case of a turbocharged gasoline engine, the latter can vary from about 80 ms to 300 ms. On figure 6.4 below, the performances of the parameterized NMPC scheme are depicted for different lengths of the prediction horizon: 100, 200, 300 and 500 ms. Again, two engine rotational speeds N_e were evaluated, namely 2,000 rpm and 5,000 rpm, and the same inlet manifold pressure set point step as before is presented. In both cases, the scaling factor a was 0.5 and, in agreement with section 6.2.2.1, $N = 2$.

It should be pointed out that, in our particular case of application, the influence of H_p on the response of the closed-loop system depends on the engine rotational speed N_e. Indeed, at low rotational speeds (left figure 6.4), it is clear that the settling time of the engine is not affected by the prediction horizon that is chosen. However, at 5000 rpm, i.e. a typically high engine rotational speed, the settling time of the system depends nonlinearly on the prediction horizon (right figure 6.4). In particular, using a prediction horizon of 100 ms considerably accelerates the engine response while for prediction horizons greater than 200 ms, the influence rapidly decreases. This can be explained by the fact that, at 5,000 rpm, 200 ms is typically greater than the settling time of the system. Then, since the control increments Δu are equal to zero beyond this time interval, there is no significant difference

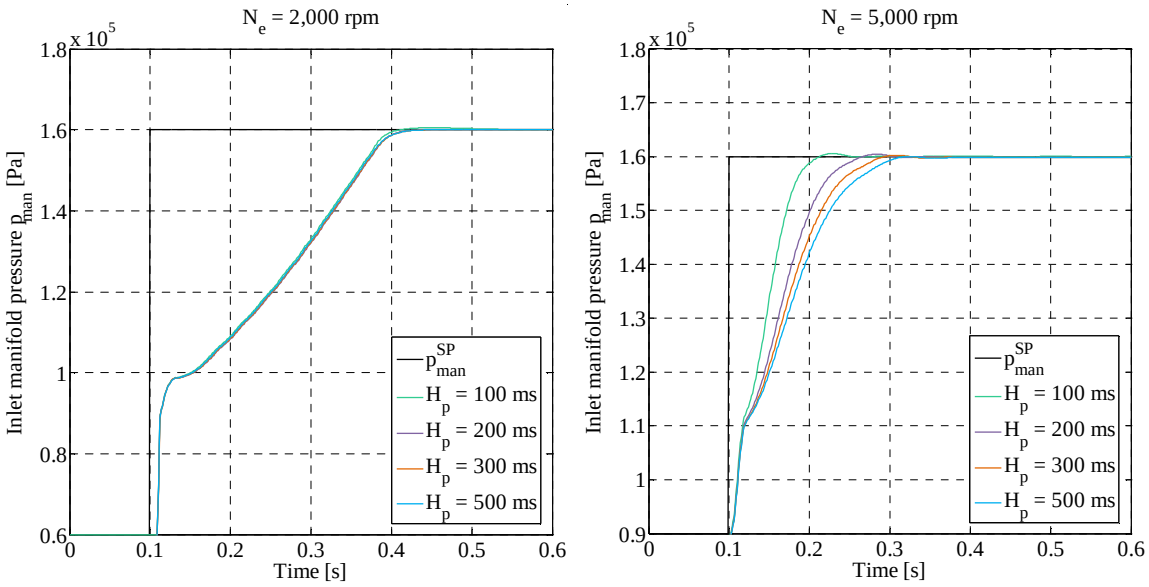

Figure 6.4 – Influence of the prediction horizon H_p on the step response of the engine at 2,000 rpm (left) and 5,000 rpm (right). At 2,000 pm, the response of the system is independent of the prediction horizon. On the contrary, at 5,000 rpm, the settling time of the system depends nonlinearly on the prediction horizon. $N = 2$ and $a = 0.5$.

The prediction horizon H_p is a tuning parameter because the NMPC formulation (6.17)-(6.24) has an embedded integral action. Hence, the following theoretical consideration must be taken into account concerning the determination of an appropriate value: the prediction horizon must be sufficiently large to include the range within the Laguerre functions decay (figure 6.1). A reasoned choice of the prediction horizon should also take into account the dynamic of the system at high rotational speeds. Here all four prediction horizons lead to acceptable performances with respect to the car manufacturer specifications. To

facilitate the comparison with the horizon-1 NMPC scheme presented in chapter 5, as well as providing a sufficient level of stability to the closed-loop system, $H_p = 200$ ms was chosen for the rest of the study.

6.2.2.3 Scaling factor a

While the number of Laguerre functions in the expansion has been shown to influence the flexibility of the control trajectory and the prediction horizon to mainly influence the dynamic at high engine speeds, the scaling factor will allow tuning of the final dynamic and level of stability of the closed-loop system. This is actually a similar philosophy to the change in the control horizon H_c in a standard NMPC scheme (section 5.3.3.2).

Figure 6.5 below presents the closed loop response of the system to an inlet manifold pressure set point step change. Different values of the scaling factor are evaluated, from 0.2 to 0.8. Once again, two cases are presented: 2,000 rpm and 5,000 rpm. In agreement with the previous sub-sections, $N = 2$ and $H_p = 200$ ms.

At low rotational speeds, the influence of the scaling factor on the settling time of the system is minor but still nonlinear: a bigger change is observed between $a = 0.2$ and $a = 0.5$ than between $a = 0.5$ and $a = 0.8$. At high rotational speeds, the same nonlinear effect is observed but the scaling factor has much more influence on the shape of the closed-loop response. In both cases, the smaller the scaling factor, the faster the controller due to a more aggressive control trajectory (figure 6.5).

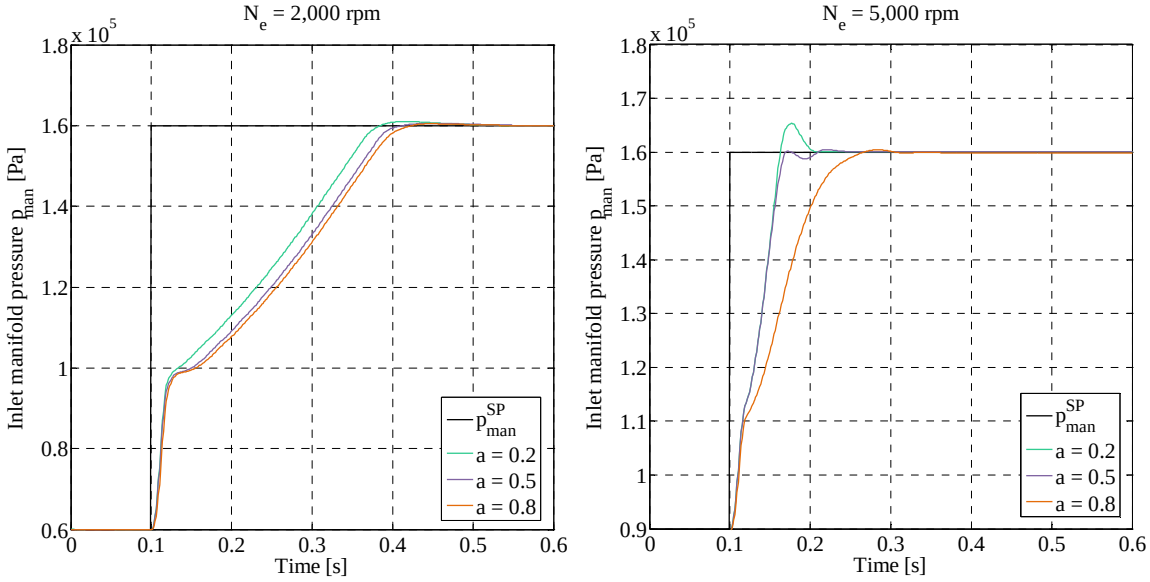

Figure 6.5 – Influence of the scaling factor a on the step response of the engine at 2,000 rpm (left) and 5,000 pm (right). It can be noticed that the scaling factor has a nonlinear effect on the step response, larger at 5,000 rpm than at 2,000 rpm. $N = 2$ and $H_p = 200$ ms.

To conclude these calibration recommendations, it is noted that once again, a reasonable choice of the scaling factor a must be done in agreement with the fastest engine dynamic.

A final point to note is that in the case of difficult multi-input systems, the closed-loop performance can be fine-tuned by selecting an appropriate pair of parameters $\{a, N\}$ for each input. For instance, a larger scaling factor along with fewer terms in the expansion corresponds to a future control trajectory with a lower decay rate.

6.3 Simulation performances

6.3.1 Transient performances

Figures 6.6 and 6.7 depict the transient performances of the NMPC law based on the parameterization of the future control increments trajectory on a set of $N = 2$ Laguerre functions (section 6.2.2.1). In the final set of calibration parameters, the prediction horizon is $H_p = 200$ ms (section 6.2.2.2) and the scaling factor (section 6.2.2.3) was set at $a = 0.7$ in accordance with the transient performances obtained on the validation cycles. These cycles represent samples of a driving sequence recorded on a vehicle equipped with the engine (figure 1.1). The engine speed varies continuously between 2,500 rpm and 5,000 rpm while the intake manifold pressure set point p_{man}^{SP} varies from 200 mbar (low load) to roughly 1,700 mbar (high load) (figures 3.11 and 3.12). The cycle includes areas where the sensitivity of the wastegate is very low, and set point change dynamics that require sudden actuator opening and closing.

In both situations, it can be seen that the closed-loop leads to tracking performances in agreement with car manufacturer specifications (section 5.1.4). In fact, the inlet manifold trajectory shows no static error and during transients, remains within a +/- 100 mbar tolerance interval.

Our preliminary conclusion to this work is that, altogether, the calibration effort that is required to tune this Laguerre functions-based NMPC scheme remains quite similar to what is required when calibrating a more standard NMPC design, or more precisely to what was presented in chapter 5. In fact, once the objective function has been defined, instead of the two control and prediction horizons (figure 5.4), only three parameters need to be tuned here, namely N, H_p and a (figure 6.2). Moreover in practice, they all carry a clear physical sense in terms of closed-loop behavior that considerably facilitates the calibration stage (section 6.2.2).

As for computational requirements, both approaches are equivalent in terms of the number of parameters in the general optimization problem (4.1)-(4.5) solved in an NMPC framework. Indeed, using a 2-level Laguerre function expansion, i.e. $N = 2$, requires solving a 4-dimension problem at each time step (2 parameters C_1 and C_2 in (6.17)-(6.24), need to be determined for each actuator). This is similar to the NMPC scheme presented in chapter 5, based on a horizon-1 formulation (figures 5.8 and 5.9). Additionally, both led to sufficiently good tracking performances within 20 iterations, in our particular case of application.

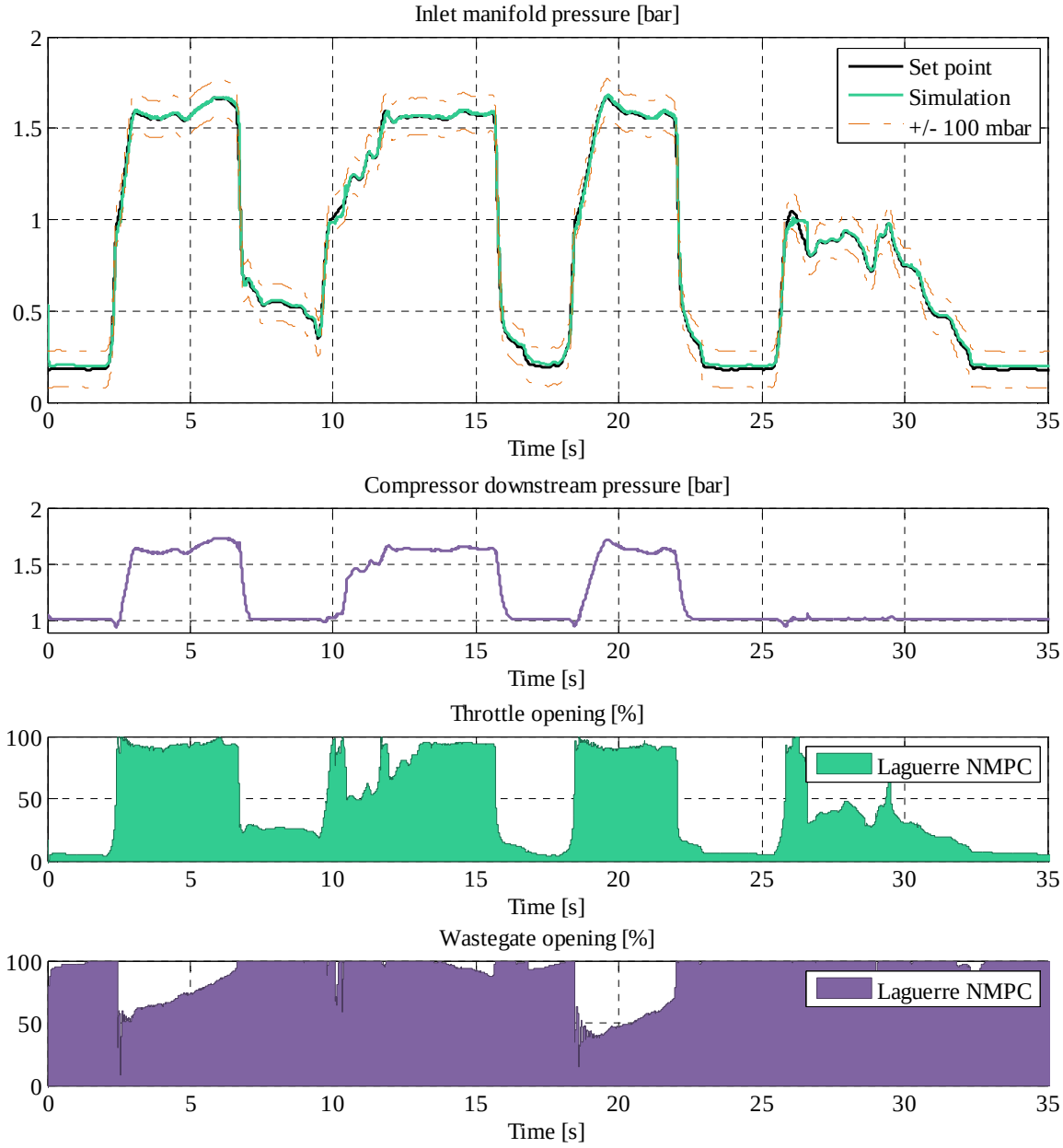

Figure 6.6 – Validation cycle #1: Inlet manifold pressure p_{man} tracking performances on a realistic driving cycle. The controller is parameterized as follows: $N = 2$, $H_p = 200$ ms and $a = 0.7$. The bottom plot respectively displays the corresponding compressor downstream pressure and actuator openings.

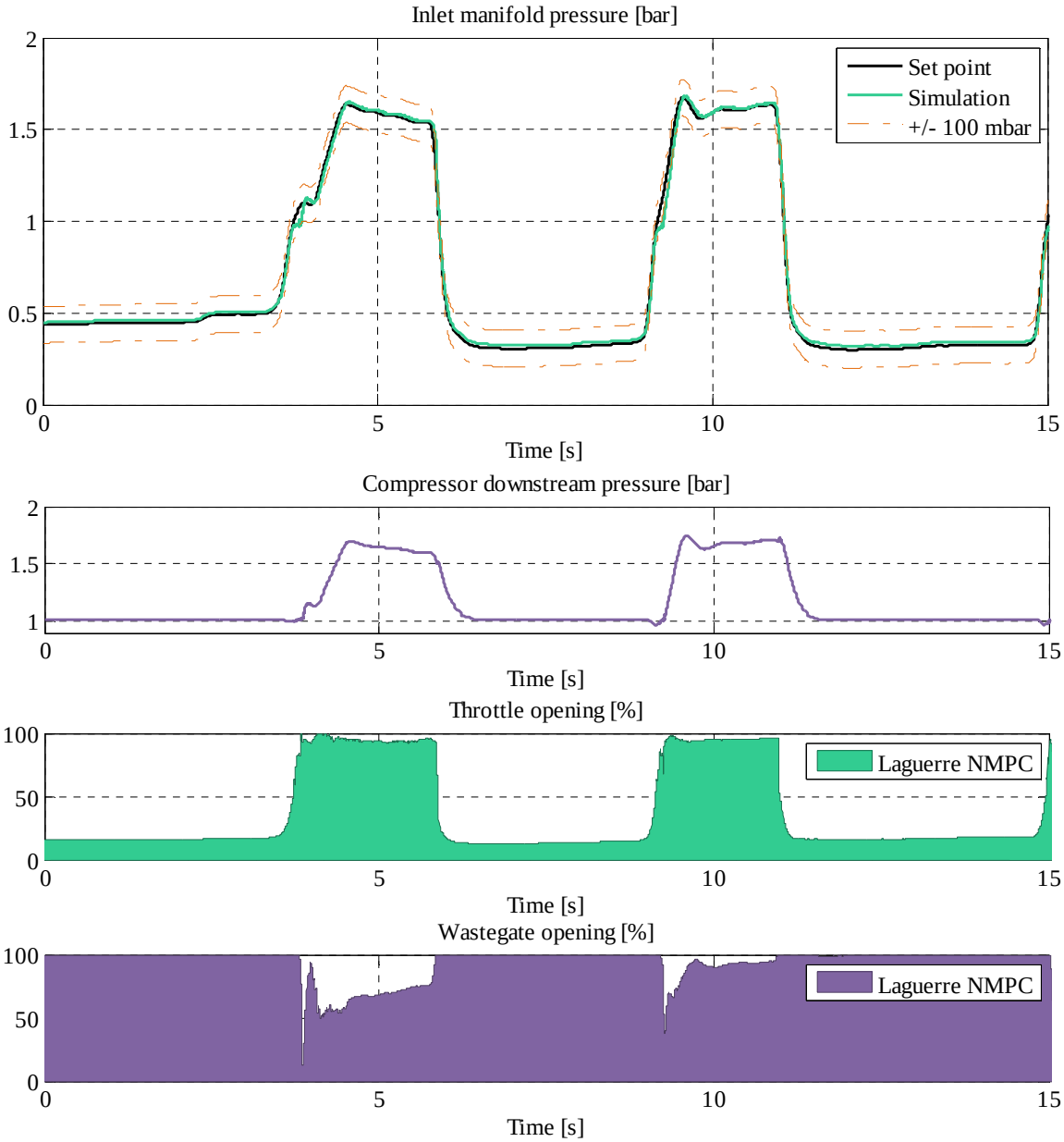

Figure 6.7 – Validation cycle #2: Inlet manifold pressure p_{man} tracking performances on a realistic driving cycle. The controller is parameterized as follows: $N = 2$, $H_p = 200$ ms and $a = 0.7$. The bottom plot respectively displays the corresponding compressor downstream pressure and actuator openings.

6.3.2 Performance analysis w.r.t. horizon-1 NMPC

When figures 5.8 and 5.9 that depict the performances of the horizon-1 NMPC case (detailed in chapter 5) are compared to the transient performances of the Laguerre-based NMPC law presented on figures 6.6 and 6.7, it can be seen that, even though both situations are acceptable w.r.t the time scale, the NMPC scheme presented in this chapter leads to an actuator positioning that fluctuates significantly less. This can be explained by the fact that whereas a satisfactory approximation of the optimal future control law trajectory of the orignial problem (4.1)-(4.5) requires a large number of forward shift operators, the increase in flexibility over the prediction horizon provided by the approach presented in this chapter directly benefits the NMPC scheme.

In practice, for a given number of terms N in the Laguerre-based NMPC framework, the flexibility over the prediction horizon H_p can be increased by tuning the scaling factor a (figure 6.1). However, if the flexibility increases with a, it also tends to slow down the closed-loop response (figure 6.5) since the future control increments trajectory becomes smoother and less aggressive (figure 6.1). The final behavior of the closed-loop is indeed the result of a compromise between stability and time response when determining an appropriate value of the scaling factor. The advantage w.r.t. the standard NMPC scheme is that in this approach this compromise is encapsulated in a tuning parameter that controls the phenomena in a monotonic fashion (figure 6.5).

6.4 Conclusion

Without appropriate tuning, the computation requirements involved in implicit NMPC laws are known to be prohibitive due to the need to solve a usually high-dimensional non-convex optimization problem. Even in simulation, the computation can quickly become time-consuming or even prohibitive when considering the use of a physics-based prediction model. In chapter 5, this issue was overcome by reducing the control horizon, i.e. by reducing the degrees of freedom of the future control trajectory. This is a well-known, common and straightforward approach to decrease the number of parameters of the optimization problem. However in practice, it suffers from a major drawback: reducing the number of actuator positions in the future control trajectory may reduce the performances of the closed-loop system in terms of settling time, stability and robustness when a large number of forward shift operators are needed to approximate the optimal future control trajectory. An alternative versatile and parsimonious parameterization of the future control trajectory has therefore been investigated and a proposal is made in this chapter.

The parameterized NMPC formulation proposed in this chapter is a direct extension to the nonlinear framework of the approach introduced by [131-133]. It maintains the computational requirements while offering a new range of trade-offs between the number of inputs of the optimization problem and the flexibility of the future control trajectory. The idea is based on the expansion of the future control increments trajectory on a set of orthonormal functions, namely Laguerre polynomials (section 6.1.2). In the nonlinear framework in which it is applied, this innovative control scheme presents several advantages. One of them is that it allows a lot more flexibility in the control trajectory, while maintaining equivalent computational requirements. In particular, the compromise between stability and speed of the closed-loop system can be entirely controlled using the scaling factor that characterizes this approach.

Along with the NMPC scheme presented in chapter 5, this parameterized NMPC scheme aims to provide a set of relevant alternatives for the design of explicit-ready engine NMPC laws. In both cases, the adaptability and the minimization of the computational requirements open up a very good perspective for the computation of the explicit solution to the associated constrained nonlinear optimization problem.

CHAPTER 7

EXPLICIT NMPC OF THE AIRPATH OF A TURBOCHARGED GASOLINE ENGINE BASED ON A PIECEWISE AFFINE APPROXIMATION

The main emphasis in this chapter is to make the final step toward a systematic approach for the design of the control of the air path of turbocharged gasoline engines. After building a physics-based model essentially calibrated from standard steady-state test bench trials in chapter 3, and after obtaining great control performances from a standard implicit NMPC approach in chapter 5, the ultimate task lies in the implementation of this implicit control scheme in real time. This usually requires solving online and at each sampling instant, a computationally overwhelming nonlinear optimization problem.

Among other approaches to deal with real-time implementation, many authors have highlighted the fact that this optimization problem can be posed parametrically, with the measured extended state vector $\tilde{x}$ as the parameter. Determined exclusively offline, the solution to the associated multi-parametric nonlinear problem provides a piecewise affine approximation of the optimal control law, mapped on a given set of hyper-rectangles covering the parameter space (figure 7.1). Then online, the computation of the actuator positions depends on the evaluation of an explicit function of state $\tilde{x}$ rather than the solution of an optimization problem.

The main outcomes of this chapter are: the modification of an existing explicit NMPC synthesis [53,72] in order to use a computationally expensive prediction model and unconventional objective functions; and a practical physics-based nonlinear case of application of the explicit NMPC paradigm in an unprecedented 6-dimension parameter space.

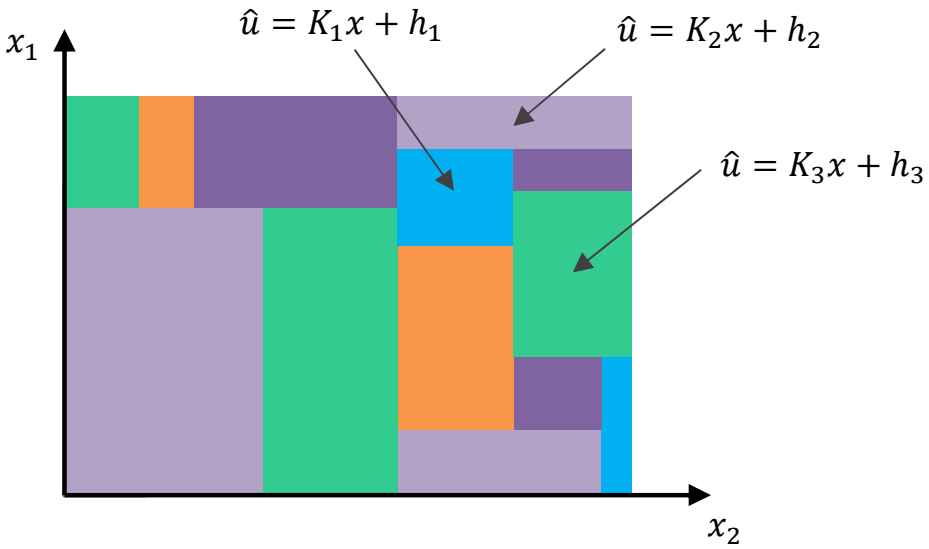

Figure 7.1 – Principle of the explicit nonlinear model predictive control strategy presented in this chapter. It should be compared with the explicit MPC approach (figure 4.5) that uses a polytopic partitioning.

Section 7.1 starts the general multi-parametric programming framework involved in the computation of the explicit solution of MPC and NMPC problems. Sections 7.2 and 7.3 present the general methodologies that are respectively used to: compute an explicit law from a given implicit NMPC scheme, and evaluate the resulting piecewise affine control law on-board. Finally, a practical case of application is presented in sections 7.4 and 7.5, namely the control of the air path of a turbocharged gasoline engine.

7.1 Multi-parametric nonlinear programming (mp-NLP)

The growing interest in parametric programming in the control community in the past few years is motivated by the possibility to reformulate certain optimal control problems as parametric programs. The fact that NMPC is one of them motivates the brief background presented below.

Multi-parametric programming is one way to address parameter variations in mathematical programs. It consists in characterizing the solution to the problem for a full range of parameter values. By nature, it involves solving repeatedly the original problem and therefore usually leads to significant computational requirements. The general appellation *multi*-parametric programming, also denoted mp-NLP, refers to problems depending on several parameters. A very good summary of the results related to multi-parametric programming can be found in [48] and an emphasis on their relation to explicit model predictive control is presented in [53].

Consider a general nonlinear mathematical program, parameterized by a vector x:

$$\mathcal{S}^*(x) = \min_u \mathcal{J}(u,x) \tag{7.1}$$

$$\text{s.t.} \quad g(u,x) \leq 0 \tag{7.2}$$

where $u \in \mathbb{R}^s$ corresponds to optimization parameters, $x \in \mathbb{R}^n$ a given set of parameters, $\mathcal{J}: \mathbb{R}^s \times \mathbb{R}^n \longmapsto \mathbb{R}$ a cost function and $g: \mathbb{R}^s \times \mathbb{R}^n \mapsto \mathbb{R}^q$ the problem constraints.

Let X be a closed polytopic set of parameters such that $X = \{x \in \mathbb{R}^n, Ax \leq b\}$. Assuming that the minimum exists in (7.1)-(7.2), multi-parametric programming consists in characterizing the solution for the set X. As detailed in [2], the solution to such a problem is a triple denoted:

$$\left(X_f, \mathcal{S}^*(x), U^*(x)\right) \tag{7.3}$$

where X_f is the set of feasible parameters and $\mathcal{S}^*$ is the optimal value function that associates to each parameter $x \in X_f$ the optimal value of the original problem (7.1)-(7.2). Similarly, U^* associates to each parameter $x \in X_f$ the set of optimizers of the original problem (7.1)-(7.2).

In a general framework, the components of the constraints function $g(u,x)$ that fulfill (7.2) at equality are called *active* constraints, in opposition to *inactive* constraints.

Let us assume that X_f is closed and that $\mathcal{S}^*$ is finite for all $x \in X_f$. For a given parameter x, if u is a feasible point of the problem (7.1)-(7.2), we denote $\mathcal{A}(u,x)$, the set of indices of active constraints:

$$\mathcal{A}(u,x) \triangleq \{i \in \{1,2,\dots,q\} | g(u,x) = 0\} \tag{7.4}$$

Then, the optimal active set $\mathcal{A}^*(x)$ is the set of indices of the components of the constraints that are active for any $u \in U^*(x)$:

$$\mathcal{A}^*(x) \triangleq \{i | i \in \mathcal{A}(u,x), \forall u \in U^*(x)\} \tag{7.5}$$

Finally, the set of parameters for which the optimal active set is equal to $\mathcal{A}$ is called critical region $CR_{\mathcal{A}}$ and defined such that:

$$CR_{\mathcal{A}} \triangleq \{x \in X | \mathcal{A}^* = \mathcal{A}\} \tag{7.6}$$

In practice, when considering a strictly convex quadratic function f and linear constraints g, the critical regions defined in (7.6) are polyhedrons. Additionally, u^* is unique, piecewise affine and continuous. These appealing properties of the optimizer partially explain the growing interest in explicit MPC. However, in the nonlinear paradigm adopted in this study, the exact solution of a multi-parametric programming problem such as (7.1)-(7.2) cannot be found and a suboptimal approximation of the optimizer function $u^*(x)$ is usually used [53].

7.2 Explicit NMPC law synthesis, using mp-NLP

Similarly to the explicit MPC philosophy (section 4.3), the objective pursued in this chapter is to construct a piecewise approximation to the optimal control law $u^*(x)$ presented in chapter 3, by solving the associated mp-NLP on the parameter space X.

In practice, determining the explicit exact solution of the multi-parametric programming problem in the general nonlinear case imposes limits on the problem definition (section 7.1) that are not compatible with the use of a physics-based nonlinear model (chapter 3) and the use of a non-quadratic objective function (chapter 5), both at the heart of this study. Instead of pursuing this objective, we favor a generic solution and propose a suboptimal approach, based on the philosophy presented in [53,72,125], to determine an approximate solution of the resulting mp-NLP.

In the NMPC paradigm, an appealing idea to achieve this is to define the constituent functions pieces on a hierarchical set of hyper-rectangles covering X (figure 7.1). The resulting hyper-rectangular partitioning then replaces the polytopic partitioning of the parameter space used in the explicit MPC framework (figure 4.5) but the use of a piecewise affine (PWA) function remains. As detailed below in section 7.3, this philosophy leads to a remarkably short online evaluation time, even for a large number of constituent functions pieces [53,125]. If convexity holds, the PWA approximation is computed using only the vertices of the hyper-rectangles. If this property is not guaranteed, the computation uses a combination of vertices and interior points.

The cornerstone of the approach consists in quantifying the accuracy of the approximation by the difference between the optimal value function $\mathcal{S}^*$ and the sub-optimal objective function value $\hat{\mathcal{S}}^*$, rather than between the exact and the approximated solution [53,72,125]. In fact, it should be noted that the difference between the optimal actuator position u^* and the result of the PWA approximation $\hat{u}^* = Kx + h$ is not taken into account during the synthesis of the explicit NMPC law.

The complete synthesis algorithm to compute the explicit NMPC is exclusively used offline. It is presented in detail from sections 7.2.1 to 7.2.5 and comprises four crucial sub-stages:

- splitting a given hyper-rectangle of the parameter space (section 7.2.1),
- generating a set of reference points Θ^j to compute the affine approximation in a given hyper-rectangle j and a set of validation points Φ^j that includes interior-points (section 7.2.2),
- computing the affine approximation $K_j x + h_j$ from the set of reference points Θ^j (section 7.2.3) and then,
- evaluating the accuracy of the affine approximation, in terms of objective function deviation, on the set of validation points Φ^j (section 7.2.4).

7.2.1 Procedure 1: splitting rule

Let X denote the complete parameter space to be explored. The partition of a given hyper-rectangle $X_j \subseteq X \subseteq \mathbb{R}^n$ is obtained by splitting the hyper-rectangle through its center θ_0^j by hyper-planes, on all parameter space axes. As a result of the splitting step, 2^n new hyper-rectangles are generated (figure 7.2).

7.2.2 Procedure 2: set of points generation

For a given hyper-rectangle X_j, we denote by $\Theta^j = \left\{\theta_1^j, \theta_2^j, \dots, \theta_{N_\theta}^j\right\}$ the set of its $N_\theta = 2^n$ vertices. This first set of points is used to compute an approximation of the optimal control law and thus represents a reference set of points.

We also denote $\Phi^j = \left\{\varphi_1^j, \varphi_2^j, \dots, \varphi_{N_\varphi}^j\right\}$ the union of all the vertices of the hyper-rectangles that would be created by using the splitting rule detailed above (section 7.2.1). This set of N_φ vertices is used to validate the approximated control law and represents the validation set of points. Note that $\Theta^j \subset \Phi^j$ (figure 7.2).

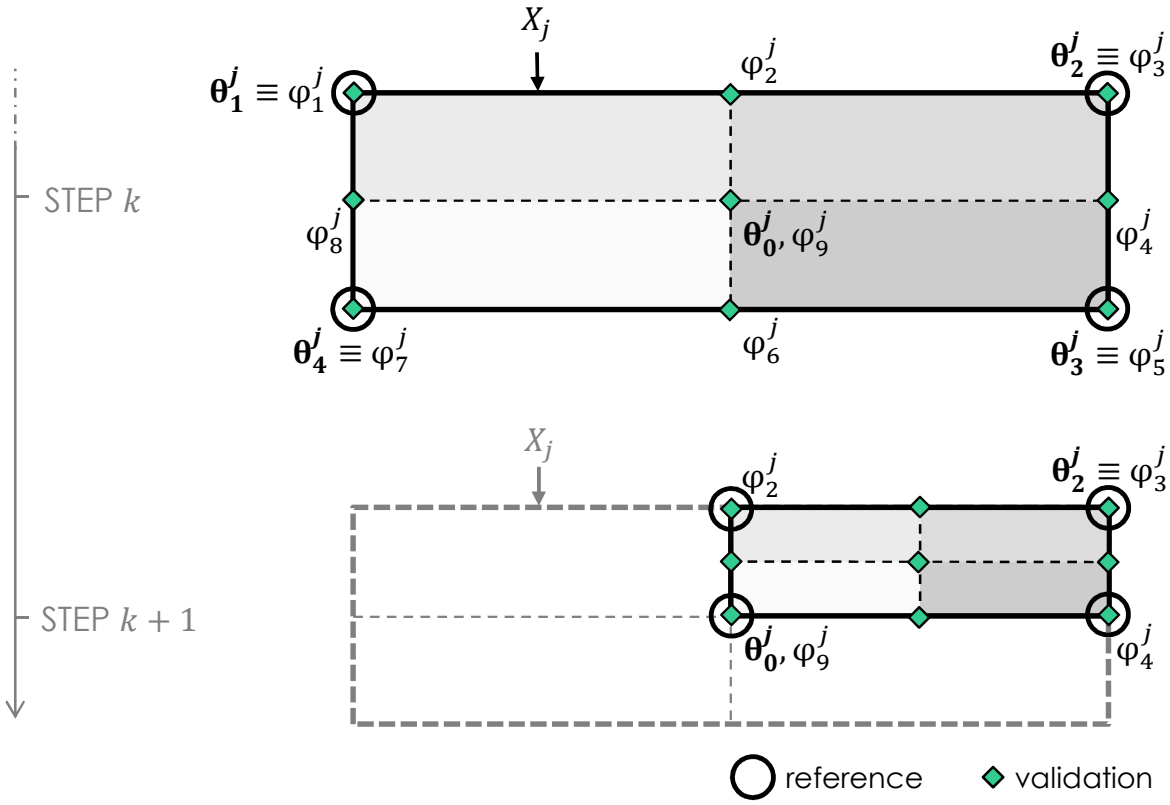

Figure 7.2 – Illustration of the splitting rule (section 7.2.1) in a 2-dimension parameter space, i.e. $n = 2$. The hyper-rectangle X_j is split through its center θ_0^j, on the two parameter space axes. This generates 2^n new hyper-rectangles. The reference and validation sets of points generated using procedure 2 (section 7.2.2) are also displayed: X_j has 2^n vertices $\Theta^j = \left\{\theta_1^j, \theta_2^j, \dots, \theta_{N_\theta}^j\right\}$ (black circles) which are used to compute the approximated control law (section 7.3.3). The control law is then validated on the set of points $\Phi^j = \left\{\varphi_1^j, \varphi_2^j, \dots, \varphi_{N_\varphi}^j\right\}$, displayed using green diamonds. They correspond to the vertices of the 2^n new hyper-rectangles.

7.2.3 Procedure 3: computing an affine approximated control law $\hat{u}_{X_j} = K_j x + h_j$

Consider any hyper-rectangle X_j and its vertices $\Theta^j = \left\{\theta_1^j, \theta_2^j, \dots, \theta_{N_\theta}^j\right\}$ as defined above. The parameters K_j and h_j of the approximated solution are obtained by linear regression analysis on the vector of u^*, the solutions at the N_θ vertices of X_j of the problem (7.1)-(7.2).

The advantage of this method w.r.t. minimizing the estimated error bound $\hat{\mathcal{S}} - \mathcal{S}^*$ at all the vertices Θ^j, as presented in [53,72,125], is that it requires less computational time by avoiding running the prediction model iteratively. However, as suggested before, the error on the estimated error bound remains the ultimate criterion to validate the approximated control law (section 7.2.5).

7.2.4 Procedure 4: error bounds approximation

Consider a hyper-rectangle X_j and its associated validation set of points Φ^j. The estimated error bound $\hat{\varepsilon}_j$ of the error bound ε_j is taken as the maximum estimated error bound obtained on the N_φ validation points Φ^j:

$$\hat{\varepsilon}_0 = max_{i\in\{1,2,\dots,N_\varphi\}}\left(\hat{\mathcal{S}}_{\varphi_i^j} - \mathcal{S}^*_{\varphi_i^j}\right) \tag{7.7}$$

where $\hat{\mathcal{S}}$ is the sub-optimal objective function value, obtained with the approximated affine control law.

7.2.5 Explicit law synthesis algorithm

Consider a given hyper-rectangle $X_j \subseteq X \subseteq \mathbb{R}^n$. Δ_x denotes the vector of lengths of the hyper-rectangle along the dimension x. Assume that the maximal tolerance $\bar{\varepsilon}_0 > 0$ of the objective function approximation error is given as well as the vector of the minimal hyper-rectangle allowed: $\underline{\Delta_x} > 0$. The PWA affine approximation can be computed using the algorithm below:

Input: The first hyper-rectangle X_0 which represents the entire parameter space to be explored. The maximum approximation tolerance $\bar{\varepsilon}$ and the vector of minimal allowed lengths of the hyper-rectangle $\underline{\Delta_x}$. We assume $\Delta_{x_0} > \underline{\Delta_x}$.

Output: Final partition $\Pi = \left\{X_1, X_2, \dots, X_{N_X}\right\}$ and associated PWA control law $\hat{u}_\Pi = \left\{\hat{u}_{X_1}, \hat{u}_{X_2}, \dots, \hat{u}_{X_{N_X}}\right\}$ where $\hat{u}_{X_j} = K_j{}^T x + h_j$.

1. Initialize the partition to the first hyper-rectangle, i.e. $\Pi = X_0$. Move the hyper-rectangle X_0 to $List\ 1$: the list of hyper-rectangles to be explored.
2. Compute Θ^0 the set of vertices of X_0 as defined in procedure 2.
3. Compute the solution $u^*_{X_0}(\theta_i^0)$ to problem (7.1)-(7.2) for each vertex $i \in \{1,2,\dots,N_\theta\}$ of X_0, i.e. every point of Θ^0.
4. **while** $List\ 1$ is not empty **do**
5. Select the first unexplored hyper-rectangle X_j in $List\ 1$. Thanks to previous calculations, its set of vertices Θ^j and the associated solution $u^*_{X_j}(\theta_i^j)$ to (7.1)-(7.2) are already available. This is also the case for the corresponding value of the objective function value: $\mathcal{S}^*_{\theta_i^j}$.
6. Compute the approximated affine control law in the hyper-rectangle X_j, i.e. $\hat{u}_{X_j} = K_j{}^T x + h_j$ as detailed in procedure 3.

7. Split the hyper-rectangle X_j as detailed in procedure 1. Store the hyper-rectangles X_k, $k \in \{1,2,\dots,2^n\}$ obtained in 2 : a temporary list of hyper-rectangles.
8. Compute the vertices of each hyper-rectangle contained in $List\ 2$ in order to obtain Φ^j as defined in procedure 2. This list will provide the validation set of points of X_j.
9. Compute the solution $u^*_{X_j}(\varphi_i^j)$ to problem (7.1)-(7.2) at each vertex contained in the validation set Φ^j. Store the corresponding values of the objective function value $\mathcal{S}^*_{\varphi_i^j}$.
10. Enhance $List\ 2$ by storing the solution $u^*_{X_k}(\varphi_i^k)$ obtained at step 9, for each hyper-rectangle X_k. Do the same for the set of vertices Θ^k of each hyper-rectangle and the corresponding objective function value $\mathcal{S}^*_{\theta_i^k}$.
11. Compute the approximate objective function $\hat{\mathcal{S}}_{\varphi_i^j}$ at each vertex contained in Φ^j, using the affine control law $\hat{u}_{X_j} = {K_j}^T x + h_j$ obtained at step 6.
12. Compute the estimated error bound $\hat{\varepsilon}_0$ in X_j, using the set of points Φ^j as detailed in procedure 4, the approximate solution $\hat{\mathcal{S}}$ computed at step 11 and the original solution value $\mathcal{S}^*$ from step 9.
13. Remove the hyper-rectangle X_j from $List\ 1$.
14. **if** $\hat{\varepsilon}_0 < \bar{\varepsilon}$ **then**
15. Save the hyper-rectangle X_j, its vertices Θ^j and the approximated affine control law $\hat{u}_{X_j} = {K_j}^T x + h_j$ obtained at step 6. Mark X_j as validated w.r.t the error bound criterion $\bar{\varepsilon}$ and the sensitivity level Δ_x.
16. **else**
17. **if** $\frac{1}{2}\Delta_x > \underline{\Delta_x}$ **then**
18. Add the hyper-rectangles contained in $List\ 2$ at the top of $List\ 1$. Clear $List\ 2$.
19. **else**
20. Save the hyper-rectangle X_j, its vertices Θ^j and the approximated affine control law $\hat{u}_{X_j} = {K_j}^T x + h_j$ obtained in step 6. Mark X_j as validated w.r.t the sensitivity level Δ_x only.
21. **end if**
22. **end if**
23. **end while**

7.2.6 Concluding remarks

Let's now summarize the important properties of the methodology presented above and dedicated to computing the explicit solution of an implicit NMPC.

The algorithm itself (section 7.2.5), guarantees that a PWA feedback control law with a finite optimal number of hyper-rectangular regions is obtained:

- The maximum number of elements in the parameter space X is a quantitative index of the exploration. It is controlled by the vector of minimum lengths along x_i of the hyper-rectangle, denoted $\underline{\Delta_{x_i}}$ at step 20 and,
- The effective number of elements is implicitly controlled at step 14 by a pre-imposed qualitative criterion on the approximated objective function, namely the error bound $\bar{\varepsilon}$.

In the adaptive method proposed here, the splitting operation is used exclusively when the nonlinear characteristics of the dynamics impose it. This property intuitively guarantees that the number of hyper-rectangles in the final partition Π will be minimized. However, minimizing the number of hyper-rectangles does not only depend on the quantitative and qualitative indexes but is also directly impacted by the splitting rule that is chosen. For instance, splitting the hyper-rectangles on selected parameter space axes instead of on all of them (procedure 1) may reduce the number of constituent functions pieces of the final explicit controller. In fact, it actually intuitively guarantees that one obtains a partition with either fewer or an equal number of constituent functions pieces but never more. The implementation of such an approach needs further investigation, since determining which parameter space axes should be selected is not straightforward. In practice, it is usually based on the analysis of the estimated error bounds $\hat{\varepsilon}_0$ even though alternatives exist [51,76,77,121].

Finally, it should be mentioned that some computationally expensive stages can be parallelized in order to benefit from the multi-core architectures of most computers, from personal computers to clusters. In particular, the time required to achieve steps 3, 9 and 11 is almost directly divided by the number of vertices that can be evaluated in parallel.

7.3 Online evaluation of a piecewise controller

The algorithm presented in the previous section leads to a PWA approximation of the solution of an mp-NLP, also known as explicit solution. However, it should be taken into account that one of the main drawbacks in the explicit framework is that the complexity of this PWA representation may be large even for low order systems (usually the partition shows thousands of regions). It therefore needs to be combined with an efficient method to evaluate online this piecewise function defined on a partition of the n-dimension parameter space.

7.3.1 About the direct approach

By direct approach we mean evaluating each region in a sequential manner to determine whether or not the current parameter x belongs to that region. It is well-known that this approach, while simple to implement is computationally demanding. In some cases, it might even exceed the computational requirements to compute the optimization problem itself. In the next few years, massively parallel computing architectures could considerably reduce the requirements of this straightforward approach but w.r.t the hardware evolution in the automotive industry (section 4.1.2), such an approach will probably impractical for several more generations of electronic control units.

7.3.2 Explicit NMPC based on binary search tree

Because the lack of hardware is not solely a problem of the automotive industry, a few computationally more efficient alternatives have been developed in the past few years [124,125].

The approach in the literature that appears to be the most appealing when considering hyper-rectangular partitioning of the parameter space X (section 7.2) is to organize the set of affine control laws $\hat{u}_{X_j} = {K_j}^T x + h_j$ in a binary search tree. In fact, at each level of a binary tree, it is possible to exclude a significant fraction of the remaining candidate regions according to the sign of a given hyperplane cut $c_j^T x + d_j$. The major advantage of this approach is that it benefits from a logarithmic complexity in the number of regions M. For instance, the search among tens of thousands of hyper-rectangles will require, once on-board, evaluating less than 20 hyperplane cuts, i.e. solving online 20 matrix inequalities to determine the current region. As suggested before, this makes it possible to considerably reduce the online computation time with respect to direct approaches, even considering parallel implementation [53].

Several algorithms that build such binary search trees are available in the literature [125]. It usually requires extensive computations to obtain a balanced binary search tree that can be evaluated more efficiently. However, since such computations are done completely offline, they can benefit from powerful computing architectures. For instance, on standard 2010 personal computer configurations, only a few hours are required to compute a balanced binary search tree for over 20,000 regions.

7.3.3 Implementation online of the explicit NMPC law

In this study, the binary search tree that describes the hyper-rectangular partitioning obtained by using the algorithm presented in section 7.2, is built using the multi-parametric toolbox (MPT) [63]. The tree is stored in a table f_{tree} of $n+3$ columns while the PWA control law requires a table of M rows and $n+1$ columns per actuator i, denoted below $f_{PWA,i}$. M is the number of regions in the n-dimension parameter space partition.

Finally, obtaining online the suboptimal actuator positions $\hat{u}$ to be applied in the next time step involves a 2-step procedure [73] :

- Searching the binary tree f_{tree} to determine the current hyper-rectangle X_j (figure 7.3) and,
- Evaluating the corresponding affine function $\hat{u}_{X_j} = K_j{}^T x + h_j$ from table $f_{PWA,i}$(figure 7.3).

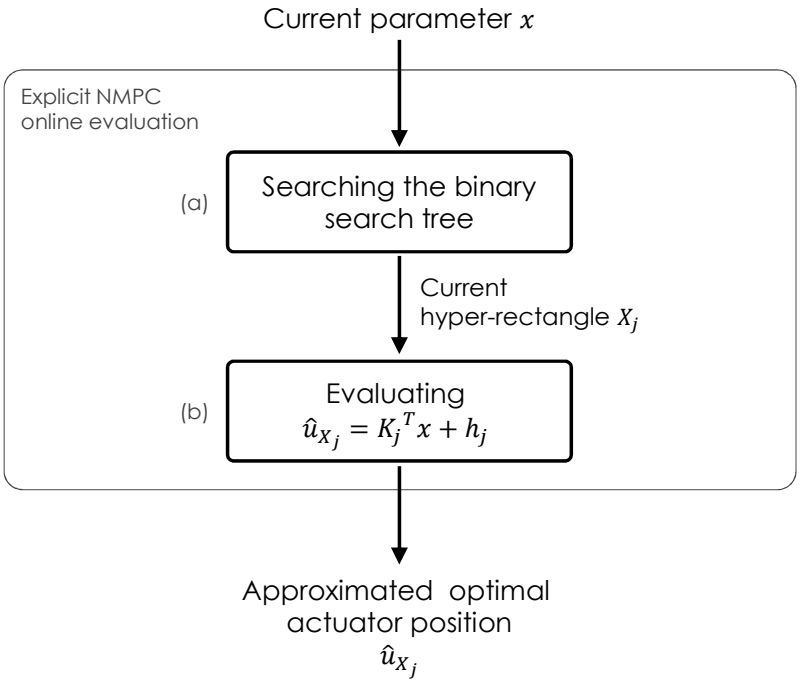

Figure 7.3 – Online computation 2-step methodology of an explicit NMPC law, stored in a binary search tree.

The table f_{tree} that contains the binary tree associates to each node and leaf the corresponding n-dimension vector c_j^T and the scalar value d_j. Both are obtained during the construction of the tree (section 7.3.2). Starting at the root node and then at each node, the hyperplane cut $c_j^T x + d_j$ is evaluated. Then, the child node is chosen in accordance with the sign of this expression and the step is repeated until reaching a leaf node. The index of the line containing the child node, i.e. the new values of c_j^T and d_j, is contained in columns $n+2$ or $n+3$, depending on the sign of the current hyperplane cut. At the leaf node j, the

control is directly given by evaluating the corresponding affine relation $\hat{u}_{X_j} = K_j^T x + h_j$ where K_j^T and h_j are obtained from the table $f_{PWA,i}$, that contains the affine control law of each region.

At each node the arithmetic operations required to evaluate the hyperplane cut are n multiplications, $n+1$ additions and 1 comparison. Assuming a partition of M polyhedrons, a rough estimate of the search tree depth D is usually given by $D = 1.7\, log_2 M$. Finally, at a leaf node, the number of arithmetic operations required to compute the approximated optimal position $\hat{u}_{X_j}$ of each actuator are n multiplications and $n+1$ additions.

7.4 Application to the control of the air path of a turbocharged gasoline engine

This section presents a practical case of application for the computation of the explicit solution of the NMPC scheme. In particular, the NMPC schemes presented in chapter 5, used for the control of the air path of a turbocharged gasoline engine, can be simply formulated as an mp-NLP (section 7.4.1). Then, the application of the methods presented in sections 7.2 and 7.3 is straightforward. Details for the problem formulation (section 7.4.1) and the performances of the resulting PWA control law performances (section 7.4.2) are provided in the following sub-sections.

7.4.1 Implicit NMPC problem formulation

For the sake of completeness, the air path NMPC formulation presented in chapter 5 is briefly summed up below:

$$\mathcal{S}^* = \mathcal{S}(u^*) = min_{u(.)}\, \mathcal{S}(x, y, u, \sigma) \tag{7.8}$$

s.t.

$$\mathcal{S} = \sum_{i=k}^{k+N_p} \mathcal{J}(x(i), y(i), u(i), \sigma) \tag{7.9}$$

$$x(k+1) = f(x(k), u(k), \sigma) \tag{7.10}$$

$$y(k) = g(x(k), u(k), \sigma) \tag{7.11}$$

$$\underline{u} \leq u(k) \leq \overline{u} \tag{7.12}$$

$$x(k) = x_0 \tag{7.13}$$

where $H_p = [k, k+N_p]$ is the so-called prediction horizon at time *k*. f and g are nonlinear functions describing the discrete-time system dynamics and based on the physics-based modeling philosophy presented in section 3.2. Finally $\underline{u}$ and $\overline{u}$ respectively stand for lower and upper bounds on the control variables and respectively define a compact subset of $\mathbb{R}^m$. The states, control inputs and exogenous inputs are given by:

$$x \coloneqq \left(p_{ape}, p_{man}, p_{avt}, \omega_t\right)^T \tag{7.14}$$

$$u \coloneqq \left(u_{thr}, u_{wg}\right) \tag{7.15}$$

$$\sigma = (N_e, p_{man}^{SP}, p_{amb}, \theta_{amb}) \tag{7.16}$$

where p_{ape}, p_{man} and p_{avt} respectively stand for the boosting pressure, the intake manifold pressure and the pressure upstream the turbine (figure 1.1). ω_t represents the turbocharger rotational speed. N_e is the engine speed, $p_{amb}$and θ_{amb} respectively represent the ambient pressure and temperature. p_{man}^{SP} is the intake manifold pressure set point. Finally, u_{thr} and u_{wg} respectively correspond to the throttle and wastegate positions that are constrained between closed and fully open:

$$0 \leq u \leq 100\% \tag{7.17}$$

The cost function $\mathcal{J}$ to be minimized contains two terms, one of which is a thermodynamic performance

index that maximizes the engine cycle efficiency:

$$\mathcal{J} = \alpha(p_{man}^{SP} - p_{man})^2 + \beta \frac{p_{avt}}{p_{man}} \tag{7.18}$$

where the weighting factors α and β are used to scale and penalize each term of this multi-objective cost function.

7.4.2 mp-NLP formulation

Let $\tilde{x}$ be the 6-parameter vector defined such that:

$$\tilde{x} = \left(p_{ape}, p_{man}, p_{avt}, \omega_t, p_{man}^{SP}, N_e\right)^T \tag{7.19}$$

Then, (7.8)-(7.18) define an mp-NLP since it is an NLP in u parameterized by the 6-dimension vector $\tilde{x}$. The latter represents the axes on which the parameter space $\tilde{X}$ will be partitioned, i.e. the four states of the physics-based model presented in chapter 3 $\{p_{ape}, p_{man}, p_{avt}, \omega_t\}$, the set point to be tracked p_{man} and here, one relevant exogenous input i.e. the engine rotational speed N_e, known to have a significant influence on the air path dynamic (chapter 5). In a general framework, this construction motivates the minimization of the number of states suggested in section 5.2.3, before designing the implicit NMPC scheme. Similarly, it can be seen that if possible, the number of set point trajectories should be minimized when designing the implicit NMPC scheme since they are necessarily all included in the resulting mp-NLP formulation. It should also be noted that the ambient conditions can also be added to the parameter vector $\tilde{x}$, as can all exogenous inputs. In practice, this would increase the dimension of the problem from 6 states to 8 states. Here we avoid such a formulation in order to minimize both offline and online computational requirements. This is motivated by the fact that the car manufacturers' approach usually consists in calibrating additional corrections to the control in order to take into account measured disturbances such as the ambient conditions (section 4.1).

7.4.3 Explicit controller

When computed using the algorithm presented in section 7.2, this mp-NLP formulation leads to a partition of 26,411 hyper-rectangles stored in a binary search tree f_{tree} that requires approximately 475 kilobytes of read-only memory. That represents about 6% of the total read-only memory available in a current standard Engine Control Unit (ECU). Each table $f_{PWA,thr}$ and $f_{PWA,wg}$, that respectively contains the 26,411 affine control laws for the throttle and the wastegate, requires about 370 kilobytes of read-only memory, so another additional total of 9% of the ECU memory. In both cases, the number of elements in each table is in agreement with current 16- or 32-bit ECUs (section 4.1.2) that can respectively handle tables of $2^{16} - 1$ and $2^{32} - 1$ elements.

Altogether, the memory required to store the three tables represents a significant part of the total memory available on current ECUs. However, other similar explicit control schemes, computed using the same methodology but based on a larger maximal tolerance index $\bar{\varepsilon}_0$ (section 7.2.5) contained significantly fewer elements. For instance, on the same case of application, i.e. the control of the air path of a turbocharged gasoline engine, an explicit NMPC law based on a partition of 3,917 hyper-rectangles was presented in [38,41] where it led to sensible performances.

The explicit NMPC law presented in this chapter is based on an extreme partitioning of the parameter space, w.r.t. the computational resources available for the study. If there is one reason which can justify why we relaxed the ECU memory constraints presented in section 4.1.2, it is the pure curiosity of discovering the optimum performances of our philosophy, on this particular case of application.

7.5 Simulation performances

In this study, the cycles on which the control schemes are evaluated were acquired on an actual vehicle equipped with the engine, and thus represent relevant engine operating conditions. As detailed in section 5.4, the performances of the implicit NMPC scheme at the origin of the explicit NMPC law presented in this chapter, are in perfect agreement with the car manufacturer's specifications introduced in section 5.1.4 and that also apply to this PWA control law.

7.5.1 Performances of the explicit NMPC law

First, by storing the PWA control law in a binary search tree (section 7.3), the average computational time required to obtain the sub-optimal actuator positions $(\hat{u}_{thr}, \hat{u}_{wg})$ is divided by a significant factor 10,000, w.r.t. the time required to obtain the optimal actuator positions (u_{thr}, u_{wg}) from the implicit NMPC scheme presented in chapter 5. These figures were obtained on a Core™ i7 CPU x8 cores without any specific Matlab® code optimization. Additionally, the average number of arithmetic operations involved at each time step is in agreement with current hardware standards with roughly 300 multiplications, 300 additions and 17 comparisons to search the binary tree and evaluate the PWA control of each actuator. Altogether, the implementation of this control law on an embedded solution becomes worth considering.

The control structure that corresponds to the strict application of the PWA solution, computed using the synthesis algorithm presented in section 7.2, is depicted on figure 7.4 below.

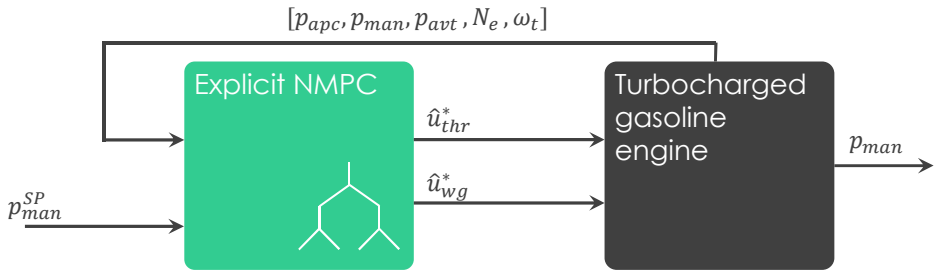

Figure 7.4 – Explicit NMPC implementation scheme. It consists in directly applying the PWA control law obtained with the synthesis algorithm presented in section 7.2 and stored in a binary search tree (section 7.3).

The performances that were obtained on our reference vehicle transient cycle are depicted on figures 7.5 and 7.6 below. It can be seen that the dynamic performances observed on the implicit NMPC scheme are very well approximated most of the time. Additionally, even if the comparison may not be relevant since the two closed-loop systems are not exactly at the same operating point, the steady-state optimal actuator positions seem to be well preserved. Consequently, the maximization of the engine cycle efficiency (7.18) is expected to be maintained with the explicit NMPC scheme.

However, since no integral action is involved in the PWA control scheme presented so far, a steady-state tracking error is present. For instance, between 3 and 7 seconds on figure 7.5, the closed-loop system shows a significant performance drop w.r.t. the implicit NMPC performances (figure 5.8). In particular, the quasi-constant quasi-steady-state error of about 70 millibars that can be observed is unacceptable with regard to the air path control objectives (section 5.1).

One way to eliminate this offset error is to introduce an integral action directly in the parametric control design by adding in (7.19) an additional integral state to the parameter vector $\tilde{x}$. However, while appealing from a theoretical point of view, this philosophy also increases the number of parameters of the resulting mp-NLP that needs to be solved (section 7.4.2). It therefore contributes to generating overwhelming offline

computational requirements. A more practical approach to overcome this issue, also motivated by the need for tuning knobs in industrial engine controllers (section 4.1), is presented in the following sub-section.

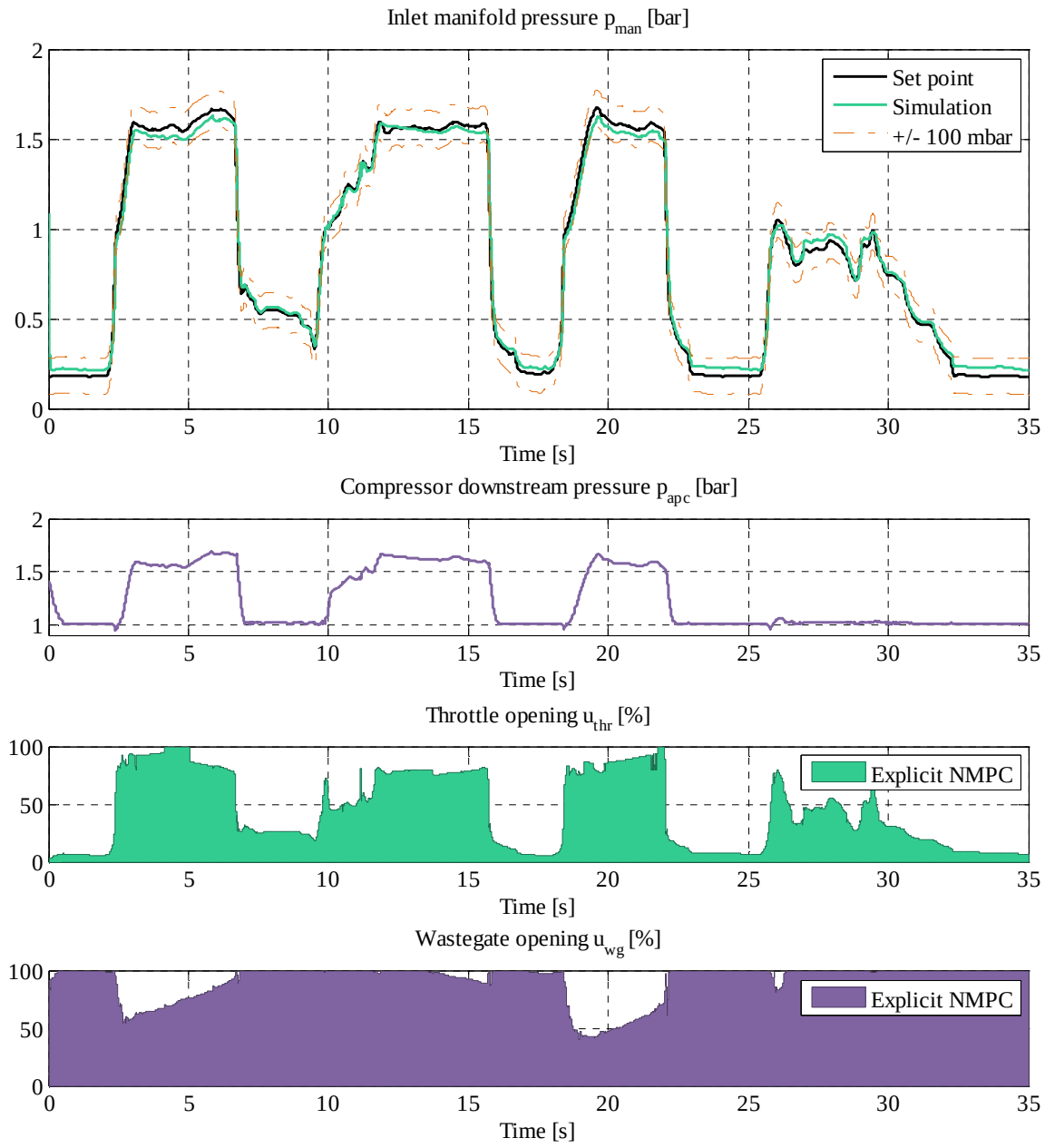

Figure 7.5 – Validation cycle #1: inlet manifold pressure tracking performances for the explicit NMPC scheme. The overall dynamic performances of the implicit MPC scheme (figure 5.8) are well captured.

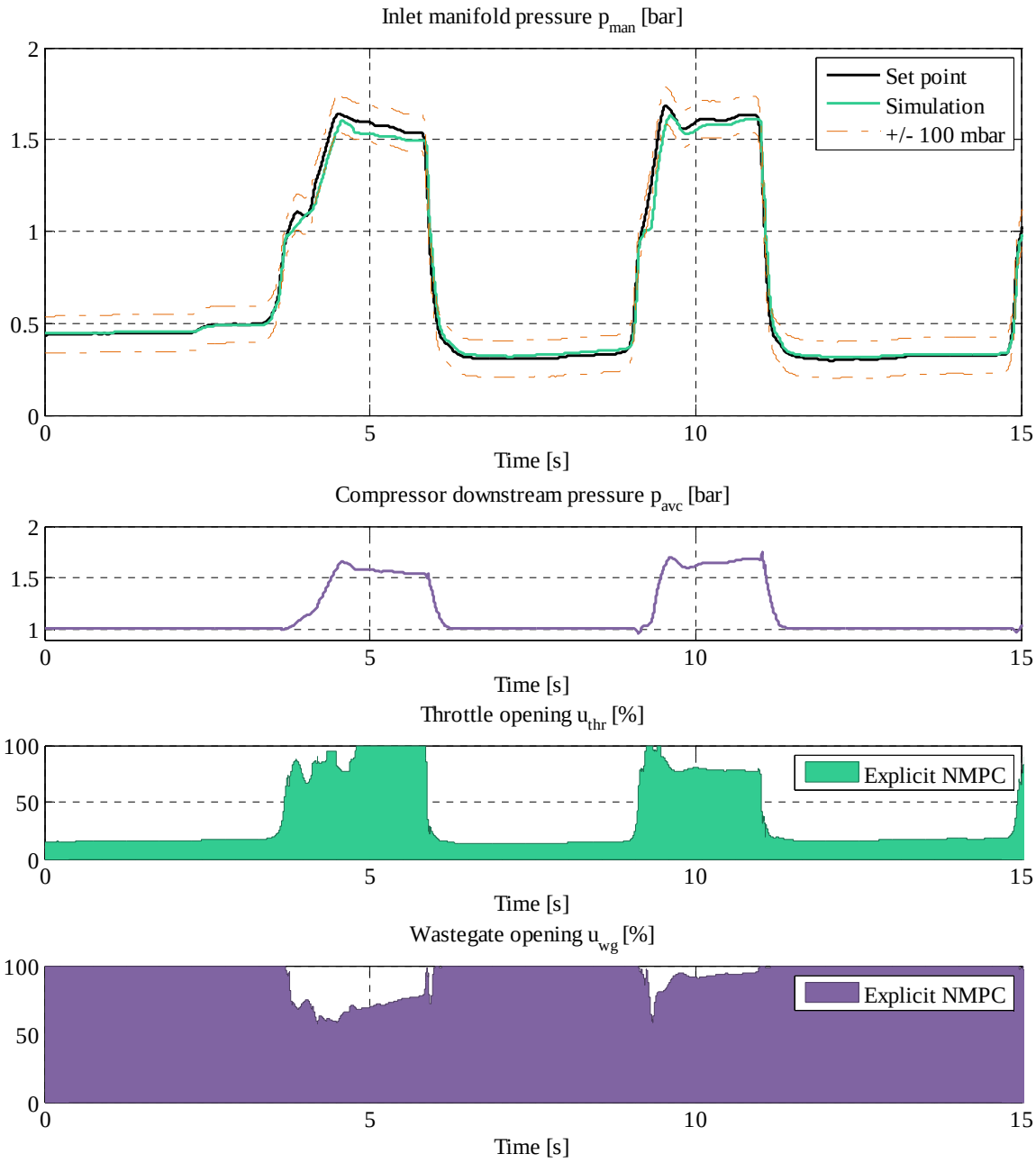

Figure 7.6 – Validation cycle #2: inlet manifold pressure tracking performances for the explicit NMPC scheme. The overall dynamic performances of the implicit MPC scheme (figure 5.9) are well captured.

7.5.2 Explicit NMPC law with integral action

In order to circumvent the steady-state error observed on figures 7.5 and 7.6, we propose to enhance the initial explicit NMPC law (section 7.5.1) by adding, at the end of the synthesis, an integral term per actuator (figure 7.7), i.e.:

$$\begin{pmatrix} \hat{u}_{thr}^{*} \\ \hat{u}_{wg}^{*} \end{pmatrix} = K_j{}^T x + h_j + \begin{pmatrix} Ki_{thr} \\ Ki_{wg} \end{pmatrix} \int (p_{man}^{SP} - p_{man}) \tag{7.20}$$

where Ki_{thr} and Ki_{wg} are constant through the entire engine operating range and calibrated using a trial-and-error calibration method. This is made possible thanks to the very good initial performances of the explicit NMPC scheme (figures 7.5 and 7.6).

In practice, the integral actions are expected to be sufficiently slow not to interfere significantly with the explicit control law during transients [38]. Additionally, in order to compensate for the typical integral-windup effect, anti-windup integral controllers were implemented. The new control structure is depicted on figure 7.7 below.

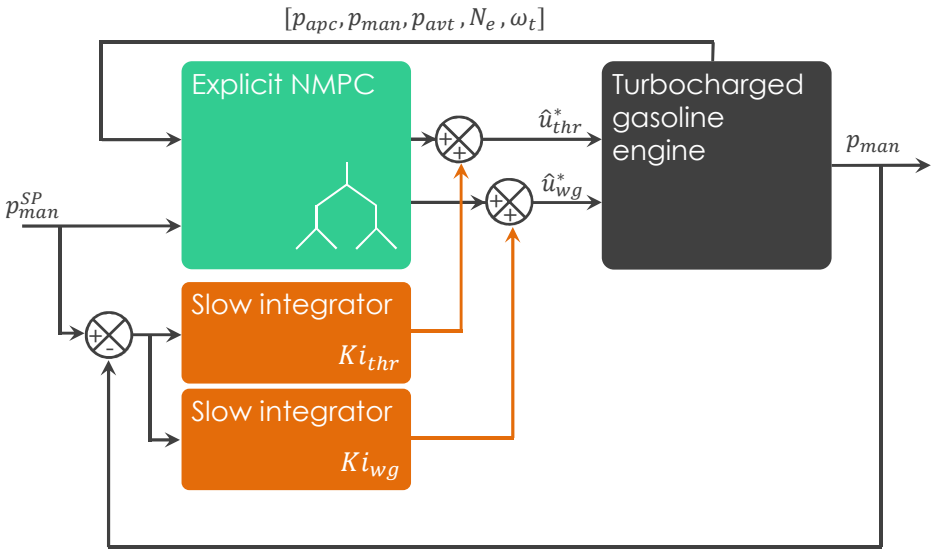

Figure 7.7 – Explicit NMPC implementation scheme with the addition of two slow integral actions, one for each actuator.

Figures 7.8 and 7.9 depict the final performances obtained with the complete controller, i.e. PWA explicit NMPC plus additional anti-windup integral action (7.20). One can see that the steady-state error is almost perfectly compensated by the slow integral action in both cases. It can also be seen the integrator correction is small w.r.t. the output of the PWA part in (7.20). This underlines the fact that most of the tracking is ensured by the explicit NMPC.

Between 8 and 10 seconds on figure 7.9, one can notice that the controller suffers from a sudden change of set point and the resulting intake manifold pressure p_{man} is slightly late w.r.t. its set point trajectory p_{man}^{SP}. This was already observed on the initial explicit NMPC scheme (figure 7.6) and can be attributed to the PWA approximation error. However, when reaching the top of the set point trajectory, at about 9 seconds on figure 7.9, the pressure trajectory p_{man} suffers from a serious overshoot that was not observed on the explicit NMPC law without integral action. Basically what happens here is that the integral actions computed previously during the p_{man}^{SP} climb are no longer appropriate and in particular, the wastegate is

too closed. By the time the slow wastegate integrator reaches a more appropriate value, in order to compensate the current PWA control law error, a quasi-steady-state error still remains.

Finally, the distinctive feature of this practical method is that, besides suppressing the steady-state error that is encountered, it also provides the controller with a tuning knob. This feature is crucial when aiming for an industrial implementation of the controller, as presented in chapter 4, since it allows the closed-loop dynamic to be to a certain extent modified afterward. In particular, all other methodologies that require the use of an augmented parameter vector $\tilde{x}$ (7.19) would require computing a substantial part of the PWA approximation again.

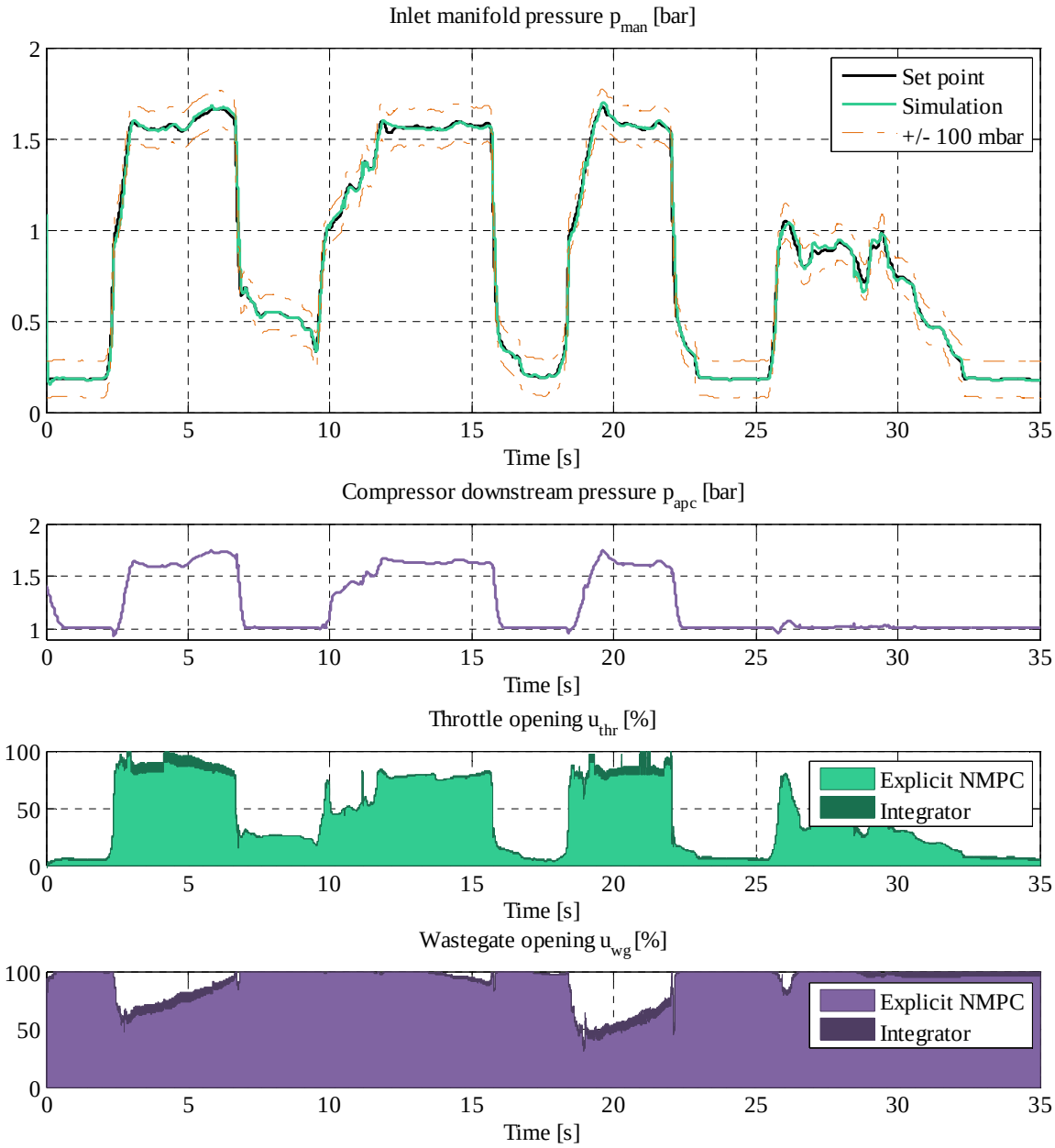

Figure 7.8 – Validation cycle #1: inlet manifold pressure tracking performances for the explicit NMPC plus integrator scheme.

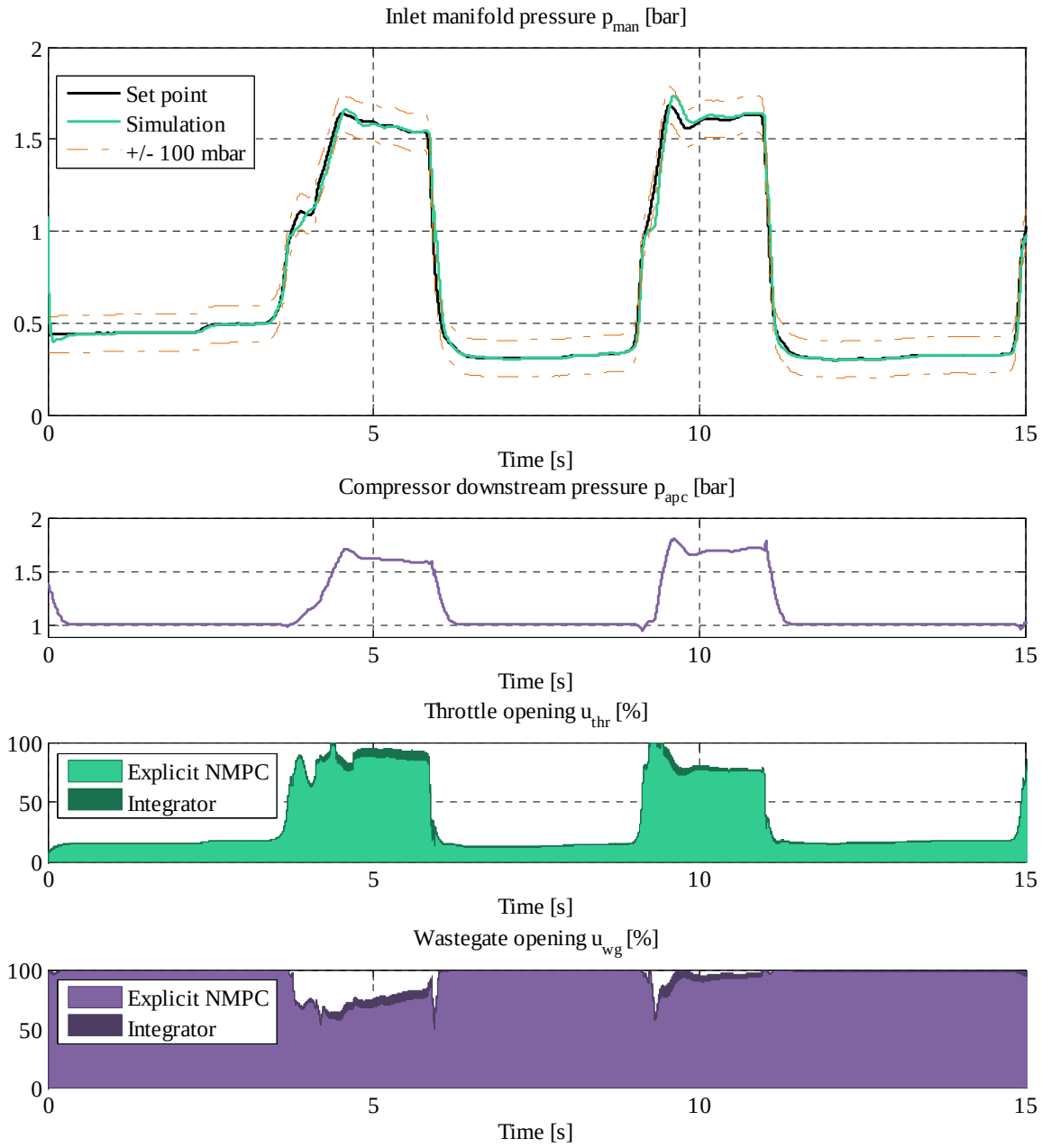

Figure 7.9 – Validation cycle #2: inlet manifold pressure tracking performances for the explicit NMPC plus integrator scheme.

7.6 Conclusion

This chapter has explained how, starting from the mp-NLP formulation of an implicit NMPC scheme, a step toward real-time implementation can be achieved following the explicit NMPC philosophy [53]. The approach proposed here consists in approximating the mp-NLP problem solution on a hyper-rectangular partition of the extended state space. It has drawn extensively on the most recent results in the field of explicit NMPC [53,72,73,125] and the main contribution consists in the practical adaptation of the philosophy to the use of a computationally expensive prediction model. In fact, while being easily parallelized, the algorithm proposed in this study also minimizes the use of the prediction model.

This chapter has also focused on the exploitation online of the resulting PWA control law. Here, the approach suggested is a direct application of the philosophy presented in [125], where a binary search tree is used to organize a set of affine control laws, also defined on hyper-rectangles. Its application in our framework is straightforward and altogether it contributes to drastically reducing the online computational requirements w.r.t. implicit NMPC schemes (section 7.3). In particular online, the evaluation of the approximated control law runs in a bounded logarithmic time.

Finally, the overall approach has been applied to our practical example of application, namely the control of the air path of a turbocharged gasoline engine (sections 7.4 and 7.5). Starting from the implicit NMPC scheme presented in chapter 5 that uses a physics-based engine prediction model, the entire synthesis of a 6-dimension explicit NMPC law has been achieved. The sole fact of presenting validation results on a realistic driving cycle, i.e. covering an extensive part of the actual engine operating range, proves the validity of the overall methodology and the fact that it can overcome ordinary computational issues. Indeed, while the explosion of massively parallel architectures such as clusters will considerably reduce computational times in the next few years, the control law presented in this chapter was computed in two months using a standard 8-core CPU. Taking into account the fact that the multiplication of cores almost directly divides the computational time, using the computational resources of a car manufacturer would reduce this figure to a question of days or even less. This also makes the approach worth considering in an industrial framework. It therefore represents the third and last step of our proposal for a systematic control design approach of the control of the air path of turbocharged gasoline engines (figure 7.10).

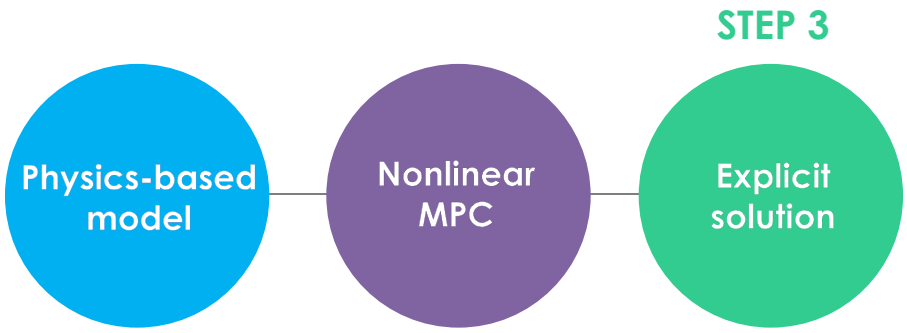

Figure 7.10 – Overview of the control design approach proposed in this study.

***

Before concluding on the overall study, it is only fair to point out that the major theoretical limitation of this PWA approach lies in the generation of a control law that can be discontinuous, unfeasible and potentially destabilizing. In fact, while the explicit NMPC law presented in this chapter mostly results in good practical performances (figures 7.5, 7.6, 7.8 and 7.9), there is no systematic procedure to prove that it will satisfy the basic requirements of feasibility (e.g. there is no guarantee to fulfill the input constraints)

and continuity of the control law. It is the development of an alternative constructive methodology to guarantee these properties, while maintaining the fast online calculation time, that distinguishes a new approach that is being developed and applied to the control of the air path of turbocharged gasoline engine. In practice, it is based on the use of a barycentric interpolation [120] of the control law within the hyper-rectangles, in opposition to the affine approximation proposed in this chapter. Figure 7.11 below depicts the very promising preliminary results obtained using this new approach and highlight the versatility of the overall philosophy introduced in this study to handle any type of approximation (section 7.2.3).

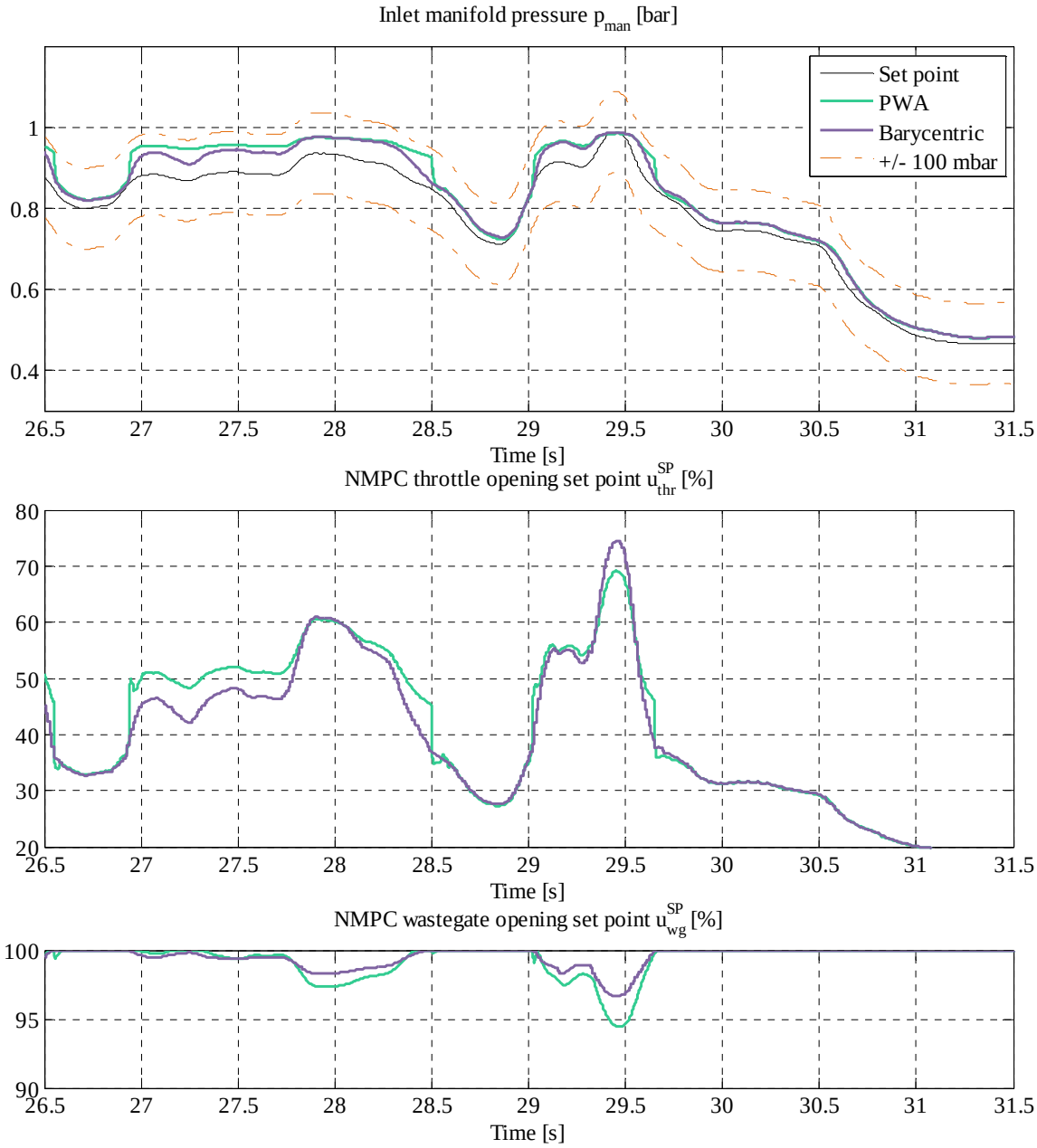

Figure 7.11 – Extract of the validation cycle #1: Comparison of the tracking performances and actuator set points obtained with a PWA approximation and a barycentric interpolation of the implicit NMPC law. While both approximations are defined on the same set of hyper-rectangles, the use of a barycentric interpolation shows actuator set point trajectories that are perfectly smooth and lead to better tracking performances. Note that the whole validation cycle could not be simulated because, at this stage, the control law has not yet been computed on the entire engine operating range.

CONCLUSION

...AND DIRECTIONS FOR FUTURE WORK

The first part of this study concerned the design of a physics-based control-oriented turbocharged engine model. The philosophy that is proposed combines a mean value engine model and zero-dimensional models to describe the phenomena involved in the air path. Both approaches are widely known in the automotive industry, which represent a major feature of the overall work w.r.t. its industrial context.

When considering turbocharged engine models, the compressor and turbine sub-models play a key role in the accuracy and reliability of the prediction results. More precisely, when considering control-oriented models, for which computational requirements are high, the performance of the model is directly inherited from a set of four static data-maps, systematically built from experimental test bench trials. The present thesis has proposed a new set of interpolation and extrapolation algorithms. Altogether, they aim to address the accuracy issues encountered in the literature when curve-fitting methods are used, and the computational requirements issues that characterize models that use a detailed description of the thermodynamic and fluid mechanics phenomena involved in each turbo-machine. The result is a similar methodology to obtain the compressor and turbine data-maps, notably based on the relation between the ideal and actual behaviour of the components. The preservation of this link in the results presented in this study considerably contributes to the overall consistency of the method.

The benefits of these results go far beyond the framework of this study even if the data-maps are at the heart of the control-oriented physics-based model presented in section 3.2 and used throughout part 2:

- The compressor pressure ratio versus mass flow rate data-map has enabled the construction of an open-loop turbocharger rotational speed estimator at Renault SAS (section 3.1). In an industrial context, this estimation structure directly benefits from its simplicity of implementation and proved experimentally to lead to great performances thanks to the new extrapolation strategy of the data-maps.
- The complete interpolation and extrapolation methodology for the compressor and turbine data-maps is being implemented in an industrial tool, in the framework of a partnership between Renault SAS and LMS®.
- Finally, the extrapolation models developed in this study also are at the heart of patented applications including for example electric turbocompounding.

The second part of the thesis addressed the control of the air path of a turbocharged engine by means of the nonlinear model predictive control (NMPC) paradigm. The latter is known to be particularly suitable to handle the multi-input multi-output constrained nonlinear nature that characterizes modern combustion engines, while standard multi-linear methods encounter difficulties in handling the entire engine operating range [46,96]. This issue is even more crucial since, due to increasing complexity, control design is becoming a bottleneck in terms of development time and cost for all car manufacturers.

When considering NMPC, two critical issues need to be considered. The first one is the construction of an appropriate nonlinear model of the system, which is the result of a compromise between accuracy and computational requirements. The second one lies in the fact that solving online the optimization problem that is at the heart of predictive control, usually leads to prohibitive sampling time requirements. The present thesis proposes two implicit control schemes that address the first issue by using the control-

oriented physics-based model developed in part 1 of the manuscript. This choice is motivated by the versatility of the modelling philosophy as well as its ability to obtain an accurate model using only standard automotive test bench trials. Additionally both control schemes benefit from the physics-based nature of the model by explicitly minimizing a thermodynamic performance index, besides ensuring inlet manifold pressure tracking. The approaches differ in the way they describe the future control trajectory during the prediction. In fact, while the first one is based on a horizon-1 predictive control scheme, the second one is based on the parameterization of the control trajectory by means of orthonormal functions, namely Laguerre polynomials, and thus belongs to the category of parameterized NMPC. Both approaches show accurate tracking performances in realistic engine operating conditions but significant computational requirements, as suggested above.

Indeed, the issue related to the real-time implementation of NMPC laws needs to be addressed by other means. In the present thesis the problem is tackled using the explicit NMPC paradigm. In practice, sub-optimal actuator positions are obtained online by searching a binary tree and computing a simple affine relation. In this particular case of application, it has consisted in determining the piecewise affine solution of a 6-dimension multi-parametric nonlinear programming problem. The offline computational requirements related to such a high dimensional problem were tackled by means of a new parallelized algorithm compatible with the horizon-1 NMPC scheme derived in this study. Thus, all the benefits of using a physics-based prediction model and minimizing a thermodynamic performance index are maintained, while leading to a remarkable drop in online computational requirements.

Altogether, three important conclusions can be drawn from this study:

- Physics-based models based on the combination of a mean value engine model and zero-dimensional models are suitable for use in an engine NMPC framework. They have the advantage of being widespread in the automotive industry, including dedicated design software, and can be obtained in a straightforward fashion from standard steady-state test bench trials. Additionally, the NMPC framework includes a performance index such as the engine efficiency.
- The expansion of the future control increments trajectory on the set of Laguerre polynomials encapsulates the compromise between complexity/optimality in an easy-to-tune set of high level parameters. This formulation shows great versatility with respect to current and future computational requirements since for instance, fine-tuning the parameters will make it possible to adapt the complexity/optimality compromise to new hardware capabilities.
- The computation of a real-time implementable controller that approximates the behaviour of such an implicit engine NMPC can be obtained by solving a multi-parametric nonlinear programming problem offline. An algorithm able to handle time-expensive prediction models such as physics-based engine models and that benefits from the explosion of massively parallel architectures is fully detailed in the present thesis.

Toward a *quasi*-systematic engine air path control design approach

Since the very beginning, the emphasis has been placed on facilitating the design of engine air path control laws, in the context of increasing requirements and development time reduction that characterize the modern automotive industry. In particular, incresingly stringent pollutant emission standards have obliged car manufacturers to considerably complicate the technical definition of internal combustion engines. This increasing complexity makes the design of a control strategy longer and more difficult if no new methods are put in place. For a few years now, model-based control has aimed to provide an answer to this challenging issue. However, in practice, it is more a question of model-based control *development*, which uses simulation intensively to validate the control law, than actual model-based control that includes physics in the control law. Only some precise cases of applications use such an approach but they have

usually required a dedicated research and development stage, which prevents them from being applied to other problems in a systematic fashion.

This study aims to provide the beginning of an answer to car manufacturers' need to develop engine air path control laws much faster. The proposal is based on the NMPC framework, which was selected for its natural optimality and versatility, and can be summed up in three steps (figure below):

- STEP 1: Obtaining a representation of the phenomena to be controlled. Physics-based models, in contrast to mathematical representations, will allow faster calibration and more robustness over the entire operating range.
- STEP 2: Deriving an implicit nonlinear model predictive scheme that achieves the performances dictated by the specifications. This represents a major step, in which an objective function must be designed in agreement with physics and mathematics. In practice, the nonlinear framework remains highly adaptable and facilitates the design.
- STEP 3: Computing the explicit solution of the optimization problem. This leads to a real-time implementable controller, i.e. proving fast and predictable computational time.

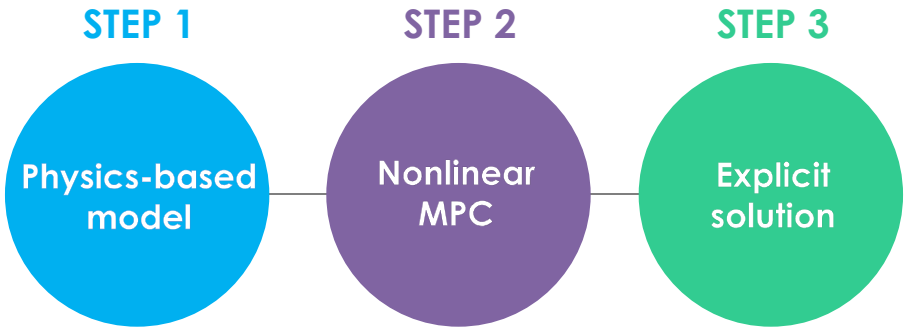

Figure – Overview of the control design approach proposed in this study

The major strength of the proposal concerns its versatility. Indeed, any step in the scheme can be adequately replaced by an alternative approach, sharing the same inputs and the same outputs. The physics-based model presented in chapter 3, can be replaced by a purely mathematical model such as a neural model. The horizon-1 NMPC scheme introduced in chapter 5 can be substituted by a more complex formulation if the available computational resources become greater. It can also be replaced by one of the formulations known as fast NMPC, known to be faster but which may still remain incompatible with real-time computational requirements. Finally, the piecewise affine approximation defined on a set of hyper-rectangles, used in chapter 7, can be replaced using any other partitioning geometry, or any alternative type of approximation.

On the particular example of the air path of a turbocharged gasoline engine, the overall approach leads to a drastic drop in computational requirements, which made a real-time implementation on-board worth considering at Renault SAS.

Perspectives

The following short-term work directions have been identified to improve and complement the methods developed in this study:

- A natural extension of the modelling philosophy presented in chapter 1 is the development of new flow restriction sub-models that can describe the phenomena involved in more complex technical definitions, including for instance, exhaust gas recirculation and multi-stage turbocharging. The case of variable valve timing is currently being addressed using neural models in [39].
- The next steps to follow concerning the interpolation and extrapolation strategy detailed in chapter 2 is the validation of the extrapolated data-maps on experimental test benches. Additionally, a precise description of the phenomena involved in the surge zone would be advantageous since it is increasingly used during transient conditions. Many research investigations are currently being conducted, and new results should soon be available [81,82]. Finally the consideration of simple geometrical characteristics of the turbo-machines can potentially increase the robustness and accuracy of the methodology. In particular, an approach to build compressor data-maps from only three standard geometrical features has been developed and published in [40]. The method is directly based on the extrapolation model presented in chapter 2 and a feedback would certainly improve the results presented in this document.
- For the design of implicit NMPC, the parameterization of the future control trajectory showed interesting properties in terms of versatility and management of the complexity/optimality compromise. Further investigations should follow a similar direction in order to confirm that a better compromise between performance and computational requirements is achieved in a systematic way.
- The explicit paradigm is a relatively young field of research in model predictive control approaches, particularly when considering the nonlinear case. In the short-term, research must focus on reducing the memory required to store the piecewise affine law and the regions on which it is defined. This is indeed a crucial feature regarding the implementation on mass production automotive electronic control units. Many solutions exist in the literature but simple additional features to the algorithm presented in chapter 7 may already lead to significant memory reductions. For instance, they include a physics-based definition of the error bound, i.e. being able to validate or invalidate a hyper-rectangle on a criterion that is more physical than the simple value of the objective function.

Additionally, the following long-term work directions have been identified to ensure the durability of the proposal presented in this study:

- First, the overall methodology can intuitively be extended to the case of diesel engines, which account for a significant part of the world's vehicle fleet. The development of a library of control-oriented sub-models, able to describe both gasoline and diesel engine technical definitions is an important step toward an industrial application of the methodology.
- Concerning the interpolation and extrapolation of the compressor and turbine data-maps, rewriting the algorithms so that they do not require any more turbocharger iso-speeds as in chapter 2, would make it possible to replace the manufacturer's operating points by actual steady-state engine test bench measurements. The actual operating conditions of the turbocharger could then be taken into account, including for instance the heat transfer occurring between the compressor and the turbine. These new methodologies could be directly integrated in the library of components suggested

above in order to obtain the compressor and turbine control-oriented sub-models directly from standard test bench trials.

- For the implicit NMPC law, one should consider that, in some cases, the optimization problem that needs to be solved may be non-convex and show several local minima, which considerably complicates the determination of a sufficiently good solution. Either recasting the problem or using a global optimization algorithm are two general solutions that would need to be integrated in the methodology in order to enable the synthesis of a black-box-like NMPC algorithm. The impact of such an approach on the offline computational time of the explicit solution would then need further investigations.
- Finally, the overall methodology, including the explicit synthesis algorithm, could be implemented in an industrial tool that would encapsulate the three stages of the methodology (figure above). This would enable car manufacturers to build quasi-optimal control laws in a straightforward fashion, with a clear benefit coming from their current efforts to obtain accurate engine models. Initially, w.r.t. current memory requirements, the latter would be used to evaluate the maximum potential of different technical definitions, early in the development process. Then, on a longer-term perspective, the increasing computational capabilities and memory available on electronic control units should enable such control laws to be implemented in mass production engines in order to speed up the integration of new technologies, in favor of pollutant emission and fuel consumption reductions.

***

It is a fact that memory requirements are the Achilles heel of explicit NMPC when considering on-board implementation. Several different directions of work will need to be investigated in order to increase the credibility of the explicit NMPC framework w.r.t. the automotive industry or to a larger extent the control community. In the next few years the explicit NMPC community will probably be working in two directions. First, developing advanced strategies to store the regions and the control laws on board. The use of binary search trees has opened up this field of research, but alternative representations may prove to give better results. The second direction concerns the solution of the multi-parametric programming itself. Indeed, alternative approximations to piecewise affine could considerably reduce the number of regions required to approximate the solution. In particular, appealing approaches using barycentric interpolation are already available in the literature, for the linear framework. The practical extension to the nonlinear framework, on the particular example of the control of the air path of a turbocharged engine, proves to be promising (figure 7.11) and in-depth results will be reported in future communications.

CONCLUSION *(in French)*

...ET PERSPECTIVES FUTURES

La première partie de cette étude porte sur la conception d'un modèle de moteur essence suralimenté, orienté pour le contrôle et basé sur la physique. La philosophie qui est proposée dans cette étude associe un modèle moyen de moteur et une approche de modélisation zéro dimensionnelle pour décrire les phénomènes impliqués dans la chaîne d'air. Les deux approches sont largement utilisées dans l'industrie automobile, ce qui représente un élément majeur par rapport au contexte industriel de ces travaux.

Lorsque l'on considère le cas des moteurs essence suralimentés, la modélisation du compresseur et de la turbine jouent un rôle clé sur la précision et la robustesse des résultats de simulation. Plus précisément, pour les modèles orientés contrôle nécessitant un temps de calcul le plus court possible, la performance du modèle découle directement d'un jeu de quatre cartographies statiques, systématiquement construites à partir d'essais expérimentaux. Cette étude propose un nouvel ensemble d'algorithmes destinés à l'interpolation et l'extrapolation de ces cartographies. Ils entendent améliorer les résultats en extrapolation obtenus dans la littérature lorsque des modèles mathématiques sont utilisés, et réduire le temps de calcul par rapport aux modèles utilisant une description détaillée des phénomènes thermodynamiques et de mécaniques des fluides mis en jeu. Une méthodologie similaire est proposée pour le compresseur et la turbine, basée notamment sur la relation entre le comportement idéal et réel de chacun de ces composants. L'utilisation de ce lien physique dans les modèles présentés dans cette étude contribue considérablement à la robustesse de la méthode.

Bien que les cartographies soient au cœur du modèle moteur présenté en section 3.2 et utilisé tout au long de la partie 2, les bénéfices de ces développements vont bien au-delà du cadre de cette étude:

- La cartographie qui donne le rapport de compression en fonction du débit traversant le compresseur permet l'implémentation d'un capteur virtuel du régime de rotation du turbocompresseur chez Renault SAS (section 3.1). Dans un contexte industriel, cet estimateur en boucle ouverte bénéficie avant tout de sa simplicité, et a également démontré une grande précision, obtenue grâce aux nouvelles stratégies d'extrapolation.
- Dans le cadre d'un partenariat entre Renault SAS et LMS®, la méthodologie complète d'interpolation et d'extrapolation des cartographies du compresseur et de la turbine est en train d'être implémentée dans un outil industriel.
- Finalement, les modèles d'extrapolation développés dans cette étude sont également au cœur d'applications brevetées, incluant notamment des turbocompresseurs à assistance électrique.

La seconde partie de la thèse répond au problème du contrôle de la chaîne d'air des moteurs essence suralimentés, au moyen d'une approche de commande prédictive non linéaire. Cette dernière est connue pour sa capacité à contrôler des systèmes multi-entrées, multi-sorties, contraints et non linéaires, tels que les moteurs à combustion interne modernes. Au contraire, les méthodes classiques multi-linéaires montrent leurs limites à contrôler le moteur sur la totalité de ses points de fonctionnement [46,96]. Ce problème est d'autant plus crucial que la complexité croissante des moteurs fait de la synthèse du contrôle, un frein pour la réduction des coûts et temps de développement des constructeurs automobiles.

Concernant la commande prédictive non linéaire, deux difficultés importantes doivent être prises en compte. La première repose sur la construction d'un modèle non linéaire du système, fruit d'un juste compromis entre précision et temps de calcul. La seconde concerne la résolution du problème d'optimisation caractérisant la commande prédictive. Cette thèse propose deux schémas de contrôle implicite qui solutionnent la première difficulté en utilisant directement le modèle moteur développé dans la partie 1. Ce choix est motivé à la fois par la flexibilité de la philosophie de modélisation, ainsi que par sa capacité à obtenir un modèle précis par le seul biais d'essais expérimentaux classiques dans l'industrie automobile. De plus, ces deux stratégies de contrôle bénéficient de la physique contenue dans le modèle en minimisant explicitement un critère de performance basé sur la thermodynamique et en assurant par ailleurs le contrôle de la pression collecteur. Les approches diffèrent dans leur description de la future trajectoire de contrôle sur l'horizon de prédiction. En effet, alors que la première est basée sur un schéma prédictif à horizon-1, la deuxième repose sur la paramétrisation de la trajectoire de contrôle au moyen de fonctions orthonormales: les polynômes de Laguerre. Cette dernière entre ainsi dans la catégorie des commandes prédictives non linéaires paramétrées. Les deux approches montrent de bonnes performances en poursuite, dans des conditions réelles d'utilisation mais requièrent des moyens de calcul significatifs.

En effet, le problème lié à l'implémentation en temps réel d'une stratégie de contrôle prédictif non linéaire se doit d'être résolu par d'autres moyens. Dans ces travaux, on utilise pour cela le cadre de la commande prédictive non linéaire explicite. En pratique, une position sous-optimale des actionneurs est obtenue en ligne en parcourant un arbre de recherche binaire puis en calculant une simple relation affine. Dans ce cas particulier d'application, cela a nécessité la détermination d'une solution affine par morceau d'un problème non linéaire multi-paramétrique de dimension 6. Les importants calculs hors ligne associés à la résolution d'un problème de si grande dimension ont été permis par un nouvel algorithme supportant le calcul parallèle et compatible avec le schéma prédictif à horizon-1 synthétisé dans cette étude. Ainsi, tous les bénéfices de l'utilisation d'un modèle de prédiction physique et de la minimisation d'un critère thermodynamique sont conservés, tout en menant à une réduction considérable du temps de calcul en ligne.

Dans son ensemble, l'étude mène à trois conclusions importantes:

- Les modèles physiques basés sur la combinaison de modèles moteur moyens et de modélisations zéro dimensionnelles sont compatibles avec le cadre de commande prédictive non linéaire. Ils présentent l'avantage d'être largement utilisés dans l'industrie automobile et peuvent être obtenus de façon systématique à partir d'essais expérimentaux en stabilisé. Le cadre prédictif non linéaire permet, quant à lui, de prendre en compte des critères de performance tels que le rendement du moteur.

- La décomposition de la future trajectoire des incréments de commande sur un jeu de polynômes de Laguerre encapsule le compromis complexité/optimalité dans un jeu de paramètres de haut niveau, simples à calibrer. Cette formulation montre un grand potentiel d'adaptabilité au moyen de calcul, puisque le simple réglage des paramètres va pouvoir permettre d'adapter le compromis à de nouveaux moyens de calcul.

- Le calcul d'un contrôle temps-réel approximant le comportement d'une telle commande prédictive non linéaire implicite peut être obtenu en résolvant un problème multiparamétrique non linéaire hors ligne. Un algorithme compatible avec les modèles de prédiction complexes tels que des modèles moteurs physiques, et capable de profiter du développement des architectures de calcul parallèle est détaillé dans ce mémoire.

Vers une approche quasi-systématique de la synthèse du contrôle de la chaîne d'air des moteurs

Dès le début, l'objectif a été de faciliter la conception des lois de contrôle de la chaîne d'air des moteurs, dans un contexte où l'industrie automobile moderne présente des exigences de plus en plus fortes et des temps de développement de plus en plus courts. En particulier, les normes anti-pollution de plus en plus strictes ont obligé les constructeurs automobiles à considérablement complexifier la définition technique de leurs moteurs. Cette complexité croissante rend la synthèse du contrôle plus longue et plus difficile si aucune nouvelle méthode n'est mise en place. Depuis quelques années maintenant, les lois de contrôle « model-based » entendent répondre à ce challenge. Cependant, en pratique, il est d'avantage question d'un développement « model-based », utilisant la simulation pour la validation des lois de contrôle, plutôt que de réelles stratégies de contrôle « model-based », intégrant de la physique. Seuls quelques cas précis d'application utilisent une telle approche, cependant ils sont souvent le résultat d'un processus de conception qui les empêche d'être systématiquement appliqués.

Cette étude entend fournir le début d'une réponse au besoin des constructeurs automobiles de développer des stratégies de contrôle de la chaîne d'air beaucoup plus rapidement. La proposition repose sur la commande prédictive non linéaire choisie pour son optimalité et sa flexibilité naturelle, et peut être résumée en trois étapes (voir figure ci-dessous):

- Etape 1: Obtenir une représentation du phénomène à contrôler. Les modèles physiques, en opposition aux modèles mathématiques, permettent une calibration plus rapide et une meilleure robustesse sur l'ensemble des points de fonctionnement.
- Etape 2: Synthétiser une commande prédictive non linéaire implicite qui atteint les performances prévues dans le cahier des charges. Dans cette étape majeure, une fonction de coût en accord avec la physique et les mathématiques doit être choisie. En pratique, la flexibilité du cadre non linéaire facilite la synthèse.
- Etape 3: Calculer la solution explicite du problème d'optimisation. Cela conduit à un contrôleur implémentable en temps réel, c'est-à-dire présentant à la fois un temps de calcul court et prévisible.

Figure – Vue d'ensemble de l'approche de synthèse du contrôle proposée dans cette étude

L'avantage majeur de la proposition repose sur sa flexibilité. En effet, chacune des étapes du schéma peut être adéquatement remplacée par une approche alternative, partageant les mêmes entrées et les mêmes sorties. Le modèle physique présenté dans le chapitre 3 peut être remplacé par un modèle purement mathématique tel que modèles neuronaux. La commande prédictive non linéaire à horizon-1 introduite dans le chapitre 5 peut être substituée par une formulation plus complexe si les moyens de calcul sont augmentés. Elle pourrait également être remplacée par l'une des formulations de commande prédictive non linéaire dite « rapide », connues pour être moins chronophages mais pouvant néanmoins rester

incompatibles avec les contraintes du calcul temps réel. Enfin, l'approximation linéaire par morceaux définie sur un ensemble d'hyper-rectangles, utilisée au chapitre 7, peut être remplacée par toute autre géométrie de découpage ou tout autre type d'approximation.

Dans le cas particulier du contrôle de la chaîne d'air d'un moteur essence suralimenté, l'ensemble de l'approche a mené à une réduction de temps de calcul suffisamment grande pour envisager une implémentation en temps réel chez Renault SAS.

A court terme, les développements suivants permettront de compléter et d'améliorer les méthodes présentées dans cette étude:

- L'extension naturelle de la philosophie de modélisation présentée dans le chapitre 1 concerne le développement de nouveaux modèles de composants pour décrire les phénomènes impliqués dans des définitions techniques de moteur plus complexes. Cela inclut notamment la recirculation des gaz brûlés (EGR) et les systèmes de suralimentation multiples. Des développements sur la modélisation de l'effet des soupapes à levée variable sont d'ores et déjà en cours [39].

- La validation expérimentale des cartographies représente la prochaine étape concernant les stratégies d'interpolation et d'extrapolation présentées dans le chapitre 2. De plus, une description précise des phénomènes mis en jeu dans la zone de pompage sera d'autant plus profitable qu'elle est de plus en plus utilisée lors des phases transitoires. De nombreux travaux sont actuellement menés et de nouveaux résultats seront bientôt disponibles [81,82]. Enfin, la prise en compte des grandeurs principales de la géométrie des turbomachines peut potentiellement augmenter la robustesse et la précision de la méthode. En particulier, une approche consistant à construire les cartographies compresseur uniquement par le biais de trois caractéristiques géométriques a été développée et présentée dans [40]. Grâce à cette méthode utilisant les modèles d'extrapolation présentés au chapitre 2, la prise en compte des informations obtenues améliorerait encore les résultats présentés dans ce mémoire.

- Pour la synthèse de la commande prédictive non linéaire implicite, la paramétrisation de la future trajectoire de contrôle a montré des propriétés intéressantes en termes d'adaptabilité et de gestion du compromis complexité/optimalité. D'autres cas d'application permettront de confirmer qu'un meilleur rapport performance/temps de calcul peut être obtenu de manière systématique.

- La commande explicite, et en particulier son pendant non linéaire, sont des champs de recherche relativement jeunes. A court-termes, les développements devraient porter sur la réduction de la mémoire nécessaire pour stocker en ligne la loi linéaire par morceaux et les régions sur lesquelles elle est définie. Cela représente, en effet, un élément crucial au regard d'une implémentation sur des calculateurs de série. Plusieurs solutions existent dans la littérature, mais une optimisation de l'algorithme présenté dans le chapitre 7 devrait déjà pouvoir mener à une réduction significative de la quantité de données à embarquer. Cela inclut par exemple l'utilisation d'une définition basée sur la physique du critère d'erreur, c'est-à-dire d'être capable de valider ou invalider une région donnée en se basant sur un critère plus physique que la simple valeur de la fonction de coût.

A plus long termes, les perspectives de développement ci-dessous permettront d'assurer la pérennité de la méthode présentée dans cette étude:

- Intuitivement, la méthode dans son ensemble doit pouvoir être étendue au cas des moteurs diesel, qui représentent un part significative du parc automobile mondial. Ainsi le développement d'une librairie de modèles de composants orientés contrôle, capables de décrire à la fois les moteurs essence ou diesel, est une étape importante à franchir en vue d'une application industrielle de la méthodologie.

- Concernant l'interpolation et l'extrapolation des cartographies du compresseur et de la turbine, réécrire les algorithmes pour se soustraire du besoin de travailler par iso-vitesse de rotation du turbocompresseur, permettrait de remplacer les données fournies par le fabricant par des mesures en stabilisé obtenues sur banc d'essais moteur. Les conditions réelles de fonctionnement du turbocompresseur pourraient dès lors être mieux prises en compte, et inclure par exemple les transferts thermiques entre le compresseur et la turbine. Ces nouvelles méthodologies pourront directement être intégrées à la librairie de composants suggérée ci-dessus, et permettre ainsi la construction de modèles de compresseurs et de turbines à partir des mesures sur banc d'essais moteur.
- Concernant l'étape de synthèse de la commande prédictive non linéaire implicite, il faudra prendre en compte que, dans certains cas, le problème d'optimisation peut être non convexe et présenter de nombreux minimums locaux, compliquant ainsi considérablement la détermination d'une solution. Reformuler le problème ou utiliser des algorithmes d'optimisation globaux représentent deux méthodes générales à intégrer à cette étape, de manière à rendre la synthèse systématique. L'impact d'une telle approche sur le temps de calcul hors ligne de la solution explicite devra également être étudié en profondeur.
- Finalement, la méthode dans son ensemble, incluant l'algorithme de construction de la loi explicite, pourrait être implémentée dans un outil industriel, encapsulant les trois étapes de la méthode (voir figure ci-dessus). Pour les constructeurs automobiles, cela permettrait de construire des lois de contrôle quasi-optimales de manière systématique, en mettant à profit les importants efforts consentis sur les aspects modélisation. Dans un premier temps, à la vue de la quantité de mémoire actuellement requise, l'outil pourrait être utilisé pour comparer différentes solutions techniques, en amont dans le processus de développement. Ensuite, à plus long termes, l'augmentation des capacités de calcul hors ligne et de la mémoire disponible dans les calculateurs devrait permettre l'implémentation de ces lois de contrôle dans les véhicules de série, accélérant ainsi l'intégration de nouvelles briques technologiques favorisant la baisse d'émissions polluantes et de la consommation de carburant.

***

Il est clairement établi que ces aspects liés à la quantité de mémoire nécessaire, représentent le talon d'Achille des approches de commande prédictive non linéaire explicite lorsque l'on considère des applications embarquées. Différentes directions de travail devront être étudiées de sorte à augmenter la crédibilité du cadre général de la commande prédictive non linéaire explicite vis-à-vis de l'industrie automobile et, à plus grande échelle, de la communauté du contrôle. Ainsi, les prochaines années verront probablement les recherche sur la commande prédictive non linéaire explicite, partir dans deux directions de travail. Premièrement, une des directions concerne le développement de méthodes avancées pour le stockage de la solution explicite. L'utilisation d'arbres de recherche binaires a ouvert la voie, mais d'autres approches pourraient encore améliorer les résultats. La deuxième voie de travail concerne la résolution du problème multiparamétrique en elle-même. En effet, des alternatives à une approximation affine par morceaux devraient pouvoir considérablement réduire le nombre de régions requises, modifiant ainsi le compromis entre temps de calcul en ligne et mémoire, pour l'instant intrinsèque à la méthodologie. En effet, les méthodes d'approximation barycentrique proposées dans la littérature dans des cas linéaires, semblent très attractives. En particulier, l'application pratique au cas non linéaire du contrôle de la chaîne d'air des moteurs essence suralimentés s'avère être prometteuse (figure 7.11). Des résultats complets à ce sujet seront bientôt publiés.

REFERENCES

[1] Akins M. D. et al., *Techniques for Determining Turbocharger Speed*, 2004.

[2] Alessio A. and Bemporad A., *A Survey on Explicit Model Control*, *Nonlinear Model Predictive Control Towards New Challenging Applications*, Springer, Heidelberg, 2009, pp. 345-369.

[3] Allgöwer F. and Zheng A., *Nonlinear Model Predictive Control*, Springer, Basel, 2000.

[4] Allgöwer F. et al., *Nonlinear Model Predictive Control: From Theory to Application*, J. Chin. Inst. Chem. Engrs., 35 (2004), pp. 299-315.

[5] Ammann M. et al., *Model-Based Control of the VGT and EGA in Turbocharged Common-Rail Diesel Engine: Theory and Passenger Car Implementation*, SAE Transactions, 112 (2003), pp. 527-538.

[6] Ayadi M. et al., *Polynomial Control of Turbocharged Diesel Engine Model*, *IEEE International Conference on Industrial Technology*, 2004, pp. 1384-1389.

[7] Baines N. C., *Fundamentals of Turbocharging*, Concepts NREC, 2005.

[8] Baotic M. et al., *Efficient On-line Computation od Constrained Optimal Control*, SIAM J. Control Optim., 47 (2008), pp. 2470-2489.

[9] Behrendt S. et al., *An Application of Model Predictive Control to a Gasoline Engine*, *18th International Conference on Process Control*, Tatranská Lomnica, Slovakia, 2011, pp. 57-63.

[10] Bemporad A. et al., *The Explicit Solution of Constrained LP-Based Receding Horizon Control*, *Decision and Control, 2000. Proceedings of the 39th IEEE Conference on*, 2000, pp. 632-637 vol.1.

[11] Bemporad A. et al., *The Explicit Solution of Model Predictive Control via Multiparametric Quadratic Programming*, *American Control Conference*, Chicago, 2000.

[12] Bemporad A. et al., *Model predictive control based on linear programming - the explicit solution*, Automatic Control, IEEE Transactions on, 47 (2002), pp. 1974-1985.

[13] Beño R. et al., *Enforcing Stability in Steady-State Optimization*, *16th IFAC Symposium on System Identification*, Brussels, Belgium, 2012.

[14] Beño R. et al., *Robust Numerical Approach to Mean-Value Modeling of Internal Combustion Engines*, *7th IFAC Symposium on Advances in Automotive Control*, Tokyo, Japan, 2013.

[15] Blauwkamp R. and Basar T., *A Receding-Horizon Approach to Robust Output Feedback Control for Nonlinear Systems*, *IEEE Conference on Decision and Control*, San Diego, USA, 1999.

[16] Borrelli F. et al., *Efficient On-Line Computation of Constrained Optimal Control*, *Decision and Control, 2001. Proceedings of the 40th IEEE Conference on*, 2001, pp. 1187-1192 vol.2.

[17] Borrelli F. et al., *Geometric Algorithm for Multiparametric Linear Programming*, Journal of Optimization Theory and Applications, 118 (2003), pp. 515-540.

[18] Borrelli F. et al., *On the Complexity of Explicit MPC Laws*, *Proceedings of European Control Conference 2009*, Budapest, Hungary, 2009.

[19] Borrelli F. et al., *Reference governor for constrained piecewise affine systems*, Journal of Process Control, 19 (2009), pp. 1229-1237.

[20] Chang T. S. and Seborg D. E., *A Linear Programming Approach for Multivariable Feedback Control With Inequality Constraints*, International Journal of Control, 37 (1983), pp. 583-597.

[21] Chauvin J. et al., *Control Oriented Model of a Variable Geometry Turbocharger in an Engine with Two EGR loops*, Oil & Gas Science and Technology - Rev. IFP Energies nouvelles, 66 (2011), pp. 563-571.

[22] Chen H. and Shaw L., *On Receding Horizon Feedback Control*, Automatica, 18 (1982).

[23] Chen H. et al., *A Game Theoretic Approach to Nonlinear Robust Receding Horizon Control of Constrained Systems*, *Amercian Control Conference*, Albuquerque, USA, 1997.

[24] Chen H. and Allgöwer F., *A Quasi-Infinite Horizon Nonlinear Model Predictive Control Scheme with Guaranteed Stability*, Automatica, 34 (1998).

[25] Christen U. and Busch R., *The Art of Control Engineering: Science Meets Industrial Reality*, *IFAC Workshop on Engine and Powertrain Control, Simulation and Modeling*, France, 2012.

[26] Clarke D., *Advances in Model-Based Predictive Control*, Oxford University Press USA, 1994.

[27] Clarke D. W. et al., *Generalized Predictive Control - Part 2 : Extensions and Interpretations*, Automatica, 23 (1987).

[28] Clarke D. W. et al., *Generalized Predictive Control - Part 1: The Basic Algorithm*, Automatica, 23 (1987).

[29] Colin G. et al., *Linearized Neural Predictive Control: a Turbocharged SI Engine Application*, SAE Technical Paper, 2005-01-0046 (2005).

[30] Colin G., *Control of Fast Nonlinear Systems : Application to a Turbocharged SI Engine with Variable Valve Timing*, University of Orleans, 2006.

[31] Colin G. et al., *Exact and Linearized Neural Predictive Control : a Turbocharged SI Engine Example*, J. Dyn. Sys., Meas., Control, 129 (2007), pp. 527-533.

[32] Cutler C. R. and Ramaker B. L., *Dynamic Matrix Control - A Computer Control Algorithm*, *Automatic Control Conference*, San Francisco, CA, USA, 1980.

[33] Del Re L. et al., *Automotive Model Predictive Control*, Springer, Berlin, 2010.

[34] Devasia S., *Should Model-Based Inverse Inputs Be Used As Feedforward Under Plant Uncertainty ?*, IEEE Transactions on Automatic Control, 47 (2002), pp. 1865-1871.

[35] Dowell P. G. and Akehurst S., *Advanced Mapping Techniques for Radial Compressor for Use in Real-Time Engine Models*, SAE Technical Paper, 2010-01-1227 (2010).

[36] Draper N. R. and Smith H., *Applied Regression Analysis* Third, Wiley, 1998.

[37] Dubravic A. and Sehic Z., *Using Orthonormal Functions in Model Predictive Control*, Technical Gazette, 19 (2012), pp. 513-520.

[38] El Hadef J. et al., *Explicit-Ready Nonlinear Model Predictive Control of the Air Path of a Turbocharged Spark-Ignited Engine*, *7th IFAC Symposium on Advances in Automotive Control*, Tokyo, Japan, 2013.

[39] El Hadef J. et al., *Neural Model for Real-Time Engine Volumetric Efficiency Estimation*, SAE Technical Paper, 2013-24-0132 (2013).

[40] El Hadef J. et al., *Geometry-Based Compressor Data-Maps Prediction*, SAE Technical Paper, 2013-01-0933 (2013).

[41] El Hadef J. et al., *Explicit Nonlinear Model Predictive Control of the Air Path of a Turbocharged Spark-Ignited Engine*, *2013 IEEE Multi-Conference on Systems and Control*, Hyderabad, India, 2013.

[42] Eriksson L. et al., *Modeling of a Turbocharged SI Engine*, Annual Reviews in Control, 26 (2002), pp. 129-137.

[43] Eriksson L., *Modeling and Control of Turbocharged SI and DI Engines*, Oil & Gas Science and Technology - Rev. IFP Energies nouvelles, 62 (2007), pp. 523-538.

[44] Feng L. et al., *Barrier Functions Nonlinear Optimization for Optimal Decompression of Divers*, *IEEE Conference on Decision and Control*, Shangai, China, 2009.

[45] Ferreau H. J. et al., *An Online Active Set Strategy for Fast Solution of Parametric Quadratic Programming in MPC Applications, Proceedings of the IFAC Workshop on Nonlinear Model Predictive Control for Fast Systems*, 2006.

[46] Ferreau H. J. et al., *Fast Nonlinear Model Predictive Control of Gasoline Engine*, in P. o. t. IEEE, ed., *International Conference on Control Applications*, Munich, Germany, 2006.

[47] Ferreau H. J. et al., *Predictive Control of a Real-World Diesel Engine Using an Extended Online Active Set Strategy*, Annual Reviews in Control, 31 (2007), pp. 293-301.

[48] Fiacco A. V. and Ishizuka Y., *Sensitivity and Stability Analysis in Nonlinear Programming*, Annals of Operations Research, 27 (1990), pp. 215-235.

[49] Foss B. A. et al., *Nonlinear Predictive Control Using Local Models - Applied to a Batch Fermentation Process*, Control Engineering Practice, 3 (1995), pp. 389-396.

[50] Fritsch F. N. and Carlons R. E., *Monotone Piecewise Cubic Interpolation*, SIAM Journal on Numerical Analysis, 17 (1980).

[51] Fuchs A. N. et al., *Optimized Decision Trees for Point Location in Polytopic Data Sets - Application to Explicit MPC*, *American Control Conference*, Baltimore, USA, 2010, pp. 5507-5512.

[52] Garcia C. E. et al., *Model Predictive Control: Theory and Pratice - A Survey*, Automatica, 25 (1989), pp. 335-348.

[53] Grancharova A. and Johansen T. A., *Explicit Nonlinear Model Predictive Control*, Springer, Berlin, 2012.

[54] Greitzer E. M., *Surge and Rotating Stallin Axial Flow Compressors*, Transactions ASME, Journal of Engineering for Gas Turbine and Power, 98 (1976), pp. 190-217.

[55] Grimm G. et al., *Examples when Nonlinear Model Predictive Control is Nonrobust*, Automatica, 40 (2004).

[56] Grüne L. and Pannek J., *Nonlinear Model Predictive Control*, Springer-Verlag, London, 2011.

[57] Guzzella L. and Onder C. H., *Introduction to Modeling and Control of Internal Combustion Engine Systems*, Springer-Verlag, Berlin, 2004.

[58] He C. and Xiao Y., *Turbo Speed Sensor Diagnostic for Turbocharge Engines*, 2011.

[59] Hendricks E. and Sorenson S. C., *Mean Value Modeling of Spark Ignition Engines*, SAE Technical Paper, 900616 (1990).

[60] Hendricks E., *Isothermal versus Adiabatic Mean Value SI Engine Models*, 3rd IFAC Workshop, Advances in Automotive Control (2001), pp. 373-378.

[61] Henson M. A., *Nonlinear Model Predictive Control: Current Status and Future Directions*, Computers & Chemical Engineering, 23 (1998), pp. 187-202.

[62] Herceg M. et al., *Nonlinear Model Predictive Control of a Turbocharged Diesel Engine*, *IEEE International Conference on Control*, 2006, pp. 2766-2771.

[63] Herceg M. et al., *Multi-Parametric Toolbox 3.0*, *European Control Conference*, Zurich, Switzerland, 2013, pp. 502-510. http://control.ee.ethz.ch/~mpt.

[64] Hermans R. M. et al., *Horizon-1 Predictive Control of Automotive Electromagnetic Actuators*, IEEE Transactions on Control Systems Technology, 21 (2013), pp. 1652-1665.

[65] Heywood J. B., *Internal Combustion Engines Fundamentals*, McGraw-Hill, 1988.

[66] Hicks G. A. and Ray W. H., *Approximations Methods for Optimal Control Synthesis*, Canadian Journal of Chemical Engineering, 49 (1971), pp. 522-528.

[67] Jadbabaie A. et al., *Unconstrainted Receding Horizon Control of Nonlinear Systems*, IEEE Transactions on Automatic Control, 46 (2001).

[68] Jankovic M. and Magner S. W., *Variable Cam Timing: Consequences to Automotive Engine Control Design*, *15thTriennal IFAC World Congress*, Barcelona, Spain, 2002.

[69] Japikse D. and Baines N. C., *Introduction to Turbomachinery*, Concepts NREC, 1994.

[70] Jensen J.-P. et al., *Mean Value Modeling of a Small Turbocharged Diesel Engine*, SAE Technical Paper (1991).

[71] Jensen P. A. and Bard J. F., *Operations Research Models and Methods*, John Wiley and Sons, 2003.

[72] Johansen T. A., *On Multi-Parametric Nonlinear Programming and Explicit Nonlinear Model Predictive Control, Decision and Control, 2002, Proceedings of the 41st IEEE Conference on*, 2002, pp. 2768-2773 vol.3.

[73] Johansen T. A. et al., *Hardware Synthesis of Explicit Model Predictive Controllers*, IEEE Transactions on Control Systems Technology, 15 (2007), pp. 191-197.

[74] Jung M. et al., *Parameterization and Transient Validation of a Variable Geometry Turbocharger for Mean-Value Modeling at Low and Medium Speed-Load Points*, SAE Technical Paper, 2006-01-0438 (2002).

[75] Kraft D., *On Converting Optimal Controls Problems into Nonlinear Programming Problems*, *Computational Mathematical Programming*, Springer-Verlag, 1985, pp. 261-280.

[76] Kvasnica M. and Fikar M., *Clipping-Based Complexity Reduction in Explicit MPC*, IEEE Transactions on Automatic Control, 57 (2012), pp. 1878-1883.

[77] Kvasnica M. et al., *Complexity Reduction of Explicit Model Predictive Control via Separation*, Automatica, 49 (2012), pp. 1776-1781.

[78] Lee J. H. et al., *State-Space Interpretation of Model Predictive Control*, Automatica, 30 (1994), pp. 707-717.

[79] Lee Y. W., *Statistical Theory of Communication*, John Wiley and Sons, New-York, 1960.

[80] Leroy T. et al., *Motion Planning for Experimental Air Path Control of a Variable-Valve-Timing Spark Ignition Engine*, Control Engineering Practice, 17 (2009), pp. 1432-1439.

[81] Leufven O. and Eriksson L., *Surge and Choke Capable Compressor Model*, *18th IFAC World Congress*, Milano, Italy, 2011.

[82] Leufven O. and Eriksson L., *A Surge and Choke Capable Compressor Flow Model - Validation and Extrapolation Capability*, Control Engineering Practice, 21 (2013), pp. 1871-1883.

[83] Limon D. et al., *Input-to-State Stability of Min-Max MPC controllers for Nonlinear Systems with Bounded Uncertainties*, Automatica, 42 (2006), pp. 797-803.

[84] Magni L. and Sepulchre R., *Stability Margins of Nonlinear Receding Horizon Control via Inverse Optimality*, Systems & Control Letters, 32 (1997).

[85] Magni L. et al., *Robust Model Predictive Control for Nonlinear Disrete-Time Systems*, International Journal of Robust and Nonlinear Control, 13 (2003), pp. 229-246.

[86] Magni L. and Scattolini R., *Robustness and Robust Design of MPC for Nonlinear Discrete-Time Systems*, *Assessment and Future Directions of Nonlinear Model Predictive Control*, Springer, Heidelberg, 2007, pp. 239-254.

[87] Martin G. et al., *Implementing Turbomachinery Physics into Data-Map Based Turbocharger Models*, SAE Technical Paper (2009).

[88] Martin G., *0D - 1D Modeling of the Airpath of Internal Combustion Engines for Control Purposes*, PhD. thesis, University of Orleans, 2010.

[89] Mayne D. Q. et al., *Constrained Model Predictive Control : Stability and Optimality*, Automatica, 26 (2000).

[90] Michalska H. and Mayne D. Q., *Robust Receding Horizon Control of Constrained Nonlinear Systems*, IEEE Transactions on Automatic Control, AC-38 (1993).

[91] Miotti A. et al., *Integrated Breathing Model and Multi-Variable Control Approach for Air Management in Advanced Gasoline Engine*, SAE Technical Paper, 2006-01-0658 (2006).

[92] Moraal P. and Kolmanovsky I., *Turbocharger Modeling for Automotive Control Applications*, SAE Technical Paper (1999).

[93] Moran M. and Shapiro H. N., *Fundamentals of Engineering Thermodynamics*, Wiley, New-York, 1992.

[94] Moulin P. et al., *Modelling and Control of the Air System of a Turbocharged Gasoline Engine*, Proc. of the IFAC World Conference (2008).

[95] Müller M. et al., *Mean Value Modelling of Turbocharged Spark Iginition Engines*, SAE Technical Paper (1998).

[96] Murilo A., *Contributions on Nonlinear Model Predictive Control for Fast Systems*, PhD thesis, Institut Polytechnique de Grenoble, 2009.

[97] Murilo A. et al., *Fast NMPC Scheme for a Diesel Engine Air Path*, *European Control Conference*, Budapest, Hungary, 2009.

[98] Murilo A. et al., *Experimental Validation of a parameterized NMPC for Diesel Engine*, *2009 IFAC Workshop on Engine and Powertrain Control, Simulation and Modeling*, France, 2009.

[99] Murilo A. et al., *A Real-Time Implementable NMPC Output Feedback for a Diesel Engine Air Path*, Oil Gas Sci. Technol. – Rev. IFP Energies nouvelles, 66 (2011), pp. 613-625.

[100] Murilo A. et al., *Multivariable Control Strategy Based on a Parameterized NMPC for Diesel Engine*, ABCM Symposium Series in Mechatronics, 5 (2012), pp. 316-324.

[101] Nagy Z. K. et al., *Real-Time Implementation of Nonlinear Model Predictive Control of Batch Processes in an Industrial Framework*, *Assessment and Future Directions of Nonlinear Model Predictive Control*, Springer, Heidelberg, 2007, pp. 465-472.

[102] Nguyen-Schäfer H., *Turbocharging Concepts*, *Rotordynamics of Automotive Turbochargers*, Springer Berlin Heidelberg, 2012, pp. 1-16.

[103] Ortner P. and Del Re L., *Predictive Control of a Diesel Engine Air Path*, IEEE Transactions on Control Systems Technology, 15 (2007), pp. 449-456.

[104] Ortner P. et al., *Nonlinear Model Predictive Control of a Diesel Engine Air Path*, *IFAC Workshop on Control Applications of Optimization*, University of Jyväskylä, Finland, 2009.

[105] Pachner D. et al., *Identification Techniques for Control Oriented Models of Internal Combustion Engines*, in D. Alberer, H. Hjalmarsson and L. Re, eds., *Identification for Automotive Systems*, Springer London, 2012, pp. 257-282.

[106] Peterka V., *Predictor-Based Self Tuning Control*, Automatica, 20 (1984), pp. 39-50.

[107] Propoi A. I., *Use of Linear Programming Method for Synthesizing Sampled-Data Automatic Systems*, Automation and Remote Control, 24 (1963), pp. 837-844.

[108] Qin S. J. and Badgwell T. A., *A Survey of Industrial Model Predictive Control Tehcnology*, Control Engineering Practice, 11 (2003), pp. 733-764.

[109] Rao C. V. and Rawlings J. B., *Linear Programming and Model Predictive Control*, Journal of Process Control, 10 (2000), pp. 283-289.

[110] Richalet J. et al., *Algorithmic Control of Industrial Processes*, Proceedings of the 4th IFAC Symposium on Identification and System Parameter Estimation (1976), pp. 1119-1167.

[111] Richalet J. et al., *Model Predictive Heuristic Control: Applications to Industrial Processes*, Automatica, 14 (1978), pp. 413-428.

[112] Ricker N. L., *Model Predictive Control: State of the Art*, *4th International Conference on Chemical Process Control*, Padre Island, Texas, 1991, pp. 271-296.

[113] Ruckert J. et al., *A Model Based Predictive Attempt to Control Boost Pressure and EGR-rate in a Heavy Duty Diesel Engine*, *IFAC Advances in Automotive Control*, 2004.

[114] Saerens B. et al., *Model Predictive Control of Automotive Powertrains - First Experimental Results*, *Decision and Control, 2008. CDC 2008. 47th IEEE Conference on*, 2008, pp. 5692-5697.

[115] Salcedo J. V. et al., *Real-Time Control and Simulations of a Nonlinear Model of Air Management in a Turbocharged Diesel Engine*, Departement of System Engineering and Control, Universidad Politécnica de Valencia, Spain (2004).

[116] Sargent R. W. H. and Sullivan G. R., *The Development of an Efficient Optimal Control Package*, *8th IFIP Conference on Optimization Techniques*, Springer, Heidelberg, Germany, 1977.

[117] Scokaert P. et al., *Discrete-Time Stability with Perturbations: Application to Model Predictive Control*, Automatica, 33 (1997).

[118] Scokaert P. et al., *Suboptimal Model Predictive Control (Feasability Implies Stability)*, IEEE Transactions on Automatic Control, 44 (1999).

[119] Stewart G. and Borrelli F., *A Model Predictive Control Framework for Industrial Turbodiesel Engine Control, Decision and Control, 2008. CDC 2008. 47th IEEE Conference on*, 2008, pp. 5704-5711.

[120] Summers S. et al., *A Multiresolution Approximation Method for Fast Explicit Model Predictive Control*, Automatic Control, IEEE Transactions on, 56 (2011), pp. 2530-2541.

[121] Szücs A. et al., *Data Compression Techniques for Complexity Reduction in Explicit MPC*, *Selected Topics in Modelling and Control*, Slovak University of Technology Press, 2011, pp. 18-23.

[122] Talon V., *Modélisation 0-1D des Moteurs à Allumage Commandé*, University of Orleans, 2004.

[123] Theotokatos G. and Kyrtatos N. P., *Diesel Engine Transient Operation With Turbocharger Compressor Surging*, SAE Technical Paper, 2001-01-1241 (2001).

[124] Tøndel P. and Johansen T. A., *Complexity Reduction in Explicit Model Predictive Control*, *IFAC World Congress*, Barcelona, Spain, 2002.

[125] Tøndel P. et al., *Evaluation of Piecewise Affine Control via Binary Search Tree*, Automatica, 39 (2003), pp. 945-950.

[126] van Nieuwstadt M. J. et al., *EGR-VGT Control Schemes: Experimental Comparison for a High-Speed Diesel Engine*, IEEE Control Systems Magazine, 20 (2000), pp. 63-79.

[127] Vitek O. et al., *New Approach to Turbocharger Optimization using 1-D Simulation Tools*, SAE Technical Paper (2006).

[128] Wahlberg B., *System Identification using Laguerre Models*, IEEE Transactions on Automatic Control, 36 (1991), pp. 551-562.

[129] Walter E. and Pronzato L., *Identification of Parametric Models from Experimental Data*, Springer, Londres, 1997.

[130] Wang L. and Cluett W. R., *System Identification Based on Closed-Loop Step Response Data*, IEE Proceedings - Control Theory and Applications, 141 (1994), pp. 107-110.

[131] Wang L., *Continuous Time Model Predictive Control Design using Orthonormal Functions*, International Journal of Control, 74 (2001), pp. 1588-1600.

[132] Wang L., *Discrete Model Predictive Control Design using Laguerre Functions*, *American Control Conference*, Arlington, USA, 2001, pp. 2430-2435.

[133] Wang L., *Discrete Model Predictive Controller Design using Laguerre Functions*, Journal of Process Control, 14 (2004), pp. 131-142.

[134] Whitfield A. and Baines N. C., *Design od Radial Turbomachines*, Pearson Education, 1990.

[135] Winkler G., *Steady State & Dynamic Modelling of Engine Turbomachinery Systems*, PhD Thesis, 1977.

[136] Winterbone D. E. and Pearson R. J., *Design Techniques for Engine Manifolds: Wave Action Methods for IC Engines*, Wiley, 1999.

[137] Winterbone D. E. and Pearson R. J., *Theory of Engine Manifold Design: Wave Action Methods for IC Engines*, Wiley, 2000.

[138] Zadeh L. A. and Whalen L. H., *On Optimal Control and Linear Programming*, IRE Transactions on Automatic Control, 7 (1962), pp. 45-46.

Jamil EL HADEF

Approche quasi-systématique du contrôle de la chaîne d'air des moteurs suralimentés, basée sur la commande prédictive non linéaire explicite

Résumé

Les centaines de millions de véhicules du parc automobile mondial nous rappellent à quel point notre société dépend du moteur à combustion interne. Malgré des progrès significatifs en termes d'émissions polluantes et de consommation, les moteurs essence et diesel demeurent l'une des principales sources de pollution de l'air des centres urbains modernes. Ce constat motive les autorités à renforcer les normes anti-pollution, qui tendent à complexifier la définition technique des moteurs. En particulier, un nombre croissant d'actionneurs fait aujourd'hui, du contrôle de la chaîne d'air, un challenge majeur.

Dans un marché de plus en plus mondialisé et où le temps de développement de moteurs se doit d'être de plus en plus court, ces travaux entendent proposer une solution aux problèmes liés à cette augmentation de la complexité. La proposition repose sur une approche en trois étapes et combine : modélisation physique du moteur, contrôle prédictif non linéaire et programmation multiparamétrique. Le cas du contrôle de la chaîne d'air d'un moteur essence suralimenté sert de fil conducteur au document.

Dans son ensemble, les développements présentés ici fournissent une approche quasi-systématique pour la synthèse du contrôle de la chaîne des moteurs essence suralimentés. Intuitivement, le raisonnement doit pouvoir être étendu à d'autres boucles de contrôle et au cas des moteurs diesel.

Mots clés : modélisation moteur, turbocompresseur, commande prédictive non linéaire explicite.

Quasi-systematic control design approach for turbocharged engines air path, based on explicit nonlinear model predictive control

Abstract

The hundreds of millions of passenger cars and other vehicles on our roads emphasize our society's reliance on internal combustion engines. Despite striking progress in terms of pollutant emissions and fuel consumption, gasoline and diesel engines remain one of the most important sources of air pollution in modern urban areas. This leads the authorities to lay down increasingly drastic pollutant emission standards, which entail ever more complex engine technical definitions. In particular, due to an increasing number of actuators in the past few years, the air path of internal combustion engines represents one of the biggest challenges of engine control design.

The present thesis addresses this issue of increasing engine complexity with respect to the continuous reduction in development time, dictated by a more and more competitive globalized market. The proposal consists in a three-step approach that combines physics-based engine modeling, nonlinear model predictive control and multi-parametric nonlinear programming. The latter leads to an explicit piecewise affine feedback control law, compatible with a real-time implementation. The proposed approach is applied to the particular case of the control of the air path of a turbocharged gasoline engine.

Overall, the developments presented in this thesis provide a quasi-systematic approach for the synthesis of the control of the air path of turbocharged gasoline engines. Intuitively, this approach can be extended to other control loops in both gasoline and diesel engines.

Keywords: mean value engine model, turbocharger maps, explicit nonlinear model predictive control.

UNIVERSITE D'ORLEANS

Laboratoire PRISME
8 rue Léonard de Vinci
45072 Orléans cedex
FRANCE

RENAULT